d|b|t|a

Technische Universität Berlin

Development of Operation Trajectories Under Uncertainty for a Hydroformylation Mini-plant

vorgelegt von
Master of Science
David Müller
aus Berlin

von der Fakultät III - Prozesswissenschaften
der Technischen Universität Berlin
zur Erlangung des akademischen Grades

Doktor der Ingenieurwissenschaften
- Dr.-Ing. -

genehmigte Dissertation

Promotionsausschuss
Vorsitzender: Prof. Dr.-Ing. Prof. e.h. Dr. h.c. George Tsatsaronis
1. Gutachter: Prof. Dr.-Ing. habil. Prof. h.c. Dr. h.c. Günter Wozny
2. Gutachter: Univ. Prof. Dr. Dr. h.c. Lorenz T. Biegler
3. Gutachter: Prof. Dr. rer. nat. habil. Reinhard Schomäcker

Tag der wissenschaftlichen Aussprache: 24.07.2015

Berlin, 2015

Acknowledgements

During my research as a Ph.D.-student I had the joy of working with numerous people from different academic fields, who have helped me advance personally and professionally.

Firstly, I would like to express my deepest gratitude to my advisor, Prof. Dr.-Ing. Günter Wozny, for letting me complete my Ph.D. at his department. I gratefully acknowledge the opportunities he has given me especially regarding the freedom to pursue various research topics as well as the possibility to attend international conferences and to expand my horizon. I am very thankful for his continuous assistance throughout the last years, both on an academic as well as personal level. Secondly, I would like to thank Prof. Dr. Larry Biegler for accepting to supervise my Ph.D. and for the research impulses he has given me directly at international conferences as well as indirectly via the students he has supervised as part of the collaboration between CMU and TUB. I am also grateful to Prof. Dr. Reinhard Schomäcker for the close collaboration on the research project as well as the fruitful discussions during my Ph.D. studies. I am very thankful for all of their continuous input and support.

Next, I wish to express my sincere thanks to the students, whose theses I have supervised and who have assisted me in my research in the last three years. Of these students, I would like to thank three in particular: Alexander Fleck, Markus Illner, and Christian Hoffmann. Alex worked for me as a student assistant for more than two years and in his Master's thesis was responsible for designing the communication scheme to enable real-time online optimization of the mini-plant. Markus, who succeeds me within the project, assisted me greatly during several stages, especially in the model design of the plant. Christian worked for me for over a year and finally wrote his thesis at Carnegie Mellon on the overall model of the mini-plant. All of their input, their ideas, and effort have added to the great success of the research project. For their continuous assistance, motivation, and devotion I am very grateful.

Next in line of the people I would like to thank are Marcel Schmidt, Tobias Hamerla, and Yasemin Kasaka from the Department of Chemistry at the TU Berlin. A special thanks hereby goes to my colleague Tobias Pogrzeba, from the Department of Chemistry, with whom I have intensively worked on solving all phase separation related issues. Additionally, I would like to thank Michael Maiwald, Korvin Walter, Klas Meyer, Nicolai Zientek, and Andrea Paul from the BAM, who have greatly assisted me on the analytic side of the project. I would also like to extend my appreciation to the entire department of DBTA, the workshop, and lab staff in particular, who have continuously helped me when things got difficult.

Finally, very special thanks goes to my friend and colleague, Erik Esche, with whom I have spent my entire academic career. We successfully studied together in the Bachelor's program, the Master's program, and finally worked together as research assistants at the Chair of Process Dynamics and Operations at TU Berlin. A large degree of my success during the last three years was achieved thanks to our mutual assistance, teamwork, and friendship. Hereby, especially the operation of the mini-plant would have been more difficult and I would have had even more sleepless nights trying to cope with day and night shifts simultaneously. Thank you for your continuous support!

This work is dedicated to my family and to Laura, who have never stopped believing in me and supporting me.

Eidesstattliche Erklärung Ich erkläre an Eides statt, dass die vorliegende Dissertation in allen Teilen von mir selbständig angefertigt wurde und die benutzen Hilfsmittel vollständig angegeben worden sind.

Statutory Declaration I hereby declare that I have authored this thesis independently, that I have not used other than the declared sources, and that I have explicitly marked all material which has been quoted either literally or by content from the used sources.

Berlin, June 12, 2015

David Müller

Publications

This thesis partially consists of already published work. Among the relevant publications are:

- Müller, D.; Kahrs, O.; Höser, S.; Arellano-Garcia, H. (2012): Durchgängige Nutzung von Prozessmodellen während des Prozesslebenszyklus: ein industrielles Fallbeispiel, Chemie Ingenieur Technik, 84, No. 11, 1971-1979. DOI:10.1002/cite.201200072
- Müller, M.; Kasaka, Y.; Müller, D.; Schomäcker, R.; Wozny, G. (2013): Process Design for the Separation of Three Liquid Phases for a Continuous Hydroformylation Process in a Miniplant Scale, Industrial & Engineering Chemistry Research, 52, No. 22, 7259-7264. DOI:10.1021/ie302487m
- Müller, D.; Minh, D.H.; Merchan, V.A.; Arellano-Garcia, H.; Kasaka, Y.; Müller, M.; Schomäcker, R.; Wozny, G. (2013): Towards a Novel Process Concept for the Hydroformylation of Higher Alkenes: Mini-plant Operation Strategies via Model Development and Optimal Experimental Design, Chemical Engineering Science, 115, 127-138. DOI: 10.1016/j.ces.2013.05.022
- Esche, E. and Müller, D.; Kraus, R.; Wozny, G. (2014): Systematic approaches for model derivation for optimization purposes, Chemical Engineering Science, 115, 215-224. DOI: 10.1016/j.ces.2013.11.041
- Müller, D. and Esche, E.; López C., D.C.; Wozny, G. (2014): An Algorithm for the Identification and Estimation of Relevant Parameters for Optimization Under Uncertainty, Computers & Chemical Engineering, 71, No. 4, 94-103. DOI:10.1016/j.compchemeng.2014.07.007
- Esche, E.; Müller, D.; Song, S.; Wozny, G. (2014): Optimization during the Process Synthesis: Enabling the Oxidative Coupling of Methane by Minimizing the Energy Required for the Carbon Dioxide Removal, 91, 100-108. DOI: 10.1016/j.jclepro.2014.12.034
- Pogrzeba, T.; Hamerla, T.; Müller, D.; Wozny, G.; Schomäcker, R. (2014): Kontinuierliche Hydroformylierung von 1-Dodecen in wässrigen Mehrphasensystemen mit nichtionischen Tensiden, Chemie Ingenieur Technik, 86, No. 9, 1486-1508. DOI: 10.1002/cite.201450078
- Meyer, K.; Zientek, N.; Maiwald, M.; Kraemer, B.; Esche, E.; Müller, D.; Wozny, G. (2014): Eine robusten Prozessanalytik für die CO_2-Abtrennung industrieller Gasströme basierend auf Online-NMR und Raman-Spektroskopie, Chemie Ingenieur Technik, 86, No. 9, 1574-1592. DOI: 10.1002/cite.201450076
- Müller, D.; Esche, E.; Pogrzeba, T.; Illner, M.; Leube, F.; Schomäcker, R.; Wozny, G. (2015): Systematic Phase Separation Analysis of Surfactant-Containing Systems for Multiphase Settler Design, Industrial & Engineering Chemistry Research, 54, No. 12, 3205-3217. DOI: 10.1021/ie5049059

- Brinkmann, T.; Naderipour, C.; Pohlmann, J.; Wind, J.; Wolff, T.; Esche, E.; Müller, D.; Wozny, G.; Hoting, B. (2015): Pilot Scale Investigations of the Removal of Carbon Dioxide from Hydrocarbon Gas Streams Using Poly (Ethylene Oxide) – Poly (Butylene Terephthalate) (POLYACTIVE) Thin Film Composite Membranes, Journal of Membrane Science, 489, 237-247. DOI: 10.1016/j.memsci.2015.03.082

Additionally, several contributions in proceedings of conferences were made.

- Müller, M.; Kasaka, Y.; Müller, D.; Schomäcker, R.; Wozny, G. (2012): A Continuous Hydroformylation Process in a Mini-Plant Scale: Equipment Design for the Separation of Three Liquid Phases, Comp. Aid. Chem. Eng., 31, 710-714. DOI:10.1016/B978-0-444-59507-2.50134-7

- Müller, D.; Kahrs, O.; Höser, S.; Arellano-Garcia, H.; Wozny, G. (2012): Optimization of Process Operation Strategies by Combining Process Models with Plant Operating Data, Chemical Engineering Transactions, 29, 1495-1500. DOI:10.3303/CET1229250

- Müller, D.; Müller, M.; Nguyen, L.A.T.; Ludwig, J.; Drews, A.; Kraume, M.; Schomäcker, R.; Wozny, G. (2012): Development of Separation Methods for a Continuous Hydroformylation Process in a Mini-Plant Scale, Proceedings of the 19$^{\text{th}}$ Int. Conference Process Engineering and Chemical Plant Design 2012, Cracow, Poland. ISSN 0011-4561 / ISSN 1897-6328.

- Esche, E.; Müller, D.; Müller, M.; Schöneberger, J.; Thielert, H.; Wozny, G. (2012): Innovative Product and Process Development With Mobile and Modular Mini-Plant-Techniques, Proceedings of the 19$^{\text{th}}$ Int. Conference Process Engineering and Chemical Plant Design 2012, Cracow, Poland. ISSN 0011-4561 / ISSN 1897-6328.

- Müller, D.; Esche, E.; Wozny, G. (2013): Phase Separation Engineering: Trajectories Through Model Regression for a Hydroformylation Mini-Plant, Proceedings of the 6$^{\text{th}}$ Int. Conference on Process Systems Engineering, Kuala Lumpur, Malaysia. Online Proceedings: http://www.sps.utm.my/download/PSEAsia2013-14.pdf

- Esche, E.; Müller, Song, S.; Wozny, G. (2013): Optimization of a Membrane-Absorption- Hybrid System for the Removal of CO_2 from OCM Product Gas, Proceedings of the 6$^{\text{th}}$ Int. Conference on Process Systems Engineering, Kuala Lumpur, Malaysia. Online Proceedings: http://www.sps.utm.my/download/PSEAsia2013-49.pdf

- Zhang, S.; Müller, D.; Arellano-Garcia, H.; Wozny, G. (2013): CFD Simulation of the Fluid Hydrodynamics in a Continuous Stirrer, Proceedings of the 11$^{\text{th}}$ Int. Conference on chemical & Process Engineering, Milan, Italy. ISBN 978-88-95608-23-5; ISSN 1974-9791

- Müller, D.; Esche, E.; Hamerla, T.; Rost, A.; Kasaka, Y.; Schomäcker, R.; Wozny, G. (2013): Enabling Hydroformylation in Micro-emulsion Systems: Long-Term Performance of a Continuously Operated Mini-plant. Proceedings of the AIChE Annual Meeting, San Francisco, CA. Online Proceedings: http://www3.aiche.org/ proceedings/ Abstract.aspx?PaperID=324238

- Esche, E.; Müller, Song, S.; Wozny, G. (2013): MINLP Optimization of a Membrane - Absorption - Hybrid System for the Removal of CO_2 from OCM Product Gas, Proceedings of the AIChE Annual Meeting, San Francisco, CA. Online Proceedings: https://aiche.confex.com/aiche/2013/webprogram/Paper324244.html

- Esche, E.; Müller, D.; Kraus, R.; Fillinger, S.; Merchan Restrepo, V.A.; Wozny, G. (2013): MOSAIC: An Online Platform for Combined Process Model and Measurement Data Management, Proceedings of the AIChE Annual Meeting, San Francisco, CA. Online Proceedings: http://www3.aiche.org/proceedings/content/Annual-2013/extended-abstracts/P324478.pdf

- Müller, D.; Esche, E.; López C., D. C.; Wozny, G. (2014): Systematic Parameter Selection for Optimization under Uncertainty, Proceedings of the 8th Int. Conference on Foundations of Computer-Aided Process Design - FOCAPD 2014, Comp. Aid. Chem. Eng. ISBN: 978-0-444-63433-7, p. 717-722.

- Bock, C.; Esche, E.; Müller, D.; Wozny, G. (2014): Superstructure Optimization: Reaction Yield Dependent CO_2 Removal from OCM Product Gas, Proceedings of the 8th Int. Conference on Foundations of Computer-Aided Process Design - FOCAPD 2014, Comp. Aid. Chem. Eng., ISBN: 978-0-444-63433-7, p. 267-272.

- Esche, E.; Müller, D.; Wozny, G. (2014): Systematic Modeling for Optimization, Proceedings of the 8th Int. Conference on Foundations of Computer-Aided Process Design - FOCAPD 2014, Comp. Aid. Chem. Eng., ISBN: 978-0-444-63433-7, p. 699-704.

- Esche, E.; Müller, D.; Tolksdorf, G.; Kraus, R.; Wozny, G. (2014): MOSAIC: An Online Modeling Platform Supporting Automatic Discretization of Partial Differential Equation Systems, Proceedings of the 8th Int. Conference on Foundations of Computer-Aided Process Design - FOCAPD 2014, Cle Elum, WA. Comp. Aid. Chem. Eng., ISBN: 978-0-444-63433-7, p. 693 - 698.

- Esche, E.; Müller, D.; Bock, C.; Wozny, G. (2014): Synthesis of a Membrane - Absorption - Hybrid System for the Removal of CO_2 from OCM Product Gas, 10th Int. Conference on Distillation and Absorption 2014, Friedrichshafen, Germany.

- Müller, D.; Esche, E.; Pogrzeba, T.; Hamerla, T.; Barz, T.; Schomäcker, R.; Wozny, G. (2014): Hydroformylation of 1-Dodecene in Microemulsions: Long-Term Mini-plant Operation Results, 20th Int. Conference Process Engineering and Chemical Plant Design 2014, Berlin, Germany. ISBN: 978-3-00-047364-7.

- Müller, D.; Illner, M.; Fleck, A.; Esche, E.; Barz, T.; Schomäcker, R.; Wozny, G. (2014): Enabling Online-Optimization for a Multiphase System in a Hydroformylation Mini-plant, 20th Int. Conference Process Engineering and Chemical Plant Design 2014, Berlin, Germany. ISBN: 978-3-00-047364-7.

- Esche, E.; Kraemer, B.; Müller, D.; Meyer, K.; Zientek, N.; Maiwald, M.; Wozny, G. (2014): Improved Desorption Control via Raman Spectroscopy, 20th Int. Conference Process Engineering and Chemical Plant Design 2014, Berlin, Germany. ISBN: 978-3-00-047364-7.

- Müller, D.; Esche, E.; Werk, S.; Wozny, G. (2015): Dynamic Chance-Constrained Optimization under Uncertainty on Reduced Parameter Sets, 12th Int. Symposium on Process Systems Engineering and 25th European Symposium on Computer Aided Process Engineering, Copenhagen, Denmark. Comp. Aid. Chem. Eng., ISBN: 978-0-444-63578-5, p. 725-730.

- Esche, E.; Müller, D.; Wozny, G. (2015): Raman-based Advanced Control of an Absorption Desorption System, 12th Int. Symposium on Process Systems Engineering and 25th European Symposium on Computer Aided Process Engineering, Copenhagen, Denmark. Comp. Aid. Chem. Eng., ISBN: 978-0-444-63578-5, p. 1523-1528.

Furthermore, contributions in form of posters or presentations with only an abstract submission were also made:

- Müller, D.; Esche, E.; Müller, M.; Wozny, G. (2012): Development of a Short-Cut Model for Three-Phase Liquid Separation Dynamics for a Hydroformylation Mini-Plant, AIChE Annual Meeting, Pittsburgh, USA.
- Hamerla, T.; Rost, A.; Kasaka, Y.; Müller, M.; Müller, D.; Wozny, G.; Schomäcker, G. (2012): Development of a Continuous Process for the Rhodium-Catalyzed Hydroformylation of Long Chain Olefins in Aqueous Liquid-Liquid Two-Phase Systems, AIChE Annual Meeting, Pittsburgh, USA.
- Esche, E.; Müller, D.; Stünkel, S.; Wozny, G. (2012): Derivation and Validation of a Short-Cut Model for the Absorption of CO2 in an OCM Mini-Plant, AIChE Annual Meeting, Pittsburgh, USA.
- Kasaka, Y.; Rost, A.; Hamerla, T.; Müller, D.; Schomäcker, R.; Wozny, G. (2012): Mikroemulsion als Medium für die rhodiumkatalysierte Hydroformylierung mit anschlieSSendem Katalysatorrecycling. Würzburg
- Esche, E.; Müller, D.; Schöneberger, J.; Thielert, H.; Wozny, G. (2013): Modellgestützte Planung einer mobilen, modularen Miniplant zur CO_2-Absorption aus industriellen Gasen, Conference on Integrated Digital Plant Design and Operation, Frankfurt a.M., Germany.
- Kasaka, Y.; Rost, A.; Müller, D.; Wozny, G. (2013): Continuous recycling of catalysts after the hydroformylation of long chain olefins in multiphase system. 46^{th} Jahrestreffen Deutscher Katalytiker, Weimar, Germany.
- Walter, K.; Müller, D.; Esche, E.; Bischoff, T.; Paul, A.; Wozny, G.; Maiwald, M. (2013): Process Monitoring of a Hydroformylation Miniplant via Raman Spectroscopy, 9. Kolloquium Arbeitskreis Prozessanalytik, Ludwigshafen, Germany.
- Zhang, S.; Baldyga, J.; Müller, D.; Dylag, M.; Wozny, G. (2013): Gas-Liquid Multiphase Dynamics in Hydroformylation Process - CFD Based Macro-instability simulation in baffled CSTR. Proceedings of the 21^{st} Polish National Conference on Chemical and Process Engineering - Kolberg, Poland.
- Wozny, G.; Zerry, R.; Kuntsche, S.; Kraus, R.; Merchan-Restrepo, V.A.; Esche, E.; Müller, D.; Minh, D.H.; Fillinger, S.; Tolksdorf, G. (2013): Trends and prospects in process modeling and optimization. Proceedings of the 21^{st} Polish National Conference on Chemical and Process Engineering - Kolberg, Poland.
- Müller, D.; Esche, E.; Paul, A.; Walter, K.; Pogrzeba, T.; Hamerla, T.; Barz, T.; Maiwald, M.; Schomäcker, R.; Wozny, G. (2014): Hydroformylation of Long-chained Alkenes in Microemulsions: Raman-spectrometer Assisted Mini-plant Operation. Proceedings of the 9^{th} Int. Symposium on Catalysis in Multiphase Reactors - CAMURE, Lyon, France.
- Pogrzeba, T.; Hamerla, T.; Müller, D.; Barz, T.; Wozny, G.; Schomäcker, R. (2014): Development of a continuous process for the hydroformylation of 1-dodecene in aqueous multiphase systems with non-ionic surfactants. Proceedings of the 9^{th} Int. Symposium on Catalysis in Multiphase Reactors - CAMURE, Lyon, France.

- Paul, A.; Müller, D.; Esche, E.; Wozny, G.; Maiwald, M. (2014): Chemometric modeling of on-line Raman spectra from mini-plant operation. 10^{th} Colloquium "Arbeitskreis Prozessanalytik", 25-26 Nov. 2014, Gerlingen, Germany.

- Meyer, K.; Zientek, N.; Maiwald, M.; Kraemer, B.; Esche, E.; Müller, D.; Wozny, G. (2014): Eine robuste Prozessanalytik für die CO2-Abtrennung industrieller Gasströme basierend auf Online-NMR- und -Raman-Spektroskopie. 10^{th} Colloquium "Arbeitskreis Prozessanalytik", 25-26 Nov. 2014, Gerlingen, Germany.

- Esche, E.; Riesenbeck, M.; Müller, D.; Wozny, G. (2015): Cyclic Steady State Process Models for Combined Pressure and Temperature Swing Adsorption. Deutsche Zeolith Tage, 25-27 Feb. 2015, Oldenburg, Germany.

- Illner, M.; Müller, D.; Esche, E.; Schomäcker, R.; Wozny, G. (2015): Hydroformylation in Microemulsions on a Mini-plant Scale: Operation Challenges and Solution Approaches. ACHEMA 2015, Frankfurt, Germany.

Supervised Theses

- Kuhlmann, C. (2012): Planung und Aufbau einer Miniplant-Anlage für die Hydroformylierung langkettiger Olefine in flüssigen Mehrphasensystemen, Studienarbeit.
- Kuhlmann, C. (2012): Entwicklung und Umsetzung eines Automatisierungskonzeptes einer Miniplant zur Hydroformylierung langkettiger Olefine in PCS7, Diploma thesis.
- Tanyolac, E. (2012): Phase Separation of The Microemulsion Systems For The Hydroformylation Reaction Of Long Chain Olefins, Bachelor's thesis.
- Ludwig, J. (2012): Untersuchung einer Dekanter-Phasentrennung und Entwicklung der analytischen Methoden für eine HPLC, Diploma thesis.
- Birkholz, M. (2013): Entwicklung und Implementierung einer Prozessführungsstrategie für die flexible CO_2-Absorption in einer mobilen, modularen Pilotanlage, Diploma thesis.
- Drescher, A. (2013): Planung, Auslegung und Konstruktion von Anlagenkomponenten für die flexible CO_2- Absorption in einer mobilen, modularen Pilotanlage, Master's thesis.
- Fleck, A. (2013): Entwicklung und Umsetzung von Automatisierungskonzepten zur Online-Optimierung einer Miniplant in PCS7, Master's thesis.
- Pfeiffer, D. (2013): Modellierung des Trennverhaltens von tensidhaltigen Mehrphasengemischen für eine Hydroformylierungsanlage, Master's thesis.
- Bischoff, T. (2013): Entwicklung einer robusten Analytik basierend auf der Ramanspektroskopie an mehrphasigen Gemischen, Bachelor's thesis.
- Leube, F. (2014): Entwicklung eines Mehrphasendekanters zur Trennung tensidhaltiger Mehrphasengemische für eine Hydroformylierungsanlage, Master's thesis.
- Illner, M. (2014): Optimierung der Prozessführung einer Hydroformylierungsanlage durch Modellbildung und Trajektorienentwicklung, Master's thesis.
- Carretero Junquera, C. (2014): Uncertainty Analysis of a Hydroformylation Process, Bachelor's thesis.
- Ruppert, J. (2015): Parameterschätzung dynamischer Prozessmodelle für Optimierung unter Unsicherheiten, Master's thesis.
- Ruiken, J. P. (2015): Entwicklung der Prozessanalytik für eine Hydroformylierungsanlage: Ramanspektroskopie von mehrphasigen Gemischen, Master's thesis.
- Hoffmann, C. (2015): Dynamic Real-Time Optimization and Moving-Horizon State Estimation for a Hydroformylation plant, Master's thesis.

Executive Summary

In most disciplines, uncertainty plays a critical role during the decision making process. Uncertainty becomes especially crucial when the development of new processes is considered. For the case of optimal operation of mini- or pilot-plants, model-assisted strategies are often employed. To combat the discrepancy between model and reality and at the same time to compensate for uncertainty in the structure of the model several different strategies exist today. In this thesis, the chance-constrained optimization approach is used to derive optimal operation strategies for a mini-plant in which the novel process concept of hydroformylation in microemulsion systems is tested.

The development of optimal operation strategies under uncertainty is tackled from a theoretical point of view and is divided into several steps. Firstly, a framework is presented, in which a structured approach is given for process systems engineers developing models for optimization purposes. This framework is enhanced by ideas concerning model reformulation and approximation strategies to improve the numerical behavior of process models used for optimization studies. Secondly, a workflow is discussed, in which the selection of uncertain parameters for optimization under uncertainty is systematically carried out. Thirdly, the model derivation framework is combined with the systematic selection of relevant uncertain parameters and the chance-constrained optimization approach.

The theoretical workflow for the development of optimal operation strategies is applied later on on the process concept mentioned above. Herefore, a systematic system analysis of surfactant containing multiphase systems is performed. Based on the results of this systematic analysis as well as a parameter estimation study for the hydroformylation reaction, a model for the constructed mini-plant at TU Berlin is developed. A simulation of a performed mini-plant operation is then successfully carried out, in which an adequate representation of the measured values from the mini-plant operation could be achieved.

Using gPROMS, both the start-up as well as the continuous operation of the plant are optimized deterministically. The model is then used in a c++/python framework for optimization under uncertainty purposes. Here, three uncertain parameters are relevant: activation energy in the hydroformylation reaction, the inhibition factor of carbon monoxide in the catalyst mass, and a variation factor in the feed pumps of the plant. For the optimal operation of the plant, two chance constraints are implemented. The first is concerned with the product purity in the product tank and the second with the amount of product in the product tank. The results of the chance constrained optimization show that with the control results from the deterministic optimization, constraints are violated for the start-up. The improved controls lead to a slightly better result regarding the objective function and avoid violation of the constraints. For the continuous operation, two theoretical cases are investigated to test the functionality of the model: an ideal case, a case in which less is produced than expected, and a case in which the wrong settler temperature has been installed.

Finally, a comparison between plant data and multiple simulation and optimization runs is carried out. Hereby, almost identical values regarding the yield and phase separation quality are attainable during the continuous operation, in which similar controls are implemented as have been suggested in the determined trajectories under uncertainty. The successful application of the derived workflow is thus shown.

Zusammenfassung

In fast allen Disziplinen spielt Unsicherheit im Entscheidungsfindungsprozess eine bedeutende Rolle. Diese kommt besonders zu tragen, wenn neue Prozesskonzepte und Verfahren entwickelt werden. Bei der Bestimmung optimaler Betriebstrajektorien von Miniplants oder Pilotanlagen werden oft modellgestützte Strategien eingesetzt. Um die Diskrepanz zwischen Prozessmodel und Realität zu minimieren und zur gleichen Zeit Unsicherheiten im Modell zu berücksichtigen, existieren heutzutage verschiedene Strategien. In dieser Dissertation wird die Methode der Optimierung unter Wahrscheinlichkeitsrestriktionen angewendet, um optimale Betriebstrajektorien unter Unsicherheiten für eine Miniplant zu erhalten, in der das neuartige Prozesskonzept, Hydroformylierung langkettiger Alkene in Mikroemulsionen mit wasserlöslichen Rhodiumkatalysatoren, untersucht wird.

Die Entwicklung optimaler Betriebstrajektorien unter Unsicherheiten wird zunächst von theoretischer Seite betrachtet und in dieser Arbeit in mehrere strukturierte Schritte unterteilt. Diese sind im groben: Modellentwicklung für Optimierungszwecke, systematische Identifikation von unsicheren Parametern und Anwendung eines geeigneten Optimierungsverfahrens für stochastische Optimierungsprobleme. Zuerst wird eine Modellierungssystematik für Systemverfahrensingenieure vorgestellt, die das Entwickeln von Modellen für Optimierungszwecke ansteben. Besonderer Fokus wird dabei auf Reformulierungen von Gleichungen gelegt, welche sich für Optimierungsrechnungen als ungünstig hinsichtlich des numerischen Verhaltens erweisen. Im zweiten Schritt wird ein Algorithmus präsentiert, welcher bei Parameterschätzproblemen seine Anwendung findet. Dieser dient dazu relevante unsichere Parameter auszuwählen basierend auf Untersuchungen bezüglich linearer Unabhängigkeit, Sensitivität gegenüber den Modellgleichungen sowie Sensitivität gegenüber einer Zielfunktion. Die als relevant identifizierten Parameter werden dann im Optimierungsverfahren für das stochastische Optimierungsproblem (in dieser Arbeit chance-constrained optimization) als unsichere Parameter im davor entwickelten Modell verwendet.

Nach der Vorstellung der theoretischen Schritte zur Entwicklung der optimalen Betriebstrajektorien werden diese auf das Fallsbeispiel der oben genannten Miniplant erprobt. Hierzu wird zusätzlich mit Hilfe einer selbstentwickelten Systematik zur Analyse tensidhaltiger Mehrkomponentensysteme das vorliegende Stoffsystem analysiert. Basierend auf den experimentell ermittelten Ergebnissen aus dieser Analyse sowie die Anwendung der o.g. Methoden wird ein dynamisches Modell der Miniplant entwickelt. Eine Nachsimulation einer getätigten Anlagenfahrt wird erfolgreich für 32 Betriebsstunden durchgeführt, bei der die Abweichungen der berechneten Werte gegenüber den Messwerten in akzeptablen Bereichen liegen (innerhalb des 3σ Bereichs der Messungen). Aufgrund dieser erfolgreichen Wiedergabe der experimentellen Werte wird das Modell für das stochastische Optimierungsproblem angewendet. Drei GröSSen werden als unsicher deklariert: die Aktivierungsenergie der Hydroformylierungsreaktion, der Kohlenmonoxidinhibitionsfaktor zur Beschreibung der aktiven Katalysatormasse, sowie die Variation der Feedströme. Ziel der Optimierung ist die Produktquantität in gegebener Zeit zu maximieren. Zusätzlich werden im Optimierungsproblem mehrere Nebenbedigungen als Wahrscheinlichkeitsrestriktionen beschrieben: Produktqualität und Rhodiumverlust. Die Optimierung wird gelöst für den Anfahrprozess sowie für den kontinuierlichen Betrieb der Anlage. Die Ergebnisse zeigen, dass im Vergleich zur deterministischen Optimierung, geringfügig bessere Ergebnisse erzielbar sind und viel wichtiger, die Nebenbedingungen im Rahmen der vorgeschriebenen Wahrscheinlichkeit nicht verletzt werden. Ein Vergleich mit einem Miniplant-Versuch mit wiederholter parallel laufender Optimierung zeigt, dass die Ergebnisse der Optimierung erzielbar sind, wenn die ermittelten Trajektorien implementiert werden.

Contents

List of Figures

All figures that do not pertain a reference have been created by the author.

List of Tables

Nomenclature

Abbreviations

Abbreviation	Meaning
Act	Activity entry regarding identifiable parameters
max	Max - function
Pr	Probability
TRIG	Trigger function
FIM	Fisher Information Matrix
HSS	Hammersley Sequence Sampling
LSCS	Linear steady-state process with uncertainties under single chance constraints
MCS	Monte-Carlo Sampling
MPC	Model-predictive control
NDCJ	Nonlinear dynamic process with uncertainties under joint chance constraints
RTO	Real-time optimization

Greek Symbols

Symbol	Meaning	Unit
α	Oil:water ratio	[g/g]
α	Probability bound	[-]
$\dot{\phi}_{Oil}$	Oil volume fraction	[cm^3/cm^3]
ϵ	Dispersed phase hold-up	[-]
γ	Surfactant concentration	[g/g]
κ	Condition number	[-]
λ	Splitting factor	[-]
μ	Expected value	[-]
Φ	Output performance criterion	[-]
ρ	Density	[kg/m^3]
ρ_F	Probability density function	[-]
σ	Standard deviation	[-]
τ	Characteristic coalescence time	[s]
Θ	Contact angle	[°]
ε	Small positive number	[-]
Ξ	Uncertain parameter space	[-]
ξ	Uncertain parameter	[-]
ζ	Friction factor	[-]

Indeces

Symbol	Meaning	Max. Value
g	Gas	[2]
i	Component	[12]
s	Stream	[25]
u	Plant unit	[23]

Latin Symbols

Symbol	Meaning	Unit
Δp	Pressure loss	[bar]
$\Delta_R h$	Heat of the reaction	[J/mol]
$\dot{H}$	Enthalpy stream	[J/s]
$\dot{r}$	Reaction rate	[mol/(l·s)]
$\overline{j}$	Normalized Jacobian matrix	[-]
$\overline{\mathcal{F}}_i$	Normalized objective function - parameter derivative matrix	[-]
A	Area	[m^2]
B	Coalescence rate constant	[-]
C	Constant	[-]
c	Concentration	[mol/l]
Cov	Covariance matrix	[-]
d	Diameter	[dm]
E	Activation energy	[J/mol]
F	Probability distribution function	[-]
F	Stream	[g/s]
f	Function: $\mathbb{R}^n \to \mathbb{R}, n \in \mathbb{N}$	[-]
f	Objective function	[-]
g	Model equations	[-]
H	Temperature dependent Henry constant	[bar]
h	Inequality constraint	[-]
$H_{1...3}$	Henry constant parameter. Unit depends on application	[-]
HU	Hold-up	[g]
K	Inhibition factor. Unit depends on application	[-]
k	Preexponential factor. Unit depends on application	[-]
K_{cat}	Catalyst inhibition factor	[$l^2/(mol^2\ g)$]
KP	Proportional gain. Unit depends on application	[-]
L	Length	[dm]
M	Molar mass	[g/mol]
m	Mass	[kg]
N	Number of droplets	[-]
n	Moles	[mol]
o	Number of coalescence events	[-]
p	Parameter	[-]
p	Pressure	[bar]
Pl	Parameter in cubic settler height function	[-]

q	Exponent	[-]
q	Shape parameter	[1/m]
R	Universal gas constant	[J/(mol·K)]
r	Correlation coefficient	[-]
$R_{i,j}$	Covariance	[-]
Re	Reynold's number	[-]
S	Sensitivity Matrix	[-]
s	Sensitivity	[-]
T	Temperature	[K]
t	Time	[h]
U	Internal energy	[J]
u	Process controls	[-]
V	Volume	[l]
v	Flow velocity	[m/s]
W	Measurement device variance matrix	[-]
w	Mass fraction	$[g/g]$
X	Yield	[-]
x	Molar fraction	[mol/mol]
x	Plant data / state variable	[-]
Y	Output variable space	[-]
y	Output variable. Unit depends on application	[-]
z	Parameter bound	[-]

Sub- and Superscripts

Symbol	**Meaning**
$*$	Optimal
0	Initial
A	Water
a	Lower parameter interval bound
B	Oil
b	Upper parameter interval bound
C	Surfactant
c	Coalescence
dpz	Dense packed zone
ds	Dispersed phase
E	End
in	Entering
$kill$	Kill switch trigger for the settler temperature
L	Limit, Liquid
l	Lower
Lvl	Liquid level
max	Maximum
min	Minimum
n	Dimension
o	Standard conditions
Oil	Oily components: 1-dodecene, 1-tridecanal, iso-dodecene, iso-tridecanal, n-dodecane

$OilLvl$	Level of oil phase in settler
out	Leaving
s	Separated oil phase
s	Subspace
$Settler$	Settler
$solved$	Dissolved amount of gas in liquids
SP	Operation set-point
t	Top
tot	Total
u	Upper
val	Validated
$WaterLvl$	Level of mixed phase in settler
SsS0	Initial subset selection
SsSI	Subset selection for model equations
SsSII	Subset selection for the objective function
SsSIII	Final subset selection

Chapter 1.

Introduction

In the last years an increase of complexity and degree of integration of chemical plants has occurred, due to the consistent rise of overall cost pressure (Müller et al., 2012c). To remain competitive, chemical companies are forced to either enhance the production efficiency as well as the operation flexibility of existing chemical plants or are required to develop new processes. However, an increasing degree of complexity of chemical processes also leads to an increase of an inherent characteristic of every process system: uncertainty. It can be found at various levels of a chemical process, ranging from process related uncertainty concerning sensors, actuators, and controls actions, to uncertainty related to model parameters and constraints. Decisions, in which uncertainty is not considered, may have critical and often safety-relevant chain-effects on a whole production line of a chemical plant. It is therefore of the utmost importance to consider and develop strategies to implement uncertainty in this decision making process.

1.1. Motivation I: Uncertainty in Chemical Engineering

Throughout all disciplines, such as economics, natural sciences, or chemical engineering, uncertainty plays an important role in the decision making process (Arellano-Garcia, 2006). Often enough, robust decisions are desired. For chemical plants this generally means robust decisions regarding design or operating conditions, which maintain all safety and environmental requirements and guarantee the reliability of production to reach a certain profit. "The chemical industry is, therefore, required to make design and operating decisions to satisfy [these] conflicting goals in an optimal and safe manner. However, uncertainty and variability are inherent characteristics of any process system. These arise due to the unpredictable and instantaneous variability of different process conditions" (Arellano-Garcia and Wozny, 2009).

"On an industrial scale, uncertainty is often compensated with conservative measures such as worst case assumptions, over-estimation of operating parameters, over-design of equipment, or implementation of risk-values to minimize possible losses of profit" (Esche et al., 2014a). In this context, simulation and optimization play a crucial role to determine economically advantageous designs of chemical processes (Arellano-Garcia et al., 2007a). Therefore, in order to optimize the systems, mathematical model-based optimization techniques are often applied. Among these techniques, online-optimization of industrial plants has become an increasingly prominent topic in the last years in different fields. Several examples of a successful implementation of model-based optimization approaches from the petro-chemical and chemical industry are available today. Some of these are:

- (Sarabia et al., 2012), in which "a strategy for the management of the whole process and an integrated optimization based framework to optimize the distribution of available hydrogen from producers to consumer facilities" is presented. The applied approach

herein is capable of systematically reducing operating costs by increasing the hydrogen recycle in the consumer facilities and reducing the production costs in the producer facilities.

- (Jalilova et al., 2008b), wherein a modeling and optimization platform for on- and offshore oil production plants is discussed. "The heart of the advisory system is a multi-purpose high-fidelity model with auto-calibration mechanisms. The advantage of this approach is that the same model that is tuned to plant conditions, can be extrapolated to new operating conditions" (Jalilova et al., 2008a). "Using an advisory software package, subsystems were integrated into a model that optimized the facility to create a 3% production increase" (Jalilova et al., 2008a).
- (Ramdial et al., 2009), in which it is shown how a process model can be combined with plant operating data to optimize a process in general. The Trinidad Field Optimizer (TFO) presented in this contribution "is an offline optimization advisory system that links to real time data sources as well as to modeling and simulation packages (Aspen HYSYS and PROSPER) to provide an overall representation of the bp Trinidad and Tobago (bpTT) gas production and conditioning facilities" (Ramdial et al., 2009).
- (Müller et al., 2012b) and (Müller et al., 2012c), wherein a systematic approach to design a technology platform is discussed, in which a validated process model is combined with plant operating data. The strategy is applied to a chemical plant of BASF SE in Ludwigshafen, Germany. Economic potentials regarding energy efficiency as well as production maximization are exposed. Furthermore, bottlenecks of the process are identified, soft sensors are created, and a general optimization of process operating strategies is performed.

In all of these contributions, to combat the model-reality mismatch and to compensate for uncertainty in the structure of the model and the process data, reconciliation and refitting techniques are applied. However, none of these contributions consider the preliminary incorporation of uncertainty into the structure of the objective function in the optimization problem. In these examples of deterministic approaches, expected values are used for the optimization calculation. However, the likelihood of results leading to violations of the constraints, such as safety requirements, when the result is implemented in the chemical plant, is statistically seen as quite high. As discussed in (Arellano-Garcia and Wozny, 2009) the existence of uncertainty leads to questions regarding the reliability of deterministic results in complying with constraints. In this context, uncertainty becomes especially crucial when the development of new processes is considered.

1.2. Motivation II: Hydroformylation in Microemulsions

An increasingly prominent topic is the utilization of multiphase systems for industrial purposes. Several examples can be found in academic contributions by Zagajewski et al. (2014), Rost et al. (2013), Brunsch and Behr (2013), Haumann et al. (2002a) as well as industry-oriented contributions by Kohlpaintner et al. (2001) or Hirasaki et al. (2011). In the transregional collaborative research center SFB/TRR63 InPROMPT, novel process concepts for substitutable base chemicals in multiphase systems are under investigation (InPROMPT, 2013). Hereby, next generation liquid-liquid processes based on innovative solvent concepts are being developed (Müller et al., 2013a). In this dissertation, a new hydroformylation process is of interest: hydroformylation of long chain alkenes in microemulsions with rhodium-based catalysts.

The production of aldehydes from short chain alkenes such as propylene or butylene via the reaction known as hydroformylation, is one of the most important applications of homogeneous catalysis in chemical industry today (Cornils, 1980), (Hamerla et al., 2013b). The annual production lies around 10 to 12 million metric tons (Wiese and Obst, 2006), (Kohlpaintner et al., 2001). Aldehydes are essential intermediate products in the chemical industry and can be used to produce alcohols, detergents, softening agents, flavors, and other chemicals in consecutive steps. The original hydroformylation reaction was first discovered in 1938 by Otto Roelen at Ruhrchemie (Roelen, 1938) (Roelen, 1943). The general idea is "to increase the chain length of unsaturated hydrocarbons by passing synthesis gas over a catalyst, thus creating an aldehyde, a core intermediate product in the chemical industry" (Müller et al., 2013c). Hereby, a linear or branched aldehyde can be produced (Müller et al., 2012d). Figure 1.1 displays a general reaction equation.

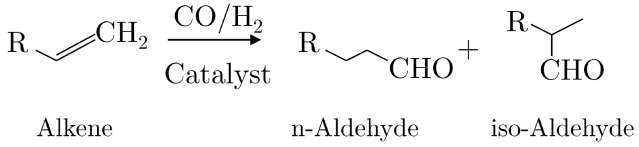

Figure 1.1.: General hydroformylation reaction.

"To date, only rhodium and cobalt are used in industrial practice" (Franke et al., 2012). Challenging in this context is establishing an economical ratio of n:iso aldehydes during the reaction. As discussed by Franke et al. (2012), this challenge can be met by modifying the catalysts with appropriate ligands. In general, the homogeneous catalysis offers the advantage of higher yields and selectivities due to increased surface area of the catalyst. A drawback though is the fact that the catalyst must be isolated from the product after the reaction. This generally results in additional process steps and higher energy expenses, thus reducing the profitability of processes applying homogeneous catalysis (Hamerla et al., 2012). The challenging task of recovering the expensive and cost-determining rhodium catalyst was solved in the Ruhrchemie/Rhône-Poulenc process by immobilization of the hydrophilic catalyst complex in the aqueous phase (Cornils et al., 1984; Kohlpaintner et al., 2001). To date, it represents the only industrial process with a water-soluble catalyst (Hamerla et al., 2013b). A drawback of the Ruhrchemie/Rhône-Poulenc process is its limitation to short chain alkenes ($\leq C_5$), because of the poor solubility of longer alkenes in the aqueous phase. To enhance production efficiency, to enable the utilization of alternative reactants, and to facilitate the creation of alternative base chemicals advancements in this field must be made.

The process concept under investigation in this thesis aims at simultaneously reaching several goals: applying a highly reactive and selective ligand-modified rhodium-based catalyst for the hydroformylation reaction, mixing two normally immiscible liquids as a pseudo-homogeneous reaction, and isolating the product from the catalyst after the reaction. Core idea of the concept, which has been patented by Tinucci and Platone (1991), is the application of a non-ionic surfactant to create a microemulsion. This concept is known as hydroformylation in microemulsions and is extensively being investigated by various groups such as (Haumann et al., 2002b),(Miyagawa et al., 2005), and (Hamerla et al., 2012). A visualization of the concept can be found in Fig. 1.2, in which the general scheme is displayed.

Through the creation of the micro-emulsion, the water soluble rhodium-ligand-catalyst applied for the reaction is brought into contact with the alkene (Kupka, 2006). By injecting syngas (H_2&CO) into the system the reaction is then started. On a macroscopic scale, a homogeneous reaction is performed. Subsequently, the reactants are led to a settler, in which

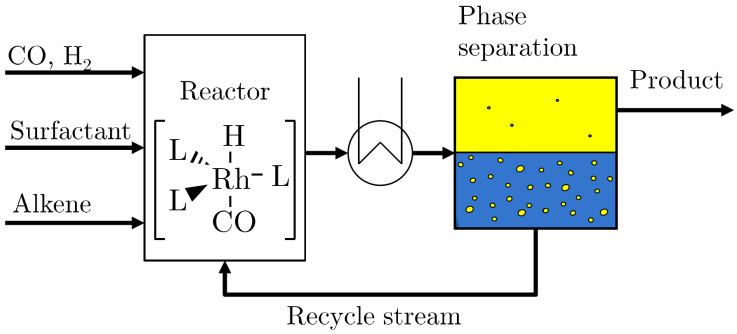

Figure 1.2.: Concept for the hydroformylation in microemulsions (Müller et al., 2012a).

the miscibility gap between the aqueous catalyst solution and hydrophobic alkene/aldehyde mixture is exploited. The valuable rhodium catalyst can be separated and an almost pure organic product phase is obtained (Müller et al., 2012d,e). As discussed by Müller et al. (2013c), the catalyst loss into the oil phase must stay at a minimum, to achieve an economically viable process. According to (Matthey, 2015), the rhodium price has swayed between 1500 and 900 $/Oz over the last two years (2012 to 2014). Despite the fact that the cost of rhodium has taken several plunges, a high average value of 1170 $/Oz (Comparison to gold: 1250 $/Oz (Finanzen.net, 2015)) remains. This fact underlines the mentioned economic influence of the loss of catalyst on the process.

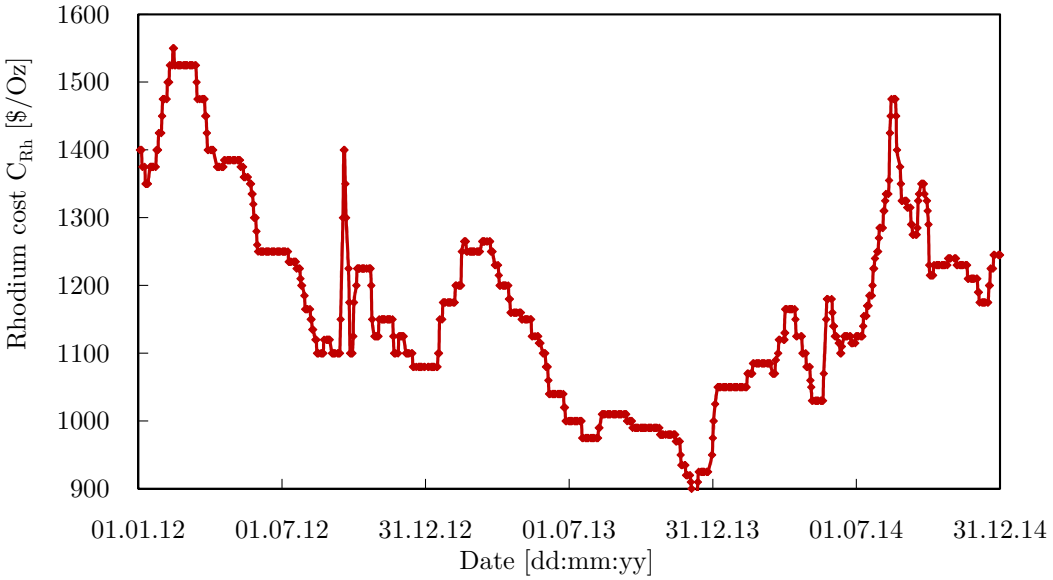

Figure 1.3.: Rhodium price development between the years 2012 and 2014 (Matthey, 2015).

Up to this point in time, no industrial-scale process at moderate temperatures (below 150 °C) and pressures (below 50 bar) exists, in which alkenes with a carbon length longer than C_{10} are reacted to aldehydes using rhodium-based catalysts in micellar media. To investigate this concept in greater detail, a mini-plant has been constructed at Technische Universität Berlin. Given that the process concept is still at an early development stage, the uncertainty of various process relevant characteristics is very large.

1.3. Research Goal

Keeping the challenges mentioned in the previous motivational sections in mind, the research goal in this thesis can be summarized as follows: The aim is to present an overall approach to develop applicable dynamic plant operation trajectories under uncertainty using the chance-constrained optimization approach, which can later be used for dynamic online-optimization. This approach is specifically applied on the industry-related example of the process concept concerning hydroformylation in microemulsions. This research goal is divided into several sub-goals, which in themselves are unique developments part of this thesis:

1. a workflow presenting critical steps of model preparation for optimization purposes,
2. mathematical reformulation strategies to improve convergence of optimization problems,
3. a selection strategy to identify relevant uncertain parameters for optimization under uncertainty,
4. a framework for the online solution of nonlinear dynamic systems considering the stochastic behavior of uncertainty in the objective function for operation trajectory determination,
5. an empirical, general phase separation model for oil-water-surfactant systems, and
6. a systematic approach for the analysis of surfactant-containing multiphase systems for process development and modeling purposes.

1.4. Thesis Overview

This thesis is dedicated to the advancement of a strategy for process systems engineers working with uncertainty. The general aim is to develop, implement, and apply a framework for dynamic online-optimization under uncertainty to develop operation trajectories. The thesis itself is structured into seven chapters.

In **Chapter 2** theoretical fundamentals required to develop the process concept as well as the optimization framework are presented. Firstly, chemical plant automation and real-time online-optimization are discussed. Secondly, uncertainty is a core topic in this thesis. Therefore, an approach for the selection of relevant uncertain parameters is discussed. This is followed by a brief presentation of numerical methods and modeling strategies regarding the systematic development of process models for optimization. Afterwards, existing stochastic optimization strategies are reviewed, whereby a focus is laid on the chance-constrained approach. Since the industrial example is concerned with microemulsions and oil-water-surfactant systems, fundamentals regarding the thermodynamic and fluid dynamic properties of oil-water-surfactant systems are shortly revisited. This is followed by a discussion of an application-related approach for analyzing surfactant containing systems, which is later required for process and model development purposes.

Chapter 3 is devoted to the presentation of the industrial example of hydroformylation in microemulsions. Hereby, a systematic analysis of applied surfactant-containing multiphase systems is carried out. This is then followed within this thesis by a presentation of the designed and built mini-plant at Technische Universität Berlin with a consideration of design and safety issues regarding the applied substances during the reaction. Additionally, issues concerning the monitoring and surveillance of the system as well as the implemented controls

of the process are discussed. Herein, the applied implementation structure, to combine the actuators of the chemical process with an optimizer is shown. For this purpose, a framework for observing the process control system and the optimizer's results is presented. A two-level strategy towards an integration of dynamic online-optimization of processes is considered, especially regarding the moving horizon problem.

Then in **Chapter 4** the mini-plant is systematically modeled. The process model as a whole represents a hybrid model, combining an empirical phase separation model with a rigorously developed and empirically modified reactor model. Herein, the systematic approach from 2.2 is applied, in order to prepare the models for optimization purposes.

Chapter 5 focuses on the actual quantification of the uncertainty in the process. This is divided into two parts: uncertainty concerning the process and uncertainty concerning the model (reaction kinetic parameters and phase separation parameters). Herein, the most relevant uncertainty required for the chance-constrained approach are determined.

In **Chapter 6** the results concerning the "proof of concept" are shown. Here, phase separation as well as reaction results of two performed mini-plant operations are shown. By implementing the actual set-points from one of these mini-plant operations into the model, the operation is simulated and a comparison between reality and simulation is carried out. Afterwards, a deterministic optimization as well as a chance-constrained optimization of the operation trajectories is performed. These results are compared to the results of the real operation and their betterment regarding the objective is discussed. In parallel to a final mini-plant operation, repeated simulation and chance-constrained optimization is carried out.

Finally, in **Chapter 7** a summary of the most important points including an outlook on potential future developments is presented.

Chapter 2.

Theoretical Fundamentals and Status Quo

This chapter focuses on presenting the theoretical background of a structured, general workflow for the development of optimal operation trajectories under uncertainty. To achieve the goal, several steps must be carried out. Fig. 2.1 presents the structure of this workflow brought into connection with the sections in this chapter, in which the theoretical fundamentals required for each step are discussed.

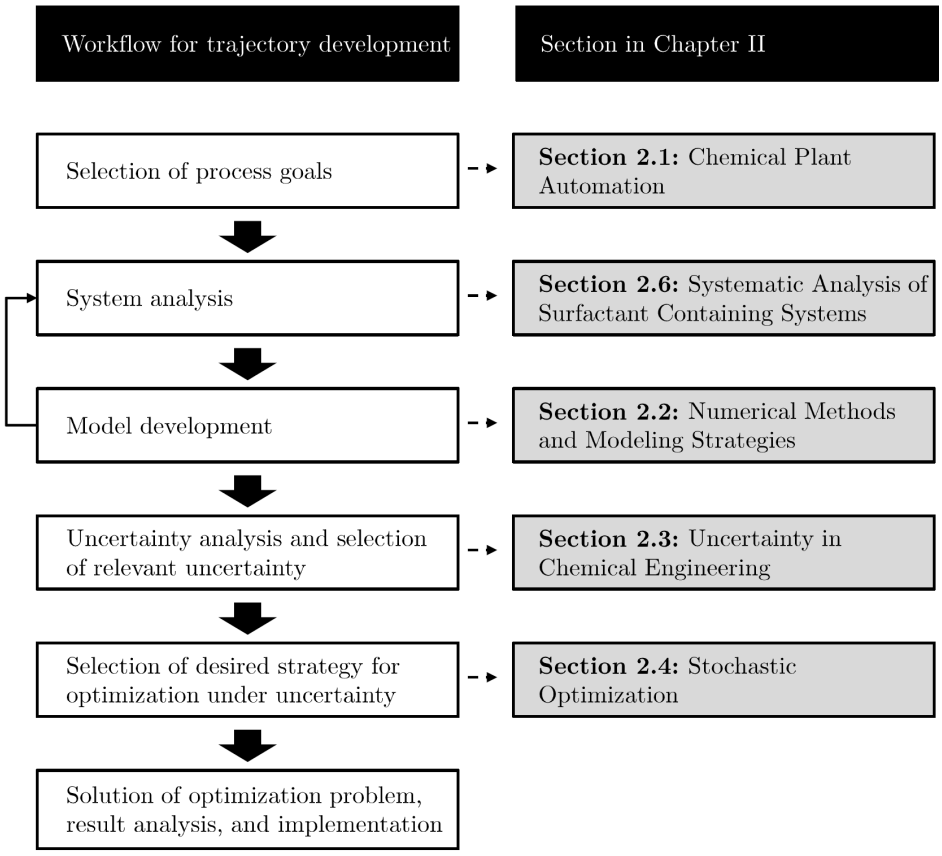

Figure 2.1.: Workflow for the development of operation trajectories under uncertainty.

First of all, a definition of the desired process goals concerning the optimal operation must be carried out. Hints on this topic can be found in (Herder et al., 1997). Therein, the result of a questionnaire for industrial design engineers regarding the question "How to define the quality of plant design and operation" is presented. Keeping in mind that the obtained result (operation trajectory) is to be implemented in a plant, the first section of this

chapter discusses the automation hierarchy of chemical plants and how a determined optimal result can be implemented. Deliberations on the importance of real-time optimization in the automation hierarchy are carried out.

After the goals have been specified, the system at hand must be analyzed in greater detail to model the process accordingly. In the case of this thesis, the system is a surfactant containing multiphase system for a hydroformylation process. Therefore, several sections in this chapter focus on the theoretical fundamentals involved with this system. Of special interest are the thermodynamic properties of oil-water-surfactant systems. The aim hereby is to present the challenges associated with microemulsions. For the workflow shown in Fig. 2.1, Section 2.6 is of relevance. Hereby, a method for the systematic analysis of surfactant containing multiphase systems is presented, whereby critical factors needed to understand and especially to model such a system are highlighted. To avoid a splitting of the mathematical and process control related topics, this part of the workflow is discussed after the fundamentals for the other sections have been presented.

The third step, after the system has been analyzed, is the development of the process model. Since the requirements for real-time optimization are the existence of an accurate as well as easily solvable model, a workflow for designing models for optimization purposes is presented in Section 2.2. This is complemented by strategic mathematical reformulation methods for improved optimization. Obviously, if additional information is required, a reanalysis of the system is needed (Recourse arrow in Fig. 2.1).

After having designed the model, an uncertainty analysis of the system should be performed. A discussion on classification, description, and quantification of uncertainty is carried out in Section 2.3. This is followed by a step containing two tasks: selection of the relevant uncertainty that is to be considered in the optimization problem as well as the selection of the desired strategy to obtain the trajectories under uncertainty. For the former, an approach for the selection of uncertain parameters from parameter estimation studies is shown in Section 2.3. For the latter, special attention is given to the approach known as chance-constrained optimization in Section 2.4. Finally, the optimization problem should be solved accordingly, the results analyzed, and eventually implemented into the process.

To avoid jumping from topic to topic this chapter is structured in such a way that firstly the mathematical and process control related topics are discussed. As a preparation for the system analysis, a review of related thermo- and fluiddynamic topics is carried out. All of the presented methods, workflows, and approaches for the system analysis as well as modeling strategies are applied later on in Chapter 3 and 4, when the process concept and the substances are presented. The strategies discussed in this chapter thus also present spin-off results of this thesis to achieve the goal of obtaining optimal operation trajectories under uncertainty.

2.1. Chemical Plant Automation

In the introduction to this thesis the aim was expressed to develop optimal trajectories under uncertainty. For this purpose, the automation hierarchy of chemical plants must be looked at in greater detail, as this yields information on how an implementation of the developed trajectories can be performed. An even closer look is hereby taken on the field of real-time optimization (RTO).

2.1.1. Automation Hierarchy

The general automation hierarchy of chemical plants is displayed in Fig. 2.2. This hierarchy consists of the different dispositive and operative parts of the plant, with the successive refinement of time scales. "This hierarchy, for which no claim of optimality is made, has evolved based on the decisions that must be made for an operating plant, with consideration to the available information uncertainties, and technology limitations" (Darby et al., 2011).

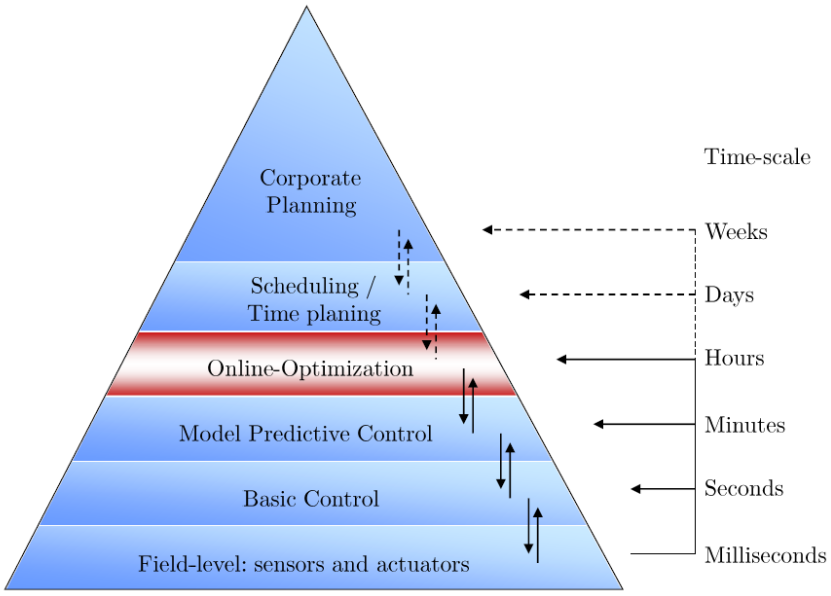

Figure 2.2.: General automation hierarchy of chemical plants. The figure is adapted from (Darby et al., 2011).

According to Darby et al. (2011) the top level, the corporate planning level, is concerned with "what and how" in terms of production choice and quantity. The decisions are made based on the present and forecasted economic situation. This level is relevant for the selection of process goals. Often enough though, these goals stand in contrast to safety and environmental restrictions.

In the second level, the scheduling level, the timing of the operative actions is carried out. Often, logistic issues are taken into account. The third level, the online-optimization, which is of interest for this thesis, is concerned with the implementation of economic decisions on the automation of a chemical plant. In general, a model of the process is connected with the process control system. The model is fitted to the current operating point and then, based on an economic objective function, an optimal operating point or operating trajectory is determined. The set-points are then forwarded to the lower layers of the automation hierarchy. Here, either model-predictive control (MPC) or basis control can adjust the operating point of the plant to a more stable performance.

The lower three layers in the hierarchy consist of MPC, basis control, and the field layer. The MPC layer consists of one or several controllers, which contain a time-discrete and often linear model. The distributed or basis control layer is responsible for the regulatory control. Below are the sensors and actuators, which monitor the plant behavior, compensate for minor disturbances, and supply the other layers with according information.

It is important to note the reaction or execution time reduction. In the planning layer, weeks are often required for a decision to be realized, while in the lowest layer milliseconds

suffice for changes to be performed.

Now, to draw the connection to the goal in this thesis, different approaches exist to improve the operation of a chemical plant:

- Experience based: This approach demands a large degree of experience from the plant operator. Often enough it takes years of expertise and knowledge about the actual operational behavior of the plant.
- Heuristic: Here, rules derived from experience from other or similar plants are followed.
- Offline trajectory development: Using model-based optimization approaches appropriate offline trajectories can be developed. These are then implemented into the operation procedure of the chemical plant. A large degree of uncertainty is taken into account, as the model is not continuously updated to the current state of the plant.
- Online trajectory development: Again, model-based approaches are used to improve the process operating strategies. However, the model is updated regularly to thus minimize plant model mismatch and thus obtain more realistic results. In the chemical industry, a data exchange with the chemical plant can be described as online if a continuous connection to the process control system of a plant exists. Information is constantly supplied regarding the state of the chemical plant as soon as this information is available. The data exchange with the chemical plant is offline, if there is no continuous connection to the process. The data set is obtained at discrete points in time, and not continuously.

In the next section, more details regarding the last mentioned approach are given.

2.1.2. Real-time Optimization

As uncertainty is an inherent characteristic in process control and optimization problems, methods must be developed to consider uncertainty in the decision making process, especially during plant operation. An important level in the automation hierarchy, where model predictions vs. reality discrepancies are minimized, is that of real-time optimization. The term 'real-time optimization' (RTO) is defined by (Forbes et al., 1994): "RTO is a model-based process control approach that uses current process information (i.e. process model and economic data) to predict the optimal operating policy for a process unit during the next RTO interval". The aim is to improve chemical plant performance, operating strategies, and profitability online and in real-time. Hereby, an extrapolation from a validated operating point or plant state is performed. It is important that the model is updated due to the existence of uncertainty, which will be discussed in the following sections in greater detail. A typical, general model-based RTO loop is displayed in Fig. 2.3.

It is important to differentiate between basic online-optimization and real-time online-optimization. For the sake of this thesis, the explanation of real-time found in (Grötschel et al., 2001) will be employed: "The required reaction time of the algorithm must be short compared to the time frame of the system". For chemical plants this means that the computation time to solve the optimization problem must be faster than the time constant of the entire chemical production process. The challenge lies in defining the time constant of the process.

This RTO loop can be divided into several steps. First of all, a measurement data set (x) from the plant is gathered, and validated. It is important to avoid implementation of gross measurement errors or outliers as they may have a drastic effect on the optimization

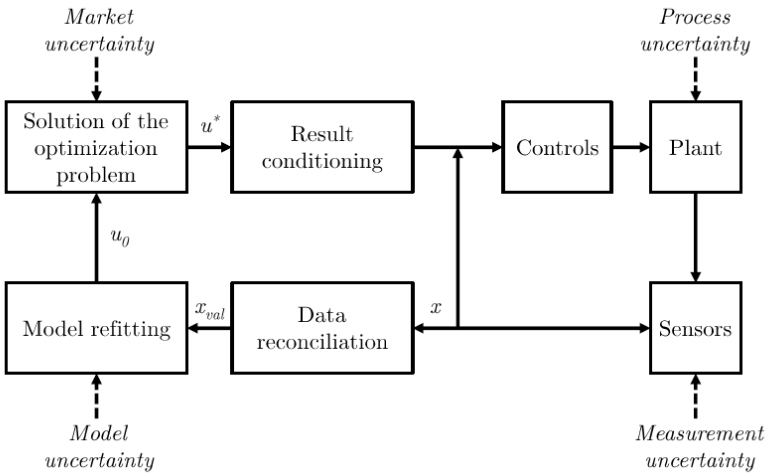

Figure 2.3.: General model-based RTO loop. The figure is adapted from (Forbes et al., 1994).

outcome. The validated measurements (x_{val}) are then used to refit the model to the current state of the plant. This is to minimize the model-reality discrepancy as much as possible. An example, where this issue has been tackled, can be found in (Faber et al., 2007). Therein, an optimization framework for parameter estimation of large-scale systems is presented. Then, using an appropriate algorithm, optimal controller set-points (u^*) from given starting values for the set-points (u_0) are calculated. These are then transferred to the process control system of the plant and thus to the controls themselves. Before this is done, the results are checked by some form of conditioning system.

Often enough though the required frequent and fast solution of the optimization problem may be problematic, especially if convergence issues of the optimizer regarding the deterministic optimization problem arise. To counter this issue and especially to enhance the reliability of the determined results, it is suggested in this thesis to solve a stochastic optimization problem. Hereby, a consideration of the uncertainty in the optimization problem is carried out and a more reliable result is obtained. Thus, even if convergence is not obtained quickly enough, a deviation from reality is kept at a lower level than in the solely deterministic optimization case.

Nevertheless, the introduction of uncertainty into optimization greatly enhances the required computational load. Therefore, fast converging models are needed. Once the model is designed so that it is appropriate for optimization purposes, an analysis of the relevant uncertainty can take place.

2.2. Numerical Methods and Modeling Strategies

In accordance with the workflow for operation trajectory development discussed at the beginning of this chapter, modeling strategies for optimization purposes are looked at now. The next step of the workflow is highlighted in Fig. 2.4. As stated before, for real-time optimization an accurate, but also quickly converging model is required. Therefore in this section, an approach for model derivation for optimization is discussed. This approach is the result of our own already published article (Esche et al., 2014a) and published conference proceeding (Esche et al., 2014b). This description is followed by reformulation and approximation strategies to improve the numerical behavior of nonlinear models. This workflow shown in the next section as well as the presented model reformulation methods are applied later on during the design of the process model for the hydroformylation mini-plant.

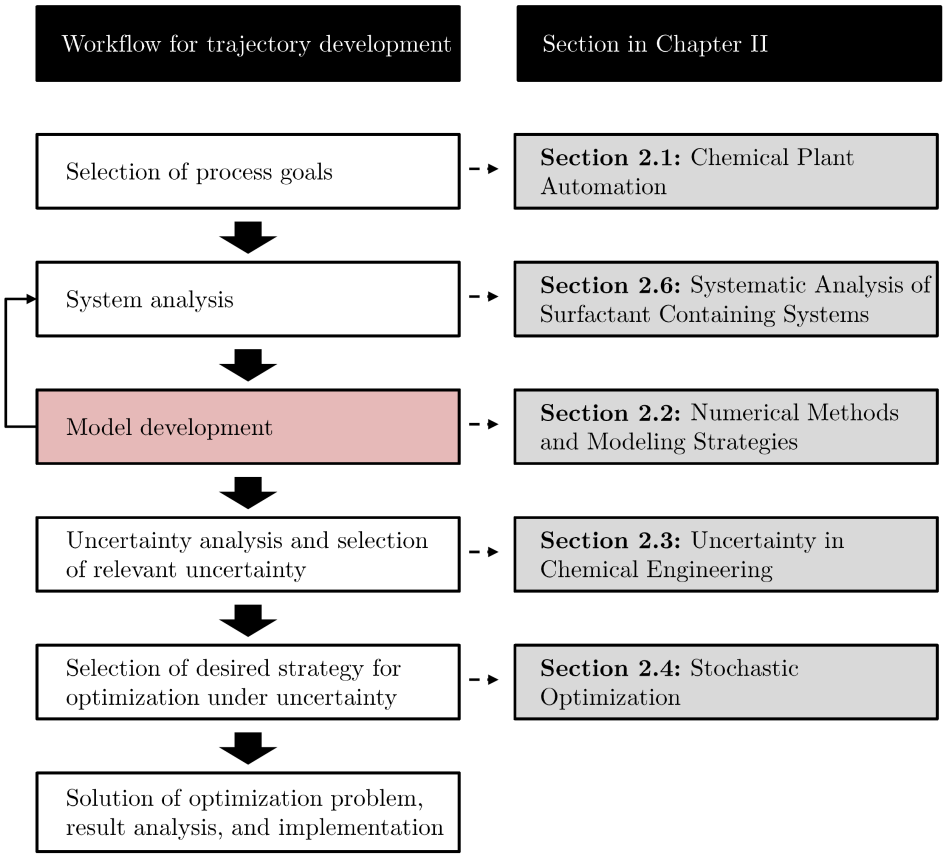

Figure 2.4.: Workflow for the development of plant operation trajectories under uncertainty: Step 3 - Model development

After the discussion on the systematic modeling approach, the uncertainty analysis and chance constraint optimization approach are presented in greater detail.

2.2.1. Workflow for Model Derivation for Optimization

> *"The solution of very large-scale nonlinear programming problems still remains pretty much an art." – Stratos Pistikopoulos, International Conference on Process Systems Engineering Asia - June 2013*

"During the last few decades great advancements in solving large-scale nonlinear and other

programming problems have been made. Despite the vast evolution of the algorithms, a large portion of the actual success to solve a programming problem still depends upon the skill of the programmer or process systems engineer preparing the model for optimization" (Esche et al., 2014a). A first step to systematize the preparation of models and thus demystify this 'art' is taken.

As discussed by Esche et al. (2014a), the success of many model-based optimizers, such as those shown in (Ramdial et al., 2009; Jalilova et al., 2008a; Müller et al., 2012b) can be ascribed to utilized models with two vital characteristics: high to reasonable accuracy regarding the process and acceptable computational effort regarding the optimization calculation. In chemical engineering a multitude of applications ranging from distillation to reaction to absorption exist. In many cases, a model of the system is desired, either for simulation, optimization, or advanced control purposes. Often, engineers will find themselves in one of the following three situations:

- Deterministic models of systems are available, which describe the phenomena, process units, or entire plants with high accuracy. Due to their non-convexity, nonlinearity, and sheer size in terms of equations and variables, application of these models for optimization purposes is seldom seen.
- In contrast to these highly accurate models is the availability of simplified standard models, such as a continuously stirred tank reactor models consisting of integral mass and energy balances. What these models make up for in computational time, they lack in accuracy. "Their viability for optimization can usually be guaranteed, but the results are scarcely ever sensible" Esche et al. (2014a).
- In the final case the possibility of no existing model, no detailed kinetics, or simply a not so well known system must be considered.

Each situation requires its own particular strategy to formulate or rework the model. The workflow to design a model suitable for optimization purposes from (Esche et al., 2014a) is shown in Fig. 2.5. Each of the steps in the model design process can be performed multiple times or left out for certain cases. Therefore in the following, every step is discussed individually. The preliminary step in the workflow demands a definition of goals and model requirements, e.g. exact description of a dynamic system for the application of a real-time optimizer for advanced control strategies. This generally means that an accurate, but computationally inexpensive and fast converging model is desired. The model requirements are thus set: nonlinearities and potential non-convexities should be avoided to prevent the appearance of local infeasibilities.

Now, with these requirements in mind, a model has to be found or designed. Thus **Step 1** of the workflow is started: the query for the existence of a model of the phenomena, process unit, unit cluster, or entire process. If a model exists, then the process engineer should move on to **Step 2**. Often enough, models can be generated by performing a systematic investigation of the system of interest. These theoretical systematics are discussed by various authors, such as (Marquardt, 1996; Rodrigues and Minceva, 2005; Heitzig et al., 2011), and can aid the engineer in designing the desired process models. If the phenomenon has not yet been described and the creation of a rigorous model is not possible, a model needs to be generated from empirical data. This leads the engineer to **Step 6**.

Step 2 demands the analysis of the accuracy of the model. This means that the relevant outputs for the optimization formulation are declared and their description is as accurate as needed. This validation should be performed on existing data of real applications. Should the accuracy be sufficient, then **Step 3** should be carried out. Otherwise, the model should

be analyzed in greater detail. This leads the engineer to **Step 5**. A detailed sensitivity analysis can be helpful here (Homma and Saltelli, 1996).

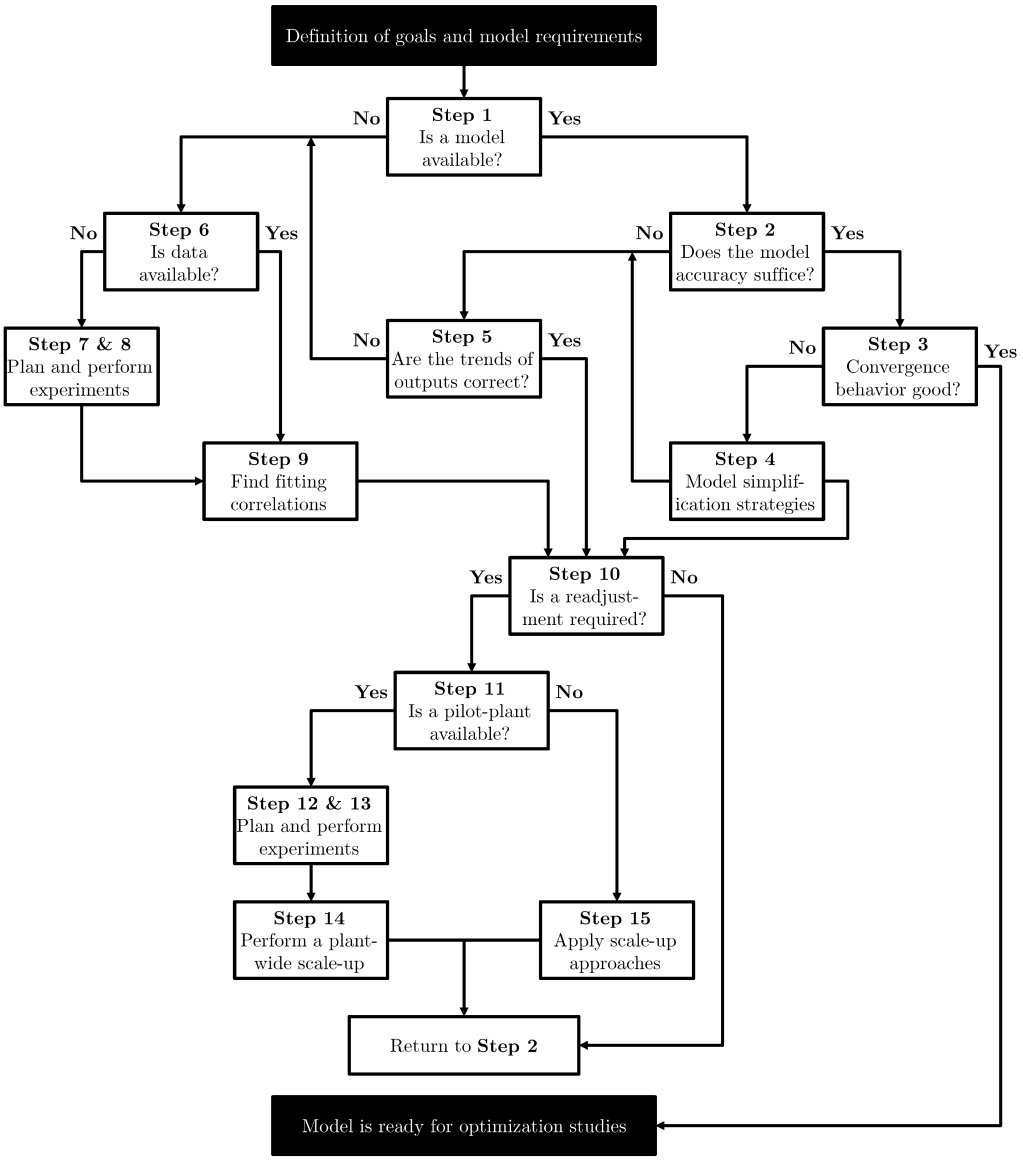

Figure 2.5.: Systematic workflow for the development of models for optimization. The original image is adapted from (Esche et al., 2014a).

In **Step 3**, the convergence behavior of the model is investigated. "Possible methods for this analysis include the test of various initial conditions or data sets for the optimization problem and the comparison of the respective number of iterations, CPU times in NLP-evaluations, and appearance of local infeasibilities. If the behavior is satisfactory, then the model is ready for optimization (step 16). Otherwise, a systematic simplification of the model is required" (Esche et al., 2014a). This is performed in **Step 4**. As this step is more extensive, it will be discussed later on.

Step 5 analyses the model that is to be used regarding its display of trends. Often enough, absolute values of outputs are of limited relevance. The gradients on the other hand are of higher interest, as the position of minima depending on the controls is important. Should the trends given by the model be correct, a readjustment to the actual application, be it plant

or lab-scale, can lead to a better representation. Should the trends be off-target though, then **Step 6** should be carried out.

For **Step 6** it is suggested to do a thorough analysis of existing, research project-specific data. Hereby the extend of information on the outputs of the model with respect to all control variables in the system is of vital importance. The derivation of an exact empirical model requires information on these outputs for a wide sampling over the input space. Should the information for fluid properties, such as viscosities, heat capacities, etc., already be available, experiments can be avoided. Depending on the extensiveness of the existing sampling over the entire input space, either **Step 7** (further experiments required) or **Step 9** have to be carried out.

The planning and execution of experiments is done in **Step 7** and **8**. For details on experimental design, literature such as (Anderson and Whitcomb, 2000) or (Montgomery, 2013) should be considered. Generally though, the following should be done: Firstly, a definition of desired correlations should be formulated. Then it must be decided, which x and u as well as inputs and outputs are of importance. Next, the range of and the density of the sampling must be defined. Regardless where the data set stems from, Esche et al. (2014a) suggest that the development of the desired correlations should be carried out in the following manner: Bivariate dependencies of outputs on their inputs should be analyzed initially. "Based on these dependencies, fitting mathematical functions can be found. Further influences of additional inputs can then be included as functions for the parameters in bivariate correlations. If this approach fails for higher dimensions of the input space, alternative strategies such as multivariate (non-)linear regression can be chosen. The correlations should then be implemented into a first principles model in the form of mass balances" (Esche et al., 2014a).

In **Step 10** a refitting of the existing model to a larger system is considered, e.g. lab- to pilot plant-scale. If necessary, **Step 11** should be performed. If a fitting was already done in the initial experiments for model derivation, the fitting can be skipped and the workflow leads the engineer to **Step 2**.

Step 11 is of course highly dependent on the available experimental facilities. If a real-sized mini- or pilot-plant is available, experiments should be planned and carried out. Thus a further adjustment of the existing model to that system (see **Steps 12 to 14**) can be done. **Steps 12** and **13** are equivalent to **Steps 8** and **7**. The main difference here lies in the application size. If no plant exists, **Step 15** should be considered on how to proceed, especially regarding scale-up techniques. If no experimental facility is available, standard heuristics for scale-up and numbering up can be considered. Since numerous applications for scale-up techniques exist, further considerations are omitted at this point.

Based on the results of the experiments in **Steps 12** and **13**, **Step 14** aims at an adjustment of the model to the larger size. Usually, the larger a plant, the more difficult it is to fully implement all controls, e.g. exact temperature to attain equilibria. Important factors such as heat loss or mixing characteristics are not to be neglected. These can often enough be described using basic correlations or even simple constants. Nevertheless, the performed adjustments of the model must be tested with respect to their accuracy and convergence behavior. This then leads the engineer to **Step 2**.

Once all requirements are fulfilled, the model is ready to be used for optimization. If this is not the case, especially regarding reformulation of model equations, further steps are required. The next section therefore focuses on **Step 4** and discusses strategies to enhance the numerical behavior of process models.

2.2.2. Structural Reformulation of Equations

Our own, already published articles (Esche et al., 2014a) and (Esche et al., 2014b) contain several of the herein listed ideas. Additionally, the topic of model reformulation has been tackled in older publications such as (Amarger et al., 1992), where the authors discuss qualitative knowledge for properly reformulating models. Since these ideas are applied for the model of the hydroformylation mini-plant later on in Chapter 4, they will be revisited in this section.

In all industrial applications in chemical engineering nonlinear behavior is very common. The effort made by process systems engineers to model a system therefore generally results in partial differential algebraic equation (PDAE) systems, which may be poorly scaled, stiff, nonlinear, and non-convex. These characteristics of process models are generally highly inconvenient, especially when process optimization is to be carried out. As stated in the section before, high accuracy criteria for correct predictions as well as ideal convergence behavior for the calculation of optima are almost always desired. Using these nonlinear models, several issues during the solution process of the optimization problem may arise. Among these issues are poorly scaled Jacobian matrices, singularities in derivatives, and indefinite Hessian matrices. Thus, process engineers still face the challenge of formulating accurate and solvable models. In the following, issues related with different equation structures are discussed. This is expanded by presenting mathematical reformulation as well as approximation strategies that may have a numerically positive effect on the solution process of optimization problems. In other words, possibilities are discussed on how process systems engineers may formulate models, so that model accuracy is maintained and numerical behavior is improved.

This section is divided into two parts. The first part focuses on numeric issues within equations. These issues can generally be broken down into several groups: singularities, power functions, large equations dependent on several variables, poorly scaled systems, partial differential equation systems, tightly bounded problems, and binary commands. For the issues that are truly of relevance for this thesis possible reformulations or approximations are presented. The focus will therefore lie on

- singularities (**Issue 1**),
- large equations dependent on several variables (**Issue 2**),
- inverse function replacement (**Issue 3**),
- tightly bounded problems (**Issue 4**), and
- binary commands (**Issue 5**).

The second part of this section looks at the structure of a process model and discusses the location, where the undesired nonlinearities can generally be found. The aim hereby is to assist process systems engineers with the questions "what numeric issue to look for", "where to look for the numeric issue", and present a possibility on "how to solve the numeric issue".

Issue 1 – Potential Singularities: One of the main reasons for the appearance of singularities is the roots of denominators. A simple equation where this can occur is shown in Eq. 2.1. This equation is generalized in Eq. 2.2, wherein f_1 and f_2 are any kind of scalar function, each of which could have multiple roots.

$$f(x) = \frac{1}{x}, \qquad x \in \mathbb{R} \setminus \{0\} \tag{2.1}$$

$$f(\vec{x}) = \frac{f_1(\vec{x})}{f_2(\vec{x})}, \qquad f_1, f_2 : \mathbb{R}^n \to \mathbb{R}, n \in \mathbb{N} \tag{2.2}$$

For the generalized form: As long as the roots of the functions $f_1(\vec{x})$ and $f_2(\vec{x})$ do not coincide, these functions can potentially cause a computational problem. Firstly, it is not possible to evaluate the exact position of the root of the denominator itself. Looking at the numerics associated with this equation, the issue can already occur for an $\varepsilon > 0$ distance away from the root. In Matlab, for example, the threshold lies at $\varepsilon = 1.0E - 309$. This value of course depends both on the applied software and the machine. Secondly, in the vicinity surrounding the denominator's root the first and second order derivatives strive to $\pm\infty$. Both of these issues are catastrophic for NLP optimization. There are several methods to counter the appearance or even or alleviate the negative effects of these singularities:

1. First of all, for non-negative denominators, the most basic solution is the addition of a small $\varepsilon > 0$ to the denominator itself (Eq. 2.3). This simple idea is decent for non-negative denominators, for which the solution to the problem lies far away from the region around the denominator's root. Then though, the problem would not occur in the first place. For the other case, in which the denominator fluctuates between positive and negative values throughout the solution process, this singularity issue is only slightly shifted. Additionally, a direct answer to the size of ε in order to avoid a falsification of results cannot be given.

$$\frac{f_1}{f_2} \approx \frac{f_1}{f_2 + \varepsilon}, \qquad f_2 \geq 0, \varepsilon > 0 \tag{2.3}$$

2. Next, if it obvious that the solution is in an area where the value of the denominator is strictly positive, an alternative approach can be taken. This approach applies an approximation of the $\max(0, f_2)$ on the denominator itself.

$$\frac{f_1}{f_2} \approx \frac{f_1}{\max(0, f_2)} \tag{2.4}$$

   For the approximation of $\max(0, b)$, several methods are known, such as Eq. 2.5 and 2.6.

$$\max{}_1(0, x) \approx \frac{x}{2} + \frac{1}{2} \cdot \left((x + \varepsilon)^2\right)^{0.5}, \qquad \varepsilon > 0 \tag{2.5}$$

$$\max{}_2(0, x) \approx \frac{x}{2} \cdot \left(\frac{x}{(x^2 + \varepsilon_1)^{0.5}} + 1\right) + \varepsilon_2, \qquad \varepsilon_1, \varepsilon_2 > 0 \tag{2.6}$$

   The advantage of both presented approximations is that the discontinuity at the denominator's root disappears. Eq. 2.6 is computationally seen more expensive.

3. The two methods shown above slightly falsify the original behavior of the system around the denominator's root. Another option is the replacement of the whole fraction by a 'dummy variable' and introducing an additional equation to describe the dummy variable. An example is shown in Eq. 2.7.

$$f(x) = \Psi \qquad \wedge \qquad \Psi \cdot f_2(x) = f_1(x) \tag{2.7}$$

   This reformulation does not directly solve the denominator's roots issue. Whenever f_2 is zero for non-zero values of f_1 the singularity remains. Nevertheless, the reformulation itself has a dampening effect on the derivatives of the system. Thus, both

first and second order derivative of the equation are well-defined, which is desirable for optimization.

Issue 2 – Complex Equations: The next issue is the appearance of equations or equation sets, which depend on a high number of variables. These could thus also have a large degree of nonlinearity. Seeing that these equations may cause a dense Jacobian matrice, computation time issues may arise. Ideas to alleviate these are partially presented in (Esche, 2011) and are revisited here. It may pay off to split the complex expression into smaller ones. This can be done by introducing 'dummy variables' and additional equations as discussed above. These can then be calculated separately and increase the sparsity of the Jacobian. Eq. 2.8 shows a simple example of a general equation of a reaction rate $\dot{r}$. Hereby K is an inhibition factor, k a preexponential factor, R is the universal gas constant, E_A the activation energy. The coefficients q_1 to q_3 are exponents. This equation is split up into three separate parts, shown Eq. 2.9.

$$\dot{r} = \frac{\overbrace{k_0 \cdot \exp\left(-\frac{E_A}{R \cdot T}\right) \cdot c_A^{q_1}}^{:=a} \cdot \overbrace{c_B^{q_2} \cdot c_C^{q_3}}^{:=b}}{\left(1 + \underbrace{K \cdot \exp\left(-\frac{\Delta H_{ad}}{R \cdot T}\right) \cdot c_C}_{:=c}\right)^2} \tag{2.8}$$

The original equation depends on four variables: c_A, c_B, c_C, and T. The new equation on the other hand is more sparse and the nonlinearity a lot better distributed across the new equations.

$$\begin{aligned} & \dot{r} = \frac{a \cdot b}{(1+c)^2} \\ \wedge \quad & a = k_0 \cdot \exp\left(-\frac{E_A}{R \cdot T}\right) \cdot c_A^{q_1} \\ \wedge \quad & b = c_B^{q_2} \cdot c_C^{q_3} \\ \wedge \quad & c = K \cdot \exp\left(-\frac{\Delta H_{ad}}{R \cdot T}\right) \cdot c_C \end{aligned} \tag{2.9}$$

Clearly, such a reformulation only makes sense for larger sets of equations with complex nonlinear interdependencies. In addition, it should of course be noted that all introduced dummy variables need to be properly initialized.

Issue 3 – Inverse Function Replacement: In chemical engineering, models may be required to describe complex geometries. Thus, the appearance of trigonometric functions, logistic behavior, or else is unavoidable. Functions such as ln, arcsin, or arccos have several singularities in the set of real values. For these functions a well-defined inverse function exists. Again, the strategy of introducing a 'dummy variable' and additional equation can be applied. This equation represents the inverse function statement. Eq. 2.10 and Eq. 2.11 show this reformulation as an example for arcsine.

$$f_1(x) \cdot \overbrace{\arcsin(x)}^{\Psi:=} = f_2(x) \tag{2.10}$$

$$sin(\Psi) = x \tag{2.11}$$

The downside to the inverse function formulation is that sine has multiple solutions. This can be countered by implementing tight bounds on the newly introduced dummy variable Ψ or some form of penalty function on the objective function to keep Ψ within the desired interval. Another possibility is by representing the expression of the trigonometric function by polynomials and accepting a small degree of error.

Issue 4 – Tight Bounding: Often enough, models in chemical engineering contain several tightly bounded variables. Examples are molar or mass fractions, which of course are only defined in the range from zero to one. Generally, the higher the number of bounds, the larger the computation time. This is especially the case if the solution of the optimization problem lies at several bounds simultaneously. Therefore, it should be preferred to develop a model in such a way that fewer bounds are required. One way of achieving this is by reformulating the model so that these tightly bounded variables are replaced. An example is the replacement of molar fractions by component mole flows. This is also applicable for component mass flows, concentrations, or partial pressures. Obviously this is not always possible as many equations, especially in thermodynamics, are formulated with molar fractions. Nevertheless, Esche et al. (2013) have shown that omitting molar fractions is feasible and advantageous compared to a more tightly bounded formulation in the optimization problem.

Issue 5 – Triggering functions: A vital part of the mini-plant model in this thesis are the functions concerning the triggers of certain events in the process, such as initiation of pressure rise, tank overflow, or the starting of a pump to feed a stream. To avoid the formulation of a mixed-integer nonlinear problem, the idea is to replace binary decision variables by continuous functions and implementing these in the respective equations. Generally, this can be done by a sigmoid function. Eq. (2.12) shows a general form of such a sigmoid function.

$$y = \frac{p_1}{1 + e^{-p_2 \cdot (x - p_3)}} \tag{2.12}$$

In the equation presented above, p_i are parameters that can be set, while x is the manipulable variable and y is its output. The parameter p_1 can change the maximum value reachable, p_1 changes the slope of the sigmoid function, and p_3 shifts the position of the switch on the x-axis. Fig. 2.6 shows the behavior of the sigmoid function for different parameters p_1, p_2, and p_3.[1]

In general, the aim is to establish an "on-off" switch in terms of 0 and 1. Thus, the parameter p_1 is left at a value of 1. The issue now arises, which value to pick for parameter p_2. Obviously a steep enough slope is required to effectively enable the switch. If the slope is too shallow, then effects such as "half actived" pumps or out flowing streams may occur. This is highly undesired. If the slope is too steep though, numeric differentiability issues may arise, as the derivative at this point may become very large. An alternative to the presented sigmoid function is shown in Eq. (2.13).

$$y = \frac{1}{2} + \frac{\frac{1}{2} \cdot (x - p_1)}{\sqrt{(x - p_1)^2 + \varepsilon}} \tag{2.13}$$

The numeric stability of this equation is higher. Since there is no exponential term in this equation. A comparison between Eq. (2.12) and Eq. (2.13) is shown in Fig. 2.7. Sig.1

[1] For the variation of parameter p_1, the following values for the different cases are used: In Case 1 $p_1 = 1$, $p_2 = 2$, $p_3 = 5$. In Case 2 only parameter p_1 is changed to $p_1 = 0.5$. In Case 3 $p_1 = 2$. For the variation of parameter p_2 the parameters used for Case 1 are $p_1 = 1$, $p_2 = 1$, $p_3 = 5$, for Case 2:$p_2 = 2$, and for Case 3 $p_2 = 10$. For the variation of parameter p_3, the parameter values for Case 1 are $p_1 = 1$, $p_2 = 2$, $p_3 = 5$, for Case 2: $p_3 = 4$, and for Case 3 $p_3 = 6$.

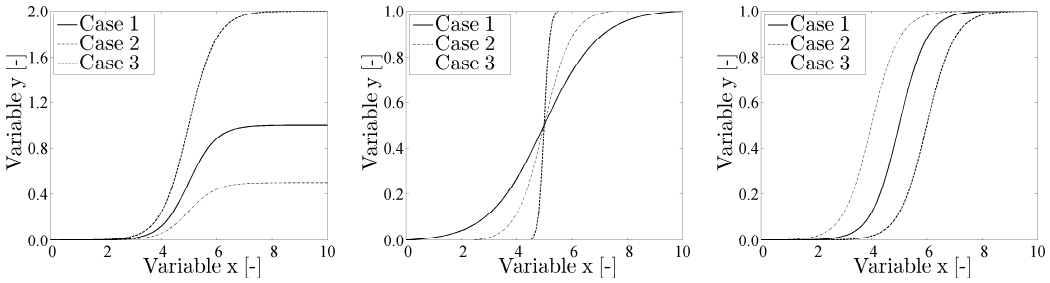

(a) Variation of parameter p_1 (b) Variation of parameter p_2 (c) Variation of parameter p_3

Figure 2.6.: Sigmoid function behavior for different vaules of p_1, p_2, and p_3.

refers to Eq. (2.12) and Sig.2 to Eq. (2.13). Hereby, $p_1 = 1$, $p_2 = 2$, and $p_3 = 5$ for the original sigmoid function. For the numerically more stable sigmoid $p_1 = 5$ for the shift and $\varepsilon = 1$. It is apparent that the differences are marginal and thus Eq. (2.13) can be used as a triggering function. It must be kept in mind though that Eq. (2.13) has a steeper slope in the vicinity of the switching point, but is more shallow later on. This can become critical if it is implemented for mass balances, as the exact values of 0 or 1 are never truly reached.

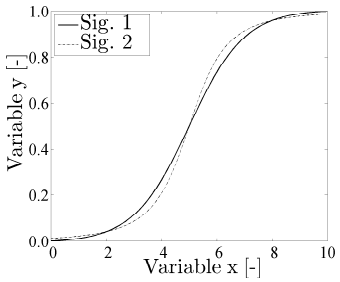

Figure 2.7.: Plot of a numerically more stable sigmoid function.

Now, several other issues such as multiple solutions and solution stability also exist. An elaboration of these issues is waived at this point, as the most relevant points for this thesis have been discussed above. For further details contributions such (Kamath et al., 2010) or (Finlayson, 1980) can be looked at. Now, after looking at improved numerical behavior involved with different formats of equations, the question arises where to look for these equations in modeling. Therefore, the next section focuses on a detailed analysis of models.

2.2.3. Systematic Model Analysis

This section focuses on thoughts and ideas published in our own articles (Esche et al., 2014a,b). As mentioned in the previous section, knowing the issues involved with equation formats does not suffice. These equations must be found in the models. To effectively perform such a model analysis, a structural dissection of the model is proposed. The entire model is separated into six parts: mass and component balances (M), equilibria formulations (E), summations (S), energy balances (H), momentum balances (I), and auxiliary equations (Aux). This section focuses on a definition of each of these parts including a discussion of possible convergence problems and strategies to alleviate these.

Mass and Component Balances: The first section is concerned with mass and component balances. Different types of these balances exist, whereby each has distinct issues which contribute differently to the convergence behavior of the model. Differentials in equations are handled separately.

- *Total mass balance:* This equation is usually linear. Thus, no further simplification is required.
- *Total mole balance:* This equation may contain source terms. This is especially the case when reactions are involved. The numerical issues therefore mainly lie within the reaction kinetics. As issues with these occur frequently, they will be dealt with later on in the section concerned with auxiliary equations.
- *Component balance (general):* This equation may also include source terms, also because of reaction kinetics. In (Esche et al., 2014a) it is suggested to deal with the nonlinearity of the kinetics separately. An evasion is possible through a reformulation of the component balances as atom balances.
- *Component balance (trace-components):* As opposed to the general case trace components must be handled differently in component balances. Here, a differentiation between vital and superfluous components is necessary. Obviously, superfluous components can be left out. Vital trace components need to be left in the balance. As the issues involved with trace components are often caused by multiple scales a manual scaling can be performed to avoid singularities in the Jacobian. To avoid this issue, the essential trace components can be divided by their initial or feed amounts. The balances may be bilinear though. This can be compensated by using component mole flows instead of mole or mass fractions.
- *Atom balances:* These equations may contain bilinear formulations and can be dealt with as stated above.
- *Scaling of differentials:* Here issues can arise, if the order of the differential is higher than one. Esche et al. (2014a) mention that "as of yet no standard procedure for scaling second order differential equations is known". Nevertheless, the separation of the differential equation into its basic phenomena can be target-oriented. Often enough, a magnitude comparison of the influence on the differential equation can be evaluated. Those phenomena with a significantly lower impact can be left out. Hereby it must be kept in mind that such a simplification is always involved with loss of model accuracy. This can become critical when coupling between differential equations and their boundary conditions is involved.

Equilibria: The next section of equation is concerned with equilibria. These equations are often a key part in phenomena-based models. In the following, the different types and their respective issues are discussed.

- *Phase Equilibria:* These sets of equations are concerned with phase equilibria describing vapor-liquid, solid-liquid, or gas-liquid combinations. In general these equations are nonlinear. Hereby, the strongest nonlinearity stems from the correction terms to describe the real fluid behavior. To reduce the nonlinearity herein, in case the correction terms are close to one, a fixing to the value one or to their current value is suggested. If they cannot be fixed to not lose the real behavior, then simplifications within the auxiliary equations are required.

- *Switch Between Phase States:* Issue often arise in the solution domain, where a switch between phases states as well as phase equilibria occurs. A simple example is the switch between a vapor-liquid equilibrium (VLE) and a vapor-liquid-liquid equilibrium (VLLE). Due to this switch, a potential non-differentiability exists in the model. A solution to this issue is a relaxation for these types of switches by implementing a sigmoid or logistic function. This function deactivates the currently non-appropriate model part. To now avoid the appearance of singularities in the Jacobian through these deactivated model parts, Esche et al. (2014a) suggest the introduction of slack variables, thus it can be ensured that at least a single variable is active. This does not solve all issues with the trivial root of equilibria though.

- *Chemical Equilibria – Reaction Equilibria:* These equations are almost always highly nonlinear and thus generally non-convex. Tackling options to avoid computational issues are the introduction of pseudo components. These can both simplify as well as replace the reaction kinetics. As mentioned in the section 2.2.2, the appearance of singularities caused by trace components is another issue. Again, manual scaling, dimensionless format, unit change, or scaling by magnitude of the respective equations are possibilities to dispatch this issue. Irrelevant trace components or those that have little to no impact on the kinetics can be fixed to their mean concentrations or even left out entirely.

- *Thermal Equilibria:* These equations are always linear and direct calculation should be possible.

- *Mechanical Equilibria:* These equations, focusing on pressure drop correlations, are also usually linear and can generally be calculated directly.

Summations: The third modeling section is concerned with summations in equations. Here, three issues are discussed.

- *Summation of Fractions:* The summation of fractions is the sum over mass, volume, or mole fractions (example is left side of Eq. 2.14 for an arbitrary stream s). This sum is always equal to one. The issue herein has already been mentioned before and lies in the fact that the variables within the sum are tightly bounded between the values zero and one. Numerically seen, this may lead to a slow convergence behavior during the solution process as solvers might continuously violate those bounds. Here again, the replacement by summation of absolute quantities might ease this issue (right of Eq. 2.14).

$$\sum_{i=1}^{n} x_{s,i} = 1 \qquad \text{vs. suggested solution:} \qquad \sum_{i=1}^{n} F_{s,i} = F_s \tag{2.14}$$

- *Empty Hold-ups:* A further, frequently appearing problem is the handling of empty hold-ups of an arbitrary unit u or non-flowing streams. A solution approach that has proven to be successful is by initializing empty tanks with an arbitrary gas component. This may increase the total number of components if a new gas has to be introduced, but it alleviates the mentioned issue.

$$\sum_{i=1}^{n} HU_{u,i} = HU_u \tag{2.15}$$

- *Summation of Absolute Quantities:* The summation of absolute quantities, such as component mole flows or component hold-ups, can be problematic in the case of poor scaling, as singularities can appear in the Jacobian matrix. Again, already discussed methods of selective manual scaling or similar is advised.

Energy Balances: The fourth group of model equations is focused on those relevant for the energy balance. Here, convergence problems are caused due to the strong influence on the entire system. In the following, the issues related with energy balances are divided into four parts.

- *Energy Balance Without Source Term:* The energy balances without a source term generally describe standard heat exchange phenomena. The nonlinearities herein can often be dealt with by linearizing the equations. An example is the logarithmic temperature difference. Of course accuracy issues have to be considered. Additionally, scaling issues can appear. This can solved though, by selecting the right units for the formulation.

- *Energy balance with source term:* Energy balances with source terms often appear due to reactions or absorptions. An example is shown in (2.16) for reactions.

$$\frac{dU}{dt} = \dot{H}_{in} - \dot{H}_{out} + V_R \cdot \sum_{i=1}^{n} \dot{r}_i \cdot \Delta_R h_i \tag{2.16}$$

  As mentioned before, nonlinearities due to reactions will be discussed later. If bilinearity should appear, e.g. in the heats of the reactions $\Delta_R h_i$, these could be fixed to an average value depending on the expected temperatures.

- *Energy balance with enthalpy of formation:* Herein, the issue exists that the reference point for a mixture often depends on the concentrations. A solution is using a unifying source term, such as heat of reactions or heat of absorptions instead.

- *Energy balance with differentials:* A similar solution can be selected here as for mass balances with differentials.

Momentum Balances: Issues in these equations are often caused by pressure loss equations.

- *Constant Pressure Problems:* Should pressure losses be neglected and constant pressure be used throughout the model, no issues should arise.

- *Pressure Loss Correlations:* The general equation for calculating pressure drop in a pipe for a given density ρ, flow velocity v, pipe length L, and diameter d is displayed in Eq. (2.17).

$$\Delta p = \zeta \cdot \frac{\rho}{2} \cdot v^2 \cdot \frac{L}{d} \tag{2.17}$$

  If the flow in the pipe is laminar, then the friction factor ζ is calculated as a function of Re:

$$\zeta = \frac{64}{Re} \tag{2.18}$$

  For the laminar flow, an implementation of this correlation into the pressure loss equation (Eq. (2.17)) leads to a linear dependency of the pressure loss Δp with respect to

the flow velocity v. The issues begin though, in the intermediate regime between laminar and fully turbulent flow. The currently existing correlations are often nonlinear. In (Esche et al., 2014a) it is suggested to carry out a local linearization. In the fully turbulent flow regime, the friction factor ζ is often enough a constant. Thus, the pressure loss turns into a quadratic equation with respect to the flow velocity v. This equation is convex and should not cause many issues. The main issues remain in the regime between laminar and turbulent flow, especially as switches between these two can cause nondifferentiabilities. Should switches be unavoidable, already mentioned solutions such as applying logistic or sigmoid functions can be implemented. These should create a smooth transition between these regions.

A discussion on simplifications regarding the Bernoulli equation or the Navier-Stokes Equations is neglected at this point, as they are not relevant for this thesis.

Auxiliary Equations: The final part is concerned with all auxiliary correlations required for the model. These generally contain additional information needed to specify certain parts of the balance equations discussed above. As these auxiliaries are vast, a focus is laid on two topics:

- *Fluid properties:* Among the equations for fluid properties are correlations for the calculation of surface tensions, viscosities, heat capacities, as well as densities. Often, polynomial functions are employed to fit experimental data to describe the behavior of pure components. The general problem herein is poor scaling and the nonlinearity associated with the polynomials. Again, these issues can be overcome by already mentioned strategies such as manual scaling and linearization in the region of interest.

- *Reaction Kinetics:* Among these issues are the appearance of reaction relevant trace components. These obviously cause scaling problems, which can be dealt with accordingly. (Esche et al., 2014a) discuss that "there is [...], a measure to simplify the existing nonlinearities by strategically tackling the multivariate interdependencies in reaction rate equation systems. Smaller, nonlinear terms within each reaction rate can be described by a newly introduced variable, which is described in an additional auxiliary equation". This measure was presented in the previous section and focused on the introduction of a 'dummy variable' and an additional equation to increase the sparsity of the system.

The main challenges relevant for designing the desired model to obtain results of optimal trajectories have thus been presented. A hence derived model can now be used in the next step with a preceding uncertainty analysis and an according optimization approach to solve the stochastic optimization problem.

2.3. Uncertainty in Chemical Engineering

Arellano-Garcia (2006) states that "in chemical industry, decisions are often made based on limited knowledge about the processes and the corresponding underlying phenomena". This generally results in poor performance of processes and thus a loss of profit. Therefore, in order to improve the decision-making process, several model-based deterministic optimization strategies have been applied and successfully implemented to various engineering problems (Ramdial et al., 2009; Müller et al., 2012c; Sarabia et al., 2012). However, due to impurities in applied materials, not perfectly implementable process operating conditions, as

well as variations in physical dimensions and scale-up issues, model reality discrepancies are always present. These discrepancies, also describable as model errors or uncertainty, are the drawback in model-based deterministic optimization approaches, as these approaches lack "the ability to achieve specified levels of constraint satisfaction especially for reliability and safety requirements" (Arellano-Garcia, 2006). This then results in over-conservative solutions or *Worst-Case-Assumptions*, again leading to a loss of profit (Li et al., 2003). Thus, the following questions arise during the development of optimal trajectories under uncertainty:

- What are the exact sources of uncertainty in chemical engineering?
- How can this uncertainty be quantified?
- Is it necessary to consider all uncertainty factors or can a focus be laid on the most relevant ones and thereby still describe the complete system?
- In what way should the uncertainty be incorporated into a model-based optimization approach?

The first three listed issues will be discussed in the following sections. The latter will be looked at more closely in section 2.4.

2.3.1. Sources and Classification of Uncertainty

All systems in the chemical industry are associated with uncertainty. From a process operation point of view, the source of uncertainty may be internal or external. The former can be inaccurate model parameters, deviations in dimensions, flaws in the model due to scale-up reasons, or inaccuracies in property functions. The latter, external uncertainty, is concerned with external events that have an influence on the process itself, such as rain showers which lead to enhanced cooling, unknown quality of the future feedstock, or sudden market-price deterioration of a product. Two approaches exist to implement uncertainty into model-based techniques: deterministic and stochastic. In the deterministic approach, the uncertainty associated with parameters can be described by lower and upper bounds or by creating scenarios in which the parameters are fixed to certain values. Several weaknesses exist hereby. Arellano-Garcia (2006) discusses that "since a number of parameters are frequently estimated at the same time from a single set of experimental data, simple lower and upper bounds may not capture the actual uncertainty". Regarding scenarios, it must be guaranteed that these depict the full scope of possible solutions. Therefore, the stochastic method on the other hand aims at describing the uncertainty by probability distribution functions to thus incorporate the uncertainty correctly. Before the exact description of uncertainty can be performed, a classification must be made. Such a classification for different uncertainty types for chemical engineering systems is discussed by Ierapetritou et al. (1996):

1. *Model-inherent uncertainty:* Physical properties, transfer coefficients, or kinetic parameters are allocated in this group. In general, this information is gained via experimental work and can supplied by e.g. approximations of a probability distribution function.
2. *Process-inherent uncertainty:* This uncertainty type contains variations of streams, temperatures, pressures, and concentrations and is often obtained from online measurements.

3. *External uncertainty:* It comprises uncertainty of data outside of the chemical plant, such as feed availability, feed price, product price and demand, or environmental conditions. To cope with this type of uncertainty, forecasting techniques based for example on historical data are generally applied to obtain corresponding probability distributions.

4. *Discrete uncertainty:* This group consists of uncertainty regarding discrete items such as equipment or discrete events. An example is the availability of a process unit in terms of failure probability. This information can be obtained from manufacturer specifications.

When modeling a process, all of the uncertainty of course has an influence on the final result, be it simulation or optimization. In this thesis, the uncertainty associated with the first two types (1. & 2.) enumerated above are of interest. After classifying the uncertainty inherent in any process system, a description and a quantification must be carried out.

2.3.2. Description and Quantification of Uncertainty

The behavior of a system subject to uncertainty is schematically depicted by Fig. 2.8. If a system is modeled with uncertain inputs, this will result in an uncertain output. The question to be answered is, how can this uncertainty be quantified?

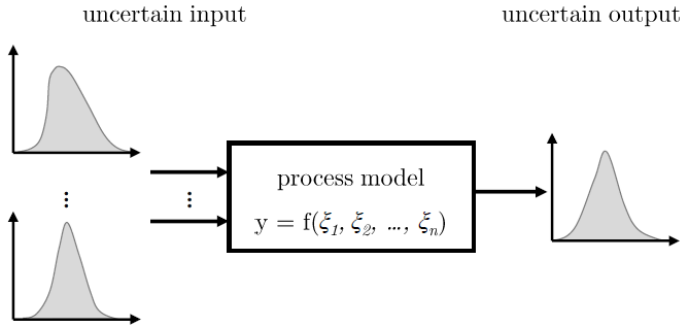

Figure 2.8.: Schematic propagation of uncertainty from uncertain inputs. The figure is based on the original image found in (Arellano-Garcia, 2006).

Before this is done though, a close look at the inputs of a system must be taken. Each of the uncertain factors in process systems engineering can be considered as a random variable or parameter. A random variable or parameter, which will be denoted as ξ for the length of this thesis, is a variable that can take on a random value within a certain region or interval. It is not possible to determine the exact value of this variable, before performing experiments. Li (2007) explains that from a mathematical point of view, this random variable can assume discrete or continuous values. The former have a certain number of possible values that the variable can take on. An example would be a six-sided dice that can yield any of the numbers one through six when rolled. Continuous random variables on the other hand can assume any value within a given range. Industrial processes are subject to continuous variables. Therefore, for the rest of this thesis, the random parameters will be viewed as continuous.

The question now is, how can these random parameters be described? Generally, for each of the random variables different distributions can be assumed based on obtainable information. This information can come from measurements, parameter estimations, or other estimates. It is assumed at this point that data sets are always available in order

to estimate the description of a parameter or set of parameters. Arellano-Garcia (2006) discusses that "in the absence of sufficient data, evaluation of realistic estimates of the parameter limits and the importance of the distributions analytical form are recommended". All in all, if no data sets are available, the confidence limits around assumed nominal values can be defined as a percentage of the nominal values.

In this thesis, the target of this quantification is to evaluate the reliability of a result and thus determine the performance of a system. One method of incorporating uncertainty is by considering the variance or standard deviation of the random parameter. This can be obtained by analyzing data, e.g. for an input mass flow, determining the expected value, μ, and measuring its standard deviation, σ. The presence of outliers can influence the variance drastically though. There are several strategies to detect and deal with outliers, which will not be discussed herein. Examples can be found in (Albuquerque and Biegler, 1996), (Arora and Biegler, 2001), or (Liu et al., 2004). For the case that the outliers are not as important as the width of the desired confidence interval, the variance can be employed as a measure to describe the uncertainty. The same can be done for a parameter, e.g. kinetic parameter, by performing a parameter estimation study based on experimental data and utilizing the inverse of the Fisher Information Matrix (*FIM*) (Bard, 1974), whose diagonal yields the variances of the parameters. All other cells of the *FIM* contain the covariances, which should be employed if the parameters are correlated. Furthermore, the random parameter is assumed to maintain its randomness over time.

Now, the quantification of an uncertain output can be handled in two ways: forward quantification and inverse quantification. The first way, known as *forward uncertainty propagation*, is the quantification of the uncertainty of one or more system outputs depending on uncertain inputs. The aim hereby is to evaluate the reliability of outputs of a system. As discussed by Lee and Chen (2009) several different techniques exist to perform this form of quantification:

- Simulation-based methods (Diwekar and Kalagnanam, 1997),
- Local expansion-based methods (Madsen et al., 2006),
- Functional expansion-based methods (Ghanem and Spanos, 2003),
- Most probable point-based methods (Fiessler et al., 1979), and
- Numerical integration methods (Seo and Kwak, 2002).

Of interest for this thesis are the techniques from the simulation based methods. Among the best known techniques of sampling a probability distribution is the Monte-Carlo Sampling method (MCS). This method is based on the use of a pseudorandom number generator to approximate a uniform distribution with a certain number of samples (Diwekar and Kalagnanam, 1997). The successively sampled points have the property that they are independent of one another. "The specific values for each input variable are selected by inverse transformation over the cumulative probability distribution" (Arellano-Garcia, 2006). All in all, the method itself is easy to employ, but requires numerous model evaluations for accurate results. The computational effort to obtain a sufficient degree of accuracy therefore depends on the number of performed samples. Another, more efficient technique, is the Hammersley Sequence Sampling method (HSS) (Diwekar and Kalagnanam, 1997). Herein, a quasi-random number generator based on Hammersley points is employed to sample points uniformly. "Although this approach preserves the uniformity properties of the stratified schemes, the optimal location of the Hammersley points is perturbed by imposing correlation structure" (Diwekar and Kalagnanam, 1997). Nevertheless, the HSS technique has a

faster convergence rate ranging anywhere from a factor of 1.5 to 100 larger than that of MCS and guarantees a more spread distribution of samples (Diwekar and Kalagnanam, 1997).

The second way is known as inverse uncertainty quantification: Data → Model parameters. Herein, experimental data sets (output) are used to estimate the values of unknown parameters in a model. Hereby, the so-called inverse problem is solved. Given that several uncertain parameters appear in a model, these can be written as a vector: $\vec{\xi} = [\xi_1, \ldots, \xi_m]^T$. Accordingly, the standard deviations can also be formulated as a vector $\vec{\sigma} = [\sigma_1, \ldots, \sigma_m]^T$.

Now to describe the shape of the probability distribution Eq. 2.19 and Eq. 2.20 will be used for the probability distribution function F and probability density function ρ_F respectively.

$$F(z_1, \ldots, z_m) = Pr\{\xi_1 \leq z_1, \ldots, \xi_m \leq z_m\} \tag{2.19}$$

$$\int_{-\infty}^{+infty} \ldots \int_{-\infty}^{+infty} \rho_F(\xi_1, \ldots, \xi_m) d\xi_1 \ldots d\xi_m = 1 \tag{2.20}$$

The boundary of the random parameter ξ_i is written as z_i. Moving on and implementing Eq. 2.20 in Eq. 2.19 leads to

$$F(z_1, \ldots, z_m) = \int_{-\infty}^{z_1} \ldots \int_{-\infty}^{z_m} \rho(\xi_1, \ldots, \xi_m) d\xi_1 \ldots d\xi_m. \tag{2.21}$$

A differentiation must now be made, between correlated and uncorrelated random variables. This correlation can be expressed with the help of the covariance matrix Cov, shown in Eq. 2.22, the covariances $R_{i,j} = Cov(\xi_i, \xi_j) = E[(\xi_i - \mu_i)(\xi_j - \mu_j)]$, and the correlation coefficient $r_{i,j}$ shown in Eq. 2.23.

$$Cov = \begin{pmatrix} R_{1,1} & R_{1,2} & \ldots & R_{1,m} \\ R_{2,1} & R_{2,2} & \ldots & R_{2,m} \\ \vdots & \vdots & \ddots & \vdots \\ R_{m,1} & R_{m,2} & \ldots & R_{m,m} \end{pmatrix} \tag{2.22}$$

$$r_{i,j} = \frac{R_{i,j}}{\sigma_i \sigma_j} \tag{2.23}$$

Matrix Cov can be rewritten in standard form:

$$Cov_S = \begin{pmatrix} 1 & r_{1,2} & \ldots & r_{1,m} \\ r_{2,1} & 1 & \ldots & r_{2,m} \\ \vdots & \vdots & \ddots & \vdots \\ r_{m,1} & r_{m,2} & \ldots & 1 \end{pmatrix} \tag{2.24}$$

Herein, $r_{i,j} = 1$ if $i = j$. Other than that, $r_{i,j}$ can assume values between -1 and 1. A positive $r_{i,j}$ means that if $\xi_i > \mu_i$ then the probability that $\xi_j > \mu_j$ is high. A negative $r_{i,j}$ means that if $\xi_i < \mu_i$ then the probability that $\xi_j > \mu_j$ is high.

According to (Li, 2007), the calculation of the probability of normally distributed random parameters for two uncertain uncorrelated parameters can be done as shown in Eq. 2.25:

$$\begin{aligned} F(z_1, z_2) = & \frac{1}{\sqrt{2 \cdot \pi \cdot \sigma_1}} \cdot \int_{-inf}^{z_1} exp\left[-\frac{1}{2} \cdot \frac{(\xi_1 - \mu_1)^2}{\sigma_1^2}\right] d\xi_1 \cdot \\ & \frac{1}{\sqrt{2 \cdot \pi \cdot \sigma_2}} \cdot \int_{-inf}^{z_2} exp\left[-\frac{1}{2} \cdot \frac{(\xi_2 - \mu_2)^2}{\sigma_2^2}\right] d\xi_2. \end{aligned} \tag{2.25}$$

Details for correlated parameters can be found in Li (2007). As a next step the optimization using these random parameters is of interest. Once the uncertain input has been defined in terms of its lower and upper bounds as well as its distribution form, "the next step is to quantitatively describe the related system outputs with regard to the performance criteria" (Arellano-Garcia, 2006). The quantification of a deterministic output performance criterion Φ can be expressed by the expected value μ. This function for a stochastic output criterion as described in (Arellano-Garcia, 2006), is shown in Eq. 2.26 and Eq. 2.27 respectively.

$$\mu\{f\left(\Phi(\xi)\right)\} = \int_{-\infty}^{+\infty} \left(\Phi(\xi)\right) \rho(\Phi)\, \mathrm{d}\Phi \tag{2.26}$$

$$\mu\{f\left(\Phi(\xi)\right)\} = \int_{\xi}^{z} \left(\Phi(\xi)\right) \rho(\xi)\, \mathrm{d}\xi \tag{2.27}$$

Within an optimization problem calculation of the probability density functions has a strong impact on the computation time. Thus, it is desired to reduce the amount of uncertain parameters.

2.3.3. Systematic Uncertain Parameter Selection

This section largely comes from our own, already published article, (Müller et al., 2014a), and conference proceeding (Müller et al., 2014b). As the topic is relevant for this thesis, the content from the two mentioned publications will be revisited here.

Today, several methods exist for incorporating the uncertainty of model parameters into optimization studies, such as (Arellano-Garcia, 2006), (Binder, 2012), or (Quaglia et al., 2013). In general, each of these approaches is computationally expensive. The computation time increases drastically with an increasing number of uncertain parameters (Dyer and Stougie, 2006). This becomes especially critical for a latter discussed approach: chance-constrained optimization under uncertainty (Wendt et al., 2002; Li et al., 2008; Arellano-Garcia and Wozny, 2009).

"The basis of all uncertainty estimation are measurements and thereon based parameter estimation. Depending on the system the parameter estimation will distribute the measurement uncertainty on all estimated parameters of the system. Usually, identifiability or relevance of parameters for the application of the model are not considered. This can lead to the effect that poorly estimated parameters, in terms of large uncertainty, can add unrealistic behavior to the system. Therefore, it is obviously not sensible to implement the uncertainty for all uncertain parameters into the entire user-defined optimization problem" (Müller et al., 2014a).

The goal in this part of the thesis is to present a method with which the most relevant uncertain parameters for optimization under uncertainty can be ranked according to their uncertainty and identifiability. Hereby, the following points are taken into account:

- the incorporation of linear independence of parameters during parameter estimation and
- a consideration of the sensitivity towards the objective function in optimization under uncertainty.

Müller et al. (2014a) discuss, that in order to design an algorithm, which selects the relevant uncertain parameters for optimization purposes, a consideration of the issues of linear independence, identifiability, and sensitivity of the parameters regarding the outputs and an objective function is required. Hereby, it is stated that identifiability theory claims

that some models, due to their structure, may not be completely identifiable. Therefore, if the model is to be used anyway, it is important to find a subset of parameters, on which it is at least partially identifiable. Müller et al. (2014a) continue and explain that "using the whole set of parameters would lead to unnecessary noise in the parameter estimation and consequently to an overestimation of the parameter variances". For optimization purposes this is undesired, because a distortion of the final optimization result would take place. Furthermore, if the applied model is able to fully depict the actual behavior of the process, the subset of identifiable parameters and their variances should be able cover the entire area of the measurement data. Still, the subset will contain additional information that for example is solely important for intermediate values in the model. The claim is made that only the behavior of certain outputs of the model with respect to a specific objective function is of importance, with respect to optimization under uncertainty. Therefore, "it should be possible to further reduce the subset of identifiable parameters to an even smaller set containing the most vital uncertain parameters, whose expected values and variance are then to be implemented into optimization under uncertainty, while all other parameters are fixed to their expected values" Müller et al. (2014a). This means that the modeler is required to formulate the objective function, before tackling the task of estimating the parameters and selecting a feasible subset.

The idea of the algorithm from (Müller et al., 2014a) is divided into several steps. Firstly, a prescreening of the parameters regarding their identifiability and their measurement data sensitivity is performed. Here, existing methods from design of experiments, also described in (Montgomery, 2013) or (Anderson and Whitcomb, 2000), can be applied. Furthermore, parameter fitting strategies, such as fixation and relaxation of parameters also already exist and have been widely investigated. Strategies for the determination and ranking of linearly independent parameters and of the sensitivities of the parameters are available and should be used (Burth et al., 1999; Brun et al., 2002). The parameters are ranked according to two types of sensitivities, regarding the model equations and regarding a user-defined objective function. In a final step, the subsets of the two rankings are combined, which thus present the relevant uncertain parameters. Additionally, next to these steps, several assumptions are made by (Müller et al., 2014a):

1. A model of the system is available or has been discriminated.
2. The model is either fully discretized or consists of a first order differential algebraic equation system.
3. Measurement data have been produced and are available for various operation points or conditions.
4. Variances for all measurement devices are available.

Keeping these basic ideas and assumptions in mind, the algorithm is developed, the general schematic of which is displayed in Fig. 2.9. In the following, this algorithm will be explained in greater detail.

The first step of the algorithm is the accumulation of measurement data and model discrimination. The general idea during the estimation of parameters is that often enough it is not obvious which parameter values can or should be fixed as constants and which should be left uncertain initially. Thus, all are originally left uncertain.

The first step of the algorithm is followed by a definition of preliminary expected values, lower, and upper bounds for these uncertain parameters. As this step is based on heuristics a relaxation of the bounds should be done, if the results of parameter estimation are not

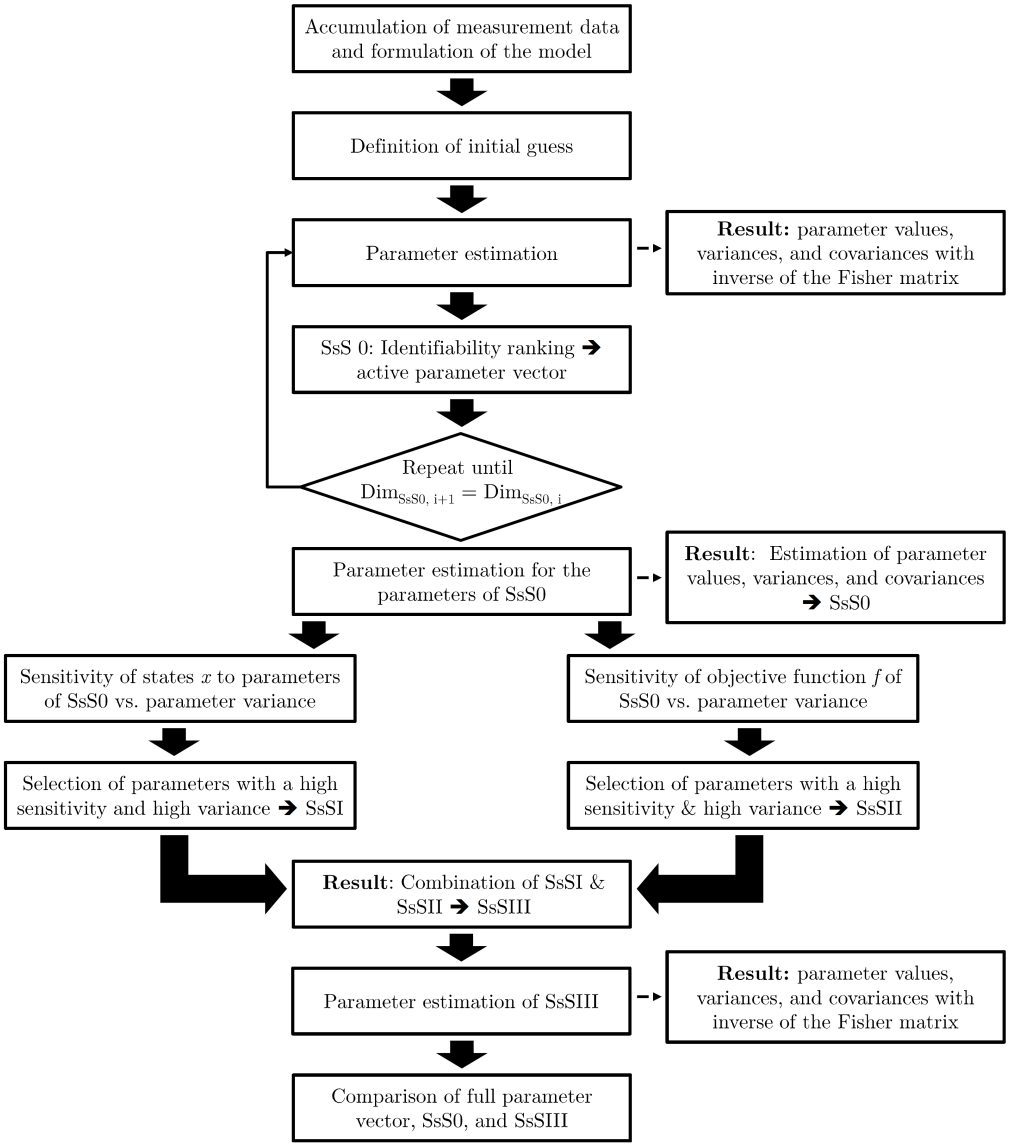

Figure 2.9.: General scheme of the algorithm for the selection of relevant uncertain parameters for optimization under uncertainty, adapted from (Müller et al., 2014a).

satisfactory (Müller et al., 2014a). The third step of the algorithm is the performance of a first parameter estimation. The parameter estimation yields the sensitivity matrix S for the output variables y with respect to the current parameter values p for all measurement points. Now, the variances for each of these estimated parameters are of interest, because these are required for a comparison with the reduced parameter set. To obtain these variances, the previously mentioned Fisher Information Matrix (*FIM*) needs to be calculated. An approximation of the (FIM) is displayed in Eq. 2.28:

$$FIM = S' \cdot W_y^{-1} \cdot S \tag{2.28}$$

FIM is the approximated Fisher Information Matrix. W_y is the measurement device variance matrix. W_y is a diagonal matrix in which for each measurement point that is to be considered the measurement variance of the measurement device σ_D^2 is noted. The variance hereby corresponds to the measurement data. As mentioned before, the inverse of the *FIM* contains the variance of each parameter in its primary diagonal (Bard, 1974). All other cells contain the covariances, which are required if the parameters are correlated.

$$S = \begin{pmatrix} \frac{\partial y_1}{\partial \xi_1} & \cdots & \frac{\partial y_1}{\partial \xi_n} \\ \vdots & \ddots & \vdots \\ \frac{\partial y_m}{\partial \xi_1} & \cdots & \frac{\partial y_m}{\partial \xi_n} \end{pmatrix} \tag{2.29}$$

$$W_y = \begin{pmatrix} \sigma_{D,y_1}^2 & 0 & \dots & 0 \\ 0 & \sigma_{D,y_2}^2 & \ddots & \vdots \\ \vdots & \ddots & \ddots & 0 \\ 0 & \dots & 0 & \sigma_{D,y_m}^2 \end{pmatrix} \tag{2.30}$$

In step 4, the first subset selection regarding linear independence, identifiability, and output sensitivity of the parameters is carried out (Müller et al., 2014a). For this purpose, a singular value decomposition (SVD) is performed on the sensitivity matrix S (López et al., 2012). The condition number κ can be calculated through a division of the largest by the smallest singular value. Generally, a high condition number indicates an almost singular sensitivity matrix, which is undesirable. As mentioned by Burth et al. (1999) and Grah (2004) a threshold κ should be set around 1000. Next, the collinearity index, which is the inverse of the smallest singular value, should be considered. Brun et al. (2002) have set the maximum of the collinearity index threshold range to 10 to 15. Herein, 10 is used (Müller et al., 2014a). López et al. (2012) mention that it can be determined, whether a parameter elimination from the active set of uncertain parameters needs to be carried out for the parameter estimation. Therefore, the parameters with the lowest sensitivity as described by Eq. 2.31 are removed from the active set, until the sensitivity matrix fulfills both thresholds of κ and collinearity index.

$$\overline{s}_{p_i} = \sqrt{\frac{1}{m} \cdot \sum_{j=1}^{m} \frac{\partial y_j}{\partial p_i}} \tag{2.31}$$

Eventually, a reduced subset of identifiable parameters is obtained. As in (Müller et al., 2014a), this subset will be referred to as SsS0. The parameters not included in this subset (those removed from the active set) are fixed to the expected value of the initial parameter estimation. These are viewed as constant parameters p. The others are seen as uncertain parameters ξ. As shown in 2.9, the sequence of successive parameter estimation and subset selection is repeated as described by López C. et al. (2013) until the subset selection stabilizes

to a fixed subset of identifiable parameters.

This leads to the fifth step of the algorithm, which is the computation of the variance for the identifiable subset, the new expected parameter values are stored as $\vec{\mu}_{SsS0}$ and their respective standard deviation $\vec{\sigma}^2_{SsS0}$. Moving on, as discussed in (Müller et al., 2014a), the aim of the algorithm is to select a reasonably small set of uncertain parameters for optimization under uncertainty. A further reduction of the number of parameters is required. Therefore the idea is to take a close look at the user-defined objective function for the process and at all the state variables x of the model (measureable as well as immeasurable). In the initial subset selection the sensitivity of the outputs with respect to all uncertain parameters ξ_i is analyzed. Next, a look at the sensitivity of all state variables with respect to the identifiable parameters is of interest. Additionally it must be mentioned, that an analysis of the outputs and their parameter sensitivities does not yield any information regarding the behavior of an arbitrary objective function. Eq. 2.32 defines such an objective function f, which is to be minimized (or maximized) by changing the control variables u accordingly. Hereby, $\vec{\xi}$ denotes the vector of fixed and uncertain parameters. The collection of state variables is x. These need to be calculated from the model equations g given in Eq. 2.33.

$$\min_u f(\dot{x}, \vec{x}, \vec{u}, \vec{\xi}) \tag{2.32}$$

$$\text{s.t. } g(\dot{x}, \vec{x}, \vec{u}, \vec{\xi}) = 0, y \subseteq x \tag{2.33}$$

To obtain the required sensitivities $\frac{\partial x}{\partial \xi} =: s$ Eq. 2.33 is differentiated with respect to all parameters ξ.

$$\frac{\partial g}{\partial \dot{x}} \cdot \underbrace{\frac{\partial \dot{x}}{\partial \xi}}_{\dot{s}} + \frac{\partial g}{\partial x} \cdot \underbrace{\frac{\partial x}{\partial \xi}}_{s} + \frac{\partial g}{\partial u} \cdot \underbrace{\frac{\partial u}{\partial \xi}}_{=0} + \frac{\partial g}{\partial \xi} = 0 \tag{2.34}$$

Thus, $\dot{s}$ (time derivative of the sensitivities) can be written as shown in Eq. 2.35.

$$\dot{s} = \left(\frac{\partial g}{\partial \dot{x}}\right)^{-1} \cdot \left(-\frac{\partial g}{\partial x} \cdot s - \frac{\partial g}{\partial \xi}\right) \tag{2.35}$$

It is assumed that all sensitivities s are zero at the starting time t_0, because this is viewed as the time before the influencing factors have an effect, e.g. before the experiment or the reaction has started. If this is the case, Eq. 2.35 can be integrated in parallel to the model equations to calculate the sensitivity for any point in time. That way the required sensitivities $s = \frac{\partial x}{\partial \xi}$ can be obtained. The total derivative of f with respect to ξ is given in Eq. 2.36. Hereby, "the first summand is the derivative of the objective function to the parameters itself and is straight forward. The second summand contains the implicit dependency of the objective function to the state variables. The third summand can be set to zero given the assumption that the parameters do not change over time" (Müller et al., 2014a).

$$\frac{df}{dp} = \frac{\partial f}{\partial \xi} + \frac{\partial f}{\partial \dot{x}} \cdot \underbrace{\frac{\partial \dot{x}}{\partial \xi}}_{\dot{s}} + \frac{\partial f}{\partial x} \cdot \underbrace{\frac{\partial x}{\partial \xi}}_{s} + \frac{\partial f}{\partial u} \cdot \underbrace{\frac{\partial u}{\partial \xi}}_{=0} \tag{2.36}$$

The control variables u are independent of the parameters ξ. All other terms appearing in Eq. 2.36 can either be calculated directly or already appear in the sensitivity integration. Given the potentially high nonlinearity and non-convexity of the problem in hand, the behavior of the model equations g and the objective function f can vary a lot with the investigated operation point. This must be kept in mind during this algorithm: $\frac{df}{d\xi}|_{u_1,t_1}$ and

$\frac{\partial x}{\partial \xi}|_{u_1,t_1}$ are calculated at the operation point of interest. Next, the elements of the former will be normalized (Eq. 2.37):

$$\overline{\mathcal{F}}_i = \frac{\left|\frac{df}{d\xi_i}\right|}{\max\limits_{j\in \mathrm{SsS0}} \left|\frac{df}{d\xi_j}\right|} \qquad \forall i \in \mathrm{SsS0} \tag{2.37}$$

Just as expressed in (Müller et al., 2014a), the elements of $\overline{\mathcal{F}}$ lie between zero and one. A sensitivity threshold of 0.1 will be used. Any parameter ξ_i for which $\overline{\mathcal{F}}_i$ is greater than 0.1 is to be considered in the subset SsSI. All others will be fixed. Each of the elements of the model equation parameter Jacobian $\frac{dx}{d\xi}|_{u_1,t_1}$ are treated as shown in Eq. 2.38:

$$\bar{\jmath}_i = \frac{\sum\limits_{j=1}^{m} \left(\frac{\partial x_j}{\partial \xi_i}\right)^2}{\max\limits_{k\in \mathrm{SsS0}} \sum\limits_{j=1}^{m} \left(\frac{\partial x_j}{\partial \xi_k}\right)^2} \qquad \forall i \in \mathrm{SsS0} \tag{2.38}$$

The elements of $\bar{\jmath}$ lie in the interval from zero to one. Just as in (Müller et al., 2014a), the same threshold value of 0.1 is used as for $\overline{\mathcal{F}}$. The parameter ξ_i of the first subset, for which $\bar{\jmath}_i$ is greater than 0.1 is selected for the subset SsSII. This selected threshold is a heuristically chosen value. It follows along the idea that choosing parameters whose influence is greater than 10 % of the influence of the most influential parameter are of importance. Future studies on this part are still required. After determining subsets SsSI and SsSII, they are joined to form subset SsSIII, which is the final result of the algorithm. In a final step another parameter estimation is performed, for which all parameters are fixed at their current expected values μ_{SsS0} and only the uncertain parameters ξ contained in SsSIII can be manipulated. An analysis of the resulting Jacobian matrix yields the standard deviation σ_{SsSIII} for the remaining parameters in SsSIII for the expected values μ_{SsSIII}.

This final subset of remaining uncertain parameters ξ_i with their according standard deviations σ_i and expected values μ_i is seen as the relevant uncertain subset for optimization under uncertainty. All other parameters are fixed to their expected values and thus viewed as constants p. In the next section, a detailed description is given on how these uncertain parameters can be implemented into a stochastic optimization problem with special focus on the chance-constrained approach.

2.4. Stochastic Optimization

The field of optimization in which optimal decision making under uncertainty is performed is known as *Stochastic Programming*. "*Stochastic Programming* handles mathematical programming problems where some of the parameters are random variables" (Prékopa, 1995).

"In most prevailing deterministic optimization approaches, the expected (nominal) values of [...] uncertainties are usually employed. In reality, however, the uncertain variables will deviate from their expected values and thus some specifications or output constraints may be violated when applying the a priori optimization results. Therefore, optimization under the uncertainties should be considered" (Wendt et al., 2002).

Today, different approaches exist to incorporate uncertainty into deterministic optimization approaches. These available techniques differ either in the way that the sources of uncertainty are implemented or in their solution policy regarding the optimization problem. According to Arellano-Garcia (2006) problems concerned with optimization under uncer-

tainty can be divided into two categories: “wait and see” and “here and now”.

2.4.1. Wait And See: Scenario-Based Optimization

The “wait and see” approach uses expected values of uncertain parameters or variables in the problem formulation. To account for this uncertainty, a number of scenarios is generated in which each parameter or variable adopts a specific value within its uncertainty range. Then, a deterministic optimization problem is solved based on these inputs of each scenario. The general form of this optimization problem can be written as shown in Eq. (2.39).

$$\begin{aligned} &\max \mu(f(u,\xi)) \\ &\text{s.t. } g(u,\xi) = 0 \\ &\quad h(u,\xi) \geq 0 \end{aligned} \tag{2.39}$$

The procedure of solving the deterministic optimization problem is repeated for each uncertain variable sample. As a final result a probabilistic representation of the uncertain output is obtained. A clustering of the output results into groups or bins can be carried out to select the most likely result. This scenario-based strategy has several drawbacks though. Firstly, the approach is mostly concerned with uncertain time-invariant parameters. Often enough, since the operation trajectory of a process is seldom known, this approach is not adequate for handling disturbances prone to time-varying behavior. Secondly, all determined actions regarding the operation of a process are determined *posterori* (Arellano-Garcia, 2006). Thirdly, in order to depict the full possible outcome, a large and representative number of scenarios depending on the number of uncertain parameters or variables must be carried out. The selection of scenarios can be done in many different ways.One example would be using a full factorial design approach in which the extreme values of uncertain parameters are used. Another example would be selecting the scenarios randomly. In any case, if the number of scenarios is too small, a misrepresentation of the possible output could result. Finally, the approach can not guarantee the satisfaction of inequality constraints (Arellano-Garcia, 2006).

In contrast to the “wait and see” approach, the “here and now” approach defines the objective function as well as the constraints in a probabilistic manner. The next section takes a closer look at this approach.

2.4.2. Here And Now: Chance-constrained Optimization

The approach of interest is known as chance-constrained optimization and has been intensively studied by various authors world wide. Tab. 2.1 presents a chronology of some of the major publications of chance-constrained methods in the last 15 years. In the following, the concept is briefly revisited. A more detailed discussion on this approach can be found in the listed contributions in Tab. 2.1.

The motivation behind the approach is based on the following thoughts: Firstly, the application of the deterministic solution may violate constraints if uncertainty is neglected and secondly, the often applied worst-case analysis yields results in which the achievable profit is drastically minimized. As stated by Arellano-Garcia (2006) the “approach [...] is capable of evaluating the balance between the reliability and the profitability of future operations”. Fig. 2.10 illustrates this motivation.

The objective function of the chance-constrained optimization problem is formulated as shown in Eq. (2.40). Hereby μ is the expected value of the time-variant performance criterion

Table 2.1.: Chronology of major publications of chance-constrained methods with application in chemical engineering.

Author	Publication and PSE application	Year
Li et al. (2000)	Robust model predictive control under chance constraints	2000
Henrion et al. (2001)	Stochastic optimization for operating chemical processes under uncertainty	2001
Li et al. (2002)	Optimal operation of distillation processes under uncertain inflows accumulated in a feed tank	2002
Wendt et al. (2002)	Nonlinear CC process optimization under uncertainty	2002
Diwekar (2003)	Optimization under uncertainty in chemical engineering	2003
Arellano-Garcia et al. (2003a)	CC batch distillation process optimization under uncertainty	2003
Arellano-Garcia et al. (2003b)	Nichtlineare stoch. Optimierung unter Unsicherheiten	2003
Henrion and Möller (2003)	Optimization of a continuous distillation process under random inflow rate	2003
Li et al. (2004)	Optimal production planning for chemical processes under uncertain market conditions	2004
Schwarm and Nikolaou (2004)	CC model predictive control	2004
Arellano-Garcia et al. (2004)	A new optimization framework for dynamic systems under uncertainty	2004
Wendt (2005)	Untersuchungen zur stochastischen Online Optimierung kont. Destillationsprozesse unter Unsicherheiten	2005
Arellano-Garcia (2006)	CC optimization of process systems under uncertainty	2006
Flemming et al. (2007)	Set-Point optimization for closed-loop control systems under uncertainty	2007
Li (2007)	Prozessoptimierung unter Unsicherheiten	2007
Arellano-Garcia et al. (2007b)	Close-Loop stochastic dynamic optimization under probabilistic output-constraints	2007
Li et al. (2008)	CC programming approach to process optimization under uncertainty	2008
Arellano-Garcia and Wozny (2009)	CC optimization of process systems under uncertainty: I. Strict monotonicity	2009
Verderame and Floudas (2009)	Operational planning of large-scale industrial batch plants under demand due date and amount uncertainty: I. Robust optimization framework	2009
Verderame and Floudas (2010)	Operational planning of large-scale industrial batch plants under demand due date and amount uncertainty: II. Conditional value-at-risk framework	2000
Geletu et al. (2011)	Monotony analysis and sparse-grid integration for nonlinear CC process optimization	2011
Klöppel et al. (2011)	Using sparse-grid methods to improve computation efficiency in solving dynamic nonlinear CC optimization problems	2011
Zhang and Li (2011)	CC programming for power flow under uncertainty	2011
Werk et al. (2012)	Performance analysis of shooting algorithms in CC optimization	2012
Geletu et al. (2013)	Advances and applications of CC approaches to systems optimization under uncertainty	2013
Zhang and Li (2013)	Application of sparse-grid technique to CC optimal power flow	2013
Geletu and Li (2014)	Recent developments in computational approaches to optimization under uncertainty and application in process systems engineering	2014
Geletu et al. (2014)	A tractable approximation of non-convex CC optimization with non-Gaussian uncertainties	2014

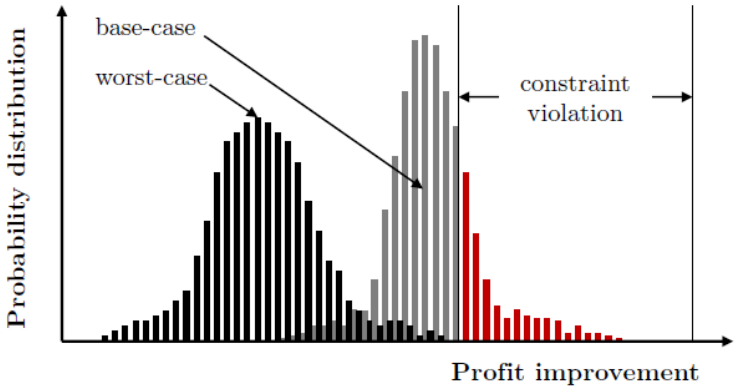

Figure 2.10.: Worst-case vs. base-case: motivation for chance-constrained optimization. The trade-off between reliability and profitability is shown. The figure is adapted from (Arellano-Garcia, 2006).

f. The minimization is to be achieved by manipulating the controls u. The states are represented by the vector x and the uncertain parameters by the vector ξ. The model contains uncertainty and thus the process output is uncertain. To avoid a constraint violation due to this uncertainty, an incorporation of uncertainty into the output constraints is required and needs to be included in the formulation of the optimization problem. Therefore, in order to cope with the uncertain factors, the vector of inequality constraints h of the optimization problem is written as shown in Eq. (2.41).

$$\min_{u} \; E\left[f(x,u,\xi)\right] \quad \text{with} \quad \xi \sim \mathcal{N}(\mu, Cov) \tag{2.40}$$

$$\text{s.t.} \; Pr\left\{h(\dot{x},x,u,\xi) \geq 0\right\} \geq \alpha \tag{2.41}$$

The probability of adhering to a certain constraint with a certain value α is of relevance. α can take on a value between 0 and 1. Thus, a relaxation of the inequality constraint is performed and the potential profit increases while keeping the constraint violation to a minimal level of 1 - α (Fig. 2.11.

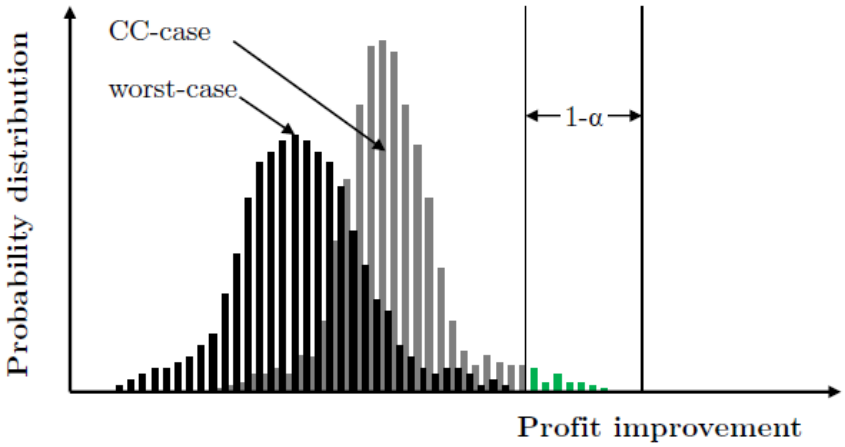

Figure 2.11.: Worst-case vs. chance-constrained-case: motivation for chance-constrained optimization. The trade-off between reliability and profitability is shown.

As stated by Arellano-Garcia (2006), it is typical that "in engineering practice, inequality

constraints are commonly used to specify or restrict some of the output variables"

$$y^{min} \leq y(u, \xi) \leq y^{max} \tag{2.42}$$

wherein y^{min} and y^{max} are the lower and upper bounds of these output variables. Eq. 2.41 can be rewritten as

$$Pr\left\{y_i^{min} \leq y(u, \xi) \leq y_i^{max}\right\} \geq \alpha_i \qquad i = 1, ..., L \tag{2.43}$$

if multiple outputs and single probabilities for each of these outputs are to be adhered to. If several outputs are subject to the same probability value α, then Eq. 2.43 can be modified to:

$$Pr\left\{y_i^{min} \leq y(u, \xi) \leq y_i^{max}, \quad i = 1, ..., L\right\} \geq \alpha \tag{2.44}$$

in which only one α is present. Eq. 2.44 is known as a joint constraint as opposed to the single constraint in Eq. 2.43. The different possible formulations for chance-constrained problems are given in (Arellano-Garcia, 2006) and can be seen in Fig. 2.12.

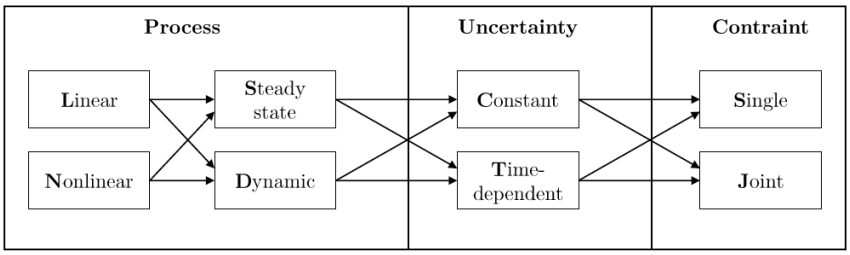

Figure 2.12.: Classification of chance-constrained problems. The figure is adapted from (Arellano-Garcia, 2006).

The initial letters in Fig. 2.12 denote the type of a chance-constrained problem. Accordingly, combinations such as linear steady-state process with constant uncertainties under single chance constraints (LSCS) or nonlinear dynamic process with constant uncertainties under joint chance constraints (NDCJ) can be considered.

Now, several different aspects must be looked at from a computational point of view to solve the probabilistic problem defined in Eq. 2.40. Because most mathematical problems in chemical engineering are subject to nonlinear characteristics the focus in this thesis will lie on nonlinear dynamic single chance-constrained optimization. In the following, a theoretical solution strategy as well as a general computation strategy to solve nonlinear chance constraints is presented.

Theoretical solution of the chance-constrained optimization problem: The theoretical solution of the chance-constrained optimization problem is derived by asking the following questions: How can the chance-constrained optimization problem be transformed to yield a deterministic solution and how can the probability as well as the according gradients of adhering to the constraints be computed? Geletu et al. (2011) catagorize the approaches to compute chance constraints into three groups: *analytic approximation*, *approximate discretization*, and *back-projection*. The latter is of interest for this thesis. Nevertheless, the first two methods will be reviewed shortly.

Regarding *analytic approximation*, this technique aims towards replacing the chance constraints with bounding confidence regions. This approach has "the danger of either over or under estimation of chance constraints, leading to conservative or unreliable approximation

of chance constraints" (Geletu et al., 2011). This behavior is undesirable and therefore this method is not focused on herein.

In the second approach, *approximate discretization*, random samples for the uncertain input variables by Monte Carlo methods are generated. Afterwards averaged sums of the function values to approximate the chance constraints are then calculated. Geletu et al. (2011) discuss that because such a large number of scenarios or samples are required to obtain a full depiction of the possible realizations of the uncertain variables, this approach is computationally intractable. An improvement can be made by replacing the Monte Carlo Sampling (MCS) methods with Latin hypercube or Hammersley sequence sampling (HSS) (Diwekar and Kalagnanam, 1997). Nevertheless, "the discrete approximations of the chance constraints may not be differentiable" (Geletu et al., 2011).

The final approach is known as *back-mapping* or *back-projection* was originally proposed by Wendt et al. (2002) and is used in a modified form in this thesis. In this approach, a transformation from the space of output variables to the space of input variables is carried out. This transformation is originally based on the assumption that a strict monotonic relationship between uncertain input and output exists. The idea here is to avoid a direct computation of the output probability distribution. Instead, a representation of the probability by mapping it back to a region of the uncertain inputs is achieved. Thus, the output probability can be computed by integration of the density function of the uncertain inputs.

To clarify this idea, the following deliberations are made: If $\xi \in \Xi$ is a random variable then any output variable $y \in Y$ that is defined as a function of ξ will also be a random variable. Hereby, $\rho(\xi)$ denotes the probability density function of ξ and $F(\xi)$ the distribution function of ξ. Fig. 2.13 shows the mapping between an uncertain input variable and an output variable to elucidate this concept. The *back-mapping* approach can be used if the requirement of a strict monotonic relationship is fulfilled. Arellano-Garcia (2006) states that "a linear relationship [between input and output] can rarely be found in process system engineering. On the other hand, the relation is nonlinear, but, it shows very often a monotonic relationship between uncertain input and constrained output". The exploitation of this characteristic as well as the application of *back-mapping* is discussed by several authors such as (Wendt et al., 2002), (Arellano-Garcia and Wozny, 2009), and (Geletu et al., 2011).

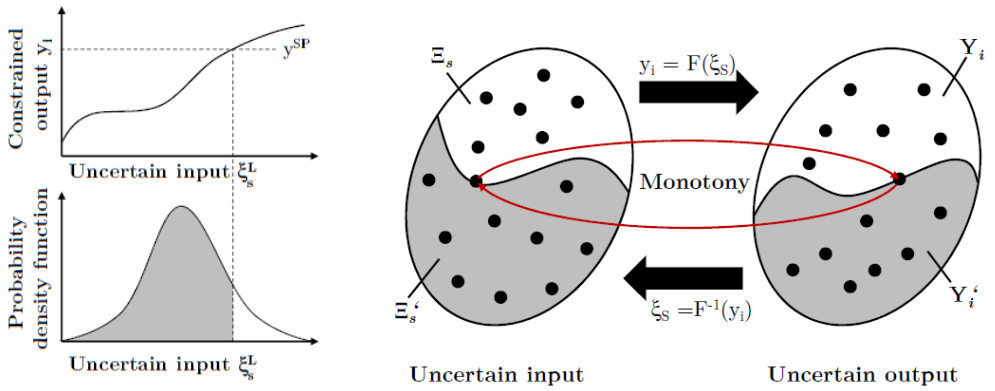

(a) Monotonic relationship.

(b) Input and output space.

Figure 2.13.: Mapping between an uncertain input variable and an output variable. The figure is adapted from (Arellano-Garcia and Wozny, 2009).

In Fig. 2.13, the constrained output variable $y_i \in Y_i$ has a strict monotonic relationship

to at least one of the uncertain input variables $\xi_i \in \Xi_s$ (Ξ_s represents a subspace of Ξ). Furthermore, a region is formed by nonlinear projection of the uncertain input region for some given controls u. The points in the set on the right of Fig. 2.13 represent possible realizations of the variables based on their distribution functions. Through the projection $y_i = F(\xi_s)$ the subspace Ξ_s leads to exactly one point in Y_i (strict monotonicity). Therefore, one point in $y_i \in Y_i$ can only lead to one ξ_s through the reverse projection $\xi_s = F^{-1}(y_i)$. As mentioned by (Arellano-Garcia and Wozny, 2009), "the boundary of the constrained value y^{SP} in the output region corresponds to a limit value ξ_s^L for ξ_s in the input region". Next in Fig. 2.13, a confined feasible region is considered (grey area), which corresponds to the bounds of the output constraints y^{SP}. This then also corresponds to a bound for the uncertain input ξ_s^L, thus creating a feasible region in the uncertain input space.

This concept can now be exploited, whereby two monotonicity cases must be considered: Case 1 - $y_i \uparrow \Rightarrow \xi_i \uparrow$(positive monotonicity) and Case 2 - $y_i \uparrow \Rightarrow \xi_i \downarrow$ (negative monotonicity). For each case, the chance constraint can be mapped differently.

$$\text{Case 1:} \quad Pr\{\xi_s \leq \xi_s^L\} \geq \alpha \tag{2.45}$$

$$\text{Case 2:} \quad Pr\{\xi_s \geq \xi_s^L\} \geq \alpha \tag{2.46}$$

In Case 2, negative monotonicity, an upper bound of the constrained output induces a lower bound on ξ (Arellano-Garcia and Wozny, 2009). In Case 1, positive monotonicity, no change between upper and lower bound occurs. It must be mentioned that the control variables u also influence the projected region. The bound ξ_s^L is therefore a reverse projection dependent on the constraint y^{SP}, the control variables u, and the other uncertain variables of ξ_i:

$$\xi_s^L = F^{-1}(y^{SP}, u, \xi_{s-1}, \ldots, \xi_1) \tag{2.47}$$

The bound of ξ can be computed by solving the model equations with known control variables u. The probability of complying with the output constraint can be transformed to a multivariate integration in the region of the uncertain inputs:

$$\begin{aligned} Pr\{y \leq y^{SP}\} &= Pr\{\xi_s \leq \xi_s^L\} \\ &= \int_{-\infty}^{\infty} \ldots \int_{-\infty}^{\infty} \ldots \int_{-\infty}^{\xi_s^L} \rho(\xi_1, \ldots, \xi_{s-1}, \xi_s) d\xi_s d\xi_{s-1}, \ldots, d\xi_1 \end{aligned} \tag{2.48}$$

Simplified examples and illustrations can be found in (Arellano-Garcia, 2006; Arellano-Garcia and Wozny, 2009), in which this *back-mapping* approach is applied. Nevertheless, even with this concept available, the actual computation of the chance constraints still poses a challenge.

Computation strategy for chance constraints: Based on the theoretical deliberations presented previously the computational strategy to solve nonlinear dynamic chance-constrained optimization problems can be formulated. In this thesis, a sequential approach is applied, which has already been presented in (Arellano-Garcia, 2006) and successfully applied in contributions such as (Arellano-Garcia and Wozny, 2009) or (Geletu et al., 2011). The approach can be divided into three layers: an optimization layer in which the objective function is solved, a multivariate integration layer, and a simulation layer with a DAE solver. A very general scheme of this approach is shown in Fig. 2.14.

The idea is that the NLP solver sends the values for the control variables u to the multivariate integrator. In general, an efficient integration approach is required in order to

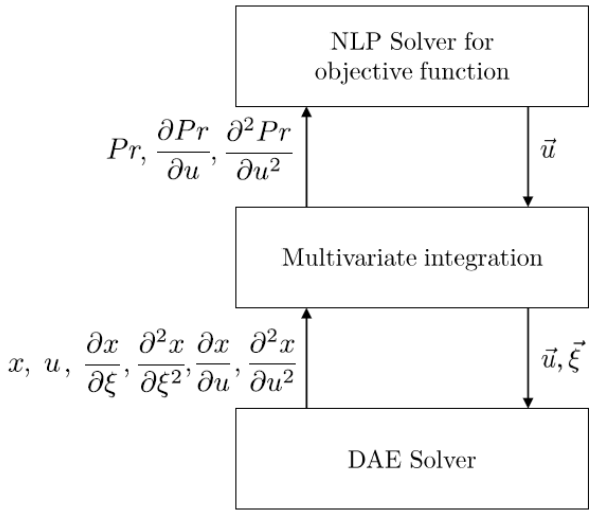

Figure 2.14.: Chance-constrained optimization framework.

compute the values and the gradients of the chance constraints and the objective function. In this thesis, the sparse-grid integration technique is used to carry out the computation of probability integrals. "The sparse-grid integration technique [...] uses a skillful combination of one-dimensional quadrature rules to generate a sparse-grid cubature rule for higher dimensions" (Geletu et al., 2011). This method has proven to be highly adequate in terms of accuracy and computation load (Geletu et al., 2014). The computation load is kept relatively low, compared to standard full-grid integration or Monte Carlo techniques. The success of this approach as well as a comparison to other approaches is shown in a detailed manner in (Geletu et al., 2011) and (Geletu et al., 2013). In the multivariate integration layer a sparse grid of the uncertain parameter space is created with the dimension $n-1$, n being the number of uncertain parameters ξ.

The grid is then sent to the DAE solver, in which a simulation for each of the u and ξ_i values of the grid is carried out. For each simulation, the computation of the boundaries of ξ by *back-mapping* is performed. In order to compute dynamic optimization problems under chance constraints, an iterative procedure is required to determine the boundary ξ_s^L. Through multiple simulations and applying either the bisectional method, a Newton approach, or others, the variable bound for ξ can be calculated. Fig. 2.15 shows such an iterative scheme as well as the graphical determination of the uncertain variable bound used by (Arellano-Garcia and Wozny, 2009). In this case the bisectional method is applied.

Within the restricted search space of $[\xi_a, \xi_b]$ the variable bound ξ_s^L is searched for. In this thesis, the starting bounds are $\pm 3\sigma$ interval of the expected value of ξ. Arellano-Garcia and Wozny (2009) state for their bisectional method, "this region corresponds to the integration area where the multivariate integration is also carried out. Firstly, the function values y_i of the corresponding interval endpoints (ξ_a, ξ_b) are defined and verified to ensure that the reverse projection value is located inside of the interval". This is then followed by a division of the area by two. The algorithm shown in the right of Fig. 2.15 thus selects the midpoints of the interval and computes the corresponding value for the output y_i. Depending on whether the y_i-value is lower or higher than the bound y_i^{SP}, the bounds of the restricted search space are adjusted accordingly. The rest of the search space is discarded and the computation of the midpoint is carried out. This basic procedure is repeated until the required bound value ξ_s^L has reached a specified tolerance.

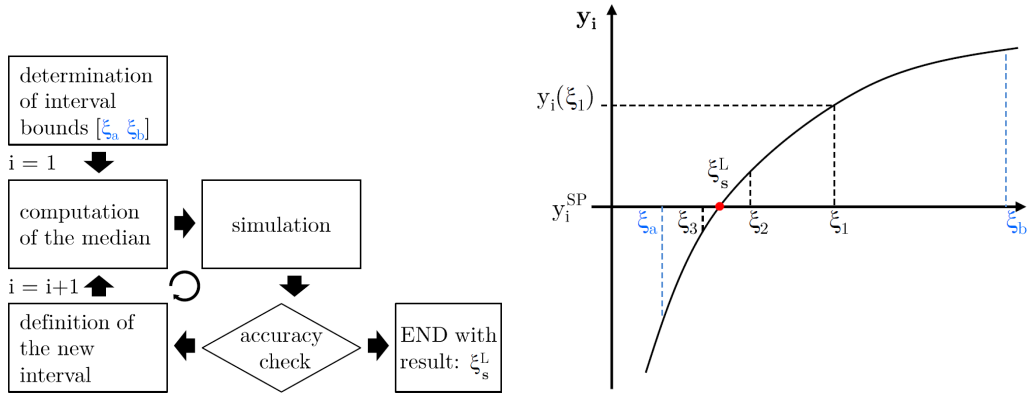

(a) Variable bound determination.

(b) Bisection method to compute ξ_s^L.

Figure 2.15.: Bisectional method for variable bound determination. The figure is adapted from (Arellano-Garcia and Wozny, 2009).

A similar concept of an iterative search for the uncertain variable bound can be applied for Newton's method or using second order derivatives for Halley's method. This has been successfully applied in our own contribution for a small example system in (Müller et al., 2015b). Using the derivative information the solution to the root-finding problem can be found faster. Additionally, the required monotonicity stated in (Arellano-Garcia, 2006) and (Wendt et al., 2002) is revoked in this thesis. Details on the implementation, especially regarding an efficient Newton approach and how multiple critical ξ_s and integration bounds can be identified, can be found in (Esche, 2015). A further, detailed discussion on this part is therefore waived at this point and only a general overview is given. Using the $n-1$ dimensional ξ sparse grid, the critical value at each point is searched for. For each sparse grid point, the values of the $n-1$ ξs is sent to the DAE solver. Three values of the n^{th} ξ are used (the upper bound, the lower bound, and the expected value) and it is determined whether or not the constraint of interest is violated ($h(\dot{x}, x, u, \xi) \geq 0$). If this is not the case, then the probability of adhering to the constraint lies at 100 %. If a change in sign takes place (one of the constraint values is negative), then it means that at least one critical ξ exists. This critical ξ is then found via a Newton approach. A convexity check helps determine, if multiple critical ξs are there. This is done by bisecting the critical region and redoing the check. As in (Müller et al., 2015b), the hybrid Newton's method is applied.

The next step in Fig. 2.14 is that the DAE solver sends the according derivative information to the multivariate integration layer. Here, a multivariate integration is carried out in which the probability that the constraints are adhered to is calculated. This is done in such a way, that for each of the points in the sparse grid, the probability of the constraint being held is determined. The information regarding the probability and the according derivatives is sent back to the optimizer.

This sequential approach is repeated, until the NLP solver finds a local minimum. Thus, the chance-constrained optimization problem can be solved. A trajectory for the dynamic problem is obtained and can be implemented into the process. It must be mentioned at this point that this sequential approach may yield unreliable results due to numerical noise caused by the DAE solver. Of special interest are noisy derivatives, as they may lead to convergence issues. This needs to be treated in future work should the issue arise frequently. A more specific description of the applied framework for the chance constraint computation

and applied software is carried out later in this thesis in Chapter 3.

Returning to the theoretical workflow for the development of trajectories, the next sections focus on the theoretical background regarding the industrial application: microemulsions and phase separation. The information on this part is required, so that the model of the process can be developed on which the chance-constrained approach should be applied on.

2.5. Thermo- and Fluid Dynamic Properties of Oil-Water-Surfactant Systems

In this section special attention is given to several thermodynamic and fluid dynamic topics, because they are relevant for the process concept presented in the introduction of this thesis. First of all, fundamentals on the general phase behavior of microemulsion systems created with non-ionic surfactants are presented. This information is the backbone of the process concept of hydroformylation in microemulsions, because the phase behavior is exploited to achieve the desired mixing and product isolation effects. Therefore, information on the binary systems of water – oil, water – non-ionic surfactant, and oil – non-ionic surfactant is presented leading to the entire separation behavior for the ternary system over multiple temperatures. Secondly, the fluid dynamics relevant for droplet coalescence are presented in greater detail. With this information in mind, existing phase separation modeling strategies are discussed.

2.5.1. Microemulsions with Non-Ionic Surfactants

Early discussions on microemulsions can be found in contributions by Schulman and Hoar (1943) and Winsor (1954). The term 'micro-emulsion' was first introduced by Schulman et al. (1959) in 1959 though. Today, microemulsions are described as "macroscopically isotropic mixtures of at least a hydrophilic, a hydrophobic and an amphiphilic component" (Stubenrauch, 2009). Essentially, microemulsions are created by a surfactant film that is formed at the oil/water interface (Stubenrauch, 2009). They are characterized by two important characteristics: their thermodynamic stability as well as their nano-structure. These characteristics are to be exploited for the process concept.

As discussed by Stubenrauch (2009) "the primary aim of microemulsion research is to find the conditions under which the surfactant solubilizes the maximum amounts of water and oil". These characteristics can be taken advantage of either for mixing or isolation purposes. Thus, the phase separation behavior of microemulsions is of high relevance, as different phase states yield different potentials for industrial processes. In order to understand the phase behavior of the ternary system consisting of an oil, water, and a non-ionic surfactant, the phase diagrams of the corresponding binary base systems must be analyzed (Kahlweit and Strey, 1985). Fig. 2.16 shows a schematic view of the phase behavior of the three possible binary combinations for an oil-water-surfactant system.

The phase behavior is shown as an 'unfolded phase prism' displaying the miscibility gaps of each of the binary systems. In Fig. 2.16, the following features can be viewed as most relevant: Between the **B** – **C** miscibility gap an upper critical solution temperature (α) exists, whereas between the **A** – **B** miscibility gap a lower critical solution temperature (β) exists. In Stubenrauch (2009) it is discussed that at low temperatures, water is a good solvent for the non-ionic surfactant. At high temperatures on the other hand the surfactant becomes increasingly soluble in oil.

With the phase behavior of the binary systems in mind, that of the ternary system can

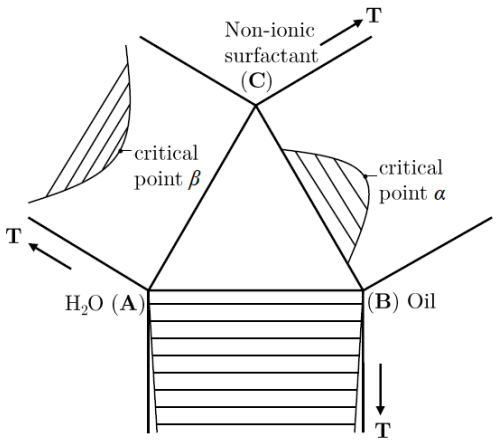

Figure 2.16.: Schematic phase behavior of the three binary systems consisting of water (**A**) and oil (**B**), water (**A**) and a non-ionic surfactant (**C**), as well as oil (**B**) and a non-ionic surfactant (**C**). The figure is adapted from (Kahlweit and Strey, 1985).

be anticipated as a result of the three miscibility gaps of the water (**A**) – oil (**B**), water (**A**) – non-ionic surfactant (**C**), and oil (**B**) – non-ionic surfactant (**C**) mixtures. Fig. 2.17 shows the phase behavior of the ternary system in the form of Gibbs phase triangles at three different temperatures:

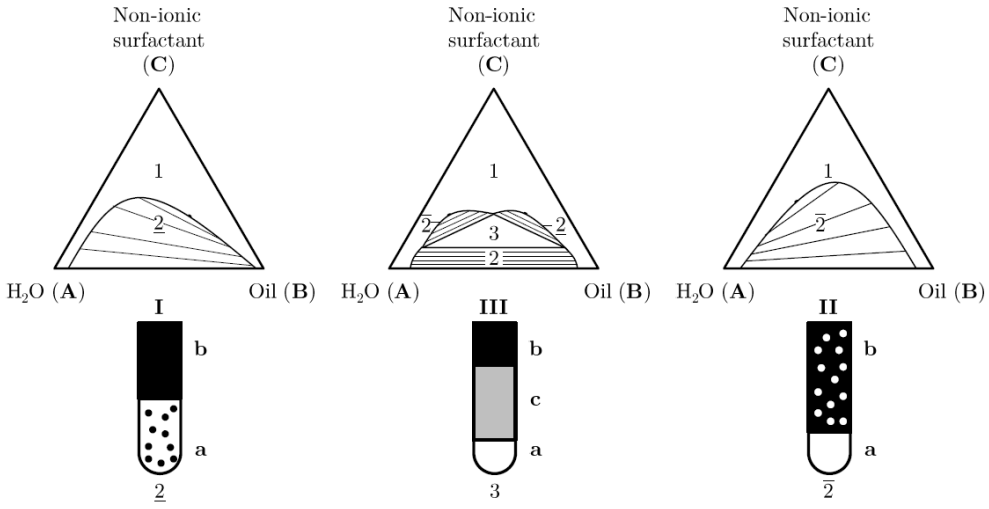

Figure 2.17.: Schematic isothermal Gibbs triangles of an oil (**B**) – water (**A**) – non-ionic surfactant (**C**) system at different temperatures. The figure is based on the original image found in (Stubenrauch, 2009).

- Starting on the left hand side at low temperatures, the solubility of the non-ionic surfactant in water is very high. Here, the phase behavior of the ternary system is dominated by a large miscibility gap. "The negative slope of the tie lines indicates that a non-ionic surfactant-rich water phase (a) coexists with an oil-excess phase (b)" (Stubenrauch, 2009). This behavior is denoted as $\underline{2}$ or Winsor I.
- As the temperature increases, a three-phase triangle with three two phase regions is

established. Hereby, a surfactant-rich microemulsion (c) is established in addition to an excess water (a) and oil phase (b). This behavior is denoted as 3 or Winsor III.

- At high temperatures, another miscibility gap dominates the phase behavior, in which a non-ionic surfactant-rich oil phase (b) coexists with an excess water phase. This behavior is denoted as $\overline{2}$ or Winsor II.

In general, Fig. 2.17 shows how an increase in temperature turns the non-ionic surfactant from hydrophilic to hydrophobic. The test tubes below the Gibbs phase triangles show the established phases in each of the temperature regions. Now, a stacking of the isothermal Gibbs triangles at several temperatures results in a phase prism displaying the temperature-dependent phase behavior of the ternary oil – water – non-ionic surfactant system discussed above (Fig. 2.18(a)).

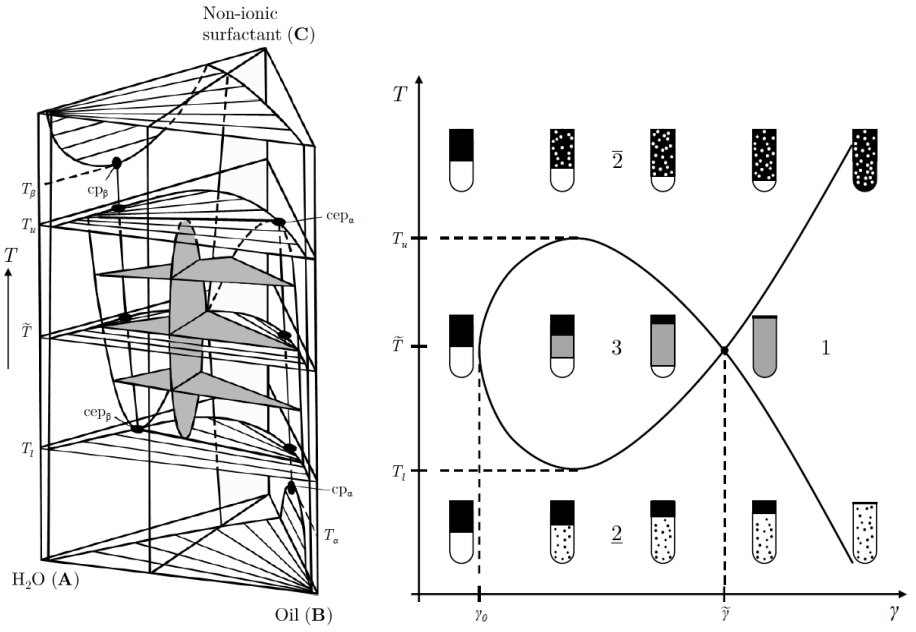

(a) General phase prism. (b) Kahlweit's fish

Figure 2.18.: General phase prism displaying the phase behavior of an oil-water-surfactant (non-ionic) mixture at different temperatures. The figures are based on the original image found in (Stubenrauch, 2009).

Herein, certain characteristic points are relevant for a potential industrial application:

- As discussed previously, at low temperatures, below T_l , the $\underline{2}$ region is established. Here, the surfactant is mainly dissolved in the aqueous phase. This lower phase is an oil-in-water (o/w) microemulsion.

- Increasing the temperature up to the temperature T_l, the surfactant-rich aqueous phase splits into two phases. The "lower water-rich phase (a) moves towards the water corner, while the surfactant-rich middle phase (c) moves towards the oil corner of the phase prism" (Stubenrauch, 2009).

- Between T_l and T_u is $\tilde{T}$, in which the largest middle phase (c) is created.
- A further increase in temperature to T_u results in a disappearance of the three phase region and a combination of the two phases (c) and (b) to a surfactant-rich oil phase. This upper phase is a water-in-oil (w/o) microemulsion.

Of importance for further discussions in this thesis is a 'slice' of the phase prism at an oil:water mass ratio α of 1:1, which is calculated as shown in Eq. 2.49. Hereby m_A and m_B are the masses of water and oil respectively.

$$\alpha = \frac{m_B}{m_A + m_B} \tag{2.49}$$

This slice results in the diagram shown in Fig. 2.18(b), also known as Kahlweit's slice or Kahlweit's Fish (Kahlweit and Strey, 1985), as it resembles a fish. The diagram shows the resulting phase states at different temperatures over various surfactant concentrations. The surfactant concentration in g/g are given by Eq. 2.50, wherein the surfactant mass is denoted by m_C.

$$\gamma = \frac{m_C}{m_A + m_B + m_C} \tag{2.50}$$

In this figure, another region becomes apparent, which is established at high surfactant concentrations. This region is the one-phase region, also known as 1 or Winsor IV. This region can be relevant for industrial purposes, where stable, one-phase emulsions are desired.

The figures discussed in this section show the phase behavior of an oil-water-non-ionic surfactant system at equilibrium. For actual industrial applications this is seldom obtained. In this thesis, the exploitation of the phase separation characteristics within the process concept is desired. The information has to be transferred into the mini-plant, both from an equipment design as well as an operation point of view. Therefore, it is important not only to consider equilibrium phenomena, but also to look at the phase separation dynamics or in other words the coalescence behavior of droplets in multiphase systems.

2.5.2. Droplet Coalescence

"The goal in separating liquid - liquid dispersions is to separate the dispersed droplets from the continuous phase, to obtain two uniform phases" (Schlieper et al., 2004). This statement is expanded in this thesis, regarding the point of obtaining two uniform phases. Since a system with three or more liquid components is used, two or more phases can be obtained. During the last decades many authors have researched the coalescence of droplets in various systems. Among these are Jeffreys and Dawies (1974); Henschke (1994); Schlieper et al. (2004); Mungma et al. (2014). Coalescence in general can be described as the process in which droplets or bubbles merge together to become larger droplets or bubbles (drop-drop coalescence). This can also occur between droplets and a layer or an interface (drop-interface coalescence). Bohnet (1976), Jeffreys and Dawies (1974), and Schlieper (2001) discuss that the coalescence behavior of droplets on a fluid layer or phase-interface can be described in five steps (Fig. 2.19).

1. The droplet approaches the phase-interface. Both droplet and interface are deformed. The film around the droplet and the phase-interface film are maintained. The kinetic energy of the droplet is partially turned into deformation work for the surfaces.
2. An oscillation of the droplet on the phase interface takes place. The viscosity of the liquids subdues this gradually.

3. A fluid film between the droplet and the main part of the fluid phase is established.
4. The fluid film is torn off or drained into the phase-interface and coalescence begins.
5. The droplet is partially or fully integrated into the fluid phase.

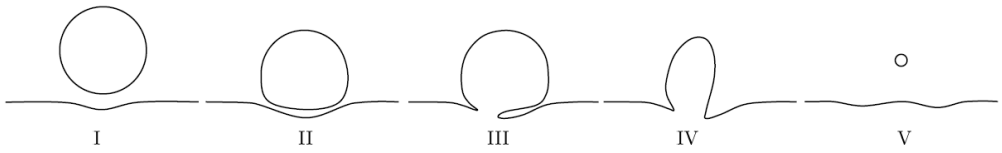

Figure 2.19.: Steps of droplet-interface coalescence. The figure is based on the original image found in (Blaß and Rommel, 1993).

The time required to carry out these steps is known as the coalescence time, during which a large amount of time is spent on step four. It is assumed by Bohnet (1976) that the coalescence speed is dependent on the tearing off of the fluid film and the integration into the fluid phase. These steps for the coalescence of one droplet obviously occur repeatedly in gravity settlers. The speed at which the coalescence occurs is of vital importance for economic reasons. The shorter the separation time in the settler is, the larger the throughput of an industrial process might be or the smaller the required settler can be. Therefore, an integral view of the entire droplet coalescence is required. The main steps of multiphase liquid separation in a settler can be described by the sedimentation and coalescence of dispersed droplets shown in Fig. 2.20. Here, the theoretical dynamic phase separation of a batch settling process is displayed, exemplarily for two liquid phases.

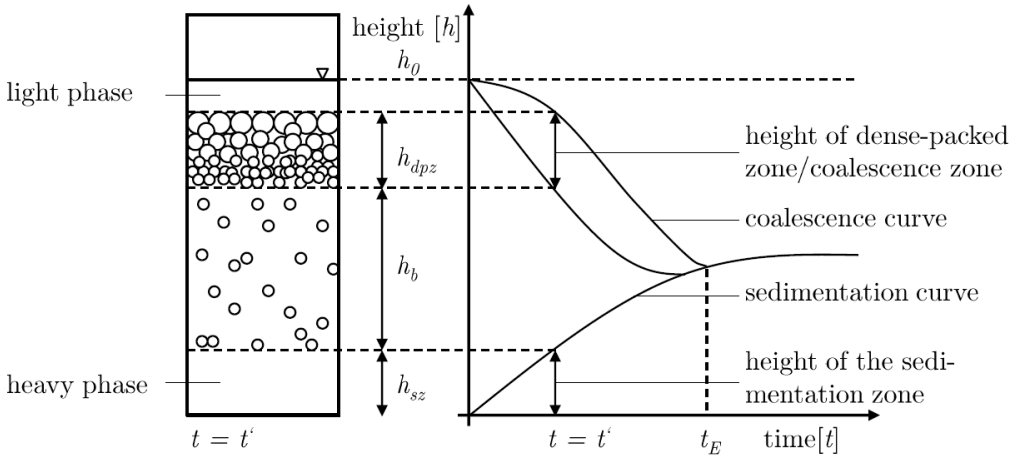

Figure 2.20.: General dynamic phase separation in a batch settling process. The figure is based on the original image found in (Henschke and Hartmann, 1993) and (Schlieper et al., 2004).

After mixing a multiphase system, a disperse and a continuous phase exist. Once the energy input into the system is stopped (e.g. the stirrer of the CSTR is stopped) the coalescence process can continue in an undisturbed manner. When this system is led into a settler, in which the phase separation is to take place, the disperse phase begins a sedimentation process and subsequently the droplets start to coalesce. The already mentioned two possible forms of coalescence may take place: drop-interface coalescence and drop-drop coalescence.

The former occurs when the droplets rise to the top of the settler and reach their own phase. For the case of Fig. 2.20, the light phase (e.g. an oil) rises to the top. If the sedimentation process is faster than the coalescence process, then a droplet packed layer/zone will be established (h_{dpz}) and is gradually reduced over time. The separation process is completed, once the droplet packed layer has disappeared and no more sedimentation takes place. This time is the 'separation end time' depicted in Fig. 2.20 as t_E . At this point in time a distinct interface between the phases can be observed (Henschke et al., 2002).

There are several factors, that can drastically influence the coalescence time. Among these is the presence of surface-active species. Among these are surfactants. These have a hydrophilic and a hydrophobic part and gather on the surface of the droplets. Fig. 2.21 shows what can occur during a sedimentation process of an oil-water-surfactant system. Schlieper (2001) discusses that a surfactant concentration gradient is established across the droplet surface (I in Fig. 2.21). After completion of the sedimentation process this gradient is equalized by transport of the continuous phase to the region between droplet and interface (II in Fig. 2.21). Thus, the coalescence process is hindered (III in Fig. 2.21).

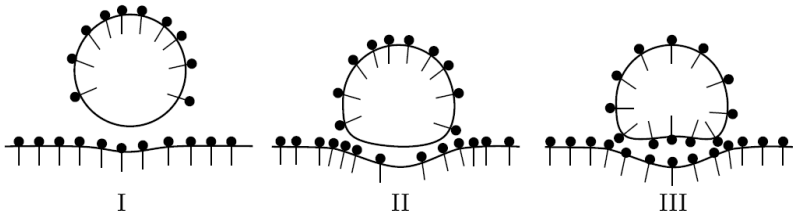

Figure 2.21.: Effect of a surface-active species on the coalescence process. The figure is adapted from (Rautenberg, 1983).

In this thesis, a continuously operated mixer-settler process is of interest. The knowledge concerning the phase behavior, the general coalescence behavior of droplets, and the coalescence in batch settling processes must now be transferred to a continuously operated units. Therefore, the following section discusses the coalescence of dispersions in continuously operated gravity settlers and relevant methods of enhancing the coalescence process.

2.5.3. Coalescence in Gravity Settlers

For continuously operated processes employing extraction technology, different options exist. Fig. 2.22 shows the different possibilities depending on the problem at hand. Herein, a liquid-liquid, single-stage mixer-settler process utilizing gravity separation is of interest (path is marked accordingly in Fig. 2.22).

Gravity separation is a method for separating two components of a mixture, which have a different specific weight. Herein, gravity is the dominant force, which is responsible for separation (Schlieper, 2001). The feeding of the dispersion occurs at the same height as the later established phase boundary. Thus, the distance for a droplet to reach the phase boundary is minimal. Fig. 2.23 shows a schematic of a settler with and without internals.

Generally, the sedimentation process of droplets, described in the previous section in Fig. 2.20, does not occur immediately (Schlieper, 2001). A certain run-in distance must be overcome. In this run-in distance (l_{in}) no coalescence takes place. This was shown in well-known measurements performed by Jeffreys et al. (1970) as well as Vijayan and Ponter (1975). This region in the vicinity of the inlet is prone to turbulence due to the expansion of the dispersion and other entry effects. The droplets are packed closely together and form

a stable configuration (Jeffreys et al., 1970). Afterwards, both forms of coalescence begin and a dispersion wedge is established.

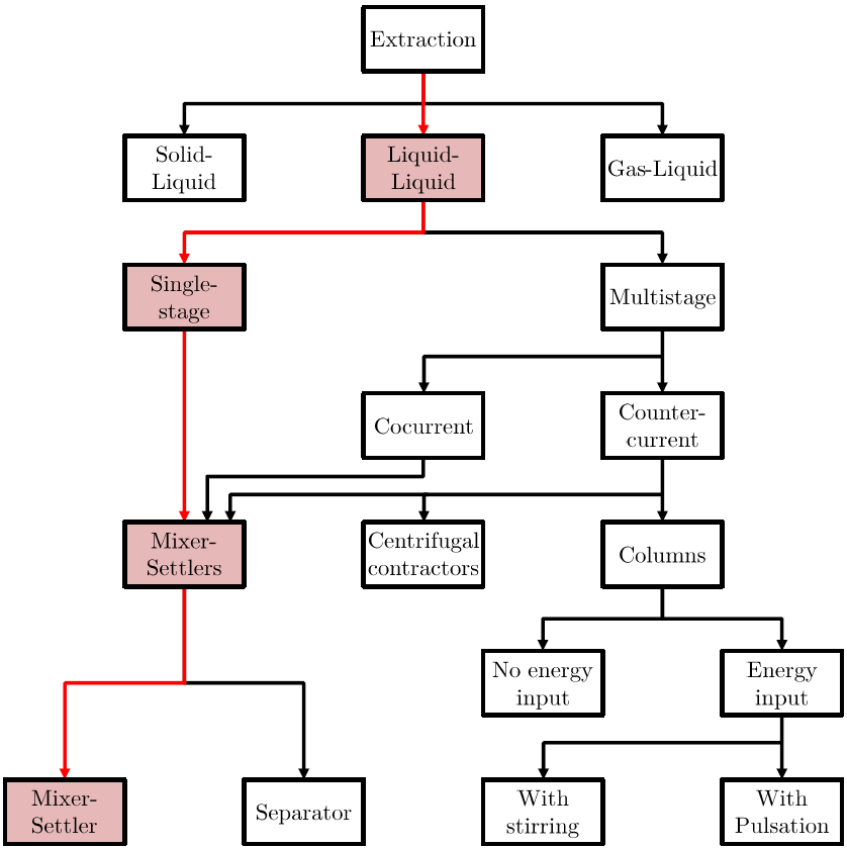

Figure 2.22.: Overview of different extraction technologies leading to different types of liquid-liquid separation processes. The figure is adapted from (Brandt et al., 1978).

The wedge is thinned along the length of the settler as more small droplets coalesce and larger droplets are integrated into their respective phase. Jeffreys et al. (1970) state that "it is evident that drop-to-drop coalescence occurs within the wedge, and droplets having a larger diameter than the mean exist at the emulsion surface. Coalescence of these droplets greatly affects the volume of the wedge and thus the capacity of the mixer settler extraction unit".

Drown and Thomson (1977) and Murray (1979) have investigated the velocity gradient of the dispersion flow within settlers. The dispersion itself flows faster than the average cross-sectional velocity of the settler. Backstreaming and circulation flows could be observed in both the lower and upper homogeneous phases. This circulating flow character leads to a dragging of smaller droplets, which do not sediment as fast as others, across the entire length of the settler. Thus, not a perfect phase separation is achieved and these smaller, fine droplets leave the settler with the continuous phase.

Several strategies exist to enhance the phase separation dynamics. In general, the separation of liquid-liquid systems is strongly dependent on the rise and sink rate of the individual droplets (and droplet swarms). One of these strategies for improving the coalescence of droplets in dispersions is concerned with leading the dispersion to solid boundaries of some form. These boundaries may be walls, plates, or knitted fabrics for example (Berger, 1986). Several authors have shown that an enhancement of the separation dynamics is possible.

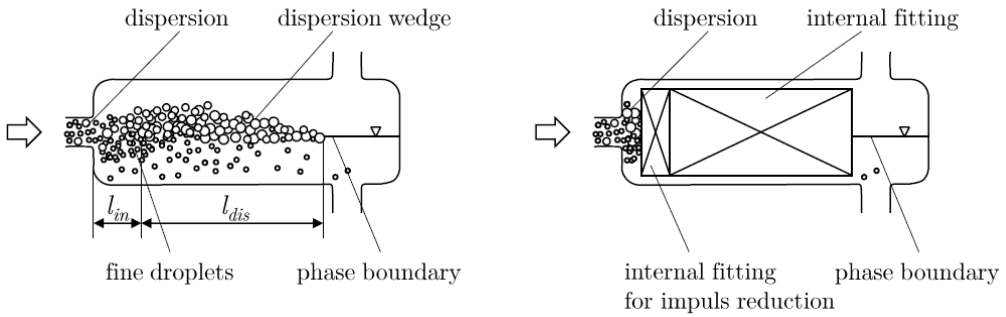

(a) Settler without internals.

(b) Settler with internals

Figure 2.23.: Schematic of a gravity settler with and without internals. The figures are adapted from (Schlieper, 2001).

Among these are Chatterjee (1998), Schlieper et al. (2004) and Mungma et al. (2014), who have investigated the influence of inclined plates in a gravity settler for the liquid - liquid phase separation of different dispersions. They showed "that internals can achieve a reduction in the separation length required of up to 75 % compared to that of a separator with no internals" Schlieper et al. (2004). In Fig. 2.24 the schematic coalescence in settlers with plates is shown for an oil - water system, whereby the oil (light phase) is the disperse phase.

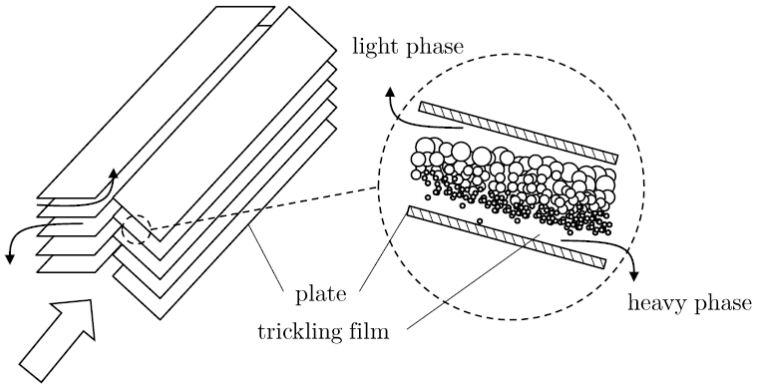

Figure 2.24.: Schematic phase separation on an inclined plate. The figure is based on the original image found in (Schlieper et al., 2004).

Due to the internals, the overall solid surface area inside the settler is larger than in a settler without internals. For all solid boundaries implemented into the settler, the wetting property of the applied material has an important influence on its effectiveness regarding enhancement of the phase separation dynamics. Hereby, the contact angle is of interest. Fig. 2.25 displays this contact angle exemplarily. The contact angle Θ of a droplet on a solid surface can be calculated with the often applied Young Equation:

$$cos(\Theta) = \frac{\sigma_{13} - \sigma_{23}}{\sigma_{12}} \tag{2.51}$$

The quality of wetting a solid surface with the disperse phase can be described by different ranges of contact angle mentioned above:

$\Theta = 0^\circ$:	The disperse phase covers the surface completely.
$0 \leq \Theta \leq 90^\circ$:	The disperse phase covers the surface well.
$90 \leq \Theta \leq 180^\circ$:	The disperse phase covers the surface poorly.

An improvement of the wetting quality can be achieved by various means, e.g. roughing up the surface or switching the material of the solid. If the wetting is good, then droplets coalesce on the solid and develop a fluid film. Thus, a more 'crude' dispersion is established and the phase separation dynamics are improved. A detailed discussion on this topic can be found in (Chatterjee, 1998).

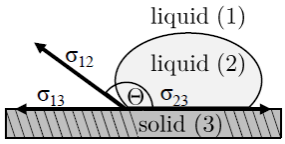

Figure 2.25.: Schematic depiction of the contact angle.

For the case of knitted fabrics, which are of interest in this thesis, the coalescence behavior is mainly affected by the sieve characteristics of the knitted fabric. If several droplets are larger than the mesh size of the fabric, they pile up against the fabric, thus coalescing with smaller incoming droplets (Bohnet, 1976). The sieve itself increases the pressure drop in the settler and simultaneously the local mass flow, as less space is available. This leads to an enhancement of the coalescence of the disperse phase, because the droplets are more likely to collide. Obviously there is an ideal mass flow rate, which differs from system to system. If the mass flow is too slow, then the fabrics have close to no influence. In general, the faster the mass flow, the larger the separation time improvement is (Schlieper, 2001). If the flow is too fast though, 'settling' is difficult to achieve.

To draw the connection to the topic of this thesis, the design of a model for the settler of the mentioned hydroformylation mini-plant is required. Therefore, the dynamic phenomena discussed in the last sections must be described mathematically.

2.5.4. Phase Separation Modeling

Different authors have suggested various strategies to solve the issue of modeling the phase separation kinetics, ranging from phenomena modeling on a molecular level (Escobedo, 2000; Kenkare and Hall, 1996), to kinetic modeling on an intermediate level (Krebs et al., 2012; Henschke et al., 2002). Of interest herein are the intermediate to integral modeling levels. In the following, a short overview of relevant ideas concerning the topic of modeling phase separation dynamics is given.

Krebs et al. (2012) suggest that "the growth rate of the volume of [the] separated oil phase V_s due to coalescence between a droplet and the oil homophase can be expressed as:

$$\frac{dV_s}{dt} = V_s \frac{do_c}{dt}, \tag{2.52}$$

whereas V_t is the average droplet volume of a droplet in the topmost emulsion layer at the oil/emulsion interface and $[o_c]$ denotes the number of coalescence events at the oil/emulsion

interface". They move on to describing the rate of coalescence as:

$$\frac{do_c}{dt} = B_{ds} N_t = \frac{N_t}{\tau_{ds}}, \tag{2.53}$$

whereby B_{ds} is the rate constant of coalescence. $1/B_{ds}$ can be viewed as the characteristic time for coalescence τ_{ds} . The number of droplets in the top layer of the emulsion N_t can be described as depicted by Eq. 2.54:

$$N_t = \frac{\pi \phi_t d_i^2}{4 A_t}. \tag{2.54}$$

The diameter of the emulsion/oil interface is given by d_i, A_t the cross-sectional area, and ϕ_t the density of the packing of emulsion droplets. Merging Eq. 2.53 with Eq. 2.54 results in an expression for calculating the coalescence time τ_{ds}:

$$\frac{1}{\tau_{ds}} = \frac{4 V_o q_t}{\pi d_i^2 \phi_t} \frac{dx_s}{dt}. \tag{2.55}$$

The shape parameter $q_t = A_t/V_t$ and the total volume of oil $V_s = x_s V_o$, whereby x_s is the volume fraction of separated oil. Krebs et al. (2012) move on discussing that the change in droplet number dN/dt can be calculated from

$$-\frac{dN}{dt} = \frac{k_{dd} N}{2}. \tag{2.56}$$

Krebs et al. (2012) discuss that "the extraction of a coalescence time distribution from the evolution of the droplet size distributions is in principle possible" and would be expedient to model the coalescence kinetics. They refrain from following this path though. The determination of droplet size distributions is associated with the necessity to perform several experiments or expensive CFD simulations.The coalescence kinetics are assumed to follow a first order process, analog to the kinetics of a uni-molecular chemical reaction. Several experiments are then performed to fit the model parameters to the equations above for their analyzed systems.

Concluding, Krebs et al. (2012) state that they "cannot make reliable predictions for the separation rate of crude oil emulsions stabilized by EOR surfactants". Due to various factors, "a scenario where the coalescence time of droplets in the crude oil/water mixture is much larger than the residence time in the separator cannot be ruled out" (Krebs et al., 2012). Nevertheless, even though these statements seem detrimental regarding the application of this model, several points can be adopted for modeling efforts discussed later on.

Additional ideas are obtained from Henschke et al. (2002). They have focused on modeling coalescence parameters in settlers from batch-settling experiments. Fur this purpose, Fig. 2.20 will be revisited here. Ideas from their model are to reduce the model to solely describe the sedimentation or coalescence curve and thus determine the 'separation end time' t_E. They describe the slope of the coalescence curve as:

$$\frac{dh_d}{dt} = \frac{2 \epsilon_{ds} d_i}{3 \tau_{ds}}. \tag{2.57}$$

In Eq. 2.57 ϵ_{ds} (roughly 1) is the total hold-up of the dispersed phase. d_i is the Sauter mean diameter of the drops at the interface and τ_{ds} represents the drop-interface coalescence time, similar to the model by Krebs et al. (2012). Also, similar to the model of Krebs et al. (2012), the hold-up of the disperse phase is also expressed as a first order decay:

$$\epsilon_p = \epsilon_{ds} - e^{(-C_1 t - C_2)}. \tag{2.58}$$

ϵ_p is the hold-up in the region $t \geq t'$. The constants C_1&C_2 can be calculated with expressions given in (Henschke et al., 2002). Finally, they present an equation to determine the coalescence time, which depends on only one parameter, r_v^*.

$$\tau = -\frac{3\pi\eta_c r_a^{5/2}}{2\sigma r_f r_v^* h^{1/2}} \tag{2.59}$$

Drawback of the model is that the solution, i.e. the calculation of settling curves, can only be obtained numerically (Henschke et al., 2002). Nevertheless, as mentioned above for the case of Krebs et al. (2012), both models contain deliberations relevant for designing models of larger units. Among these is the idea of assuming the kinetics to follow a first order process. At this point, the ideas from these models will partially be adopted and developed to fit oil-water-surfactant systems. Therefore, certain critical factors must be taken into account. Among these is the influence of trace components. Henschke et al. (2002) mention that "trace impurities present one problem in modeling phase separation in the batch-settling experiment as well as in steady-state operated technical settlers". Furthermore, neither model above takes an extreme temperature dependency into account. As described in section 2.5.1, oil-water-surfactant systems are strongly dependent on temperature changes, resulting in different phase states. For the correct dynamic modeling of a settler with an oil-water-surfactant system the following information is required:

- the temperature interval in which the desired phase separation takes place,
- the dependency of this temperature interval on concentration changes (e.g. trace components), and
- the separation end time t_E in the temperature interval.

Thus, a systematic approach to analyzing surfactant-containing systems is necessary. A detailed discussion can be found in the following section.

2.6. Systematic Analysis of Surfactant Containing Multiphase Systems

This chapter revisits deliberations found in our own, already published contribution (Müller et al., 2015a). The effort regarding phase separation modeling of multiphase systems show that a large degree of empirical studies are required to correctly depict the behavior of these systems. Obviously, the high demand for empirical studies is cost intensive in terms of time, financial, and chemical resources. Therefore, in the following a workflow to systematically analyze non-ionic surfactant containing multiphase systems regarding their applicability for technical application in mixer-settler processes is discussed.

Several of the initial thoughts and performed experiments stem from other authors such as (Kahlweit et al., 1983), (Kahlweit and Strey, 1985), and (Sottmann et al., 2002). In their work different aspects of non-ionic technical-grade surfactants are discussed. In addition, ideas concerning the operating point determination for mini-plants from (Müller et al., 2013c) are taken. In (Müller et al., 2015a), the initial thoughts are summarized and expanded to a general guideline which is used in this thesis for the system in hand. In the following, the guideline is presented. It can roughly be divided into six steps: clarification of system goals, definition of the investigation range, prescreening of the system, preliminary settler design, full system mapping, and equipment design. The steps preliminary settler design and final equipment design are omitted herein, as the focus lies on understanding of the system.

In **Step 1** of the guideline, precedes the actual experimental analysis of the system. The system goals for the mixer-settler system are defined. Hereby, variables such as the desired system throughput in terms of feed and recycle streams, the maximal residence time in the settler for the phase separation as well as the separation quality are set.

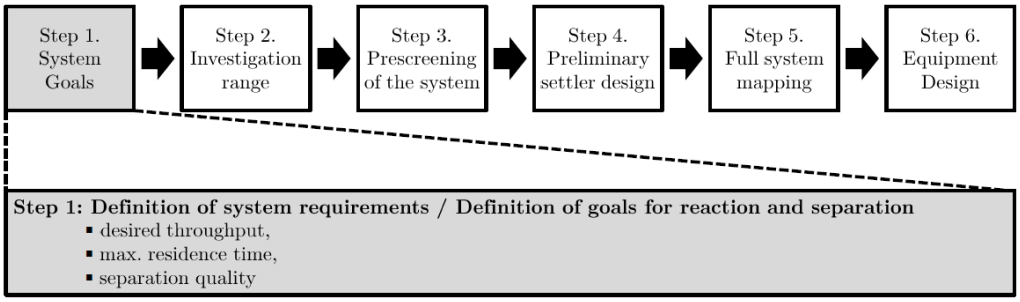

Figure 2.26.: Step 1 of the guideline for the analysis of surfactant containing systems (Müller et al., 2015a).

Once these points have been decided on, **Step 2** can be carried out. In this step a list of all influencing variables in the multiphase system in the mixer-settler process is set up. As discussed by Müller et al. (2015a), the idea here is to perform a theoretical prescreening and definition of the investigation range. The variables that may have an influence on certain properties of the multiphase system need to be analyzed. An example is given in Fig. 2.27 for the pressure influence.

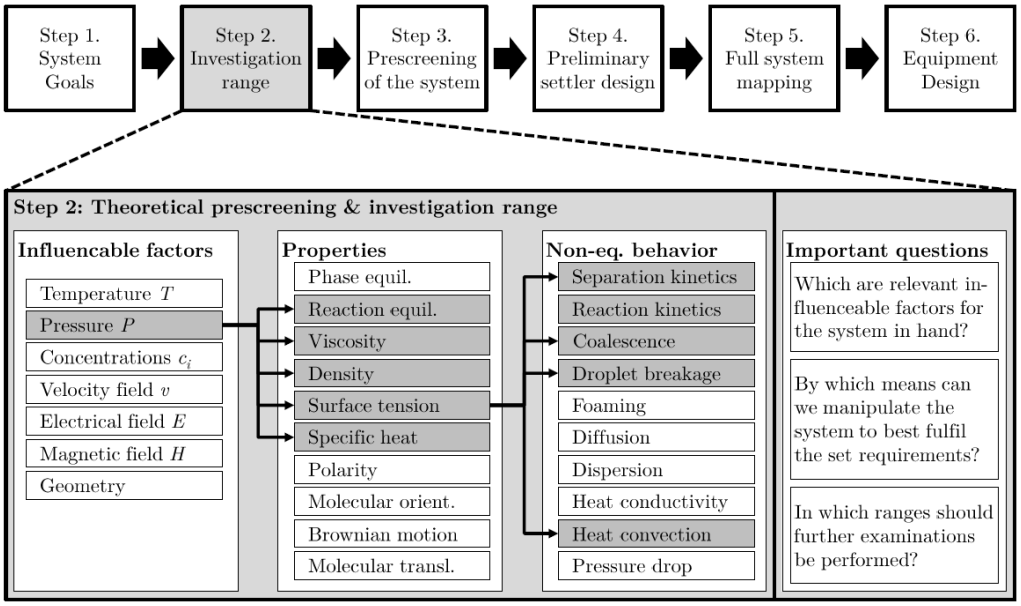

Figure 2.27.: Step 2 of the guideline for the analysis of surfactant containing systems (Müller et al., 2015a).

Obviously the pressure has an influence on the reaction equilibrium. Thus, concentrations in the system may change more or less quickly. Furthermore, the pressure can influence the overall viscosity, density, and surface tension of the multiphase system. This is important, as these rheological characteristics may have a drastic influence on the separation time and quality. Thus as part of this theoretical prescreening, the contribution of this property on the non-equilibrium behavior of the system must be characterized. Taking surface tension as an

example: it is possible to manipulate the surface tension in such a way that the coalescence behavior of the droplets changes drastically and thus also changes the separation kinetics. Therefore, this prescreening is a vital step in the guideline.

Furthermore, it is important to define the individual variable ranges. This range determines the amount of required experiments to characterize the system correctly. In general, the ranges can be selected according to known thermodynamic properties of the pure components of the system such as viscosities, vapor pressures, densities, critical mixing temperatures, etc. If data sets are available for the three-phase behavior of a similar system, this could be employed as an estimate. This is now followed by the more detailed prescreening of the system. Fig. 2.28 shows the workflow within **Step 3**.

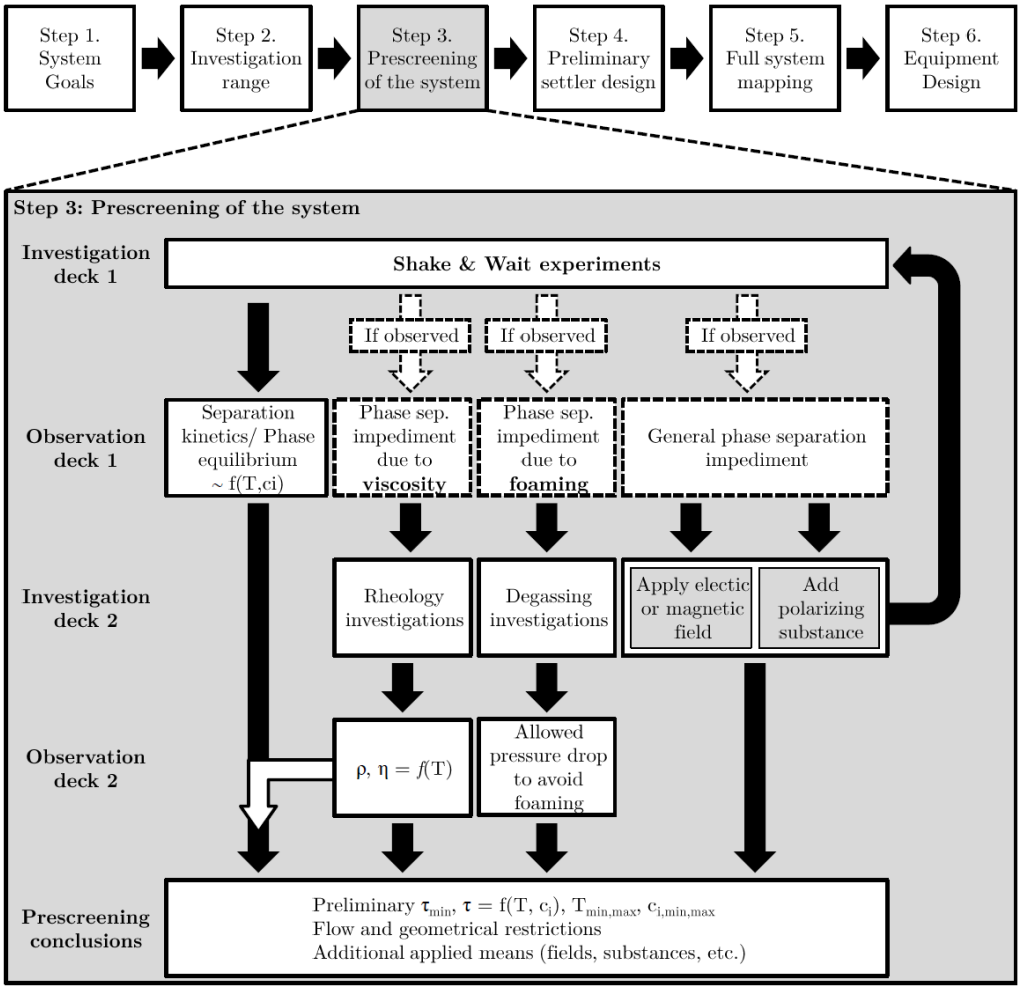

Figure 2.28.: Step 3 of the guideline for the analysis of surfactant containing systems (Müller et al., 2015a).

Thereby, an overview of the separation characteristics of the system is to be obtained. The focus lies on getting a rough idea of the answer to the following questions:

- How long does the separation of the multiphase system take?
- In what regions are the different phase states?
- How large are each of the phases?
- Where do desirable separations take place (concentrations and temperatures)?

- How much product, reactant, and catalyst is found in each of these phases?

The answers to these questions can currently only be found experimentally. Müller et al. (2015a) discuss that "from the authors' experience, so-called "shake and wait" experiments are of use. Multiple test tubes with varying compositions of the water-oil-surfactant system are prepared, immersed in thermostatic baths, and heated to temperatures within the range set above. Once the desired temperature is reached, the test-tubes are removed from the bath, shaken, and then returned to the bath to maintain the temperature. Afterwards, the phase separation for each composition is observed for a fixed time frame". This systematic experimental process is repeated for a multitude of temperatures and concentrations within the defined range from **Step 2**.

Several answers can be obtained here: the size of each of the phases, the separation time, and the feasible temperature and concentration range. The procedure in **Step 3** is divided into different categories seen as observation and investigation decks. In the investigation decks, the experiments which are to be planned are of interest, while in the observation decks the information taken from these experiments is focused on.

These initial experiments are part of "Investigation Deck 1". It must be kept in mind that circumstances may exist under which the system does not separate fast enough. The performed "shake and wait" experiments must be limited to a certain time frame, ideally one that corresponds to the maximum allowed residence time in the settler in the plant.

Furthermore, an impediment of the phase separation is possible due to various reasons. In Fig. 2.28 in "Observation Deck 1" several reasons are listed. Among these are high viscosities in certain concentration ranges, enhanced foaming, or coalescence hindrance through surface active components. Müller et al. (2015a) mention that "obviously, if the system's viscosity is too high or if a large degree of foaming is noticed, a technical application becomes questionable. If such an impeding factor is observed, further steps are required. These may be further investigations ("Investigation Deck 2") of the rheology of the system, degassing investigations or additional phase separation enhancement strategies such as applying magnetic or electric fields or even adding polarizing substances.

In the latter cases, the "shake and wait" experiments have to be repeated under these new conditions. The conclusions are a preliminary minimal settling time τ_{min}, the separation time τ as a function of temperature and concentrations as well as lower and upper temperature and concentration bounds". This leads the engineer to **Step 4**, which is concerned with the preliminary settler design. As this step is not of interest here, it will not be discussed.

The determination of the feasible operating area in terms of temperature and concentration is followed by a detailed mapping of this area. For the process concept under investigation, the oily components must be removed. This implies two things: the phase separation must be sufficiently fast and the established product phase has to be large and pure enough for adequate removal. The focus in this detailed mapping step is the analysis of the phase separation dynamics. Step by step, different factors such as the stirrer type, stirrer speed, pressure, and gas presence are analyzed.

In mixer-settler processes the reaction step is just as critical as the separation step. The formation of the mixture, which usually accompanies the reaction step, requires an adequately fast stirring speed. The higher the speed of the stirrer is, the better the reaction (up to a certain degree). In the reactor a high stirring speed leads to a decrease of the droplet size of the emulsion and hence an increase in the overall reaction rate (a plateau or maxima may be reached as well) (Hamerla et al., 2013b). This now stands in contrast to the goal in the separation step. Müller et al. (2015a) discuss that "high stirrer speeds may cause a too effective breakage of the droplets leading to the establishment of a stable

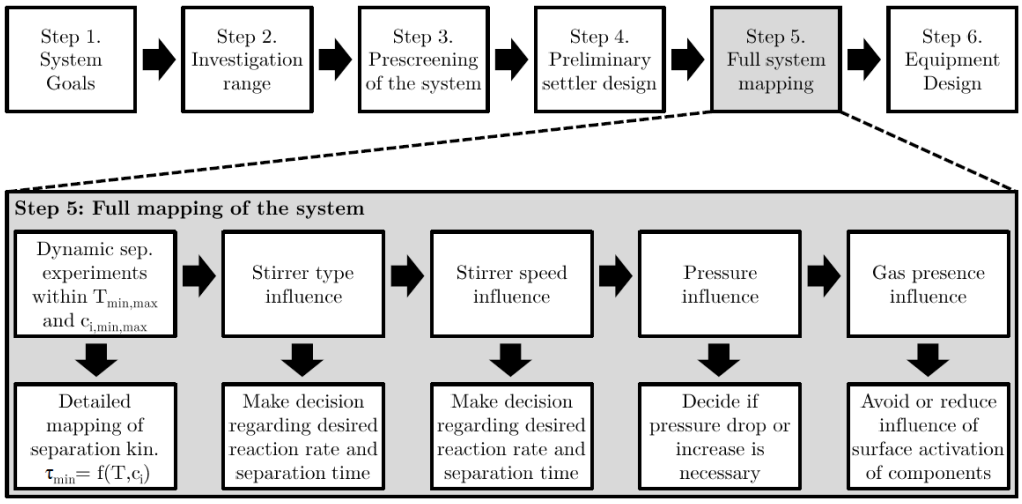

Figure 2.29.: Step 5 of the guideline for the analysis of surfactant containing systems. The original image is found in (Müller et al., 2015a).

microemulsion. In these cases, the separation time increases drastically. An optimum [or critical stirrer speed] has to be found, at which the reaction can effectively be carried out and the required separation time does not cause an overly large hold-up of the settler".

The next factor of interest is the pressure. It is well known that low to medium pressure has a negligible influence on the thermodynamic equilibrium of the phase separation. This is true for the equilibrium state. For the influence on the separation dynamics, the case may be different. It is possible that due to the physically dissolved gas in the system the coalescence may be hindered. "The partial pressures of various gases can change the behavior of the system entirely by catalyst activation or else. Hence, if relevant for the investigated system, these aspects should be included in the analysis" (Müller et al., 2015a).

Using the information obtained from this systematic analysis of the surfactant containing system, the required phase separation model can be designed. In the next Chapter, the realization of the process concept "hydroformylation in microemulsions" is presented in the form of a mini-plant. Special attention is given to the herein presented workflow, which is applied on the substances of interest.

Chapter 3.

Hydroformylation in Microemulsions

In the introduction of this thesis the concept of hydroformylation in microemulsions was discussed. In this chapter the realization of this concept is presented. To date, it is impossible to operate a process such as this successfully without knowing the exact phase separation characteristics of the microemulsion system. Therefore, this chapter focuses on two parts: the systematic analysis of the system at hand and the realization of the concept in the form of a mini-plant. Later, the process monitoring devices and the implementation of the online-optimization is discussed.

3.1. Systematic Systems Analysis

In Chapter 2 an approach was presented, in which a workflow for the systematic analysis of surfactant containing systems was discussed. This guideline is applied for the substances used in the process concept presented in the previous section. The information obtained is vital for equipment design, process operation, and modeling purposes.

3.1.1. Applied Substances

Before beginning with the actual workflow, the substances applied during the reaction are presented:

- The main component used in the reaction is the educt 1-dodecene (CAS: 112-41-4) obtained from the company MERK KGaA.
- The catalyst required for the reaction is water soluble. Therefore deionized water is used as a solvent.
- To enable the creation of the microemulsion the non-ionic surfactant Marlipal 24/70 (CAS: 68439-50-9) obtained from the company Sasol Germany GmbH is applied[1].
- The syngas (CAS: 630-08-0) for the reaction has a composition of 1:1 vol.-% of CO:H_2 with a purity of 99.999 %.
- The main product in the reaction is 1-tridecanal (CAS: 10486-19-8) obtained from the company Alfa Aesar.

The catalyst employed for the reaction consists of two parts. The first part is the rhodium-based precusor (Acetylacetonato)dicarbonylrhodium(I) [Rh(acac)(CO)2] (CAS: 14874-82-9). The precursor is obtained from Umicore NV. The second part is the ligand. Goedheijt

[1]The surfactant was sponsored by Sasol Germany GmbH

et al. (1998) state that by sulfonating the bidentate ligand 4,5-bis(diphenyl-phosphino)-9,9-dimethylxanthene (XantPhos) the water-soluble bidentate ligand [2,7-bis-(SO_3Na)-4,5-bis(diphenylphosphino)-9,9-dimethylxanthene] (SulfoXantphos) is formed. "With this modification the ligand is highly water soluble but completely insoluble in 1-dodecene" Hamerla et al. (2013b). Thus, a highly selective catalyst complex is formed, which can be separated by a simple phase separation step. Fig. 3.1 shows the structure of sulfonated Xantphos.

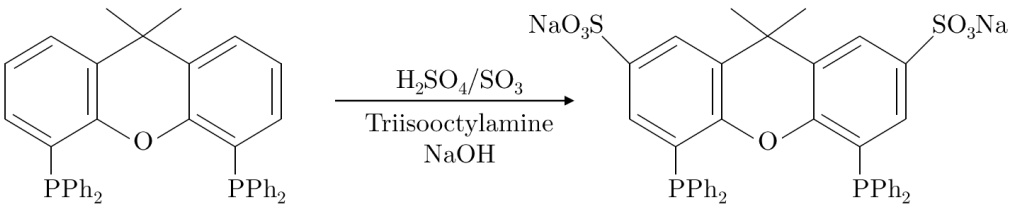

XantPhos SulfoXantPhos

Figure 3.1.: Ligands: Xantphos and sulfonated Xantphos (Goedheijt et al., 1998).

Next, the guideline presented in section 2.6 is applied for the components used in the hydroformylation mini-plant. The information obtained from this systematic analysis is used to design a settler and to develop a model for the phase separation step in the mini-plant.

3.1.2. Phase Separation Influence Factors

Step 1: The guideline starts with the specification of process goals. For this purpose, three points should be specified: maximum throughput of the system, minimal residence time in the settler, and desired yield.

The alkene feed in the plant can reach values of 1500 g/h, which is equal to the maximum throughput of the system. For the residence time of the settler, the recycle flow must be considered additionally. The pumps P05, P06, and P07 each can pump roughly 500 g/h. If the settler had a volume of 1000 ml, a residence time of roughly $\tau = 20$ minutes can be attained. Of course, if the feed stream is smaller and not all recycle pumps are activated at the same time, a larger residence time can be set. An expected feed stream of 100 g/h and a recycle stream of 500 g/h is desired. Consequently, the settler can be expected to have a residence time of over 1.5 hours. This means that an ideal separation time in the settler of the process would lie between 0 to 90 minutes. The yield of the system after four hours of reaction should be between 20 to 40 %

Step 2: Here, the theoretical prescreening of the system as well as a definition of the investigation range is carried out. The following influencing factors are determined:

- The first important influencing factor is concerned with the concentrations of educt (1-dodecene), product (1-tridecanal), surfactant Marlipal 24/70, and water. Depending on these concentrations, different phase states and phase sizes are possible.
- The second influencing factor is the system pressure, seeing that it has an influence on the micelles as well as the gas solved in the system.
- On top of that, the presence of CO & H_2 is important, because it has a strong influence on the surface activity of the catalyst. Surface activity can hinder the coalescence of the droplets in the system.

- The fourth factor of interest is the system temperature, as it dominates the phase state of the system.
- The final factor of interest is the stirring speed of the stirrer in the reactor, which can determine the droplet size before the separation.

For these variables of interest the according ranges are defined in Tab. 3.1. These ranges have been specified based on results from previous investigations such as (Hamerla et al., 2012, 2013b) and (Rost et al., 2013; Rost, 2013).

Table 3.1.: Investigation ranges for phase separation influencing factors.

Factor	Description	Lower bound	Upper bound
α	Oil:Water ratio	10 %	90 %
γ	Surfactant concentration	1 %	15 %
X	Yield	0 %	40 %
$T_{Settler}$	Settler temperature	50 °C	110 °C

Additionally, it is well known that this water-oil-surfactant system tends to foam in certain concentration regions. This is a factor that needs to be closely observed. Based on these defined ranges the next step is carried out.

Step 3: In this step the actual prescreening of the system is performed according to the defined ranges. The separation behavior of the microemulsion system is a function of composition and temperature. Müller et al. (2015a) describe that "the challenging aspect of operating a process with these systems is the shifting of the ideal separation region to different temperatures due to concentration changes, i.e. the reaction starts and product is produced, surfactant concentration changes due to purging with the product, or changing the water:oil ratio". Therefore, a mapping of the phase behavior is required in preparation of running a continuous process. Since almost no thermodynamic information for the system with all technical grade components exists, the mapping depends fully on empirical studies, a result of which is shown in Fig. 3.2.

Therein the behavior of the phase separation for one concentration for a range of temperatures is depicted. The two visible surfaces show the different heights of the phases. The upper surface is the boundary between the mixed and the oil phase. The region in which a "valley" is visible is the temperature interval where a large product phase is created. This temperature interval is desired for the process. The shake and wait experiments are carried out for the large concentration range. Hereby, the following information is derived:

- The separation for each of the concentrations in the ideal temperature region occurs in an adequately short time frame (below 10 minutes).
- The temperature interval in which this desired separation occurs is relatively small (4 K). This is can be seen in Fig. 3.2.
- Foaming of this system can be avoided if an oil:water ratio greater than 30 % is realized.
- It is observed that the catalyst is activated through the presence of CO in the system. This effect causes a hindrance to the coalescence of droplets. In the activated form, phase separation is not observed. This issue is a problem for the process concept, because the catalyst remains active after the reaction step due to the high CO pressure in the settler. If the system is deactivated by depressurization or degassing, the

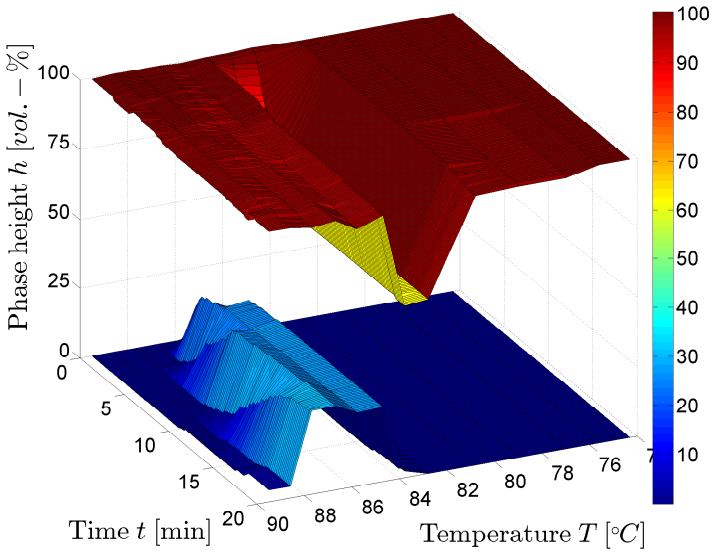

Figure 3.2.: Experimental results, which are valid for a mixture consisting of 9 wt.-% Marlipal 24/70, 22.75 wt.-% alkene, 22.75 wt.-% aldehyde, 45.5 wt.-% water, and a concentration of 298 ppm precursor (Müller et al., 2014f).

phase separation occurs again though. It can be seen in Fig. 3.3, how no oil phase is established.

- The presence of product leads to a dead-time for the phase separation. This result can also be seen in Fig. 3.3 for the line 1100 rpm 1 bar (deactivated). Here, product was created due to previous activation of the catalyst. The final phase height after several hours is the same as for the case without product though.
- A change in the surfactant concentration of Marlipal 24/70 of 1 wt.-% leads to a temperature shift of the optimal region of roughly 3 to 5 °C.
- A change in the water to oil ratio leads to a temperature shift as well as to a change in oil phase height. The exact behavior will be presented later on.

Step 4: In the fourth step, a preliminary design of the settler is performed. The quality analysis of the system with the offline gas chromatograph takes roughly one hour. Therefore, a concentration controlled settler is not ideal, as a continuous and fast analysis of the components would be required. Since the separation is highly dependent on the temperature though, a temperature controlled settler is sufficient.

Step 5, part one: Based on the observations from the preliminary screening, new variable ranges are defined. As it is known that CO activation of the catalyst hinders the phase separation, 1 wt.-% Na_2SO_4 is added to counter the effect. Additionally, the influence of the factors stirrer speed and system pressure on the separation dynamics are analyzed. Tab. 3.2 shows these new ranges.

For the full mapping of the system a fully fledged factorial design of experiments is planned. Different compositions of the reaction mixture are prepared according to Fig. 3.4. In total, 27 compositions are prepared with $\alpha = [40, 50, 60]$, $\gamma = [6, 8, 10]$, and $X = [0\ 20\ 40]$.

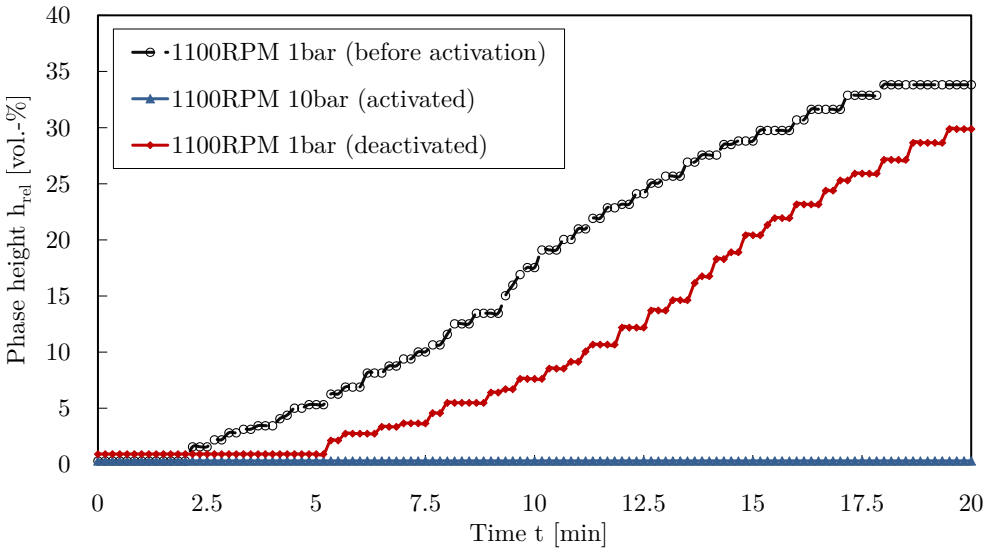

Figure 3.3.: Here, the influence of catalyst before activation with CO, after activation with CO, and after degassing of CO (deactivation) on the phase separation is visible. During the activation with CO no phase separation takes place and thus no oil phase is established.

Table 3.2.: Updated investigation range for phase separation influencing factors.

Factor	Description	Lower bound	Upper bound
α	Oil:Water ratio	40 %	60 %
γ	Surfactant concentration	6 %	10 %
X	Yield	0 %	40 %
$p_{reactor}$	System pressure	1 bar	15 bar
$S_{reactor}$	Stirring speed	700 rpm	1500 rpm
$T_{Settler}$	Settler temperature	50 °C	110 °C

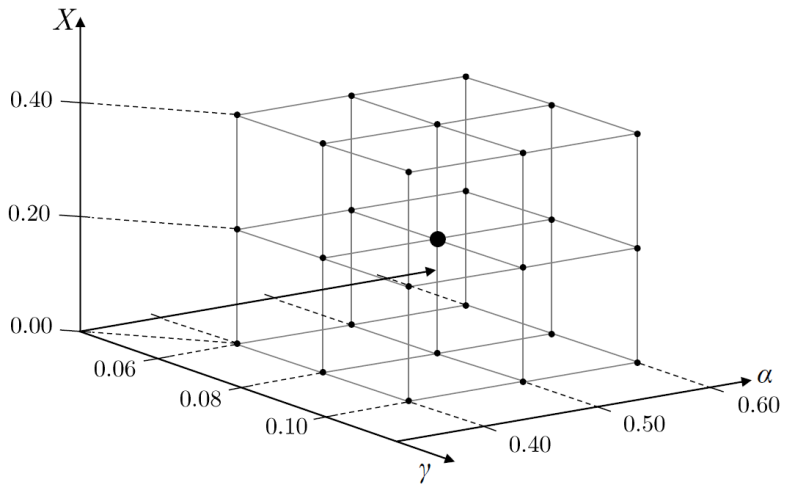

Figure 3.4.: Full mapping: factorial design of experiments for various concentrations of product (X), surfactant (γ), and oil to water ratio (α). The black dots show the concentrations that are to be analyzed.

Firstly, only experiments without syngas addition are carried out. The issue hereby is that syngas has an effect on the catalyst surface activity but simultaneously initiates the reaction. Therefore, observing the phase separation under syngas presence is difficult, because the concentrations of the prepared samples change over time. The idea now is to examine the phase separation behavior in the inactivated state of the catalyst (without syngas) and then to take a reduced number of sampling points and repeat the experiment with syngas present at 9 bar.

The experiment is carried out in a batch reactor with a total volume of 500 ml. Fig. 3.5 shows the experimental set-up. The double shell glass reactor is connected to a thermostat, thus enabling temperature control. Furthermore, it contains a gassing stirrer. The stirring speed can be controlled as well up to a maximum value of 1500 rpm. Due to cost, waste-amount, and safety reasons only 100 to 150 ml of samples are prepared each time. The reactor is capable of withstanding pressures of up to 11 bar (absolute).

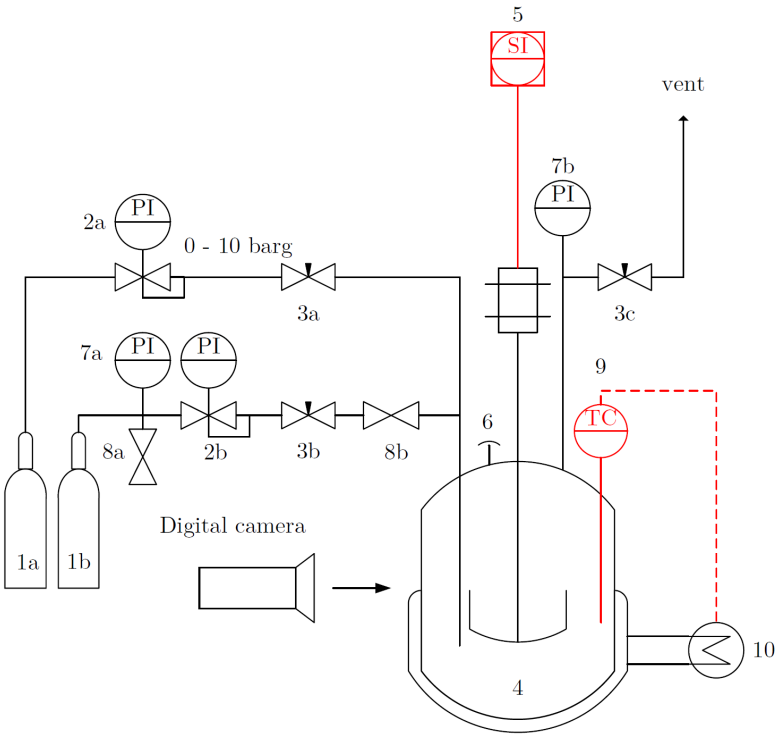

Figure 3.5.: Experimental set-up: batch experiment phase separation. 01 a/b: gas bottles (Argon/Syngas), 02 a/b: pressure control valve, 03 a/b/c: needle valve, 04: glas reactor & stirrer, 05: stirring control unit, 06: burst disc, 07 a/b: manometer, 08: needle valve, 09: thermo couple,10: thermostat. The red dotted line symbolizes the temperature control.

The samples are prepared in the following steps:

1. One mass percent of Na_2SO_4 is filled into the glass reactor.
2. The oily components, 1-dodecene and 1-tridecanal, as well as the surfactant are filled into the reactor.
3. The desired sample is prepared with deionized water. Additionally, the water is flooded with nitrogen for at least 20 minutes and simultaneously heated to roughly 80 °C. Thus, little oxygen is left, which may deactivate the catalyst complex.

4. The prepared highly concentrated catalyst solution is filled into the reactor with a syringe.

After the sample has been prepared and filled into the reactor, the experiment is carried out. Hereby, the following steps are performed:

1. The reactor is closed, tightly sealed, and the heating via the thermostat is started.
2. The vacuum pump is started, creating a vacuum of roughly 50 mbar in the reactor.
3. The system is flooded and purged with nitrogen three times.
4. The stirrer is started with a rotation speed of 1100 rpm.
5. The system is flooded and purged with nitrogen three more times.
6. Once the desired temperature in the reactor is reached, the stirring is stopped and a digital camera started. The system is filmed for ten minutes.
7. After the ten minutes the stirring is started again and the reactor temperature increased by 1 K.
8. This procedure is repeated until the three-phase area disappears or the maximum thermostat temperature has been reached.
9. The film is exported into a matlab script, in which each of the phase heights is analyzed.

As mentioned before, the phase separation is firstly carried out for samples without syngas present. After the full mapping has been performed, selected samples are repeated with syngas. Fig. 3.6 shows the batch reactor with a mixture of 1-dodecene, 1-tridecanal, water, catalyst solution, and Na_2SO_4 at the best separation temperature.

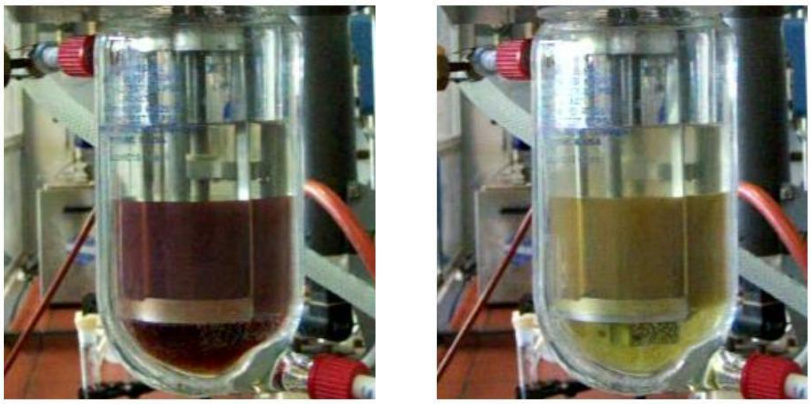

(a) Phase separation, no syngas (b) Phase separation, 10 bar syngas

Figure 3.6.: Photos of the phase separation batch experiment with and without syngas.

It was observed that the presence of syngas has no effect on the optimal phase separation temperature interval, if the surfactant concentration is equal to or lies above 8 wt.-%. For low surfactant concentrations, an upwards shift of roughly 4 to 7 K is observed to find the same separation state. It seems that at low surfactant concentrations, a non-ideal ratio of catalyst to surfactant is present in the system. The surface active catalyst hinders the phase separation from taking place at the same temperature as for the inactivated case. For

the process concept and especially for the operation of the mini-plant, this information is vital. For our case it means that an operation should be carried out at higher surfactant concentrations. Furthermore, the oil:water ratio should be higher, because a larger oil phase can be established after the reaction, thus enabling an eased product phase removal.

In general, the results of the mapping of the ideal temperature region is shown exemplarily in the two diagrams in Fig. 3.7. The diagram on the left contains the results for no product in the system. The diagram on the right contains the results for a constant oil:water ratio of 40 %. The dots represent the lower and upper ideal temperature for each concentration. All results are listed in the appendix in Tab. A.1.

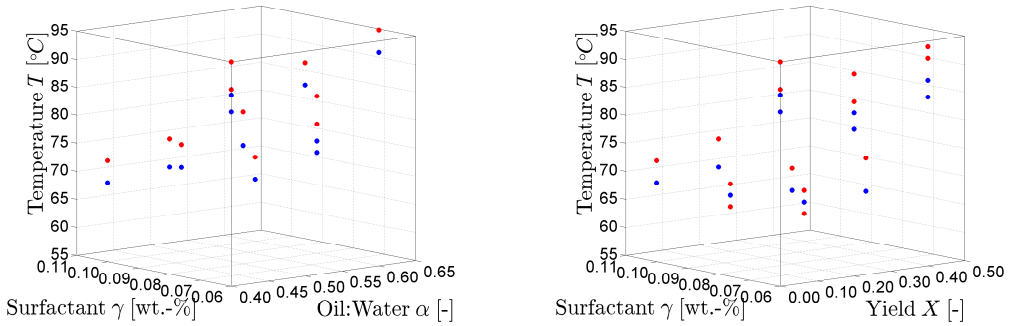

(a) Temperature interval for $X = 0$ %

(b) Temperature interval for $\alpha = 40$ %

Figure 3.7.: Mapping of the phase separation batch experiment results. The red dots show the maximum temperature for a certain concentration whereas the blue dots present the lowest temperature for the same concentration. Thus, the operating point should be between the two temperatures.

Step 5, part two: With the optimal separation temperature interval in mind, the other experiments are carried out to investigate the influence on the separation dynamics. Among these factors of interest are pressure and stirrer speed influence. To investigate these factors a mixture of $\alpha = 50$ %, a surfactant concentration $\gamma = 8$ %, a product concentration $X = 0$ %, and a catalyst concentration of 298 ppm with a metal to ligand ratio of 1:4 is filled into the reactor. No salt is used in this experiment. For this composition an ideal separation temperature of 85 °C is set.

The procedure mentioned in the previous section for analyzing the phase separation is firstly repeated for stirring rates of 700 to 1500 rpm in 200 rpm steps and for 1, 5, and 10 bar absolute pressure of Argon. Each phase separation experiment is performed two times to thus ensure reproducible results. The stirring is performed for 20 minutes each time. In general, for all experiments, the obtained results were reproducible with minimal deviations. The results are summarized in Fig. 3.8. The development of the oil phase height during the phase separation process in the glass reactor over time is exemplarily shown. The figure on the left shows the results for different stirring speeds and the figure on the right for different pressures at 1100 rpm.

As discussed in (Müller et al., 2015a), "it becomes apparent that the stirring speed in the analyzed range with the applied four-bladed gassing stirrer has no influence on the dynamics of the phase separation. The pressure on the other hand clearly has an influence on the dynamics. The relative phase height after 20 minutes of separation of 1 to 10 bar differs by roughly five percentage points. Higher pressures could not be investigated, due

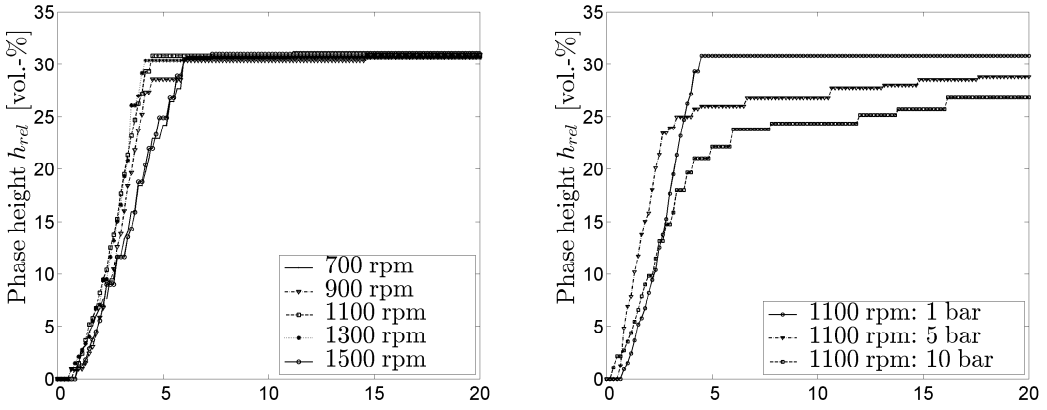

(a) Oil phase height for different stirrer speeds

(b) Oil phase height for different pressures

Figure 3.8.: Stirrer speed and pressure influence on the phase separation speed. Both have a negligible influence on the development of the oil phase (Müller et al., 2015a).

to the maximum allowed pressure of the glass reactor. Given that the mini-plant shall be operated at 15 bar, the influence of the pressure on the dynamics of the phase separation is negligible".

Step 5, part three: Additionally to the already performed experiments, investigations regarding coalescence accelerators are carried out. For the case that the phase separation in the settler takes longer than expected, coalescence enhancers may be of use. Therefore, an experimental set-up depicted in Fig. 3.9 is constructed. A mixture similar that from the previous section is prepared, heated, and stirred in a continuously stirred tank reactor (CSTR). Depending on the pumping frequency, different settler residence times can be set and the phase separation can be analyzed. For this purpose, the height of the established oil phase in the settler at a certain residence time is measured. Afterwards, the mixture is fed back to the reactor. It is assumed that the reactor volume is at least five times larger than that of the settler. Therefore, the overall composition does not drastically change.

Next, different types and geometries of knitted fabrics sponsored by Rhodius GmbH are tested in the set-up. These types are shown in Fig. 3.10. A photograph of the relevant cases for this thesis is displayed in Fig. 3.11. Starting on the left, Fig. 3.11 shows a stainless steel accelerator. For further discussions this will be case 1. The structure of this internal fitting resembles that of a cylinder made of steel wool. The next is a combination of stainless steel and PTFE. Case 3 is a modified stainless steel separation accelerator with a PTFE block in the middle. The last two presented internals are modifications of the third internal. As mentioned by Müller et al. (2015a), cases 1 and 3 are discussed in greater detail, due to the successful results obtained in the continuous phase separation experiments.

Fig. 3.12 depicts the results of the continuous phase separation experiments for the three cases. It shows the oil volume fraction $\dot{\phi}_{Oil} = \dot{V}_{oil}/\dot{V}_{feed}$ over the settler residence time. In the first experiment, the phase separation in an empty settler, without a coalescence enhancer, is measured. In the second experiment, the stainless steel knitted fabric is implemented in the settler. As described by Müller et al. (2015a), compared to the result of the first test a significant increase in the oil phase height is achieved. In the third, the modified stainless steel fabric is analyzed (case 3). "Since the centerpiece of the knitted fabric is

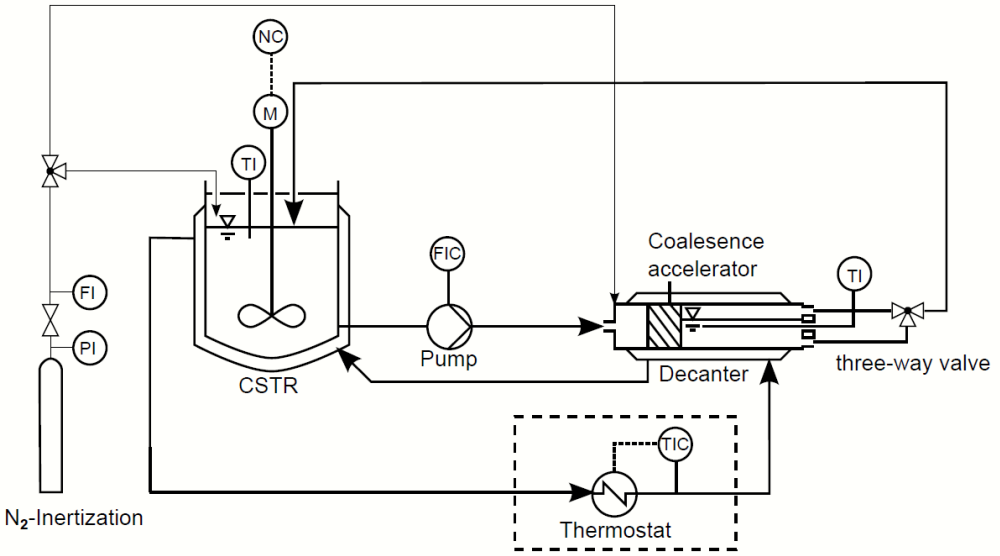

Figure 3.9.: Experimental set-up: effect of internal fittings in the settler (Müller et al., 2015a).

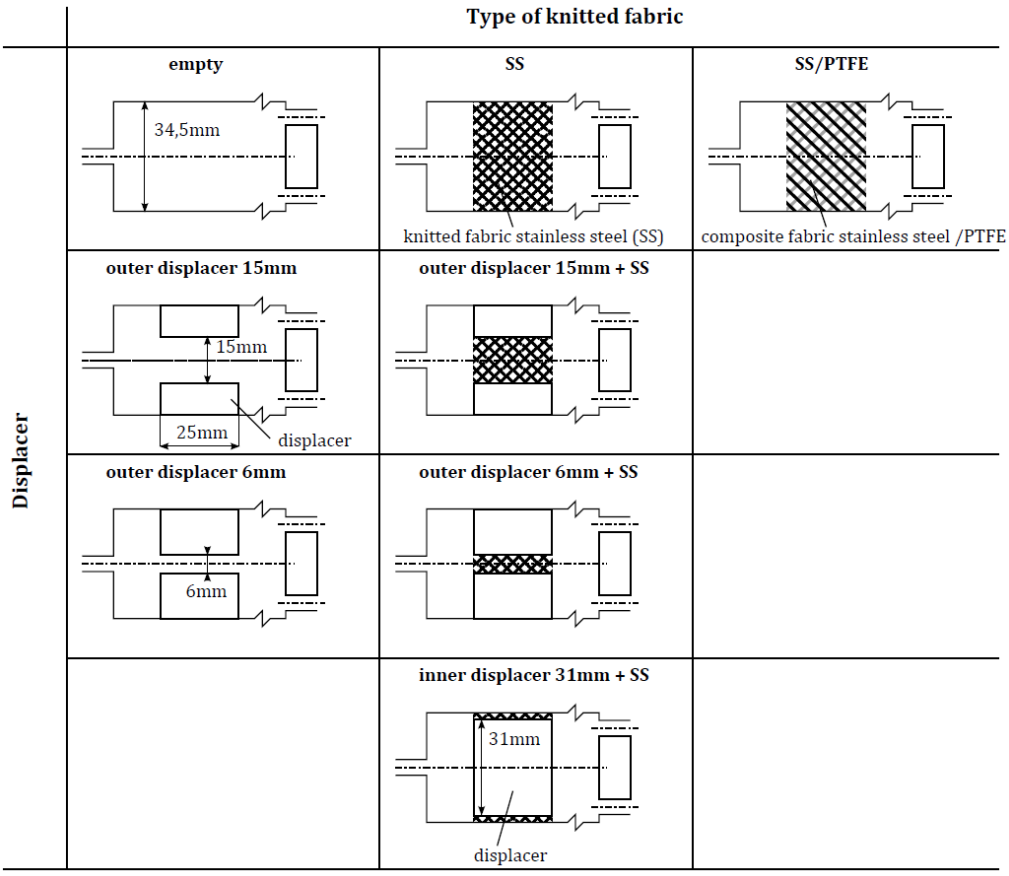

Figure 3.10.: Experimental set-up: types of implemented internal fittings in the settler (Müller et al., 2015a).

Figure 3.11.: Experimental set-up: photograph of investigated internal fittings in settler. Stainless steel (SS) fabric, SS/PTFE fabric, SS fabric with PTFE displacer inside, SS fabric with outer displacer (6mm), SS fabric with outer displacer (15mm) (Müller et al., 2015a).

replaced by a solid PTFE cylinder, the multiphase system is forced to pass directly along the wall of the settler. Here, the maximum oil phase height is almost immediately reached" Müller et al. (2015a).

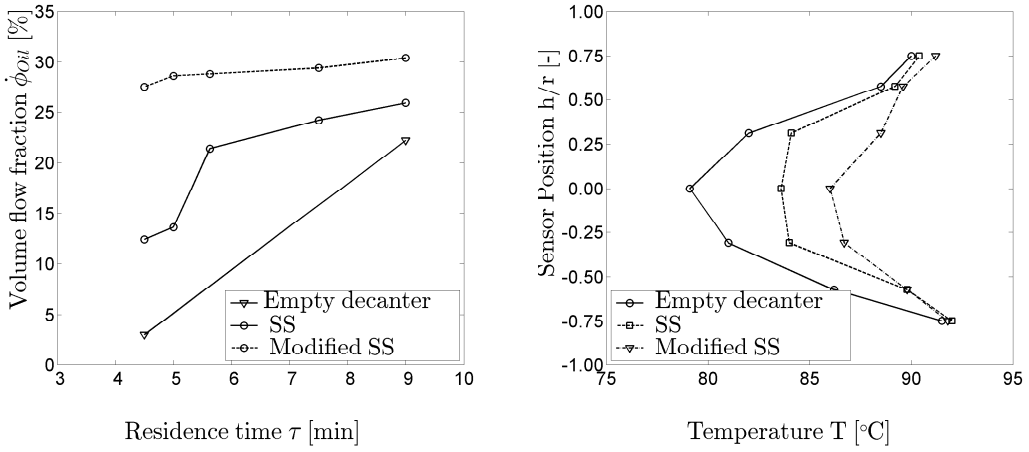

(a) Oil phase height for different internal fittings

(b) Temperature profile for different internal fittings

Figure 3.12.: Comparison of the relative oil phase height over separation time (left) and temperature profile (right) in the settler for three tests: empty settler, stainless steel fabric (SS), modified stainless steel fabric (Modified SS) (Müller et al., 2015a).

The following deliberations on three system characteristics give a first explanation regarding these obtained results: surface tension, pressure drop, and temperature.

Firstly, the stainless steel knitted fabric acts as a tightly knitted net. The droplets of oil, water, or surfactant are caught in this net or cling onto the steel fibers of this net. Because of the different surface-tension properties of each of the components, some cling onto the net better than others. Thus, those clinging onto the net are more likely to come into contact with those passing by. That way the probability of two droplets of similar composition meeting and coalescing becomes larger.

Additionally, pressure drop may be another cause for the enhanced phase separation. The stainless steel net leads to a reduction of available space in the settler. The liquid mass flow is therefore increased locally in the area of the internal fitting and a pressure drop is induced. Thus, again the probability for a coalescence of similar droplets is increased as the droplets are compressed more tightly.

Furthermore, the probably most important cause for these positive results from internal fitting implementation is the temperature homogenization. It is apparent from Fig. 3.12 that the temperature along the radius of the settler has a relatively large profile for the case of the settler without internals. A large temperature drop from the top to the middle of the settler can be seen. For this case, the wall temperature was exemplarily set to 95 °C. Already at 75% settler radius, a temperature of roughly 92 °C is measured. Now, the closer the temperature in the middle of the settler is measured, the larger the temperature drop is. In other words, the optimal separation temperature required for a fast separation is not truly implemented or obtained in a large part of the settler. For the case of the settler without inner fixtures the separation will either take a drastically larger amount of time or will not occur at all. The other two cases analyzed show that a homogenization of the temperature is possible. The third case shows the most homogeneous temperature profile. Here, the fastest phase separation also takes place. This can be explained by the fact that the liquid directly passes along the wall of the settler. The middle of the settler is blocked with the PTFE cylinder. Therefore, the exact desired temperature is reached. The positions of the temperature measurement points are shown in Fig. 3.13.

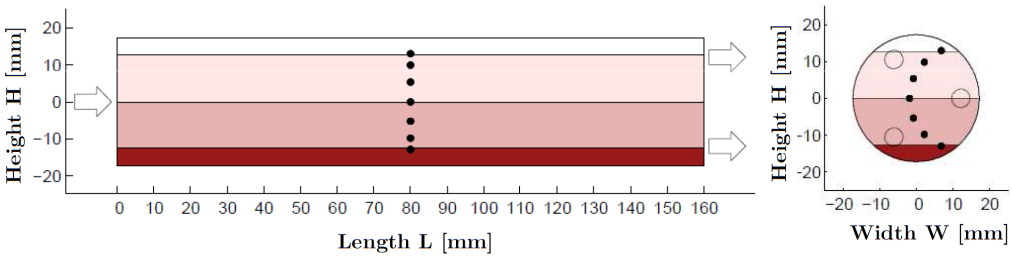

Figure 3.13.: Temperature sensor positions in the glass settler. The different shades in the settler indicate the possible phases during the phase separation at the correct temperature. (Müller et al., 2015a).

Concluding it can be said that with the information gained from the systematic analysis of the system, first development criteria are determined to design a modular, multiphase settler as well as design the mini-plant. Additionally, the foundation is laid for first modeling ideas for the settler model.

3.2. Realization: Mini-plant

The plant roughly consists of three sections: feed-, reaction, and product storage section. Fig. 3.14 displays a three-dimensional construction of the mini-plant. Additionally, the general design of the mini-plant is shown in the piping and instrumentation diagram in appendix A.1. The feed section is located in the basement, while the reaction and product storage section are on the ground and on the first floor.

In general, the surrounding area around the plant is defined as an “Explosion Zone II”, since hazardous and explosive components are employed. Therefore, all units are constructed or bought accordingly. To prevent an explosion from spreading to other areas, the mini-plant has been built in a separate room. All auxiliary equipment not designated for an “Explosion Zone II” such as thermostats, the offline gas chromatographs, gas feeds, control cabinet of the process control system as well as the control room are located outside of this room. To monitor the H_2 & CO concentrations in the building, stationary sensors have been placed on each level. To prevent an accumulation of syngas in the building, a corresponding

ventilation system is installed. In case of emergency, the magnetic valves enabling the feed of syngas are closed and nitrogen is flooded into the plant.

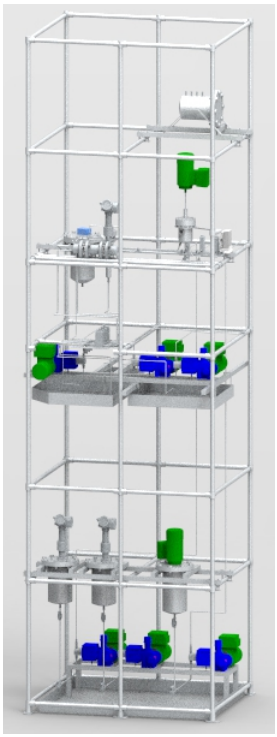

Figure 3.14.: 3D set-up of the hydroformylation mini-plant at Technische Universität Berlin.

3.2.1. General Design of the Mini-Plant

As mentioned before, the plant consists of three sections. The first section is the feed section (Fig. 3.15), in which the alkene (container B01), the surfactant (container B03), and catalyst solution (container B02) are each stored separately. With a pump for each container (P01, P02, P03) the substances are fed into the reaction section.

Here, the containers B01, B02, and B03 including the stirrer (from left to right) as well as the pumps P01, P02, and P03 (from left to right) are depicted. The pump for the alkene can feed up to 1500 g/h, while the pumps for catalyst solution and non-ionic surfactant can be regulated to a maximum value of 500 g/h each.

The reaction section consists of a reactor (C01), a settler (X01), and three recycle pumps (P05, P06, and P07). The reactor has a maximum capacity of 1500 ml, whilst a drain is fixed at 50 % height (roughly equalling 50 % liquid capacity). The reactor contains a gassing stirrer, which has a maximum rotational speed of 2880 rpm. In this section, pressures of up to 25 bar with Syngas and temperatures of 150 °C can be implemented. The settler and the reactor can be heated separately with the thermostats W01 and W02. Since the settler is a vital unit in this process, special attention is given to its design in the following section. After the phase separation in the settler, the heavier aqueous phase is recycled directly back to the reactor via pump P07. Pump P05 recycles a middle phase, if the non-oily components reach the top outlet of the reactor. The lighter organic phase is stored in the product storage container B04. From this container it can be flashed into the product storage section or recycled with pump P06.

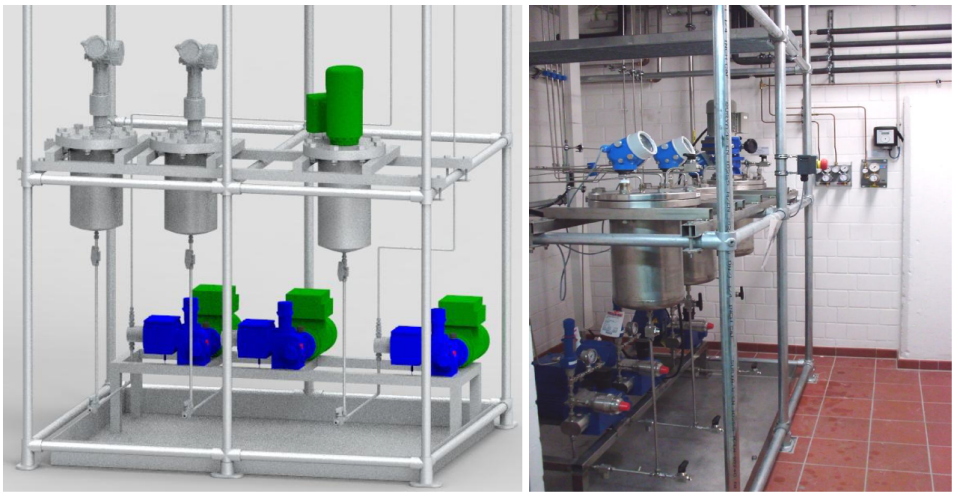

Figure 3.15.: 3D set-up and photo of the hydroformylation mini-plant: feed section.

The product storage section consists of the product container and a gas depressurization container for the removal of syngas from the system. Additionally, a vacuum pump has been installed above B06 to guarantee the removal of oxygen from the system before the reaction as well as the removal of syngas after the mini-plant operation has been carried out. Fig. 3.16 shows the 3D image of the reaction and product storage sections of the mini-plant.

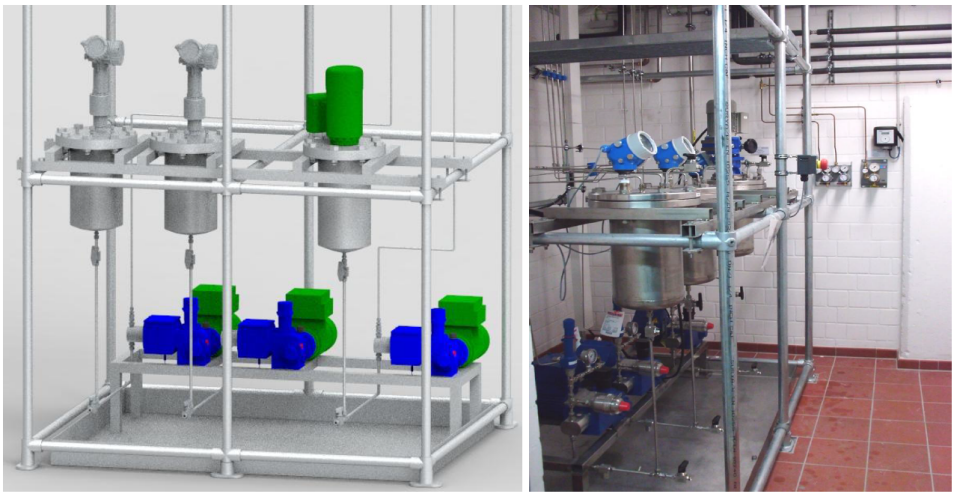

Figure 3.16.: 3D set-up and photo of the hydroformylation mini-plant: reaction and product storage section.

To guarantee the safe operation of the plant, an extensive HAZOP analysis has been made. The room, in which the plant is situated in, contains a carbon monoxide sensor on each floor and a hydrogen sensor on the upper floor. Additionally, a tenfold air exchange per hour is realized, so that no accumulation of explosive gases can occur. In case of liquid leaking out of any of the process units or pipes multiple collection basins have been added. Finally, each sub-system (feed, high pressure, product storage) can be flooded with nitrogen separately.

Additionally, the plant is fully automated with SIEMENS PCS7. Thus, a surveillance of

alarms is possible at all times. In the following figures (Fig. 3.17 to Fig. 3.19) screenshots of the user interfaces of the process control system are shown.

The first figure shows the plant as a whole. Here, it is possible to monitor the temperatures of the pipes and whether or not the pipes have liquid in them. Important in this section is the temperature in each of the pipes (top diagram on the right of the figure). Since the surfactant Marlipal 24/70 is being applied, there is a risk of the pipes coming blocked if the temperature is too low. From this overview section, the other sections such as feed section (liquids), feed section (gases), control authorization section (Freigabe), mixer-settler section, or optimizer section (Optimierer) can be selected.

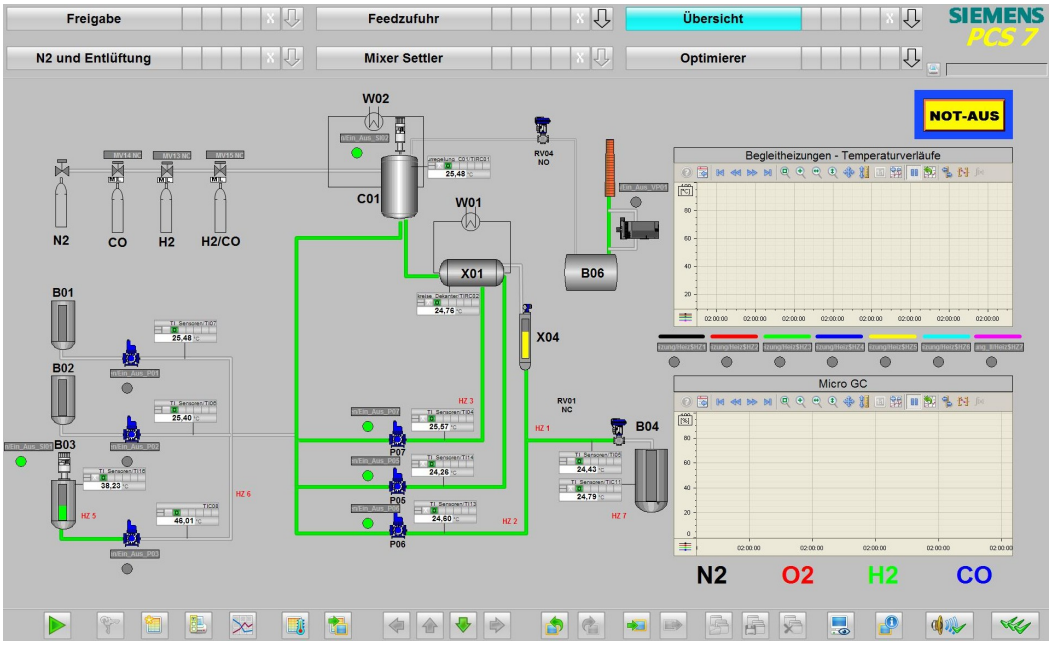

Figure 3.17.: Hydroformylation mini-plant at Technische Universität Berlin: process control system - overview.

The second figure shows the liquid feed section of the plant, in which the levels of the feed tanks, the mass flow fed by the feed pumps, and the densities of these flows are observable.

The mixer-settler section enables the control of the recycle pumps, the temperatures of reactor and settler, and the product release into the product storage tank.

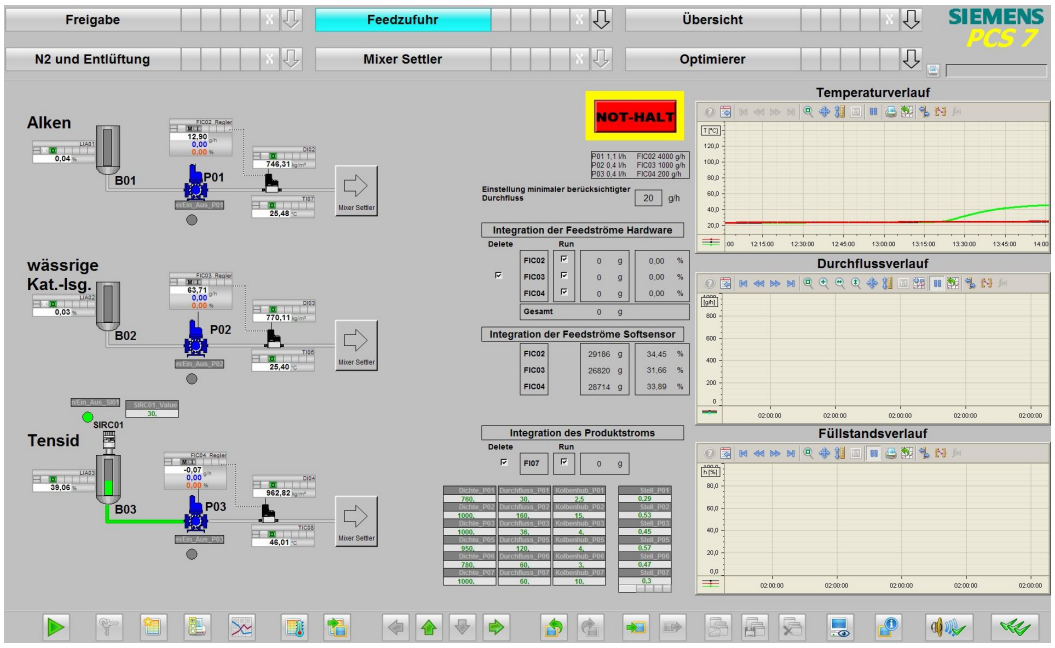

Figure 3.18.: Hydroformylation mini-plant at Technische Universität Berlin: process control system - feed section.

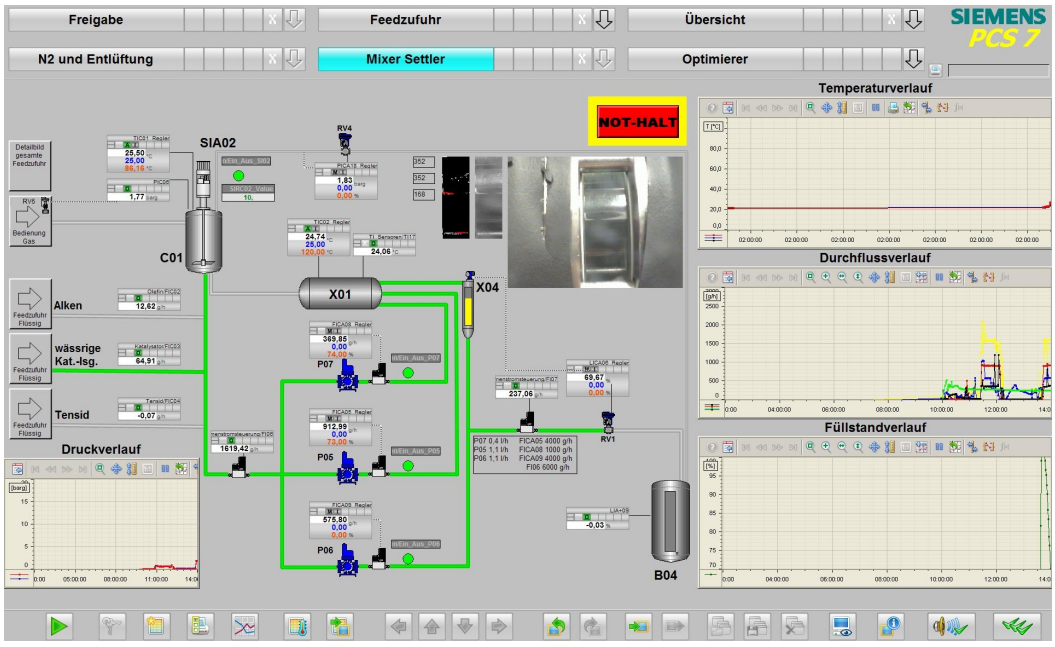

Figure 3.19.: Hydroformylation mini-plant at Technische Universität Berlin: process control system - mixer settler section.

3.2.2. Design of a Modular Multiphase Settler

In (Müller et al., 2015a) the general requirements for the design of the settler are defined. These are divided into three categories: general operational criteria, automation and observability, and modularization. The requirements as well as their implementation are discussed in the following.

"Regarding the operational criteria, the settler will be operated at up to 120 °C and at up to 20 bar. To guarantee temperature, pressure, and chemical stability, stainless steel of type EN steel no. k.h.s. DIN 1.4571 is used. The sealings consist of PTFE. The gauge glasses in the settler are made of borosilicate glass" (Müller et al., 2015a). Additionally, as mentioned in step 1 in Section 3.1.2 a settler residence time of $\tau = 90$ minutes would be desirable. Therefore, the settler should have a volume of at least 1000 ml.

As a next step the requirements for automating the settler are defined. These are mainly concerned with the actual observability of the system. As discussed before, the temperature has an significant influence on the phase separation. If the temperature in the settler is not in the correct interval, the separation will not take place fast enough. Therefore, knowledge of the temperature profile along the settler length is required. To observe the temperature, several Pt100 measurement devices are installed. In (Müller et al., 2015a) it is shown how each developed segment of the settler is connectable to a thermostat. That way it can be guaranteed that the optimal temperature is set in each segment separately. Settler sight glasses are introduced between the segments, so that visual observability of the phase separation is possible. Additionally, an optional conductivity probe is installed through the top of one of the settler segments. This measurement device allows for immediate observation of the oil phase development. Finally, a pressure sensor is added to monitor the pressure in the settler.

The third settler design specification is concerned with the modularization of the settler. Depending on the currently desired application, various settler modules are developed. The modules relevant for this thesis are shown in Fig. 3.20.

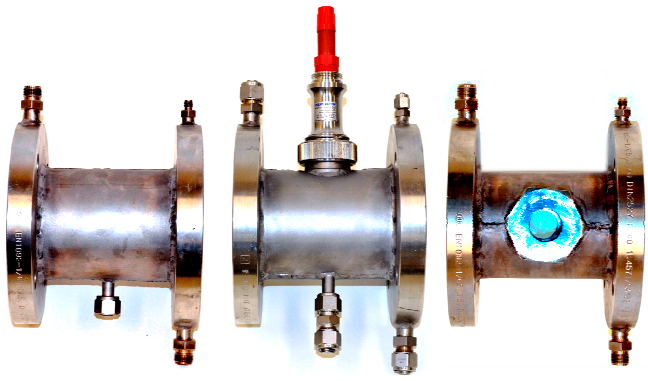

Figure 3.20.: Empty settler module for internal fittings (left), module with conductivity sensor (middle), module with sight glass (right), (Müller et al., 2015a).

"Apart from two end pieces for feeding and removing the substances from the settler, three modules are developed. Firstly, a module is desired in which different internal fittings and coalescence accelerators can be tested. This module mainly consists of flanges, a temperature sensor, and a double shell as a heating jacket. Differently designed internal fittings can be inserted herein. Secondly, a module is required for the conductivity measurement. Similarly to the first module, it features an additional temperature sensor and the double shell. The conductivity probe is inserted in the topside of the module. The third module contains

two mirror-inverted sight glasses to observe the phase separation. Between each of these modules, cylindrical glass segments are used to enhance the observability" (Müller et al., 2015a).

In a 3D model, displayed in Fig. 3.21 of the settler, the inserted internal fitting is sketched. Because the settler can be opened before or after operation, different types of knitted fabrics can be tested. Additionally, the flow of the heating fluid in the heating jacket is displayed. A complete design of the actual settler in the mini-plant is shown in Fig. 3.22.

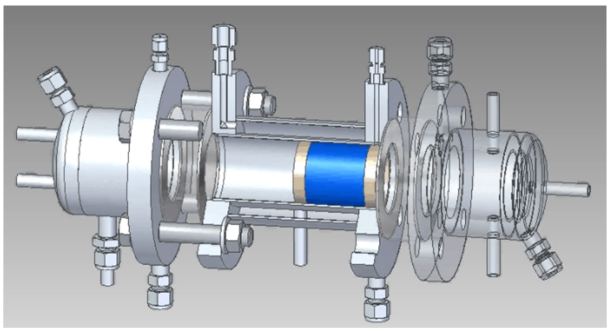

(a) Internal fitting

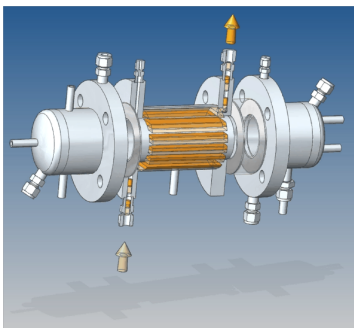

(b) Heating fluid

Figure 3.21.: 3D settler: with internal fitting and heating fluid in the jacket of the settler (Müller et al., 2015a).

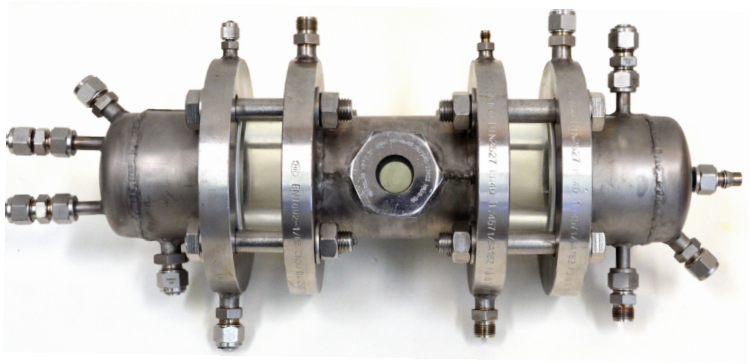

Figure 3.22.: Settler construction with one module containing the two mirror-inverted sight glasses and the two cylindrical glasses (Müller et al., 2015a).

3.3. Process Monitoring and Control

To operate the process the plant is monitored and controlled with a wide range of devices. In this section, the available process monitoring devices, existing control loops, applied analytics, and the general communication scheme of the online-optimization are discussed.

3.3.1. Process Monitoring

The information regarding the process monitoring devices is important, because that way the possible model update is specified. In the plant, different devices are used and connected to the process control system of the plant. Among these are level, temperature, pressure, mass flow, density, and stirring speed.

As shown in the PFID in the appendix of this thesis the plant has seven major units capable of containing a noteworthy liquid hold-up. These are the three feed containers B01, B02, and B03, as well as the reactor C01, the settler X01, the product containter X04, and the product storage tank B04. Of these seven containers the reactor and settler do not have a level sensor. The reason for this is that they are too small and no adequate ATEX-conform sensor that can work at pressures up to 100 bar is implementable here. Therefore, both the reactor and settler have a gauge glass allowing the operator to look into the container if necessary. Therefore sensors LIA01 - LIA03, LICA06, and LIA09 are available. Hereby, the first three are of importance, as they inform the operator when a refilling of the feed tank is required. The sensor LICA06 is relevant for the purging of the product. If enough oil phase has been created and the tank X04 is full or at least half full with oil, then the oil can be purged into the product tank.

Additionally, several temperature sensors are installed throughout the plant. Next to the required temperature sensor in the reactor to control the reaction (TIRC01) and the temperature sensor in the settler to control the phase separation (TIRC02), temperature sensors are installed in several pipes to observe the temperature. The currently applied surfactant Marlipal 24/70 turns solid around 17 °C. The streams need to be warm enough before they are led into the reactor. Therefore, the piping going from B03 to the reactor, from the reactor to the settler, from the settler back to the reactor, and from the settler to the product container, is fitted with electric trace heating. In each of the feed streams temperature sensors have been positioned to observe the temperature of the liquid flowing into the high pressure part of the plant (TI 06 - TI08). Additionally, temperature sensors can be found in the recycle streams (TI04, TI13, TI14) and the product stream as well as the product and surfactant containers themselves (TI05, TI11, TI16).

Thirdly, the pressure is monitored at several different positions in the plant, as different pressure levels are present here. The pressure of the nitrogen for the intertization is measured with PI05. The inert gas is fed to each unit in the plant. The first unit group with an identical pressure level is the set of feed and product containers. Here PIC12 and PIA19 monitor the pressure. Generally, 1 to 3 bar absolute pressure are expected here. Next, B03 and B06 have their own pressure sensor, PIC13. Again, pressures of 1 to 3 bar absolute are expected here. In the high pressure part of the plant, two pressure sensors are present. One is inside the reactor (PIC08) and another in the settler (PICA18). In this section, pressures of up to 100 bar can be measured.

The next devices, which are probably the most vital for the model, are the flow sensors. Each of the feed streams (FIC02 - FIC04) as well as the recycle and product streams (FICA05, FICA08, FIC09, FI07) are fitted with flow sensors. The first three can also measure the density of the streams. Thus, it is possible to observe whether or not the correct liquid is being fed into the system. Additionally, the gas flow into the plant is also monitored via FI01, FFC11, and FI12. These last three sensors are not used for the model currently, but are available once a model modification occurs.

Furthermore, the stirring speed of the surfactant tank and reactor can be controlled via SIRC01 and SIRC02. Because it was observed that foaming can become an issue during the operation of the plant with the surfactant Marlipal 24/70 the stirring speed in the reactor is kept around 700 rpm. At this level, the gassing stirrer does not cause a too strong foaming in the reactor.

Even though a multitude of sensors are present in the plant, only a selection of these can actually be applied later on. Tab. 3.3 shows the relevant process monitoring sensors for updating the model during the online-optimization. There are no redundant measurements in the plant, except for FI06 for the summation of the recycle streams. The measurement

errors are calculated from the information of the individual manufacturer documents. Hereby it is assumed that the operating conditions are at a reactor pressure of 15 bar and a reactor temperature of 368 K. The data for the level sensors is taken from (Endress+Hauser, 2015a) and (Endress+Hauser, 2015b). The calculation information for the temperature sensors is taken from (WIKA, 2015a) and for the pressure sensors from (WIKA, 2015b). The error for the mass flow measurement is obtained via a telephone interview with the company Bronkhorst.

Table 3.3.: Process monitoring: sensors for updating the model.

Sensor name	Sensor type	Unit	Additional description	Error
FIC02	Mass flow	[g/h]	Alkene stream	4.7 %
FIC03	Mass flow	[g/h]	Catalyst solution stream	4.7 %
FIC04	Mass flow	[g/h]	Surfactant stream	4.7 %
FICA05	Mass flow	[g/h]	Recycle stream - water phase	4.7 %
FICA08	Mass flow	[g/h]	Recycle stream - middle phase	4.7 %
FICA09	Mass flow	[g/h]	Recycle stream - oil phase	4.7 %
FI06	Mass flow	[g/h]	Recycle stream - total	4.7 %
FI07	Mass flow	[g/h]	Product stream	1.7 %
TIRC01	Temperature	[°C]	Reactor temperature	0.9 %
TIRC02	Temperature	[°C]	Settler temperature	0.9 %
PIC08	Pressure	[bar]	Reactor pressure	0.5 %
LIA01	Level	[%]	Alkene tank level	6.3 %
LIA02	Level	[%]	Catalyst solution tank level	5.0 %
LIA03	Level	[%]	Surfactant tank level	9.3 %
LICA06	Level	[%]	X04 tank level	12.2 %
LIA09	Level	[%]	B04 tank level	9.3 %

3.3.2. Applied Analytics

The analytics are important for the online-optimization of the process, as they yield information about the current state of the plant and are the main determining factors concerning the recalculation of the optimal solution. Since no single device is able to measure all components participating in the reaction, a multitude of different offline and online analytics are installed to observe the reaction and the quality of the phase separation in the process. Among the offline analytics are two gas chromatographs, an ICP, and a Karl-Fisher titrator. For online measurements a micro gas chromatograph, and a raman spectrometer are installed. In the following, the offline analytics and the online analytics together with their calibration will be discussed.

Gas Chromatography for Liquids: The gas chromatographs are required to identify and analyze the components 1-dodecene, iso-dodecenes, 1-tridecanal, iso-tridecanal, and n-dodecane. The applied column is an Agilent HP-5 column (Crosslinked 5 % PH ME Siloxane) with a film thickness of 0.25 μm, and a length of 30 m. The detector is a flame ionization detector (FID).

The challenge of analyzing the liquid phases of the process, be it product or catalyst phase, is that a phase separation inside the sample takes place. This of course is undesirable during analyses, because drastic errors would occur. Therefore, the samples are mixed with acetone (quality 99.9%). An amount equaling five times the mass of the sample is added. That way a phase separation inside the sample can be avoided. To determine the linear model,

different mixtures containing the substances are prepared for each gas chromatograph. The compositions of these mixtures are displayed in Tab. 3.4 and Tab. 3.5.

Table 3.4.: Mixtures prepared for calibrating the first gas chromatograph.

Probe [Nr.]	1-dodecene [wt.-%]	1-tridecanal [wt.-%]	n-dodecane [wt.-%]	Marlipal 24/70 [wt.-%]	Acetone [wt.-%]
1	14.702	0.000	0.000	1.935	83.363
2	14.566	0.317	0.070	1.783	83.263
3	14.119	0.691	0.186	1.659	83.344
4	13.435	1.267	0.298	1.648	83.353
5	13.032	1.609	0.432	1.524	83.403
6	12.324	2.187	0.573	1.497	83.419
7	11.722	2.882	0.714	1.369	83.312
8	10.965	3.325	0.849	1.234	83.626
9	9.924	4.429	0.988	1.327	83.332
10	9.923	4.883	1.076	0.769	83.350
11	9.191	5.696	1.170	0.601	83.343

For the actual calibration, the amount of acetone, which is inert for our purposes, is not included in the concentration determination. In Fig. 3.23 and Fig. 3.24 the calibration curves for the substances 1-dodecene and 1-tridecanal are shown. It is assumed that the response factor for the iso-dodecene peaks are similar to 1-dodecene and for iso-tridecanal are similar to 1-tridecanal. A separate calibration for these substances is therefore not carried out.

The accuracy of the models are reasonably high leading to a coefficient of determination of 0.9925 for 1-dodecene, 0.9999 for 1-tridecanal, and 0.9984 for n-dodecane. For the surfactant Marlipal 24/70 no reasonable calibration is possible with the gas chromatographs with the currently available columns (the peaks are strongly smudged).

Inductively Coupled Plasma - mass spectrometry: Of great interest for the economic assessment of the process is the measurement of catalyst and ligand loss during the operation of the plant. Since it is not possible to measure the concentrations of the catalyst or the ligand with the available gas chromatographs, another analytic method is required. For this purpose, inductively coupled plasma mass spectrometry (ICP-MS) is used. Neither the catalyst precursor nor the ligand are directly measurable with the the ICP-MS. Instead, rhodium and sulfur are visible. Since the amount of rhodium in a precursor molecule and the amount of phosphorus in a ligand molecule are known, the measured values of rhodium and

Table 3.5.: Mixtures prepared for calibrating the first gas chromatograph.

Probe [Nr.]	1-dodecene [wt.-%]	1-tridecanal [wt.-%]	n-dodecane [wt.-%]	Marlipal 24/70 [wt.-%]	Acetone [wt.-%]
1	16.620	0.000	0.000	0.000	83.380
2	10.739	4.592	0.724	0.624	83.321
3	9.618	4.278	1.369	1.426	83.309
4	8.261	3.865	2.278	2.252	83.344
5	6.845	3.263	3.317	3.368	83.207
6	4.865	2.690	4.515	4.595	83.334
7	2.791	2.063	5.890	5.811	83.444
8	1.833	0.970	6.835	6.851	83.512

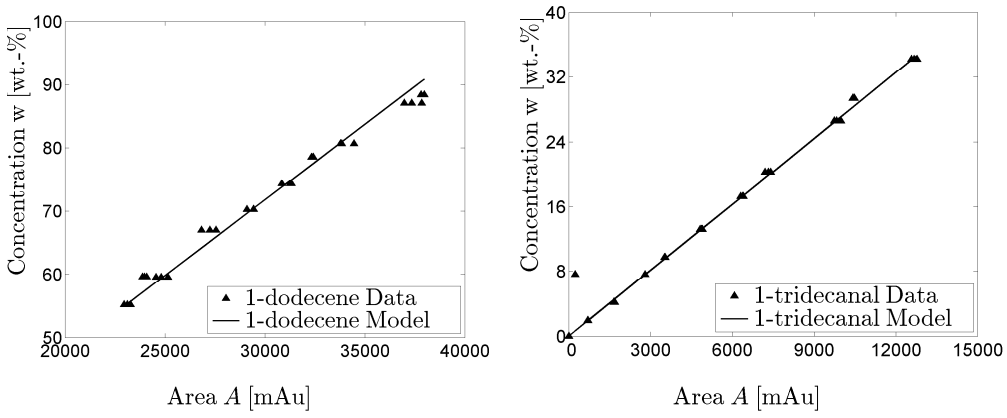

(a) 1-dodecene (b) 1-tridecanal

Figure 3.23.: Calibration curves of the liquids in the first offline gas chromatograph.

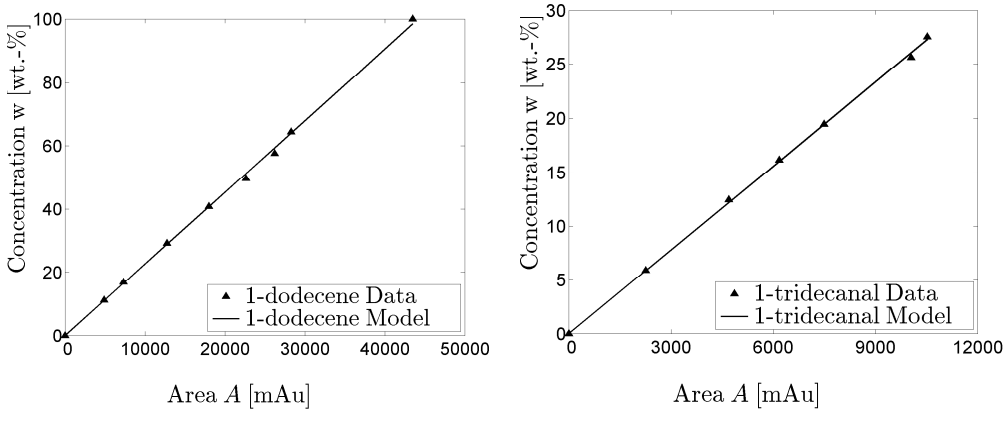

(a) 1-dodecene (b) 1-tridecanal

Figure 3.24.: Calibration curves of the liquids in the second offline gas chromatograph.

sulfur can directly be correlated to the precursor and the ligand. The offline measurements performed during the operation of the plant are carried out by the Department of Chemistry at Technische Universität Berlin.

Gas chromatrography for gases: In order to measure the gas composition in the reactor, a micro gas chromatograph (micro-GC) from the company *Agilent* and ATEX-modified by *Analytical Solutions and Products B.V. - ASAP* is installed. With this chromatrograph, the concentrations of hydrogen, carbon monoxide, oxygen and nitrogen are measurable. The micro-GC is of the model 490-GC and is certified for an ATEX Zone 2. It has a molsieve 5Å column, which is capable of analyzing the target components H_2, N_2, O_2, CH_4, and CO. As a carrier gas argon is used. The measuring time is roughly 3 minutes and the results are sent directly to the process control system of the mini-plant.

Gas in the plant can be measured from two points: the reactor and the product container. From these two points, the gas is led to a pressure regulator, to guarantee a constant inlet pressure for the micro-GC. Furthermore, the micro-GC is thus protected from sudden pressure leaps. Afterwards, the gas is led into a condensation trap to remove water. The presence of water during a micro-GC measurement can heavily distort the result.

The micro-GC is calibrated in three stages and for each stage the adsorption peaks and retention times are noted. First, the mini-plant is flooded with synthetic air with a concentration of 80% nitrogen and 20% oxygen. The mini-plant is then evacuated and repeatedly flooded with nitrogen to enable a 100% nitrogen atmosphere. At this point, another measurement is performed. Afterwards, carbon monoxide and hydrogen are let into the mini-plant. A fixed concentration of 50:50 CO to H_2 is used. Again, the measurement of the adsorption peaks and retention times is carried out. Each measurement is performed six times, to guarantee accuracy and repeatability of the measurements. The mean of the six adsorption peaks for each component is then used for the calibration information.

Raman Spectrometry: Since online-optimization is to be performed, a fast and accurate method to analyze the composition of the liquids is required. For this purpose, a Raman spectrometer is installed in the plant at the product drain of the settler. The spectrometer is borrowed from the Federal Institute for Materials Research and Testing (Bundesanstalt für Materialforschung und -prüfung BAM) and is calibrated with the assistance of the Process Analytics Group.

The analytic method measures the inelastic scattering of monochromatic light. A laser light, usually near close to the infrared or ultraviolet range, interacts with the molecules, leading to an energy shift of the laser photons. The positive aspects of Raman spectrometry are, that measurements can be carried out in situ and within less than 30 seconds. The accuracy of these measurements is adequate. Differing from the offline gas chromatograph measurements, the applied Raman spectrometer is not capable of measuring the isomers iso-dodecene and iso-tridecanal. For operating the process and for online-optimization this is acceptable though, because an accumulation of these components has not been observed. The calibration of the Raman spectrometer is performed based on offline GC measurements and online Raman spectra. Results will be presented in Chapter 6.

3.3.3. Communication and Optimization Structure

The implementation of the online-optimization scheme is discussed in this section. The general idea how the communication between each of the participants in the online-optimization works is displayed in Fig. 3.25. The communication between several different participants

needs to be realized: Computer 1 for the optimization, Computer 2 with the process control system of the plant, and the plant itself with its sensors and actuators. Between these different participants, the information needs to be stored, transferred, and processed.

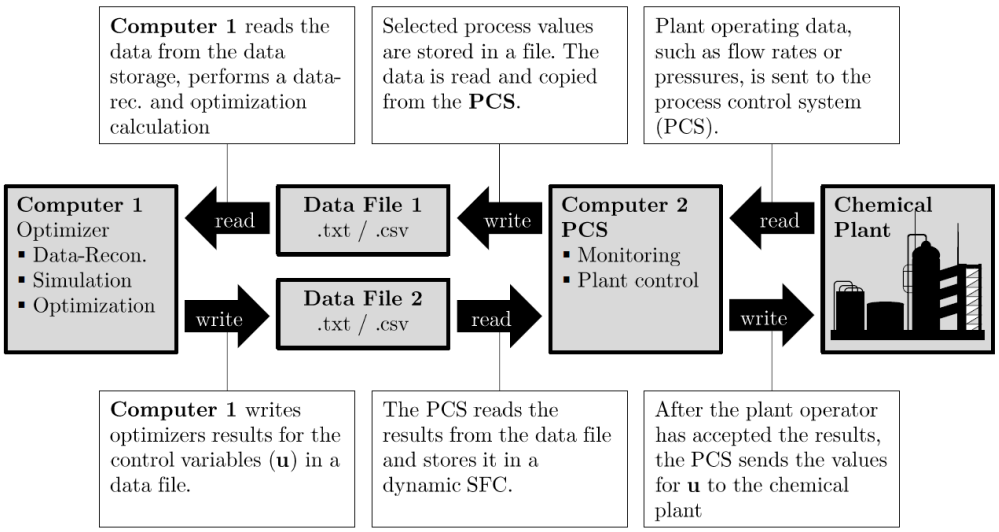

Figure 3.25.: General information exchange between the process model, the process control system, and the chemical plant. Core step in the communication scheme is the upload of information (result of the optimizer) into the process control system and the storage of this information in the dynamic sequential function chart (SFC).

A more detailed communication scheme[2] for the hydroformylation plant is displayed in Fig. 3.26.

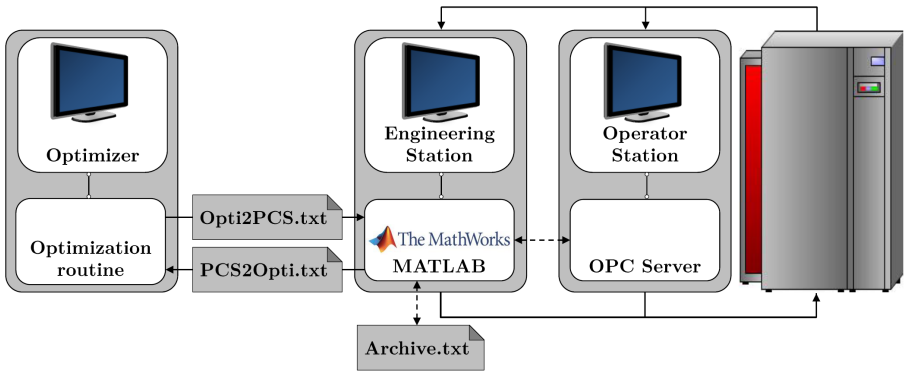

Figure 3.26.: Information exchange between the process model, the process control system, and the chemical plant. The MathWorks logo is taken from http://de.mathworks.com/ [Date: 02.01.2015].

Communication needs to be established between the following actors:

- hydroformylation plant $\rightleftarrows$ peripheral devices,
- peripheral devices $\rightleftarrows$ engineering station,

[2]The following communication scheme has been developed during the supervision of Mr. Alexander Fleck's Master's Thesis.

- peripheral devices ⇄ operator station client,
- engineering station ⇄ operator station, and
- engineering station ⇄ optimizer.

Plant and Process Control System: The first required communication is the connection of the plant with the process control system. All signals from the sensors and actuators of the plant are connected to the control cabinet to the *Automation Station* (AS) (SIMATIC 400 CPU) along the *Profibus*. From the AS, the information is sent to the engineering and operator stations (ES and OS) via an ethernet cable, the *Plantbus*. The *Terminalbus* is an ethernet network that connects the engineering station with all operator clients and servers. This network communication to the various stations is displayed in Fig. 3.27.

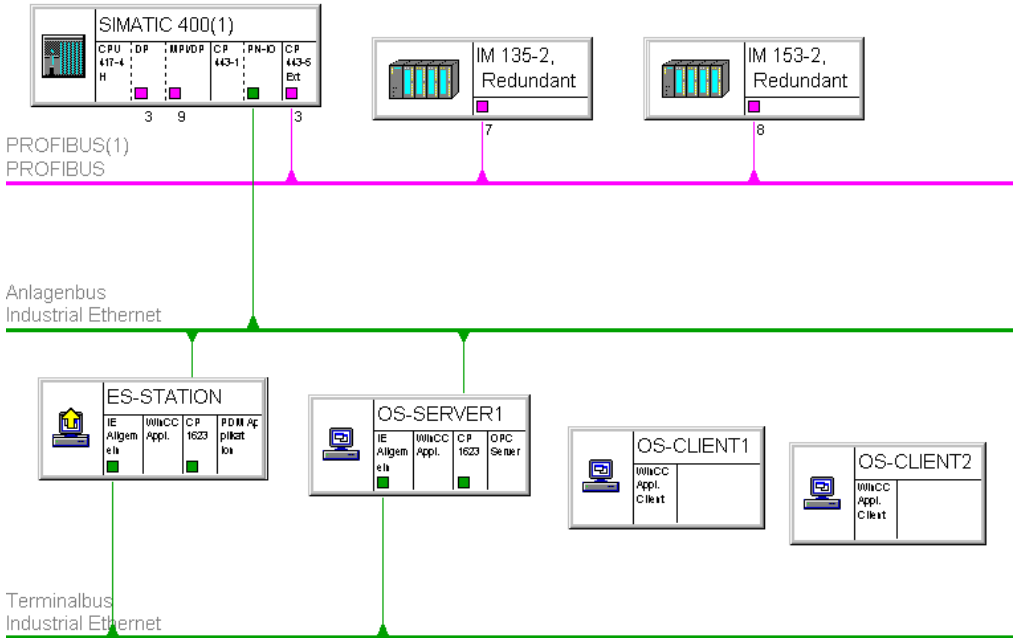

Figure 3.27.: Network configuration for the communication between the plant and engineering station.

Process Control System and Optimizer: The next communication step is acquiring the data sets from the process control system and transferring it to the computer, on which the model and the optimizer is located. For this purpose, a MATLAB script is used to continuously access and store the data set defining the current state of the chemical plant from the OPC-Server. This script accesses the set and stores it in a .txt file. This is the *Archive.txt* shown in Fig. 3.26. When the user desires to perform online optimization, the next step is is performed. Another .txt file is created called PCS2Opti.txt (Process Control System to Optimizer), which is also created with a MATLAB script. In order to send this file to the optimizer, an FTP server is used on another computer. The reason for this is that the process control system of the plant is fully isolated from the internet, to avoid external access. In Fig. 3.28 this communication is shown.

On the computer, where the model of process is stored, the data set is imported to thus present the starting values for the simulation and consecutive optimization calculation. On this computer a simulation for a time span of two process hours is carried out. Using this

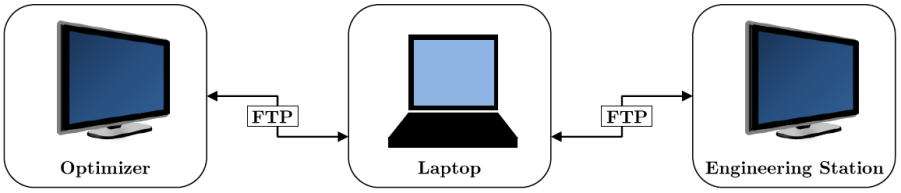

Figure 3.28.: Communication between process control system and optimizer.

information from the simulation the process is optimized regarding a user-defined objective function. Hereby, values for the set-points of the control variables (u) are determined. The manipulable variables of the process are:

- the flow rates controlled by the three feed pumps,
- the temperature of the reactor,
- the temperature of the settler,
- the flow rates of the three recycle pumps, and
- the opening of the control valve for CO/H_2.

The time steps for changing the setpoints are variable for the optimizer. A matrix consisting of 8 x N_u is obtained, whereby N_u is the number of manipulable variables. The columns of the matrix are the time steps and the rows of the matrix the set-points of the manipulable variables. This matrix is stored in the .txt file called Opti2PCS.txt shown in Fig. 3.26 and is then sent to the process control system via the FTP-Server on the laptop.

Process Control System and Plant: The Opti2PCS.txt file containing the matrix is imported into the process control system automatically via MATLAB. The visualization of the results starts with a table consisting of 13 columns. Fig. 3.29 shows the imported set-point matrix in the process control system. As an example, the set-points for the three feed pumps monitored via FIC02, FIC03, and FIC04 as well as the recycle pump P06 are displayed.

On / Off	Control	g/h / %	300	1200	150	300	200	150	100	1200
☑	FIC02	☑	500	750	0	0	250	250	100	100
		☐	33,33	50,00	0,00	0,00	16,66	33,33	6,66	6,66
☑	FIC03	☑	500	500	0	0	100	250	0	0
		☐	100,00	100,00	0,00	0,00	20,00	50,00	0,00	0,00
☑	FIC04	☐	50	50	0	0	0	50	0	0
		☑	40,00	40,00	0,00	0,00	0,00	40,00	0,00	0,00
☐	P06	☐	0	0	0	0	300	300	300	300
		☐	0,00	0,00	0,00	0,00	25,00	25,00	25,00	25,00

Figure 3.29.: Example of the set-point matrix in the process control system.

At this point, the operator has the opportunity to analyze the set-point-values and decide, if these should be implemented into the process or not. Thus, entire rows can be excluded, if the results are illogical. On the left hand side the operator has the choice to activate or deactivate the determined set-point for a certain actuator. This is achieved by checking or

unchecking the box in the column **On / Off**. The description of the actuator is in the column **Control** to the right of the column **On / Off**. For the case of the pumps, the operator has the choice to use the optimizer's results in **g/h** or in **%** of the maximum frequency of the pumps. This can become important if the control parameters of the actuator are not tuned for a certain set-point. Depending on which result the operator selects, the not-selected one is grayed out. Taking a closer look at Fig. 3.29 these different selection possibilities are shown. The actuator FIC02 and FIC03 are on and operated by controlling the **g/h** of the stream. The actuator FIC04 on the other hand is also on, but operated by **%** of the frequency of the pump. Finally, as an example, the results of P06 are not used, which again is visualized by the grayed out results.

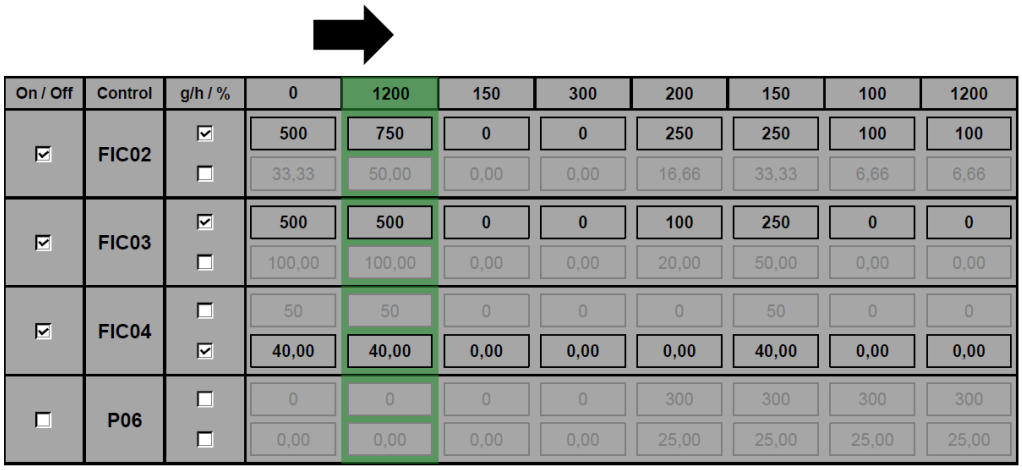

Figure 3.30.: Activation of the second time step of the set-point matrix.

Furthermore, the operator has the possibility to change the values in the matrix, if deviating set-points are desired. If a value above the maximum value of the set-point is entered, this value is automatically reduced to the allowed maximum. Once the operator has accepted the set-points, the first set is sent to the process units, such as pumps or thermostats, in the plant. Above the set-point values is the time for each interval. These time intervals are determined by the optimizer as optimal time segments for the control. Fig. 3.29 starts with 300 seconds for the first time interval. The active time interval is highlighted by the green background of the set-points. The remaining time for the time segment is displayed above the set-points. After the time runs out, the next time segment is started. Fig. 3.30 shows this switch, as the second interval with 1200 seconds is started (dark background behind 1200). Instead of constant controls for the time intervals, ramps can also be operated. This may be the case for units which require a certain temperature control. The controllers within PCS7 would therefore operate a ramp using the current set-point value and the value in the next interval. Thus, smooth controls may be implemented if necessary.

Optimization Framework and Optimizer: The data sent from the process control system contains information regarding the controls used in the last hours of operation as well as the measured concentrations. Fig. 3.31 displays the time frame in which the optimization and implementation of results takes place.

Firstly, an implementation of the first optimization trajectory in time frame of $t = t_0 +$ [04] h is performed. Every hour, a sample of the concentrations in the reactor is taken. It takes roughly 0.5 to 1 h to prepare and analyze these samples. After two hours of operation, a simulation of the process for the time frame $t = t_0 +$[08] h is performed. For the time frame

$t = t_0 + [02]$ h, controls have been implemented and concentrations have been measured. For the time frame $t = t_0 + [24]$ h on the other hand, only optimization results exist. For $t = t_0 + [48]$ h, constant controls are used. The duration of this simulation takes roughly 0.5 h. The results are used as starting values for the optimization, which is carried out after 2.5 h of operation. The computation duration is roughly 0.5 h. Additionally, a computation buffer time of 1 h is added, in case the optimization takes longer. A trajectory is determined for a duration of up to eight hours. As soon as the result is there, the second optimization trajectory can be implemented into the process for the time frame $t = t_0 + [48]$ h. If the optimization is available sooner than after four hours, it can immediately be implemented into the process.

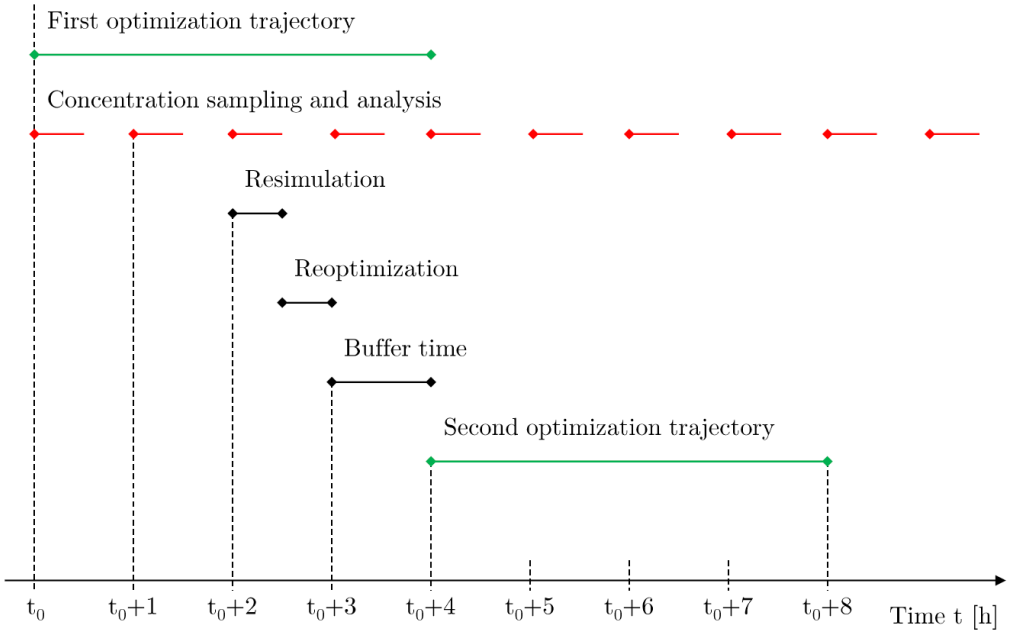

Figure 3.31.: Optimization time frame. The figure is adapted from (Müller et al., 2014e).

An implementation scheme of the actual optimization to determine the trajectories under uncertainty is presented and discussed in (Müller et al., 2015b). This general solution approach for the applied chance-constrained optimization in this thesis can be divided into six steps. For these six steps, the three layers already discussed in Section 2.4 are defined: The optimization layer, the integration layer, and the simulation layer.

Firstly, in **Step 1**, the controls u from the optimizer are sent to the Chance Constraint Evaluator (CC Evaluator). Within this thesis, the CC Evaluator is the dynamically optimized chance constraint evaluator, also known as the DoCCE. In the second step, the information is used in the DoCCE to perform a sparse-grid sampling of the uncertain parameters ξ. Here, different settings can be made by the user. Among these are "the grid width (e.g. 3σ), the grid resolution (number of samples within width), as well as the grid depth of the sample" (Müller et al., 2015b).

In the third step, the controls, as well as the defined samples of ξ are sent to the solver, which also contains the process model. Here, using the given controls and parameters ξ, the solver discretizes the DAE into an AE and solves the model. As a result, the sensitivity matrix of the states regarding the controls is determined. For the calculation of the probability of constraint adherence, further information is required: the sensitivity of the states regarding the parameters ξ as well as the sensitivity of the states regarding the controls u.

These are determined in **Step 4** and are sent back to the DoCCE. In **Step 5**, the probability Pr of adhering to the constraints is calculated. The solution to the so-called root-finding problem, in which the boundary of ξ is found, thus determining the course of the constraints h. In the last step the optimizer obtains three sets of information:

1. the probability of adhering to the constraints,
2. the sensitivity of the probability regarding the controls, and
3. the second derivative of the sensitivity regarding the controls.

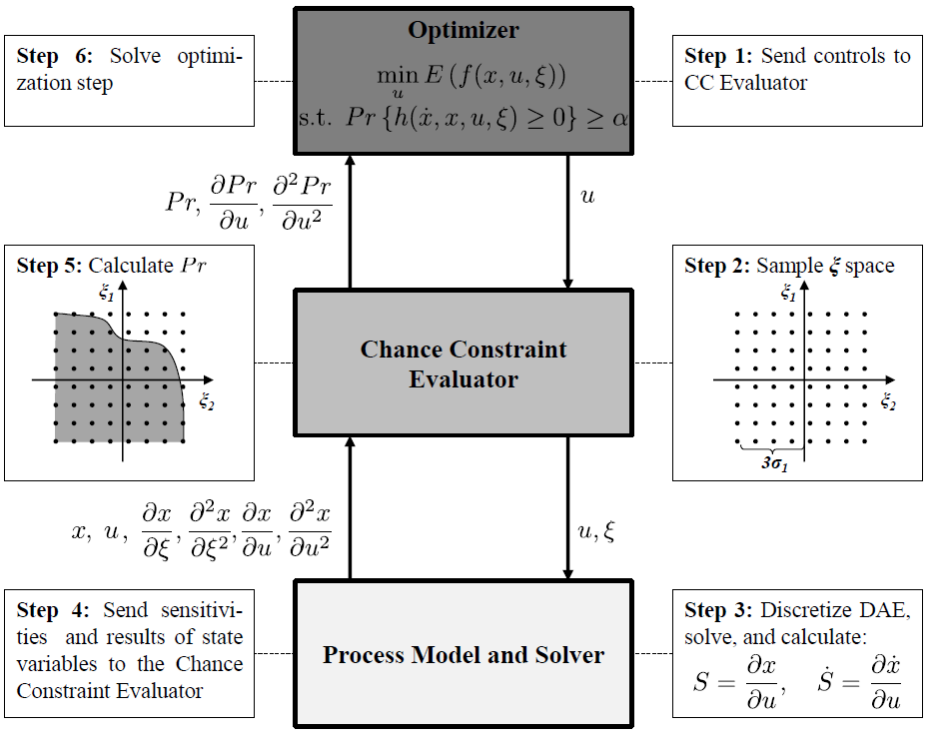

Figure 3.32.: Chance-constrained optimization structure. Figure is adapted from (Müller et al., 2015b).

Just as in (Müller et al., 2015b), the optimization problem is implemented in Python using a framework for the chance constraint calculation presented in (Wendt et al., 2002) and (Werk et al., 2012). Ipopt by (Wächter and Biegler, 2006) is used as an NLP solver and the sDACl developed by (Barz et al., 2011) for the solution of the DAE and determination of the desired gradients using UMFPACK described in (Davis, 2004). The exact set-up of the communication between each of the parts, which results are sent to which level, and how critical issues such as infeasible solutions or result recycle are handled, are more closely discussed (Esche, 2015).

Chapter 4.

Mini-plant Model Development

This chapter focuses on modeling the mini-plant at Technische Universität Berlin. The model is set up in the web-based modeling environment MOSAIC from (Kuntsche et al., 2009, 2010, 2011). That way, a fast export to any desired modeling environment such as AspenPlus, MATLAB, or C++ is possible. Concerning the hydroformylation mini-plant, it is important that the model is capable of representing several different operating phases or conditions of the plant. In particular, the phases ranging from the start-up of the process, to the process stabilization phase, and finally to the continuous operation are of interest. For this purpose, a systematic approach is selected. Firstly, based on the P&ID shown in the appendix the vital units and streams in the plant are selected. Each of these vital units (including both gas and liquid hold-ups) as well as the vital streams in the plant numbered. The hereby developed model scheme is shown in Fig. 4.1. All in all, the model consists of 23 units and hold-ups, 25 streams, and 12 components. A description of each of these units u can be found in Tab. 4.1 and a list of all components i applied in the model is presented in Tab. 4.2.

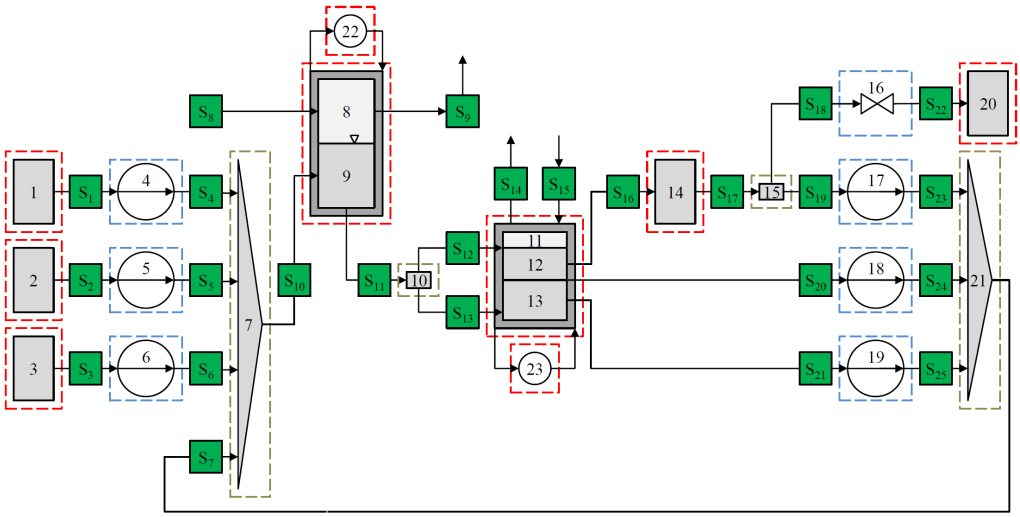

Figure 4.1.: General model scheme of the hydroformylation mini-plant at Technische Universität Berlin.

To explain the model, the scheme from Fig. 4.1 is divided into 4 sections: feed, reaction, separation, and recycle. For each of these listed sections, the systematic approach for modeling the mini-plant structures equations in the form of the MESH approach:

- Mass balances
- Equilibrium equations

- Summation equations
- Energy balances
- Momentum balances

Hereby, not all equations from the MESH approach are used, since the focus here lies on designing a model for real-time optimization. Therefore, unnecessary equations are left out. On the other hand, several auxiliary equations, such as gas solubilities or triggering functions needed to model certain effects or phenomena are required. These auxiliary equations are discussed in the final section in this chapter.

Table 4.1.: Units in the model scheme of the mini-plant.

Unit Index u	Unit description	Section
1	Feed tank containing 1-dodecene	Feed
2	Feed tank containing the catalyst solution	Feed
3	Feed tank containing the surfactant	Feed
4	Feed pump for 1-dodecene	Feed
5	Feed pump for the catalyst solution	Feed
6	Feed pump for the surfactant	Feed
7	Mixer for the feed streams	Feed
8	Reactor - gas phase	Reaction
9	Reactor - liquid phase	Reaction
10	Settler - "Water-Oil" Splitter	Separation
11	Settler - gas phase	Separation
12	Settler - oil phase	Separation
13	Settler - mixed phase	Separation
14	Buffer tank for the oil phase	Recycle
15	Splitter for recycle and product stream	Recycle
16	Valve for product stream	Recycle
17	Recycle pump for oil stream	Recycle
18	Recycle pump for mixed stream	Recycle
19	Recycle pump for catalyst stream	Recycle
20	Storage tank for the product	Recycle
21	Mixer for the recycle streams	Recycle
22	Heat exchanger for the reactor	Reaction
23	Heat exchanger for the settler	Separation

Furthermore, certain general equations exist, which are used in all sections. These are displayed here. The first is concerned with the liquid hold-up HU in the unit u. The liquid hold-up in the reactor, settler, or tank is equal to the sum of the component hold-ups in the respective reactor, settler, or tank:

$$HU_u^L = \sum_{i=1}^{Ni} HU_{u,i}^L \tag{4.1}$$

This equation is of course only relevant for the units in the process that contain a hold-up. Next, the component mass flows (Eq. (4.2)) in reformulated form including the summation

Table 4.2.: Component index i

Index i	Component	Description
1	1-dodecene	Reactant
2	Iso-dodecene	Reactant
3	Iso-tridecanal	Byproduct
4	n-dodecane	Byproduct
5	1-tridecanal	Product
6	Hydrogen (H_2)	Reactant gas
7	Carbon monoxide (CO)	Reactant gas
8	Nitrogen (N_2)	Inert gas
9	Water (H_2O)	Catalyst solvent
10	Rhacac$(CO)_2$	Catalyst precursor
11	SulfoXantPhos	Catalyst Ligand
12	Marlipal 24/70	Surfactant

equations are given (Eq. 4.3):

$$w_{s,i} \cdot F_s = F_{s,i} \tag{4.2}$$

$$\sum_{i=1}^{Ni} F_{s,i} = F_s \tag{4.3}$$

In Eq. 4.2 w stands for the mass fraction of component i given in g/g of stream s, F for the stream in g/s.

4.1. Mini-plant Section 1: Feed Section

The first section in the mini-plant model is the liquid feed section. It consists of the three containers for the liquids (units 1 to 3), the feed pumps (units 4 to 6), and the mixer of the feed and recycle streams (unit 7). Fig. 4.2 shows the model scheme for the feed section. Streams one (S_1) to three (S_3) are the liquid streams leaving the feed containers. These are fed to the mixer as streams four (S_4) to six (S_6). Additionally, a stream from the recycle section, stream seven (S_7), is fed to the mixer as well. The entire mixture leaves the mixer as stream ten (S_{10}).

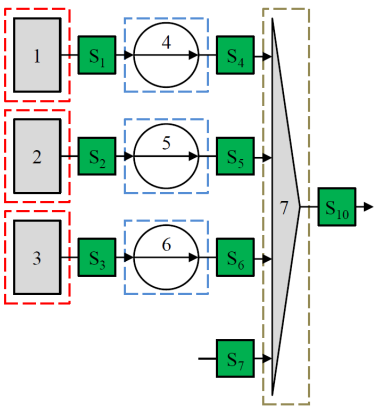

Figure 4.2.: Model scheme of the feed section of the hydroformylation mini-plant at Technische Universität Berlin.

Following the MESH systematic, the first step is the formulation of the hold-up equations. The hold-up for each of the containers can be defined with

$$HU_u^L \cdot \sum_{i=1}^{Ni} \frac{w_{s,i}}{\rho_i} = A_u \cdot L_u \tag{4.4}$$

HU_u^L represents the liquid hold-up L in the unit u, A_u is the area and L_u height of the unit u. The remaining two variables are $w_{s,i}$, the mass fraction of component i in stream s given in g/g and ρ_i is the density of component i. Thus, the mass balance for each of the containers can now be formulated:

$$\frac{dHU_u^L(t)}{dt} = -F_s \quad \text{for } u, s = \{1...3\} \tag{4.5}$$

The mass balances for the pumps (Eq. 4.6) and the mixer (Eq. 4.7) obviously do not contain a hold-up term. These can be written as:

$$F_{s,i} = F_{s+3,i} \quad \text{for } s = \{1...3\} \text{ and} \tag{4.6}$$

$$F_{s=10,i} = F_{s=4,i} + F_{s=5,i} + F_{s=6,i} + F_{s=7,i} \tag{4.7}$$

F_s is the total mass flow and $F_{s,i}$ the component mass flow. For all other streams, the component mass flows and summations are formulated in the same manner. Additionally, specific feeding equations are implemented, to control the process. These equations are mainly relevant for the feed pumps:

$$F_{s=4} = F_{s=4}^{SP} \tag{4.8}$$

$$F_{s=5} = F_{s=5}^{SP} \cdot (1 - TRIG_{Settler}^{Lvl}) \tag{4.9}$$

$$F_{s=6} = F_{s=6}^{SP} \cdot (1 - TRIG_{Settler}^{Lvl}) \tag{4.10}$$

The superscript SP stands for set-point. The set-point of these streams is to be calculated during the optimization using this model. The set-point variable thus represents a manipulable variable or decision for the optimization. The term $TRIG_{Settler}^{Lvl}$ is a triggering function used to initiate or terminate the feeding into the system via the according pump. In this case the feeding is carried out until the level in the settler has reached a critical value. A detailed discussion on the exact formulation of this triggering function as well as the applied critical value can be found in the modeling section with the auxiliary equations.

In this section, no other equations such as equilibrium or heat equations are required. Therefore, the modeling of the reaction section, is carried out.

4.2. Mini-plant Section 2: Reaction Section

Core section in the mini-plant is the reactor itself. Fig. 4.3 shows the section in greater detail. Basically, it consists of the reactor with two hold-ups, one for the gas and one for the liquid phase. Stream eight (S_8) is the incoming gas stream of syngas (CO & H_2, 1:1 vol.-%). The gas that is not used in the reaction leaves the reactor as stream nine (S_9). Stream ten (S_{10}) is the incoming liquid stream consisting of the mixture that has left the feed section. Stream eleven (S_{11}) is the liquid mixture leaving the reactor.

Before beginning with the modeling of the reaction section, some reaction-specific background information is given. Then, the details on the reaction parameter fitting are discussed. This is brought in connection with the framework for selecting relevant uncertain

parameters for optimization under uncertainty presented in section 2.3.3. Then, the MESH equations are presented followed by required auxiliaries.

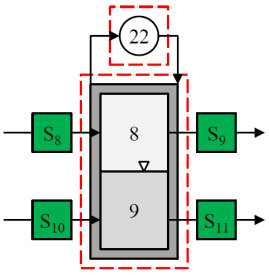

Figure 4.3.: Model scheme of the reaction section of the hydroformylation mini-plant at Technische Universität Berlin.

4.2.1. Reaction-specific Background Information

In the sub-project **A3** of the *Collaborative Research Center InPROMPT*, the reaction network of the hydroformylation network has been investigated extensively (Hamel et al., 2012) (Kiedorf et al., 2014). "It is well known that side reactions like isomerization and hydrogenation of 1-dodecene and its isomers occur during the process. Furthermore, side- or subsequent reactions leading to adols, alcohols, and acids may occur. However, since the latter side reactions have not been observed during the preliminary experiments [of **A3**], they are not considered" (Müller et al., 2014f). This network is displayed in Fig. 4.4, in which a total of six possible reactions can occur.

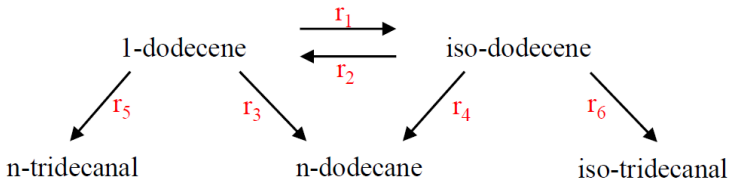

Figure 4.4.: Simplified hydroformylation reaction network.

The first reaction is the isomerization of 1-dodecene to iso-dodecene. Hereby, all isomers of dodecene are summed-up to iso-dodecene. From a modeling perspective, the reverse isomerization reaction is viewed as a second reaction (4.2). Reactions three and four are the hydrogenation of dodecene and iso-dodecene to dodecane (4.3 & 4.4). The fifth reaction is the desired hydroformylation reaction, in which the product 1-tridecanal is created from 1-dodecene (4.5). Reaction six represents the creation of iso-tridecanal from iso-dodecene (4.6). A seventh reaction, the direct creation of iso-tridecanal from 1-dodecene, is not considered.

$$\text{n}-\text{Dodecene} \longrightarrow \text{iso}-\text{Dodecene} \quad \{4.1\}$$

$$\text{iso}-\text{Dodecene} \longrightarrow \text{n}-\text{Dodecene} \quad \{4.2\}$$

$$\text{n}-\text{Dodecene} + \text{H}_2 \longrightarrow \text{n}-\text{Dodecane} \quad \{4.3\}$$

$$\text{iso}-\text{Dodecene} + \text{H}_2 \longrightarrow \text{n}-\text{Dodecane} \quad \{4.4\}$$

$$\text{n}-\text{Dodecene} + \text{CO} + \text{H}_2 \longrightarrow \text{n}-\text{Tridecanal} \quad \{4.5\}$$

$$\text{iso}-\text{Dodecene} + \text{CO} + \text{H}_2 \longrightarrow \text{iso}-\text{Tridecanal} \quad \{4.6\}$$

The experiments are planned and carried out together with the researchers from subproject **A2** of the *Collaborative Research Center InPROMPT*. The temperature range of interest lies between 75 °C and 95 °C and the pressure range between 15 and 40 bar. This temperature range is determined based on results from preliminary experiments. Here it was discovered that a maximum reaction rate can be achieved in the three phase region. For the surfacant Marlipal 24/70 this three phase region is very small and lies around 85 °C for a starting composition of the reaction mixture of $\alpha = 50$ %, $\gamma = 8$ %, and $X = 0$ %. The pressure range is selected, because a certain pressure is required for syngas to be dissolved in 1-dodecene and water. If the pressure is too high though, an inhibition of the catalyst occurs. Here, the ligand no longer attaches to the precursor, but carbon monoxide takes its place instead, thus turning the catalyst into an undesired complex.

The desired catalyst concentration in the reactor is 300 ppm for the precursor and 4500 ppm for the ligand. As an example for the reaction results, Fig. 4.5 displays the reactant amounts at 15 bar and 95 °C for a performed hydroformylation reaction.

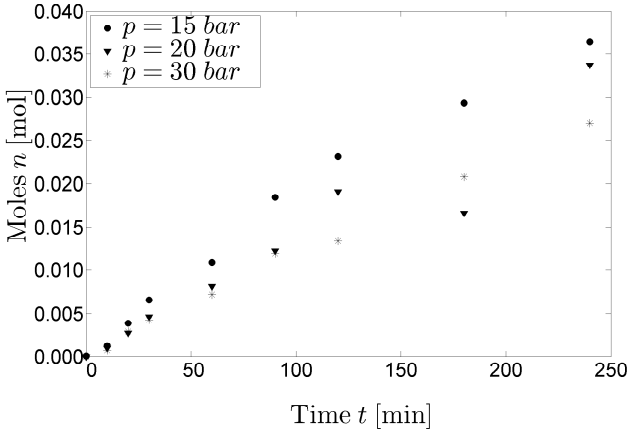

Figure 4.5.: Hydroformylation reaction at 15 bar and 95 °C.

In total, nine experiments are performed to analyze the temperature and pressure dependence of the system. In Fig. 4.6 the temperature dependence of the system is shown. The focus lies on the production of the desired product 1-tridecanal. It becomes obvious that a clear temperature dependence exists, whereby the largest molar amount of 1-tridecanal is reached at the highest temperature of 95 °C. The reason for this is the increased reaction rate at higher temperatures. At this point in time, the reaction rates at even higher temperatures were not systematically analyzed yet. Regarding pressure change no significant dependence can be observed.

For further calculations it is assumed at this point that the reaction is carried out as a pseudo-homogeneous reaction. From a microscopic point of view, the system is not homogeneous, because the phase separation is constantly taking place. From a macroscopic point of view though, the system is homogeneous, especially if

- the surfactant concentration is above the critical micelle concentration so that the surface tension between water and oil is reduced and
- if the stirring speed of the stirrer in the reactor is high enough.

For our application, a surfactant concentration in the range of 8 to 10 wt.-% is used. As mentioned by Hamerla et al. (2013a), above 8 wt.-%, the macroscopic surface tension of

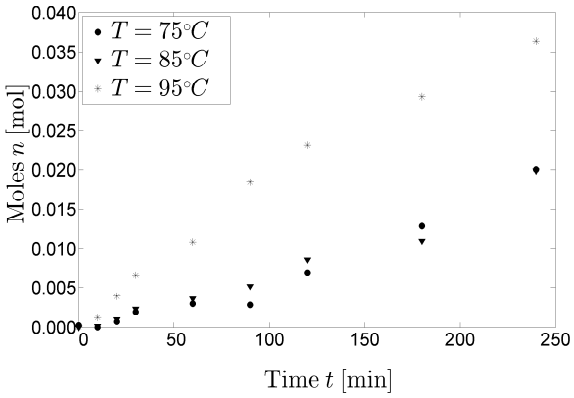

(a) Pressure = 15 bar.

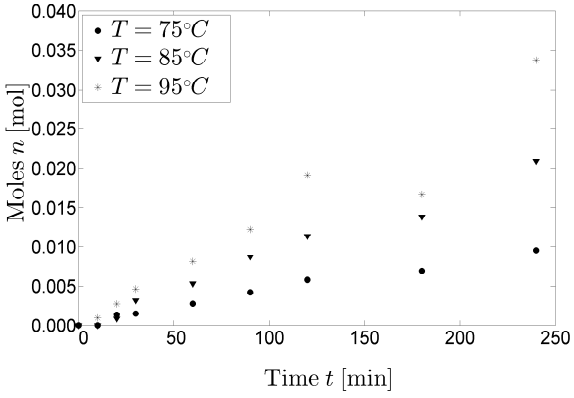

(b) Pressure = 20 bar.

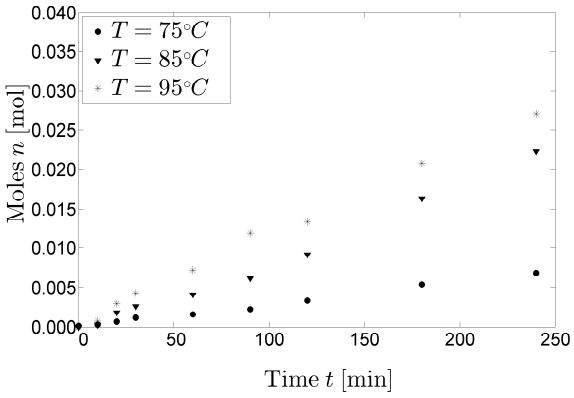

(c) Pressure = 30 bar.

Figure 4.6.: Temperature dependence of the reaction in micellar systems for different pressures. This presented experimental data set stems from Tobias Hamerla, Technische Universität Berlin, Department of Chemistry.

the mixed phase is greatly reduced in comparison to a binary system of water and oil, thus allowing for an enhanced mass transport. Additionally, Hamerla et al. (2013a) look at the influence of stirring speed on the micellar system. It is shown that for a four-bladed gassing stirrer, a stirring speed of 1200 rpm is optimal regarding the reaction rate. Above a stirring speed of 500 rpm adequate reaction rates are already observable. This result is underlined with an endoscopic image of the stirred system at 300 and 400 rpm. In Fig 4.7, taken from (Hamerla et al., 2013a), the oil-in water droplets are visible. Obviously, the faster the stirring is done, the more disperse the system becomes.

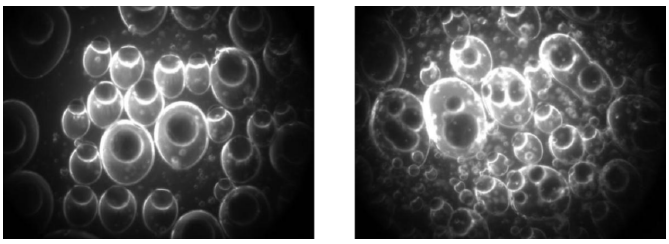

(a) 300 rpm. (b) 400 rpm.

Figure 4.7.: Endoscopic image of micellar media being stirred (Hamerla et al., 2013a).

To underline the assumption of a homogeneous reaction on a macroscopic scale, two photos of a glass autoclave are shown in Fig 4.8. In both cases the glass autoclave contains a system consisting of 8 wt.-% surfactant and a water to oil ratio of 50 %. It can clearly be seen that the mixture is homogeneous. The difference between the two photos is that the left one is being stirred at 1100 rpm and the right one is not being stirred at all. For the case of the photo on the right an ill-suited temperature is chosen. Even after 10 minutes of resting, the separation is extremely slow and no phases are visible.

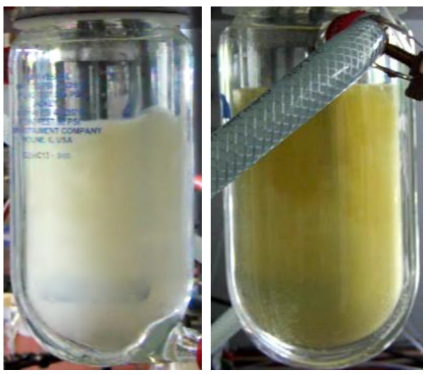

Figure 4.8.: Macroscopic homogeneity of micellar media consisting of 8 wt.-% surfactant and a water to oil ratio of 50 %. The left photo shows a syngas activated system being stirred at 1100 rpm. The right photo shows a system not being stirred.

4.2.2. Reaction Kinetics - Parameter Estimation

To effectively operate the process later on, a fitting of the reaction kinetics to the exact system is required. The main uncertain parameters in the hydroformylation mini-plant model are thus those found in the reaction kinetics. In Section 2.3.3 a method was presented

how relevant uncertain parameters for optimization under uncertainty can be selected. This strategy is expanded and applied in this section.

Often enough, the resulting expected values of uncertain parameters in parameter estimation problems are strongly dependent on the initial values or initial guess of these parameters. Due to this fact, an infinite combination of ideal solutions is possible. For the case of the mini-plant model, a solution is desired that most accurately depicts experimental results. The root-mean-squared-error (RMSE) of the parameter estimation problem should be as small as possible. Therefore, a multitude of initial guesses could lead to the desired result. To avoid the computational burden of standard approaches, a sampling technique presented in (Diwekar and Kalagnanam, 1997) is employed. This efficient sampling technique for uncertain parameters generates and inverts the Hammersley points. According to (Diwekar and Kalagnanam, 1997) it is an "optimal design for placing n points uniformly on a k-dimensional cube to provide a representative sample for multivariate probability distributions".

The idea now is to use this sampling technique for the uncertain parameters and generate a certain number of initial values. The initial value set that has the lowest RMSE in a preliminary parameter estimation is used as a starting value for the method from section 2.3.3. The resulting solution is used for further studies. The entire modified workflow is presented in Fig. 4.9. It must be mentioned though, that the best initial guess (the initial guess with the lowest RMSE) does not automatically mean the best final result after subset selection. Nevertheless, this method is employed as it has proven to yield sufficiently applicable results and simultaneously keeps the calculation time low. Otherwise, a subset selection would have to be performed of each sampled set. This would increase the calculation time drastically.

Step 0 - Data accumulation: The set of measurement data has already been presented in the previous section. It consists of nine experiments for the temperatures 75, 85, and 95 °C and the pressures 15, 20, and 30 bar. Of these nine sets, three are viewed as faulty (T = 75 °C, 30 bar, T = 95 °C, 15 & 20 bar). Therefore these data sets are removed from the parameter estimation.

Step 1 - Model formulation: As a next step, the formulation of the model is carried out. This is started with the component balances[1] in the semi-batch reactor used to perform the experiments. The change of concentration c of component i is analyzed.

$$\frac{dc_{i=1}}{dt} = -r_1 + r_2 - r_3 - r_5 \tag{4.11}$$

$$\frac{dc_{i=2}}{dt} = r_1 - r_2 - r_4 - r_6 \tag{4.12}$$

$$\frac{dc_{i=3}}{dt} = r_6 \tag{4.13}$$

$$\frac{dc_{i=4}}{dt} = r_3 + r_4 \tag{4.14}$$

$$\frac{dc_{i=5}}{dt} = r_5 \tag{4.15}$$

On top of that, expressions to describe the reaction rates are required. For these reactions, several kinetic expressions have been developed, which have been derived by the research group **A3** based on the Wilkinson-catalyst cycle (Kiedorf et al., 2014). Eq. 4.16 to Eq. 4.21 present the general form of these kinetic equations in the reactor (u = 9).

[1] As a reminder: 1 = *1-dodecene*, 2 = *iso-dodecene*, 3 = *Iso-tridecanal*, 4 = *n-dodecane*, 5 = *1-tridecanal*

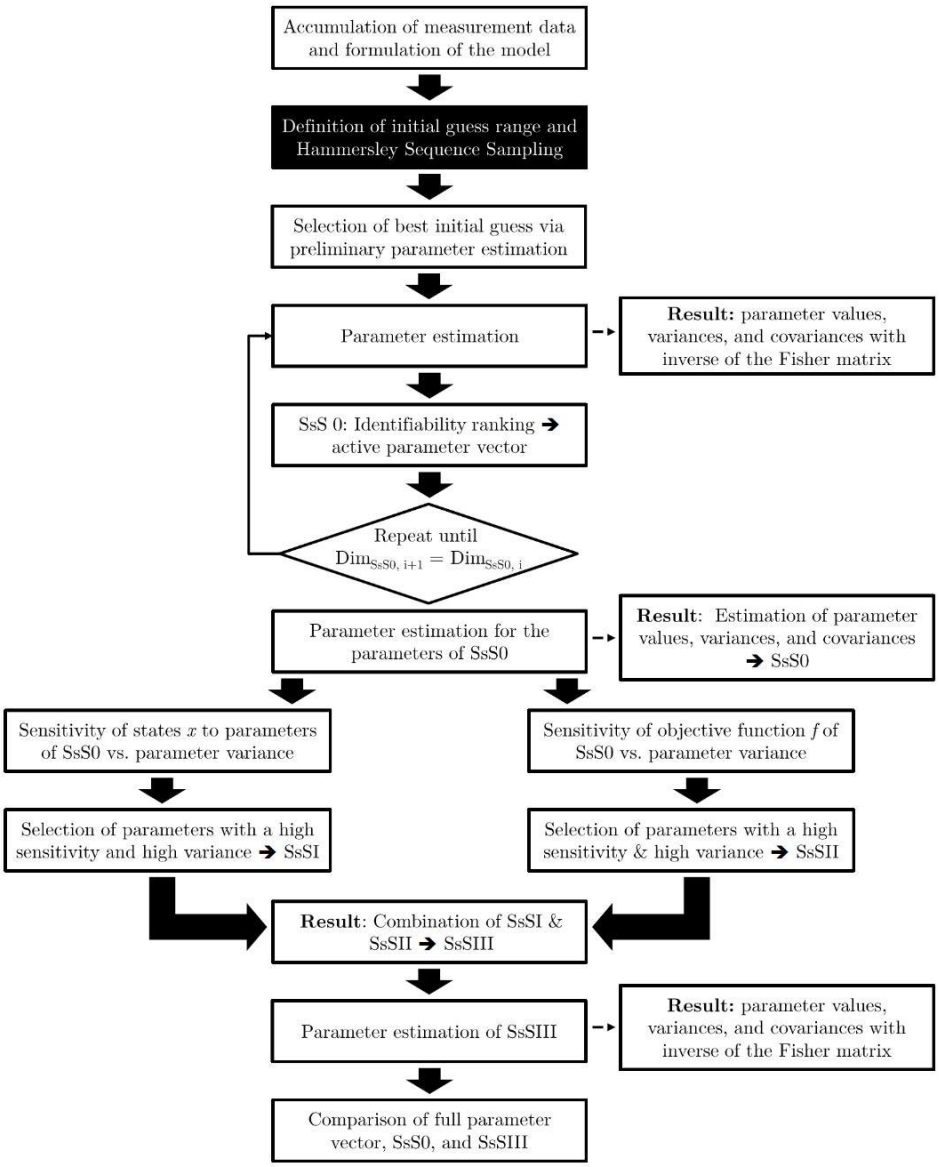

Figure 4.9.: General scheme of the advanced algorithm for the selection of relevant uncertain parameters for optimization under uncertainty.

$$r_{r=1} = \frac{m_{cat}}{(1 + K_{cat} \cdot c_{i=7})} \cdot \frac{k_{r=1} \cdot \exp(-\frac{E_{r=1}}{R \cdot T}) \cdot c_{s=11,i=1}}{(1 + K_{r=1,e=1} \cdot c_{s=11,i=1})} \tag{4.16}$$

$$r_{r=2} = \frac{m_{cat}}{(1 + K_{cat} \cdot c_{i=7})} \cdot \frac{k_{r=2} \cdot \exp(-\frac{E_{r=1}}{R \cdot T}) \cdot c_{s=11,i=2}}{(1 + K_{r=2,e=1} \cdot c_{s=11,i=2})} \tag{4.17}$$

$$r_{r=3} = \frac{m_{cat}}{(1 + K_{cat} \cdot c_{i=7})} \cdot \frac{k_{r=3} \cdot \exp(-\frac{E_{r=3}}{R \cdot T}) \cdot c_{s=11,i=1} \cdot c_{i=6}}{(1 + K_{r=3,e=1} \cdot c_{s=11,i=1})} \tag{4.18}$$

$$r_{r=4} = \frac{m_{cat}}{(1 + K_{cat} \cdot c_{i=7})} \frac{k_{r=4} \cdot \exp(-\frac{E_{r=3}}{R \cdot T}) \cdot c_{s=11,i=2} \cdot c_{i=6}}{(1 + K_{r=4,e=1} \cdot c_{s=11,i=2})}. \tag{4.19}$$

$$r_{r=5} = \frac{m_{cat}}{(1 + K_{cat} \cdot c_{i=7})} \cdot \frac{k_{r=5} \cdot \exp(-\frac{E_{r=5}}{R \cdot T}) \cdot c_{s=11,i=1} \cdot c_{i=6} \cdot c_{i=7}}{(1 + K_{r=5,e=1} \cdot c_{s=11,i=1} + K_{r=5,e=2} \cdot c_{s=11,i=1} \cdot c_{i=7})} \tag{4.20}$$

$$r_{r=6} = \frac{m_{cat}}{(1 + K_{cat} \cdot c_{i=7})} \cdot \frac{k_{r=6} \cdot \exp(-\frac{E_{r=5}}{R \cdot T}) \cdot c_{s=11,i=2} \cdot c_{i=6} \cdot c_{i=7}}{(1 + K_{r=6,e=1} \cdot c_{s=11,i=2} + K_{r=6,e=2} \cdot c_{s=11,i=2} \cdot c_{i=7})} \tag{4.21}$$

Several reformulations in the equations Eq. 4.16 to Eq. 4.21 are carried out. Among these are the replacement of the repeatedly appearing fraction of $m_{cat}/(1 + K_{cat} \cdot c_{i=7})$ with a dummy variable ψ_{cat} and simultaneously avoiding the fraction itself. The reformulation is shown in Eq. 4.22.

$$\psi_{cat} = \frac{m_{cat}}{(1 + K_{cat} \cdot c_{i=7})} \quad \Rightarrow \quad \psi_{cat} \cdot (1 + K_{cat} \cdot c_{i=7}) = m_{cat} \tag{4.22}$$

These reformulations are exemplarily shown for the isomerization reaction of 1-dodecene to iso-dodecene in Eq. 4.23 and are carried out for all other kinetic equations as well. Additionally, the fraction reformulation is also performed for the inhibition term in the equation $(1 + K_{r=1,e=1} \cdot c_{s=11,i=1})$).

$$r_{r=1} \cdot (1 + K_{r=1,e=1} \cdot c_{s=11,i=1}) = \psi_{cat} \cdot k_{r=1} \cdot \exp(-\frac{E_{r=1}}{R \cdot T}) \cdot c_{s=11,i=1} \tag{4.23}$$

Summarizing, the unknown parameters in this model are the following:

- $E_{r=1,3,5}$, activation energies for reactions 1 to 6 (3 Parameters).
- $k_{r=1...6}$, preexponential factor for reactions 1 to 6 (6 Parameters).
- K_{cat}, catalyst inhibition factor (1 Parameter).
- $K_{r=1...6,e=1}$, carbon monoxide inhibition factor (6 Parameters).
- $K_{r=5,6,e=2}$, carbon monoxide inhibition factor for the isomers (2 Parameters).

Step 2 - Hammersley Sequence Sampling: As discussed previously, the solution of the parameter estimation problem is strongly dependent on the initial guess of the uncertain parameters. Therefore, Hammersley Sequence Sampling is employed for generating initial guesses. For each of the parameters listed above, a certain lower and upper bound is defined. The Hammersley method then semi-randomly samples sets of parameters within this bound. As an example, Fig. 4.10 shows the sampling of Hammersley points for the activation energies $E_{r=1}$ and $E_{r=5}$.

Since the bounds of the parameters span several magnitudes, the sampling is carried out logarithmically. Fig. 4.11 exemplarily shows this logarithmic sampling for the three activation energies $E_{r=1}$, $E_{r=3}$, and $E_{r=5}$. The reason for the logarithmic sampling is that it needs to be guaranteed that the different starting values of the parameters with orders

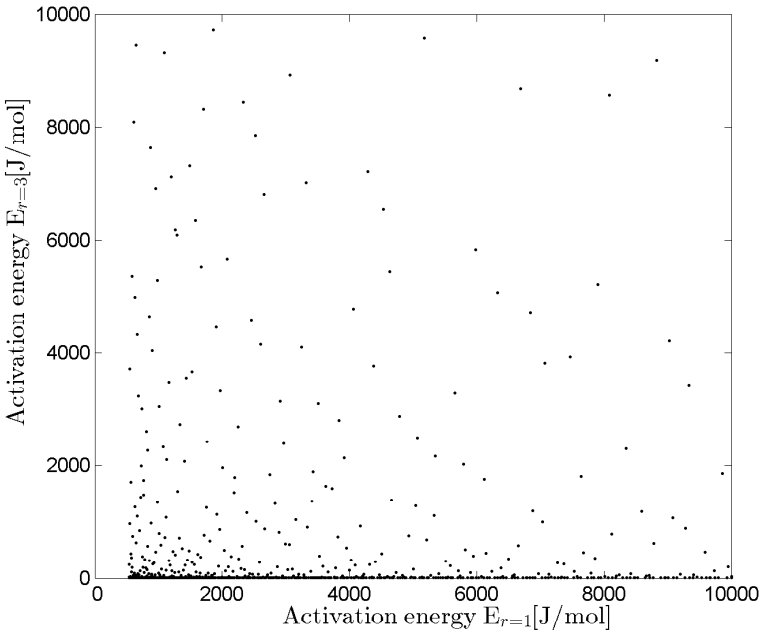

Figure 4.10.: Logarithmic Hammersley Sequence Sampling (1000 points) for the activation energy $E_{r=1}$ and $E_{r=5}$.

of magnitude are tested as opposed to variations on a single magnitude. In total, 1000 Hammersley Sequence Samples are tested.

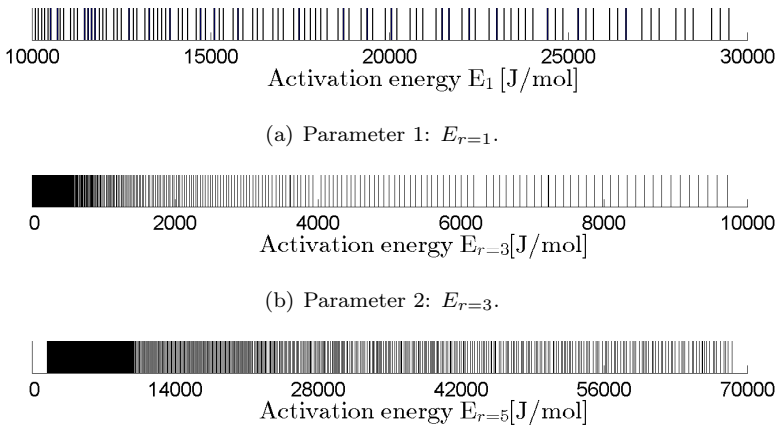

(a) Parameter 1: $E_{r=1}$.

(b) Parameter 2: $E_{r=3}$.

(c) Parameter 3: $E_{r=5}$.

Figure 4.11.: Distribution of the Hammersley points for three exemplary parameters.

The selected bounds for each of the parameters are shown in Tab. 4.3. In preliminary parameter estimation studies using various parameter initial values differing in magnitudes, a set of results was obtained. Based on the minimal and maximal values of this set the ranges in Tab. 4.3 were defined.

The parameter bounds are selected based on several deliberations. First of all, the aim of the performed parameter estimation is not to find the true values of the kinetic parameters, such as the actual activation energy of each reaction. Instead, an ideal combination of values is targeted, which when used in the kinetic equations is capable of adequately representing

Table 4.3.: Applied lower bounds (LB) and upper bounds (UB) for the uncertain parameters.

	$E_{r=1}$ $[J/mol]$	$E_{r=3}$ $[J/mol]$	$E_{r=5}$ $[J/mol]$	$k_{r=1}$ $[l/(mol\ g)]$	$k_{r=2}$ $[l/(mol\ g)]$	$k_{r=3}$ $[l/(mol\ g)]$
LB	$5.4 \cdot 10^2$	$5.0 \cdot 10^{-3}$	$1.5 \cdot 10^3$	$1.6 \cdot 10^4$	$3.5 \cdot 10^1$	$3.3 \cdot 10^6$
UB	$4.1 \cdot 10^4$	$1.0 \cdot 10^4$	$6.9 \cdot 10^4$	$1.8 \cdot 10^5$	$6.2 \cdot 10^{10}$	$1.0 \cdot 10^{11}$
	$k_{r=4}$ $[l/(mol\ g)]$	$k_{r=5}$ $[l^2(mol^2\ g)]$	$k_{r=6}$ $[l^2/(mol^2\ g)]$	K_{cat} $[l/mol]$	$K_{r=5,e=1}$ $[l/mol]$	$K_{r=5,e=2}$ $[l^2/mol^2]$
LB	$6.4 \cdot 10^3$	$3.9 \cdot 10^9$	$4.4 \cdot 10^7$	$3.2 \cdot 10^2$	$1.2 \cdot 10^0$	$1.3 \cdot 10^3$
UB	$5.3 \cdot 10^{10}$	$6.0 \cdot 10^{10}$	$9.8 \cdot 10^8$	$2.9 \cdot 10^3$	$2.3 \cdot 10^3$	$5.7 \cdot 10^5$
	$K_{r=1,e=1}$ $[l/mol]$	$K_{r=2,e=1}$ $[l/mol]$	$K_{r=3,e=1}$ $[l/mol]$	$K_{r=4,e=1}$ $[l/mol]$	$K_{r=6,e=1}$ $[l/mol]$	$K_{r=6,e=2}$ $[l^2/mol^2]$
LB	$1.1 \cdot 10^3$	$1.6 \cdot 10^4$	$3.9 \cdot 10^2$	$1.0 \cdot 10^3$	$1.2 \cdot 10^0$	$1.3 \cdot 10^3$
UB	$5.8 \cdot 10^4$	$5.0 \cdot 10^{10}$	$4.0 \cdot 10^3$	$5.9 \cdot 10^{10}$	$2.3 \cdot 10^3$	$5.7 \cdot 10^5$

the measured values from the batch reaction. Hereby, the focus is laid on numerical properties and structural identifiability. Activation energies of the hydroformylation reaction for similar components (1-dodecene, $HRh(CO)(PPh_3)_3$ catalyst) can be found in currently available literature such as (Bhanage et al., 1997), where a value of roughly 57 kJ/mol is presented. Other papers, such as (Kiedorf et al., 2014), also analyze the reaction of 1-dodecene. Here however Biphephos is used as a ligand. The activation energy of the hydroformylation reaction is given at 113 kJ/mol. In (Kiedorf et al., 2014), values for the isomerization and hydrogenation reactions can also be found, both larger than 70 kJ/mol. A negative aspect of using these high values is that the exponential term becomes very small. On the other hand this forces the parameter estimation to assume very large values for the preexponential factors, which lets the system become poorly scaled. Therefore, the decision has been made to use smaller activation energies (J instead of kJ) so that smaller, but sensitive preexponential factors can be determined.

Step 3 - Best initial guess: In the third step the values presented in Tab. 4.4 are used, as they have the lowest starting RMSE of all 1000 Hammersley samples.

Table 4.4.: Applied initial values of kinetic parameters with lowest starting RMSE.

$E_{r=1}$ $[J/mol]$	$E_{r=3}$ $[J/mol]$	$E_{r=5}$ $[J/mol]$	$k_{r=1}$ $[l/(mol\ g)]$	$k_{r=2}$ $[l/(mol\ g)]$	$k_{r=3}$ $[l/(mol\ g)]$
$3.2 \cdot 10^3$	$8.2 \cdot 10^{-2}$	$8.5 \cdot 10^3$	$1.9 \cdot 10^4$	$2.6 \cdot 10^7$	$4.0 \cdot 10^{10}$
$k_{r=4}$ $[l/(mol\ g)]$	$k_{r=5}$ $[l^2(mol^2\ g)]$	$k_{r=6}$ $[l^2/(mol^2\ g)]$	K_{cat} $[l/mol]$	$K_{r=5,e=1}$ $[l/mol]$	$K_{r=5,e=2}$ $[l^2/mol^2]$
$9.7 \cdot 10^4$	$4.3 \cdot 10^{10}$	$3.3 \cdot 10^8$	$5.0 \cdot 10^2$	$1.8 \cdot 10^1$	$2.9 \cdot 10^4$
$K_{r=1,e=1}$ $[l/mol]$	$K_{r=2,e=1}$ $[l/mol]$	$K_{r=3,e=1}$ $[l/mol]$	$K_{r=4,e=1}$ $[l/mol]$	$K_{r=6,e=1}$ $[l/mol]$	$K_{r=6,e=2}$ $[l^2/mol^2]$
$3.7 \cdot 10^3$	$4.4 \cdot 10^5$	$9.2 \cdot 10^2$	$6.0 \cdot 10^5$	$1.8 \cdot 10^1$	$2.9 \cdot 10^4$

Step 4...6 - Parameter estimation and subset selection: The resulting expected parameter values as well as their corresponding activity in the final subset are listed in Tab. 4.5. The activity in the final subset describes whether or not the parameters are identifiable. If

they are not identifiable, the parameters have been fixed to their current value and their activity entry *Act* is equal to 0. If they are identifiable on the other hand, then they have a variance and their activity entry *Act* is equal to 1. The parameters that remain active (*Act* = 1) are the uncertain parameters used later on for optimization under uncertainty.

Table 4.5.: Resulting expected values of kinetic parameters after the final parameter estimation.

	$E_{r=1}$ $[J/mol]$	$E_{r=3}$ $[J/mol]$	$E_{r=5}$ $[J/mol]$	$k_{r=1}$ $[l/(mol\ g)]$	$k_{r=2}$ $[l/(mol\ g)]$	$k_{r=3}$ $[l/(mol\ g)]$
μ	$6.3 \cdot 10^{-3}$	$5.3 \cdot 10^{4}$	$1.9 \cdot 10^{4}$	$2.2 \cdot 10^{5}$	$1.9 \cdot 10^{7}$	$2.3 \cdot 10^{10}$
	$k_{r=4}$ $[l/(mol\ g)]$	$k_{r=5}$ $[l^2(mol^2\ g)]$	$k_{r=6}$ $[l^2/(mol^2\ g)]$	K_{cat} $[l/mol]$	$K_{r=5,e=1}$ $[l/mol]$	$K_{r=5,e=2}$ $[l^2/mol^2]$
μ	$3.4 \cdot 10^{2}$	$6.2 \cdot 10^{10}$	$2.8 \cdot 10^{8}$	$4.2 \cdot 10^{2}$	$1.8 \cdot 10^{-2}$	$2.1 \cdot 10^{4}$
	$K_{r=1,e=1}$ $[l/mol]$	$K_{r=2,e=1}$ $[l/mol]$	$K_{r=3,e=1}$ $[l/mol]$	$K_{r=4,e=1}$ $[l/mol]$	$K_{r=6,e=1}$ $[l/mol]$	$K_{r=6,e=2}$ $[l^2/mol^2]$
μ	$3.9 \cdot 10^{3}$	$3.3 \cdot 10^{5}$	$9.2 \cdot 10^{-1}$	$6.4 \cdot 10^{5}$	$1.8 \cdot 10^{-2}$	$2.1 \cdot 10^{4}$

Tab. 4.6 shows the development of the activity of the parameters during the application of the algorithm from (Müller et al., 2014a). After the first subset selection (SsS 0) five of the sixteen parameters are viewed as identifiable and linearly independent. The first two remaining uncertain parameters are the activation energies of the hydrogenation (p_2) and hydroformylation (p_3) reactions. From an engineering point of view this result is logical, because these two parameters have the largest influence on the output of the system (production of the two main products, 1-tridecanal and n-dodecane). Next, is the parameter K_{cat} (p_4), which is present in all reaction kinetic equations and thus also has a large influence on the output of the system. The remaining uncertain parameters are the preexponential factor of the hydroformylation of iso-tridecanal (p_9) and the inhibition factor of the isomerization of 1-dodecene (p_{10}). In the subsequent subset selections (SsS I - SsS II) only the activation energy of the hydroformylation reaction and the parameter K_{cat} remain active. These two parameters will be used as uncertain parameters in the optimization studies.

Table 4.6.: Development of the activity of uncertain parameters during each parameter estimation and subset selection computation.

	p_1	p_2	p_3	p_4	p_5	p_6	p_7	p_8
SsS 0	0	1	1	1	0	0	0	0
SsS I	0	0	1	1	0	0	0	0
SsS II	0	0	1	1	0	0	0	0
SsS III	0	0	1	1	0	0	0	0
	p_9	p_{10}	p_{11}	p_{12}	p_{13}	p_{14}	p_{15}	p_{16}
SsS 0	1	1	0	0	0	0	0	0
SsS I	0	0	0	0	0	0	0	0
SsS II	0	0	0	0	0	0	0	0
SsS III	0	0	0	0	0	0	0	0

Exemplarily, to visualize the result of the parameter estimation, Fig. 4.12 displays results from the experiment using 85 °C and 15 bar. Here, the model using the determined kinetic parameters from the parameter estimation is compared to experimental data. Additionally,

the result for 95 °C and 30 bar is shown, because these conditions are of interest for the reaction, at which not too many byproducts are created. Other results can be found in the Appendix in Fig. A.2 to A.3.

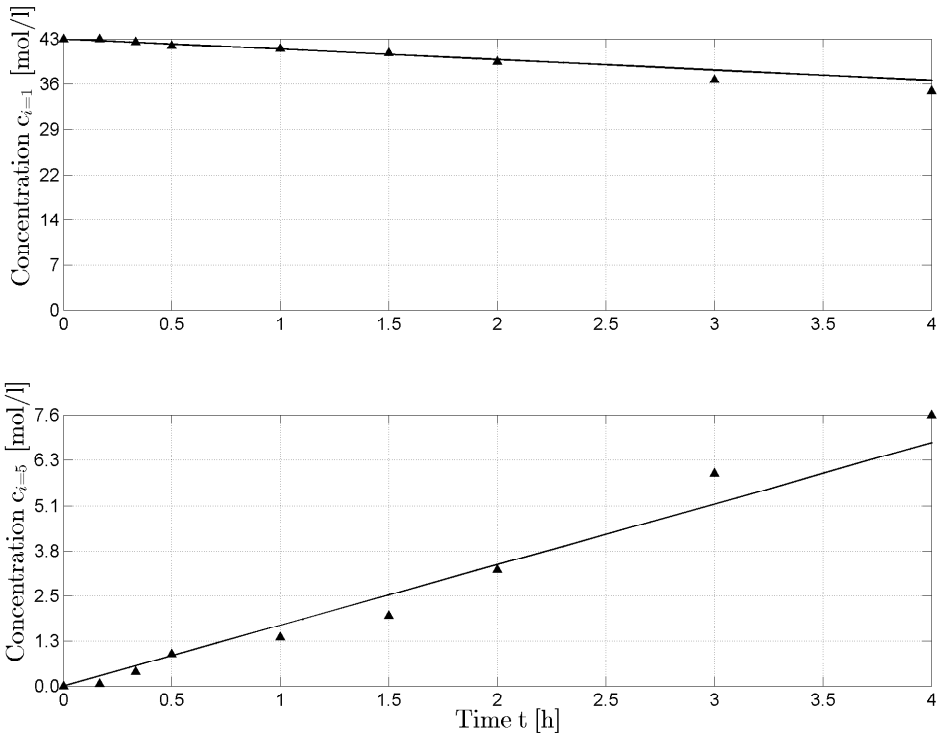

Figure 4.12.: Parameter estimation result for 85 °C and 15 bar: main components.

These results show that the reaction parameters for the main components, 1-dodecene and 1-tridecanal, are determined adequately. The experimental results for 1-dodecene are represented almost exactly with minimal deviations at all points. For 1-tridecanal, the slight fluctuations in the experimental results make it difficult for the model to represent these values in all points. Nevertheless, no real over- or underestimation of the data is visible.

For the byproducts, however, further experimental results are required. Here, especially for the estimation of n-dodecane and for iso-tridecanal, more sensitive measurements are needed. Especially for n-dodecane there seems to be an issue in the experimental results. The first actual point is only determined after two hours of reaction. It is possible, that n-dodecane was created before, but the concentration was too small to be detected by the measurement device. The results show an overestimation of the experimental values of n-dodecane. For the mini-plant modeling, these values will have to be adjusted. Otherwise misleading results may be obtained if optimization criteria in the objective function, such as keeping the byproduct amount below a certain value, are used. Next, for iso-dodecene, the experimental results seem to be totally insensitive. No large change of the experimental values is visible in any of the experiments. Therefore, of course, the sensitivity of the parameter estimation function to the according kinetic parameters of iso-dodecene is quite low and no adequate determination is possible.

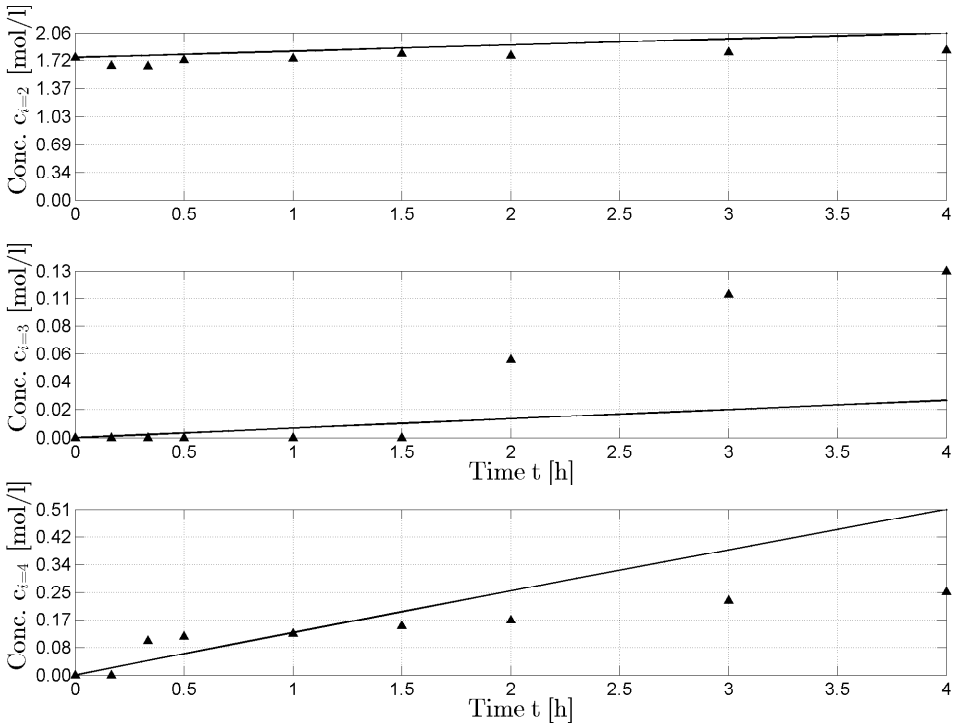

Figure 4.13.: Parameter estimation result for 85 °C and 15 bar: byproducts.

4.2.3. First Principles Model for the Reaction Section

The reactor can be modeled with the following mass balance:

$$\frac{dHU_i^{Reactor}}{dt} = F_{s=8,i} - F_{s=9,i} + F_{s=10,i} - F_{s=11,i} + M_i \cdot L_{u=9} \cdot A_{u=9} \cdot r_i \tag{4.24}$$

Since the reaction kinetics have been presented in the previous section, a repeated presentation of these equations at this point is waived. The reactor consists of two hold-ups: liquid ($u = 9$) and gas ($u = 8$). These are firstly modeled with the following equations:

$$HU_i^{Reactor} = HU_{u=9,i}^{L} + HU_{u=8,i}^{V} \tag{4.25}$$

$$HU_{u=8,i}^{V} = w_{s=9,i} \cdot HU_{u=8}^{V} \tag{4.26}$$

$$HU_{u=8}^{V} = \sum_{i=1}^{Ni} HU_{u=8,i}^{V} \tag{4.27}$$

$$HU_{u=9,i}^{L} = w_{s=11,i} \cdot HU_{u=9}^{L} \tag{4.28}$$

$$HU_{u=9}^{L} = \sum_{i=1}^{Ni} HU_{u=9,i}^{L} \tag{4.29}$$

The composition of the gas hold-up is described via the outflowing gas stream S_9 and the liquid hold-up via the outflowing liquid stream S_{11}. The amount of gas dissolved in the liquid hold-up is calculated with Eq. (4.30) and (4.31).

$$HU_{u=9,i=7}^{L} = c_{u=9,i=7} \cdot M_{i=7} \cdot A_{u=9} \cdot L_{u=9} \tag{4.30}$$

$$HU_{u=9,i=6}^{L} = c_{u=9,i=6} \cdot M_{i=6} \cdot A_{u=9} \cdot L_{u=9} \tag{4.31}$$

The concentrations are calculated via Henry's law. A discussion is carried out later in this chapter in the section concerning the auxiliary equations. To avoid a starting of the reaction (especially the isomerization of 1-dodecene) it is necessary to implement certain triggering functions in the reaction section. The first is the component switch of the gas phase. The idea here is that at the beginning during the filling process of the plant, only nitrogen is present. As soon as the reaction is started the composition switches to CO and H_2.

$$\sum_{i=1}^{Ni} w_{s=8,i} = 1 \tag{4.32}$$

$$w_{s=8,i=6} = w^{SP}_{s=8,i=6} \cdot TRIG_{u=9} \tag{4.33}$$

$$w_{s=8,i=7} = w^{SP}_{s=8,i=7} \cdot TRIG_{u=9} \tag{4.34}$$

$$w_{s=8,i=8} = 1 - TRIG_{u=9} \tag{4.35}$$

The partial pressure of each of the gases is determined with the ideal gas law, as shown in Eq. 4.37 and Eq. 4.37.

$$\sum_{i=1}^{Ni} \left(\frac{HU^V_{u=8,i}}{M_i}\right) = \frac{p_{u=8} \cdot 100 \cdot (V^{Reactor} - A_{u=9} \cdot (L_{u=9}))}{R \cdot T_{u=9}} \tag{4.36}$$

$$\frac{HU^V_{u=8,i=6}}{M_{i=6}} = \frac{p^V_{i=6} \cdot 100 \cdot (V^{Reactor} - A_{u=9} \cdot (L_{u=9}))}{R \cdot T_{u=9}} \tag{4.37}$$

$$\frac{HU^V_{u=8,i=7}}{M_{i=7}} = \frac{p^V_{i=7} \cdot 100 \cdot (V^{Reactor} - A_{u=9} \cdot (L_{u=9}))}{R \cdot T_{u=9}} \tag{4.38}$$

Moving on to the liquid part of the reactor, the composition can be described with Eq. 4.39 and the outflowing stream with Eq. 4.40:

$$\sum_{i=1}^{Ni} \left(\frac{HU^L_{u=9,i}}{\rho_i}\right) = A_{u=9} \cdot L_{u=9} \tag{4.39}$$

$$F_{s=11} = TRIG_{u=9} \cdot (F_{s=10} + KP_{u=9} \cdot (L_{u=9} - L^{SP}_{u=9})) \tag{4.40}$$

4.3. Mini-plant Section 3: Separation Section

The next section in the mini-plant model is the separation section with the settler in which the phase separation of the microemulsion system takes place. For this purpose Fig. 4.14 should be regarded. This section is made up of three units: a splitter, the settler, and the heat exchanger for the settler. The settler itself is split up into three hold-ups which symbolize the gas phase as well as an oil and mixed phase.

This step is important for the process as it determines the economic viability of the process concept. Several ideas for the development of a model for the separation section of the hydroformylation mini-plant are already published in own contributions such as (Müller et al., 2014f; Esche et al., 2014a; Müller et al., 2013b). In the following, the development of the separation model as a whole will be described. This development is split up into three parts. First of all, ideas and preliminary thoughts important for modeling the system are highlighted. Secondly, the development of an empirical phase separation model according to the systematic discussed in section 2.6 is shown.

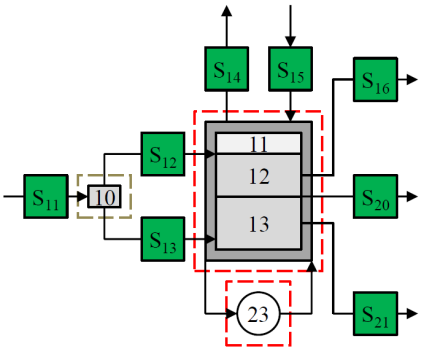

Figure 4.14.: Model scheme of the separation section of the hydroformylation mini-plant at Technische Universität Berlin.

4.3.1. Preliminary Modeling Thoughts and Ideas

There are several issues involved with modeling the separation section of the plant. Firstly, no experimental data set for the current system with all components is available. Secondly, real components are used in the process. These are generally not pure, single molecule components. The challenge of describing the ideal separation region under the influence of all effects in the mini-plant is required.

Based on the results from the preliminary analyses of the system, further experiments are performed. The Kahlweit's fish displays the phase separation at equilibrium. For dynamic modeling, equilibrium results may not be satisfied. A model would have to cover a larger number of operating points, i.e. several temperatures for several different compositions, yielding the required separation time. "Due to the lack of thermodynamic data for microemulsion mixtures and reliable existing simulations, design and operation of the phase separation unit strongly depends on experimental data. Therefore, the determination of the area in which the phase separation takes place quickly is desired. For the separation within the hydroformylation mini-plant both the two-phase and three-phase region are applicable" (Müller et al., 2014f).

"The idea behind the [design of a] phase separation model is that the optimal separation time at a certain temperature indirectly represents the necessary length in a horizontal flow [settler]" (Müller et al., 2014f). A discussion of this concept can be found in the contribution by Reissinger et al. (1981), in which the minimal necessary settler length L_{min} is determined according to Eq. 4.41:

$$L_{min} = \frac{\dot{V} \cdot t^*}{A} \tag{4.41}$$

Hereby $\dot{V}$ is the velocity of the liquid entering the settler and A is the cross sectional area of the settler. Reissinger et al. (1981) mention that depending on the type of system at hand, the optimal separation time for the continuous settler operation is often equal to one to two times the settling time in a batch experiment. This is often the case as a superposition of the velocities of vertically rising or sinking droplets and the horizontal flow of the incoming emulsion takes place. In other words, if the settler is long enough, a separation at an ideal temperature can be achieved. In the plant at Technische Universität Berlin, both temperature and superficial velocity of the reactor inlet stream can be controlled. Thus, the required separation time can be achieved.

4.3.2. Systematic Phase Separation Modeling

To develop the model, the workflow presented in Fig. 2.5 is followed. The exact steps that have been taken are displayed in Fig. 4.15.

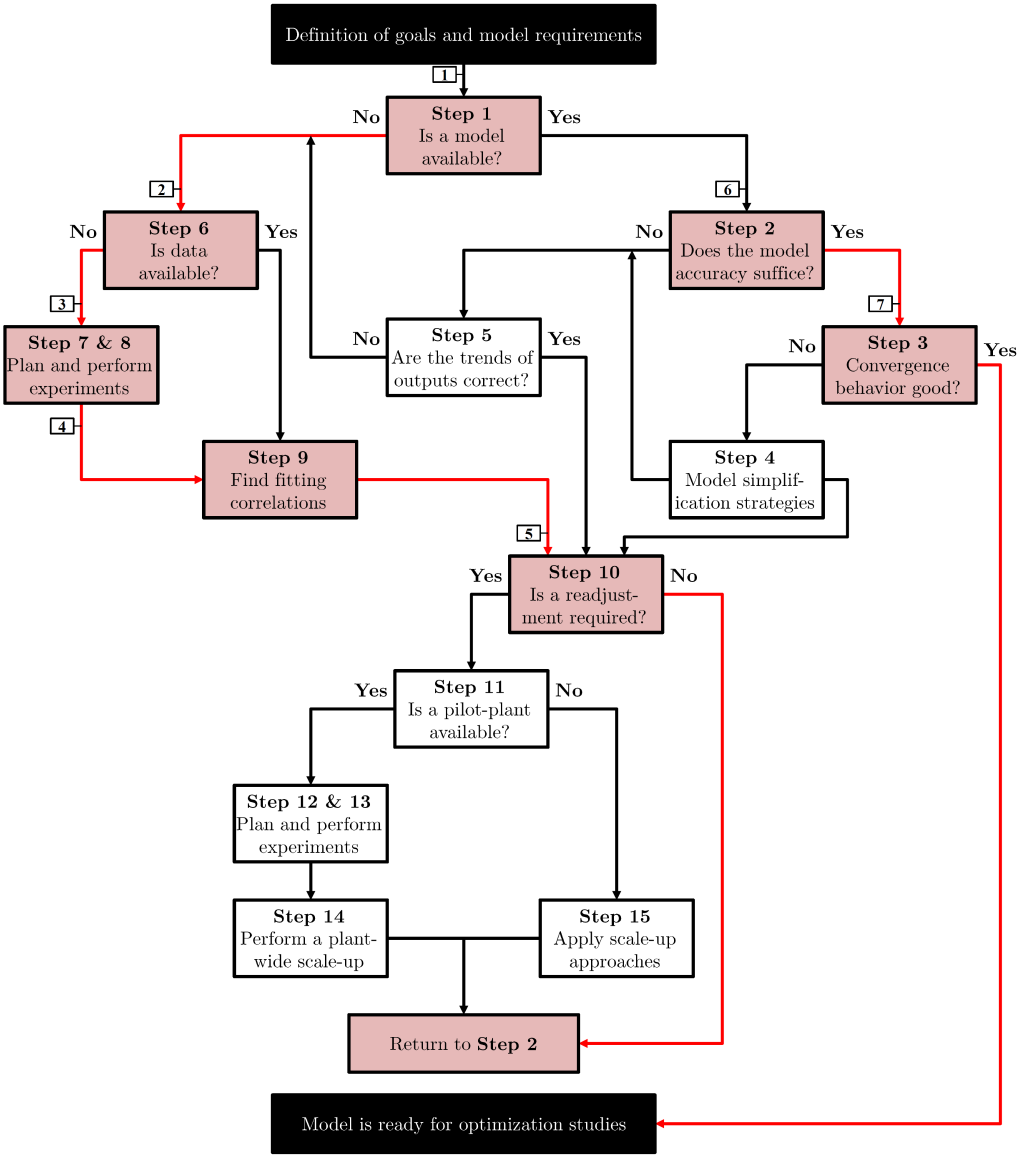

Figure 4.15.: Application of the systematic workflow to design the phase separation model for optimization.

The workflow begins with a definition of the goals and requirements for the model. The general aim is to create a model, which is capable of predicting the heights of each of the relevant phases for the phase separation depending on the influencing variables of temperature, time, and concentration. A correlation between the phase separation and the following variables is of interest:

- the separation time t,
- concentration of 1-dodecene,
- concentration of the product 1-tridecanal,

- concentration of the surfactant marlipal 24/70,
- concentration of the catalyst complex,
- the temperature T, and
- catalyst activation through syngas.

Following the query in **Step 1**, because no model is currently present that is capable of yielding this desired information, **Step 6** is carried out. As already mentioned, since little to no thermodynamic information on the phase separation behavior of the system is available, the decision is made to create an empirical model. Therefore, according experiments need to be planned and carried out (**Step 7 & 8**). Here, the results of the systematic systems analysis presented in section 2.6 with the results from 3.1 are used.

In order to describe the concentrations above, three values often used to describe oil-water-surfactant systems, where have already been discussed in Chapter 2, are revisited here:

- Oil-Water-Ratio:

$$\alpha = \frac{m_{\text{oil}}}{m_{\text{oil}} + m_{\text{water}}}$$

- Surfactant concentration:

$$\gamma = \frac{m_{\text{surfactant}}}{m_{\text{oil}} + m_{\text{water}} + m_{\text{surfactant}}}$$

- Product concentration:

$$X = \frac{m_{\text{1-tridecanal}}}{m_{\text{oil}} + m_{\text{water}} + m_{\text{surfactant}}}$$

m_{oil} is the sum of $m_{\text{1-dodecene}}$ and $m_{\text{1-tridecanal}}$. In total, six variables are implemented into the phase separation function: $h = f(\gamma, \alpha, X, t, T, c_{\text{catalyst}})$ Esche et al. (2014a). The starting concentrations of the hydroformylation process are a water to oil-ratio of $\alpha = 50$ %, a surfactant concentration of $\gamma = 8$ %, a product concentration of $X = 0$ %, a catalyst concentration of roughly 298 ppm, and a ligand concentration of 4500 ppm (Hamerla et al., 2013b). The range of interest is therefore defined accordingly:

- α = [40 ... 60] %,
- γ = [6 ... 10] %,
- X = [0 ... 40] %,
- T = [60 ... 95] °C, and
- t = [0 ... 10] min.

Based on the experiments described in (Müller et al., 2012e) and (Müller et al., 2012d), the necessary data are obtained. "The key idea of these experiments is to create a mixture representing the liquid leaving the reactor" (Müller et al., 2014f). Now, the results from section 3.1 are used. Here, oil phase height information at each concentration at different temperatures T is used. For one concentration a three-dimensional diagram is created in which the optimal phase separation region is shown. An example for a mixture consisting of 9 wt.-% surfactant (Marlipal 24/70), 22.75 wt.-% alkene, 22.75 wt.-% aldehyde, 45.5 wt.-%

water, and a concentration of 298 ppm rhodium precursor and no added sodium sulfate (Na_2SO_4) is displayed in Fig. 4.16(a).

In order to design a function to represent this surface, bivariate dependencies are analyzed. It is obvious, that several sigmoid functions are capable of portraying this surface. The first set of sigmoid functions is used to describe the height-temperature dependency. The basic function is presented Eq. 4.42, whereby p_i are parameters that still need to be fitted.

$$h(T) = \frac{p_1}{1 + p_2 \cdot e^{p_3 - T}} + \frac{p_4}{1 + p_5 \cdot e^{p_6 - T}} \tag{4.42}$$

The next bivariate dependency is the height as a function of time. Just as before, a sigmoid function is capable of describing the separation behavior.

$$h(t) = \left(100 - \frac{p_7}{1 + p_8 \cdot e^{p_9 - t}}\right) \tag{4.43}$$

A parameter estimation problem of the following form is solved:

$$\min_{p_i} \sum_{i=1}^{121} \sum_{j=1}^{14} (h(t_i, T_j) - \widetilde{h}(t_i, T_j))^2 \tag{4.44}$$

Since it is not sensible to have an equation with 121 times the number of parameters, the parameters are replaced by functions of time. Thus, the amount of parameters can be reduced to nine, which is more acceptable to describe the surface. A further elaboration at this point will be waived. The resulting surface function for the oil phase height with respect to the temperature is shown in Fig. 4.16(b). This result is very satisfying in terms of accuracy (average error is below 0.9 vol.-% height for reach data point).

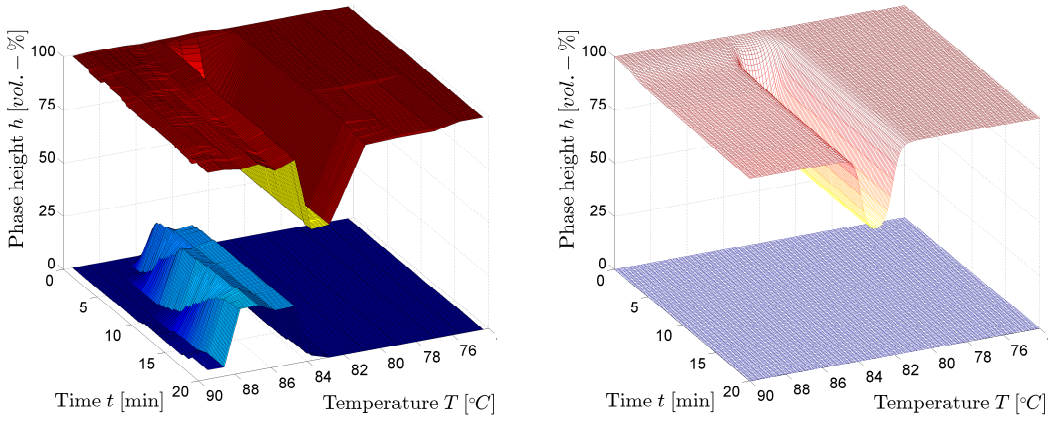

(a) Experimental results.

(b) Phase separation surface model.

Figure 4.16.: Phase separation experimental results and oil phase surface model. The results are valid for a mixture consisting of 9 wt.-% surfactant (Marlipal 24/70), 22.75 wt.-% alkene, 22.75 wt.-% aldehyde, 45.5 wt.-% water, and a concentration of 298 ppm rhodium precursor and no added sodium sulfate (Na_2SO_4). The original data set has been published in (Müller et al., 2014f).

Seeing that the phase separation is relatively fast in the ideal temperature interval (maximum 5 min) and almost always yields an oil phase height of over 20 vol.-%, an elaborate modeling on this part is not necessary. Since the aim is to perform optimization, an accurate

and quickly converging model is desired. Obviously, in terms of accuracy, the current model fulfills this requirement. For convergence, the picture may be a bit different. If the height function is transformed as to fit a cylinder, an expression as shown in Eq. 4.45 for the heights of the phases is needed. To test if this function fits reality, an experiment in a continuously operated settler was carried out. A comparison of the results between continuous settler experiment and cylinder separation function is shown in Fig. 4.17(a) and Fig. 4.17(b).

$$\frac{(d^{Settler} - 2 \cdot L_{fe,cp}^{L,Settler})}{d^{Settler}} = \cos(\Psi_1 + \Psi_2) \tag{4.45}$$

$$\Psi_1 = \frac{V^{L,Settler} \cdot 4}{(d^{Settler})^2 \cdot l^{Settler}}$$

$$\Psi_2 = (\frac{d^{Settler}}{2} - L^{L,Settler}) \cdot \frac{4 \cdot \sqrt{(d^{Settler} \cdot L^{L,Settler} - (L^{L,Settler})^2}}{(d^{Settler})^2})$$

It is obvious that the results are similar. There is a difference in the first 300 seconds as effects such as dispersion or circulation of liquid in a real flow cannot be modeled just by analyzing the phase separation. Already after 10 minutes of separation it becomes apparent that the differences of phase heights are marginal (Müller et al., 2014f).

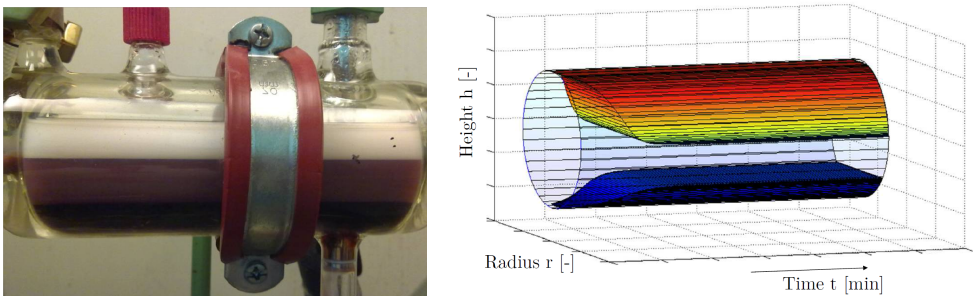

(a) Continuous settler experiment.

(b) Transformed phase separation function.

Figure 4.17.: Validation experiment for the phase separation function (Müller et al., 2014f). In this image, no CO-activated catalyst is used.

Seeing that the phase separation function is highly nonlinear in its cylindrical form, which may cause issues in the later desired optimization calculations, simplifications as presented in Chapter 2.2 are applied. The model is already quite accurate. Now the idea is not to describe the entire phase separation area, but to reduce it to the relevant temperature domain. This can now be described as **Step 9** in the workflow. The fitting correlations to describe this temperature domain are needed. First of all, the region in which the upper phase is greater than 20 % of the beaker height is of interest. This region is adequate for operating the mini-plant. Two parameters can be defined as critical at this point: $T_{min}(\gamma, \alpha, X)$ and $T_{max}(\gamma, \alpha, X)$. These parameters are equivalent to the previously described p_3 and p_6, which in mathematical terms lead to nothing else but the horizontal shift of the sigmoid functions. In the case of this example, they stand for the critical lower and upper temperature, below and above which the desired phase separation does not take place.

Instead of using the entire sigmoid function, an equation is created which calculates $T_{min}(\gamma, \alpha, X)$ and $T_{max}(\gamma, \alpha, X)$ using them as inequality constraints for the later performed optimization run. The height of the oil phase is modified, so that a constant phase height of 20 % is reached. The question now to be asked is, how do $T_{min}(\gamma, \alpha, X)$ and $T_{max}(\gamma, \alpha, X)$ shift with varying concentrations? If the experimental results from section 3.1 are recalled

at this point, this question can be answered. Using the data already obtained the bivariate dependencies are analyzed. Fig. 4.18 displays the bivariate behavior for three cases: T with varying α (Fig. 4.18(a)), T with varying γ (Fig. 4.18(b)), and T with varying X (Fig. 4.18(c)). The other variables are kept constant during each of the cases. Based on these figures, the idea is derived that a quadratic model may be sufficient to describe the temperature bounds.

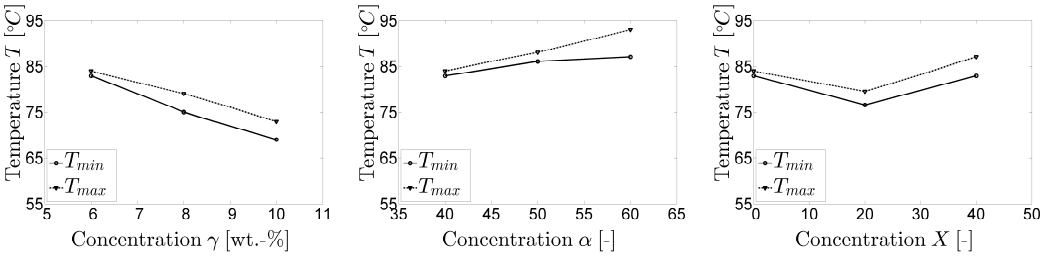

(a) $\alpha = 40\%$, $X = 0\%$. (b) $\gamma = 6\%$, $X = 0\%$. (c) $\gamma = 6\%$, $\alpha = 40\%$.

Figure 4.18.: Ideal temperature interval shift due to concentration changes.

Using multi-nonlinear regression, the equations for $T_{min}(\gamma, \alpha, X)$ and $T_{max}(\gamma, \alpha, X)$ are determined. The final result is displayed in Eq. (4.46) and Eq. (4.47) . The format of both equations is similar, but the parameters of course are different. Thus, two sets of parameters are obtained for $T_{min}(\gamma, \alpha, X)$ and $T_{max}(\gamma, \alpha, X)$ respectively. These are displayed in Tab. 4.7. The quality of the fitting is depicted in the diagrams in Fig. 4.19.

$$\begin{aligned} T_{min} = P_{ps=1}^{Tmin} &+ p_{ps=2}^{Tmin} \cdot \alpha_{s=11} + p_{ps=4}^{Tmin} \cdot \gamma_{s=11} + p_{ps=6}^{Tmin} \cdot X_{s=11} \\ &+ p_{ps=3}^{Tmin} \cdot (\alpha_{s=11})^2 + p_{ps=5}^{Tmin} \cdot (\gamma_{s=11})^2 + p_{ps=7}^{Tmin} \cdot (X_{s=11})^2 \\ &+ p_{ps=8}^{Tmin} \cdot \alpha_{s=11} \cdot \gamma_{s=11} \\ &+ p_{ps=9}^{Tmin} \cdot \alpha_{s=11} \cdot X_{s=11} \\ &+ p_{ps=10}^{Tmin} \cdot X_{s=11} \cdot \gamma_{s=11} \\ &+ p_{ps=11}^{Tmin} \cdot (\gamma_{s=11})^2 \cdot (\alpha_{s=11})^2 + 273.15 \end{aligned} \tag{4.46}$$

$$\begin{aligned} T_{max} = p_{ps=1}^{Tmax} &+ p_{ps=2}^{Tmax} \cdot \alpha_{s=11} + p_{ps=4}^{Tmax} \cdot \gamma_{s=11} + p_{ps=6}^{Tmax} \cdot X_{s=11} \\ &+ p_{ps=3}^{Tmax} \cdot (\alpha_{s=11})^2 + p_{ps=5}^{Tmax} \cdot (\gamma_{s=11})^2 + p_{ps=7}^{Tmax} \cdot (X_{s=11})^2 \\ &+ p_{ps=8}^{Tmax} \cdot \alpha_{s=11} \cdot \gamma_{s=11} \\ &+ p_{ps=9}^{Tmax} \cdot \alpha_{s=11} \cdot X_{s=11} \\ &+ p_{ps=10}^{Tmax} \cdot X_{s=11} \cdot \gamma_{s=11} \\ &+ p_{ps=11}^{Tmax} \cdot (\gamma_{s=11})^2 \cdot (\alpha_{s=11})^2 + 273.15 \end{aligned} \tag{4.47}$$

Using these parameters, the following parity plots can be created. It is obvious that the deviation from the model is fairly small. For most of the measurement data, the deviation lies within a 1.5 K range. This is sufficient for optimization purposes.

Coming back to the workflow, after determining the desired correlations, **Step 10** can be started. It is assumed that the settling time in the settler is equivalent to its length in connection with the inflowing stream. As the settler is fairly large and a minimum settling

Table 4.7.: Lower and upper temperature bound parameters.

Bound	$p_{ps=1}$	$p_{ps=2}$	$p_{ps=3}$	$p_{ps=4}$	$p_{ps=5}$	
T_{min}	292.26	-313.12	217.37	-4,199.14	19,050.35	
T_{max}	267.98	-217.68	101.48	-3,905.84	16,060.69	
	$p_{ps=6}$	$p_{ps=7}$	$p_{ps=8}$	$p_{ps=9}$	$p_{ps=10}$	$p_{ps=11}$
T_{min}	-38.67	70.37	3,570.86	61.66	-372.08	-27,947.00
T_{max}	-30.23	73.14	3,631.63	56.97	-459.40	-24,948.76

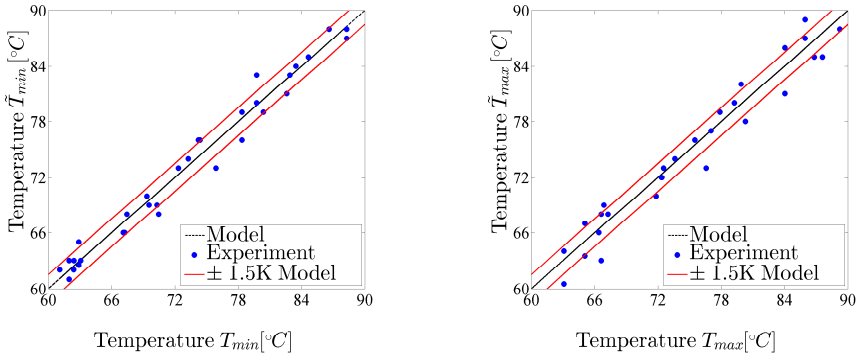

(a) Parity plot for T_{min}.

(b) Parity plot for T_{max}.

Figure 4.19.: Parity plots for the models for the lower and upper temperature bounds.

time of 30 minutes can be achieved, a readjustment is not required. As a next step, the accuracy has to be checked. This has already been performed; the accuracy of the model is high enough for optimization purposes. This then leads to **Step 3** in which the convergence behavior is analyzed. The two temperature functions are explicit and quadratic in the dimensions of γ, α and X. The convergence for any known concentration can be calculated immediately. Thus, this part of the model is ready for optimization studies.

4.3.3. First Principles Model for the Separation Section

After having designed equations to describe the behavior of the ideal temperature separation region, the settler unit must be modeled. This settler consists of basically two units: a splitter and a settler with hold-ups. The idea here is that the if the ideal separation temperature is ensured in the settler, a separation of the entering stream S_{11} takes place. It can be viewed as the activation of a splitting factor set to 30% of stream S_{11}, as this height was observed in the batch settling experiments. Thus, the value of stream S_{12} is calculated.

If the temperature of the settler is outside of the ideal temperature interval between T_{min} and T_{max}, then the entire stream S_{11} goes to the settler as stream S_{13}. Now, several variables in the settler are required:

- the hold-ups and volumes of the liquid and gas phases,
- the levels of each of the phases, and
- the streams leaving the settler.

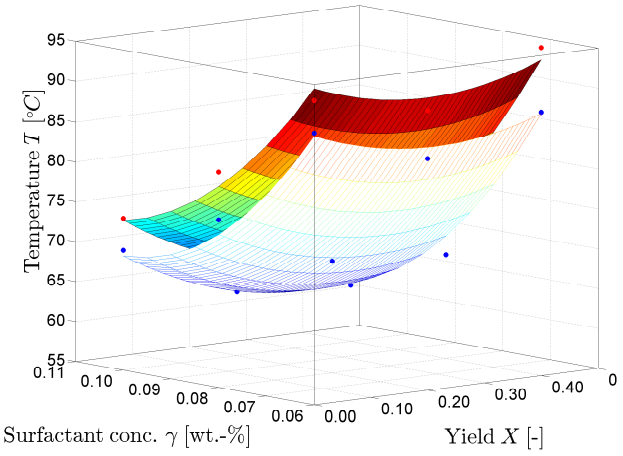

(a) $\alpha = 50\%$.

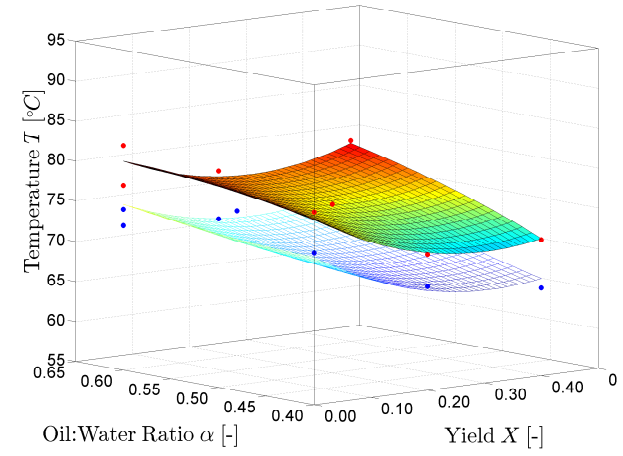

(b) $\gamma = 8\%$.

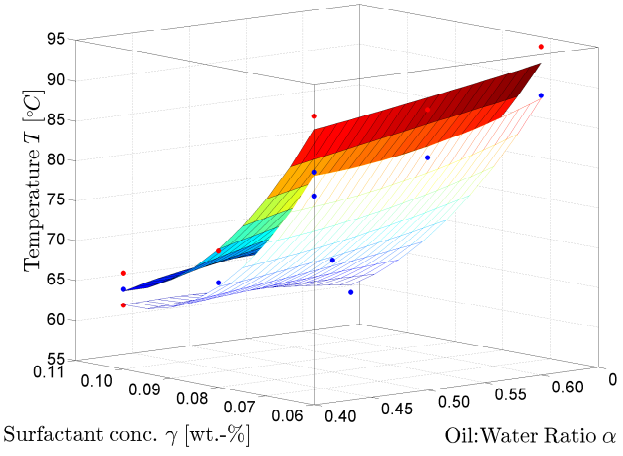

(c) $X = 20\%$.

Figure 4.20.: Model for lower and upper temperature bound.

A step-by-step description to calculate each of these is presented in the following. This is complemented by a discussion of the relevant triggers to activate each of the outflowing streams.

Firstly, the hold-ups in the settler are determined, whereby $HU^{V}_{u=11}$ is the gas hold-up (calculation via ideal gas law) and $HU^{tot,L}_{Settler,i}$ is the total component specific liquid hold-up. $HU^{tot,L}_{Settler,i}$ is split up into two parts: oil phase (u=12) and mixed phase (u=13).

$$\frac{dHU^{V}_{u=11}}{dt} = F_{s=14} - F_{s=15} \tag{4.48}$$

$$\frac{dHU^{L}_{u=12,i}}{dt} = F_{s=12,i} - F_{s=16,i} \tag{4.49}$$

$$\frac{dHU^{L}_{u=13,i}}{dt} = F_{s=13,i} - (F_{s=20,i} + F_{s=21,i}) \tag{4.50}$$

A further description of the hold-ups can be found in Eq. 4.51 and Eq. 4.52.

$$HU^{V}_{u=11} \cdot \sum_{i=1}^{Ni} (\frac{w_{s=9,i}}{M_i}) = \frac{p_{u=11} \cdot 100 \cdot (V_{Settler} - V^{L,tot}_{Settler})}{R \cdot T_{Settler}} \tag{4.51}$$

$$HU^{tot,L}_{Settler,i} = HU^{L}_{u=12,i} + HU^{L}_{u=13,i} \tag{4.52}$$

After defining the hold-ups in the units, the streams must be calculated so that the dynamic behavior of the hold-ups can be determined (Eq. 4.48 to 4.50). The two streams entering the settler are $F_{s=12}$ for the oil phase and $F_{s=13}$ for the mixed phase. If the correct temperature in the settler is set, then a split of the reactor outlet stream occurs.

$$F_{s=11} = F_{s=12} + F_{s=13} \tag{4.53}$$

$$F_{s=12} = \lambda^{Oil}_{u=10} \cdot w^{Oil}_{s=11} \cdot F_{s=11} \cdot TRIG^{Tmax} \cdot TRIG^{Tmin} \tag{4.54}$$

$$\tag{4.55}$$

Before the other streams can be calculated though, the different heights in the settler are required, as these will be used in the stream triggering functions. Now, to evaluate the different phase heights, the total liquid volume in the settler is determined with Eq. 4.56. Additionally, the volume of the mixed phase is calculated, as it is needed to determine the volume of the oil phase in Eq. 4.58.

$$V^{tot,L}_{Settler} = \sum_{i=1}^{Ni} \frac{HU^{tot,L}_{Settler,i}}{\rho_i} \tag{4.56}$$

$$V_{u=13} = \sum_{i=1}^{Ni} \frac{HU^{L}_{u=13,i}}{\rho_i} \tag{4.57}$$

$$V_{u=12} = V^{tot,L}_{Settler} - V_{u=13} \tag{4.58}$$

Next, the total liquid level in the settler is required, as it activates or deactivates the outflowing streams of the settler in the latter presented triggering functions. The total liquid level is equal to the liquid height of the oil and the mixed phase.

$$L^{tot,L}_{Settler} = L_{u=12} + L_{u=13} \tag{4.59}$$

In the previous section it was discussed that the height of liquid in the settler can be calculated analytically. For this purpose, the settler was approximated as a horizontal cylinder. This leads to a complex nonlinear equation where the liquid height is a function of the liquid volume $L^V_{Settler} = f(V)$. As this complex equation is undesired, an approximation is carried out with a third degree polynomial equation. This equation for calculating the settler's total liquid level from the total liquid volume is given in Eq. 4.60. For the parameters the values $Pl1$ = 0.844, $Pl2$ = -0.836, and $Pl3$ = 0.523 are used. In Fig. 4.21 the difference between the analytical and the approximation is shown. It is obvious that the difference is marginal and thus the approximation can be used.

$$L^{tot,L}_{Settler} = Pl1 \cdot V^{tot,L}_{Settler} + Pl2 \cdot (V^{tot,L}_{Settler})^2 + Pl3 \cdot (V^{tot,L}_{Settler})^3 \tag{4.60}$$

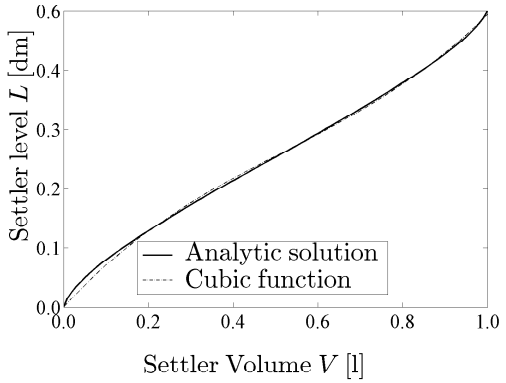

Figure 4.21.: Comparison of equations to calculate the settler liquid level.

As a calculation from the bottom of the cylinder to the top of the middle phase and from the bottom of the cylinder to the top of both phases is possible, the necessity of Eq. 4.58 becomes clear. The aim is to use this information to trigger the streams. For this purpose, several height-criteria for the streams are defined: critical total liquid level $L_{c,tot}$, critical oil phase level $L_{c,13}$, and critical mixed phase level $L_{c,13}$.

First of all a minimal mixed phase liquid height in the settler is required. Secondly, the mixed phase is not allowed to surpass a certain level, because it should not enter the product drain (this leads to high catalyst loss). Thirdly, a minimal oil phase height is required for the product stream to be activated. If the oil phase height is too small, then there is the possibility that some mixed phase enters the product drain. After this criterion has been defined, an evaluation of the different possible cases concerning the phase heights in the settler is required. Based on this evaluation the according triggering functions for the stream definitions can be specified. These different cases are displayed in Fig. 4.22. Twelve possible cases can be imagined:

- The first case is the empty cylinder. Here, obviously non of the outflowing streams are allowed to be active, since the total liquid level in the settler $L^{tot,L}_{Settler}$ is below the minimum mixed phase level $L_{c,13}$.
- The second case is the half full cylinder. Again, $L^{tot,L}_{Settler}$ is smaller than $L_{c,13}$. As in the first case, no stream is allowed to be active.
- In the third case the liquid level is above the middle outlet in the settler, $L^{tot,L}_{Settler}$ is larger than $L_{c,13}$. Here it is important to activate the streams S_{20} and S_{21} to hinder

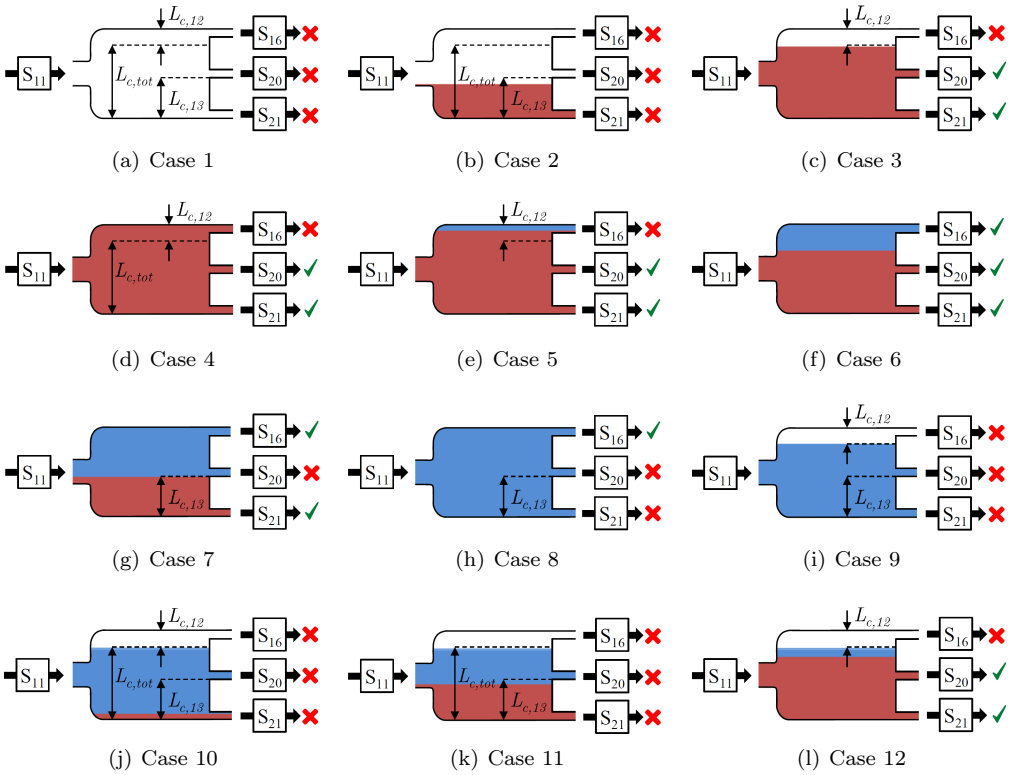

Figure 4.22.: Possible cases of oil and mixed phase levels in the settler.

some mixed phase from entering the product drain. Should the mixed phase level L_{13} reach the product drain, it would be disastrous for the economic viability of the process concept.

- The fourth case is the disaster case, in which the total liquid level is above $L_{c,13}$ and within the critical zone. Since no oil phase has been established streams S_{20} and S_{21} must be active. It is not desired that the middle phase flows into the top outlet, as this is the product outlet. With according triggering functions, this case should never appear.

- In the fifth case, an oil phase has been established. The height of the oil phase h_{oil} is not large enough though, as it is smaller than $L_{c,12}$. The middle phase can potentially flow out through the top outlet. Thus, S_{20} and S_{21} must be active and S_{16} inactive.

- The sixth case represents the ideal situation, in which the phase separation works as desired. The overall liquid level in the settler is larger than the minimally required liquid level, the mixed phase is below the critical level, and the oil phase is large enough. All streams are active in this case.

- In the seventh case, enough oil phase is there and just enough mixed phase. Hence, only the middle stream is turned off.

- In case 8, the entire settler consists of oil. This situation is unlikely in the process. Nevertheless, it is considered here. Even though enough oil is present, there is no mixed phase. Therefore, the two bottom streams must be turned off.

- In the ninth case, the oil phase is large enough, but the overall liquid in the settler is too small. Consequently, all streams are deactivated. The same applies for case 10 and 11.
- For case 12, enough mixed phase is there, but not enough oil phase and the overall height is too small. Therefore, streams S_{20} and S_{21} are activated but stream S_{16} is turned off.

Now, using these levels as triggers, the streams leaving the settler are determined. This begins with the oil stream S_{16}. The stream is calculated via Eq. 4.61. If the trigger $TRIG^{Lvl}_{Settler}$ regarding the overall liquid level in the settler (enough liquid is in the settler) and the trigger $TRIG^{OilLvl}_{Settler}$ regarding the oil level is active, then the oil stream is determined as:

$$F_{s=16} = TRIG^{Lvl}_{Settler} \cdot (TRIG^{OilLvl}_{Settler}) \cdot F_{s=12} + KP_{u=12} \cdot (L^{tot,L}_{Settler} - L^{tot,L,SP}_{Settler})) \tag{4.61}$$

$$\tag{4.62}$$

Should the water level in the settler be too high, then stream S_{20} is needed. Just as before, the triggers $TRIG^{Lvl}_{Settler}$ and $TRIG^{WaterLvl}_{Settler}$ need to be activated as shown in Eq. 4.63. From a practical point of view, this means that if too much mixed phase is in the settler, the liquid in the settler is replaced by the amount of S_{12} to thus allow for an increase of the oil phase to take place. One must keep in mind though that this double trigger formulation may lead to inaccurate behavior, due to the sigmoid functions. Next, the set-point for the pump u_{18} is given. Therefore, the outflowing stream is described via stream S_{24}.

$$F_{s=24} = F_{s=20} \cdot TRIG^{Lvl}_{Settler} \cdot (1 - TRIG^{OilLvl}_{Settler}) \tag{4.63}$$

This leaves the final equation, Eq. 4.64, to calculate the last outflowing stream in the settler. Stream S_{21} (again via S_{25}) is only allowed to flow out if the settler's mixed phase level is high enough ($TRIG^{WaterLvl}_{Settler}$). The stream is corrected by a level-specific set-point.

$$F_{s=25} = TRIG^{WaterLvl}_{Settler} \cdot (F_{s=21} + KP_{u=13} \cdot (L^{tot,L}_{Settler} - L^{tot,L,SP}_{Settler})) \tag{4.64}$$

The two mixed phase streams leaving the settler are brought together via Eq. 4.65.

$$F_{s=13,i} = F_{s=20,i} + F_{s=21,i} \tag{4.65}$$

Concentrations in the settler: A critical and highly relevant question for the optimization of the process operating strategies is the concentration development within the settler and each of the phases. For this part, since no actual concentration analysis has been carried out, several assumptions are made:

- The concentration ratios of the oily components in the oil and in the mixed phase streams (S_{12} and S_{13}) are the same as those of the incoming stream S_{11}.
- The catalyst precursor and ligand are solved in water. Their concentration ratio is therefore only dependent on the concentration of water in the according phases.
- The isomer iso-dodecene behaves as 1-dodecene.
- The byproduct n-dodecane behaves as 1-dodecene.

Going forward, assumptions regarding the purity of the oil phase are made. In a first mini-plant operation it has been observed, that the purity of the oil phase is somewhat dependent on the concentration of 1-tridecanal. In case of the absence of 1-tridecanal (before the reaction initiation in the process) the mass fraction of the sum of oily components is almost 100 wt.-%. For an average mass fraction of 10 wt.-% 1-tridecanal in the incoming stream, the purity regarding oily components in the oil phase is reduced to roughly 96 wt.%. This can be seen in Fig. 4.23 between 40^{th} to 60^{th} operation hour.

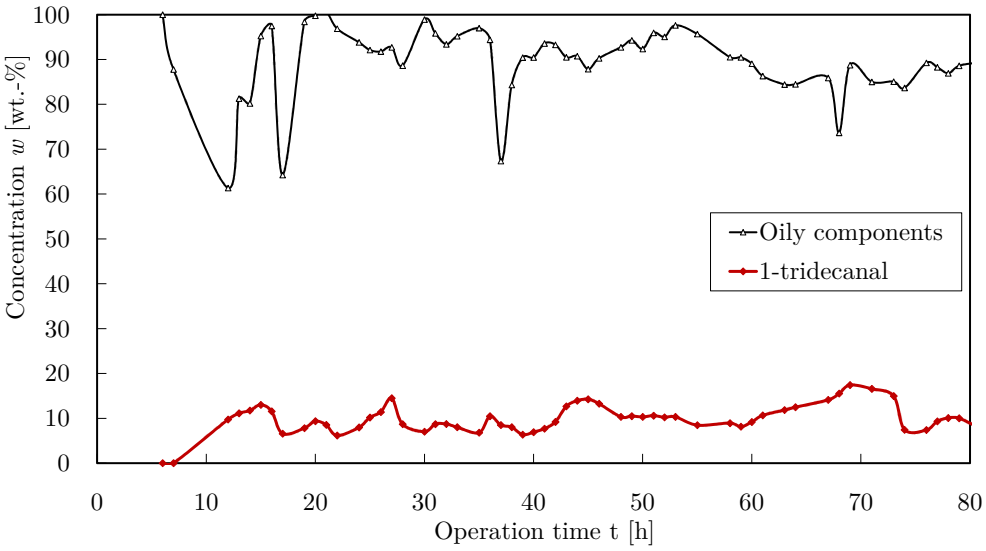

Figure 4.23.: Settler concentration modeling: oil and 1-tridecanal concentration during a first mini-plant operation.

In this figure, the spikes are omitted at which the concentration of the oily components is drastically reduced, because the phase separation did not work there. Once the concentration of 1-tridecanal reaches higher values of around 20 wt.-% (65 - 75 operating hours) the average concentration of oily components lies around 92 wt.-%. This result is logical, because 1-tridecanal is more hydrophilic than 1-dodecene. It acts somewhat as a surfactant increasing the water and actual surfactant concentration in the oil phase. Based on this qualitative observation, a first simple concentration model is developed. Eq. 4.66 to Eq. 4.71 show the resulting concentration equations.

$$w_{s=12}^{Oil} = \frac{0.92 - 1.00}{0.2} \cdot (w_{s=11,i=5} + w_{s=11,i=3}) + 1 \tag{4.66}$$

$$w_{s=12}^{Oil} = w_{s=12,i=1} + w_{s=12,i=2} + w_{s=12,i=3} + w_{s=12,i=4} + w_{s=12,i=5} \tag{4.67}$$

The idea in Eq. 4.66 is that the purity of the oil phase depends on the 1-tridecanal concentration. If the concentration of 1-tridecanal is 0 wt.-%, then the oil phase is pure. If the concentration rises, then 1-tridecanal "pulls" water and surfactant into the oil phase, thus diminishing the purity (via a linear equation). The mass fraction of oil in the oil phase, $w_{u=12}^{Oil}$, can expressed as the sum of oily components ($i = 1, ..., 5$), as shown in Eq. 4.67. The concentration of water ($i = 9$) can be determined via Eq. 4.68.

$$w_{s=12,i=9} = 1.00 - w_{s=12}^{Oil} - w_{s=12,i=12} \tag{4.68}$$

It must be emphasized at this point that several assumptions are made here, which may not be accurate in reality. These assumptions are currently necessary, as no detailed mea-

surement data are available. These are concerned with the precursor, the ligand, and the surfactant (Eq. 4.69 to Eq. 4.71).

$$w_{s=12,i=10} = w_{s=12,i=9} \cdot \frac{w_{s=11,i=10}}{w_{s=11,i=9}} \tag{4.69}$$

$$w_{s=12,i=11} = w_{s=12,i=9} \cdot \frac{w_{s=11,i=11}}{w_{s=11,i=9}} \cdot 0.01 \tag{4.70}$$

$$w_{s=12,i=12} = w_{s=12,i=9} \cdot \frac{w_{s=11,i=12}}{w_{s=11,i=9}} \cdot 0.01 \tag{4.71}$$

The surfactant concentration entering the setter via the oil stream split stays in the same ratio as in the original mixture coming from stream S_{11}, which is shown in Eq. 4.71. As mentioned above, it is assumed that the catalyst remains in water. Thus, the water concentration in the oil phase indirectly represents the catalyst concentration (Eq. 4.69 and Eq. 4.70). The value is multiplied by 1 %, which represents a loss to the oil phase of 1 % in accordance with experiemntal data. In Tab. 4.8 rhodium concentrations with respective alkene, water, and surfactant concentrations are shown. In the results of lab[2] and mini-plant experiments, in which the concentrations of the oil phase were analyzed, concentrations below 0.5 ppm rhodium were measured. For the mini-plant experiments, results are listed for which the rhodium concentrations surpass 0.03 ppm, which is the detectability bound of the ICP.

Table 4.8.: Rhodium concentrations in lab-scale analyses of the oil phase. Samples Oil I and Oil II are lab-scale analyses results. The rest are results from the mini-plant operation.

	Oily components [wt.-%]	1-tridecanal [wt.-%]	rhodium precursor [ppm]
Oil I	100	0	0.165
Oil II	100	0	0.026
Oil III	90.4	8.1	0.022
Oil IV	90.5	12.3	0.065
Oil V	85.9	14.9	0.097
Oil VI	95.2	16.6	0.121
Oil VII	81.3	17.1	0.089

As an example for the rhodium concentration calculation: a stream leaving the reactor contains 6.6 wt.-% 1-tridecanal, 39.4 wt.-% 1-dodecene, 8 wt.-% surfactant, and 46 wt.-% water. The catalyst concentration in the water lies at around 650 ppm. If the splitting from Eq. 4.66 is assumed, then an oil phase of 97.36 wt.-% with 16.8 wt.-% 1-tridecanal is established. Of the remaining 2.64 wt.-% roughly 0.46 wt.-% would be surfactant. With the manually selected factor of 0.01 in the equations, the measured values from Tab. 4.8 are slightly overestimated. For this example (6.6 wt.-% 1-tridecanal feed), which roughly equals sample "Oil VI", a catalyst concentration of around 0.28 ppm would be carried into the oil phase. In the future, more focused measurements are required, which analyze these concentrations more accurately.

For the later to be performed optimization this means that in order to keep the rhodium loss low, the 1-tridecanal production needs to be limited. Otherwise too much water would enter the oil phase. For an actual concentration model though, more detailed concentration measurements must be carried out in the future.

[2]The results are taken from Felix Leube's Master's thesis, p. 58.

4.4. Mini-plant Section 4: Recycle and Product Storage

The final section is the recycle and product storage section. Fig. 4.24 shows the model scheme for the recycle and product storage section. Basically, eight vital process units can be found here. These are

- the buffer tank for the oil phase after the settler (unit 14),
- the splitter splitting the product stream to the recycle and product storage (unit 15),
- the valve for product release (unit 16),
- three pumps for the recycle of the mixture back to the reactor (units 17 to 19),
- the product storage tank (unit 20), and
- the mixer of the recycle streams (unit 21).

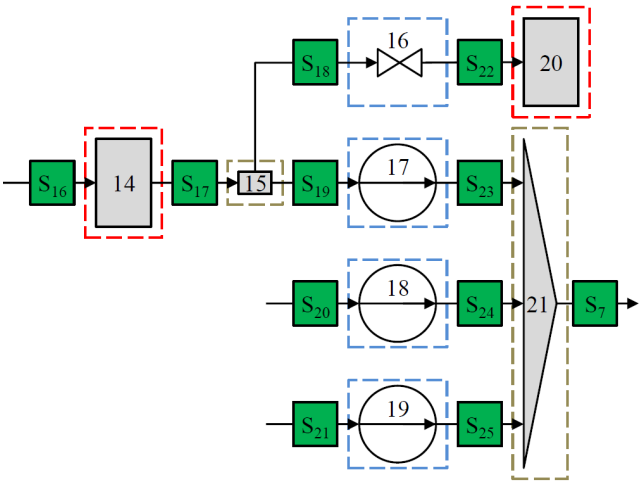

Figure 4.24.: Model scheme of the recycle and product storage section of the hydroformylation mini-plant at Technische Universität Berlin.

As for the feed section, no critical equations besides the standard MESH equations are required in this section. Nevertheless, the description is divided into equations concerning solely the recycle and those concerning the product storage. As the product storage is reached before the recycle part, it will be explained first.

Product Storage Section: The equations leading to the product storage section are defined in the following. Firstly, the storage tank u_{14} including the component streams is described:

$$\frac{dHU^{L}_{u=14,i}}{dt} = F_{s=16,i} - F_{s=17,i} \tag{4.72}$$

$$HU^{L}_{u=14,i} \cdot F_{s=17} = HU^{L}_{u=14} \cdot F_{s=17,i} \tag{4.73}$$

$$\sum_{i=1}^{Ni} \frac{HU^{L}_{u=14,i}}{\rho_i} = L_{u=14} \cdot A_{u=14} \tag{4.74}$$

Should a successful separation in the settler be achieved, then a stream S_{16} enters the storage tank u_{14}. The amount leaving this tank is described with stream S_{17}. A triggering function describing the stream going to the product storage tank is needed. In the real

plant, the control valve u_{16} itself has already been tuned for a certain range of set-points. Eq. 4.75 and Eq. 4.77 are formulated to describe the outflowing stream S_{18}:

$$F_{s=17,i} = F_{s=18,i} + F_{s=19,i} \tag{4.75}$$

$$F_{s=18,i} \cdot HU^{L}_{u=14} = HU^{L}_{u=14,i} \cdot F_{s=18} \tag{4.76}$$

$$F_{s=18} = TRIG^{Lvl}_{u=14} \cdot (F_{s=16} - F_{s=23}) \tag{4.77}$$

In the former, the mass balance of the splitter u_{15} is defined. This is influenced by with the mass balance concerning the value of stream S_{18}. The idea is that the stream S_{16}, which is being fed into container u_{14}, is equal to the recycle stream S_{23} and the product stream S_{18}. If the level of container u_{14} is too low, then stream S_{16} and S_{23} are deactivated. Thus, no product leaves the system.

Finally, the amount of product entering the product tank u_{20} is given in Eq. 4.78.

$$\frac{dHU^{L}_{u=20,i}}{dt} = F_{s=22,i} \tag{4.78}$$

Recycle Section: For the recycle section the main focus lies on the three pumps and the mixer. First of all, the mass balances around the pumps and the mixer are formulated:

$$F_{s,i} = F_{s+4,i} \quad \text{for } s = \{19...21\} \text{ and} \tag{4.79}$$

$$F_{s=7,i} = F_{s=23,i} + F_{s=24,i} + F_{s=25,i} \tag{4.80}$$

To complement these, triggering functions for the pumps are required. These are mainly dependent on the different liquid levels in the settler. The conditions are:

- If the settler is empty, no pump should be activated.
- If the liquid in the settler is above the critical level of the water phase, then pump u_{18} may be activated.
- If there is no oil phase in the settler, then pump u_{17} may not be activated.

Thus, the product and recycle section are fully described. Next, the auxiliary equations need to be formulated.

4.5. Mini-plant Auxiliary Equations

The mini-plant model contains several auxiliary equations. Among these are the triggering functions and the gas solubilities. In the following, these will be discussed.

4.5.1. Triggering Equations

As mentioned in the previous sections, for different actions various triggering equations are required. The first triggering equation is concerned with the outflowing stream of the reactor. When a liquid height equaling 70 % of the absolute reactor height is reached, the stream starts to flow out. This is shown in Eq. (4.81). Important variables in this equation are $L_{u=9}$, which is the height of the liquid hold-up in the reactor, and $L^{SP}_{u=9}$, which is the

mentioned 70 % absolute reactor height.

$$TRIG_{u=9} = \frac{1}{2} + \frac{\frac{1}{2} \cdot (L_{u=9} - L_{u=9}^{SP})}{\sqrt{(L_{u=9} - L_{u=9}^{SP})^2 + \epsilon_{u=9}}} \tag{4.81}$$

The next relevant triggering functions are found in the settler. A detailed discussion on each of these has already been done in the previous sections. Therefore, only the relevant switching values are presented here. The format of the triggering equation stays the same as in Eq. (4.81), only that $L_{u=9}$ and $L_{u=9}^{SP}$ are replaced accordingly.

- Trigger 1 for phase separation (minimum temperature): $T_{Settler}$ vs. $T_{min} = f(\alpha, \gamma, X)$.
- Trigger 2 for phase separation (maximum temperature): $T_{Settler}$ vs. $T_{max} = f(\alpha, \gamma, X)$.
- Trigger checking the total level in the settler: $L_{Settler}^{tot,L}$ vs. $L_{Settler}^{tot,L,SP} = 0.53$ dm
- Trigger checking the oil phase level: $L_{u=13}$ vs. $L_{u=13}^{SP} = 0.08$ dm
- Trigger checking the mixed phase level: $L_{u=12}$ vs. $L_{u=12}^{SP} = 0.27$ dm
- Trigger to check the maximal oil phase level which equals twice the minimal oil phase level.

The applied ϵ values for each of the triggers can be taken from the variable specifications stored in the web-based modeling environment MOSAIC[3].

4.5.2. Gas Solubility

The other auxiliary equations are concerned with the gas solubility. To model the reaction correctly knowledge regarding the amount of CO and H_2 dissolved in the mixture in the reactor is required. Hereby, the following assumptions are made:

- The molar content of syngas dissolved in the reaction mixture can be split up into moles of CO and moles of H_2 at a molar ratio of 1 to 1:

$$n_{syngas}^{solved} = n_{CO}^{solved} + n_{H_2}^{solved} \tag{4.82}$$

- Since to the current point in time measurements of the solubility of syngas in mixtures containing all components of the hydroformylation system discussed herein have not been performed, a workaround is used. It is assumed that the total mole amount of the gas dissolved in the system, $n_{CO}^{tot,solved}$ and $n_{H_2}^{tot,solved}$, is equal to the sum of the moles of gas dissolved in each component, $n_{g,i}$ in the system. The index g stands for CO or H_2 and i for each of the components in the system. Of course this means that an interaction between the different components regarding the solubility is neglected. Eq. (4.83) to Eq. (4.85) show this assumption exemplarily for CO.

$$n_g^{tot,solved} = \sum_i^{N_i} n_{g,i} \tag{4.83}$$

$$x_{g,i} = \frac{n_{COini}}{(n_i + n_{g,i})} \tag{4.84}$$

$$n_{g,i} = \frac{n_i}{1 - x_{g,i}} - n_i \tag{4.85}$$

[3] www.mosaic-modeling.de

- The mole amount of gas dissolved in surfactant is negligible.
- Furthermore, the different components have different solubility kinetics. These kinetics are neglected. Research on this part has yet to be performed for the current system.

In the following the solubility of syngas in each relevant component during the reaction is determined. For this purpose, Henry's law is applied:

$$p_g = H_{g,i} \cdot x_{g,i} \tag{4.86}$$

Next, the temperature dependency of the Henry constants $H_{CO,i}$ and $H_{H_2,i}$ are modeled, if not explicitly stated otherwise, with a quadratic function. Thus, the mole fraction of gas g dissolved in the solvent i, can be calculated from Eq. (4.86) and Eq. (4.87).

$$H_{g,i} = H_{0,g,i} + H_{1,g,i} \cdot T + H_{2,g,i} \cdot T^2 \tag{4.87}$$

Syngas solubility in dodecene: Very few authors have published experimental results regarding syngas solubility in the solvent 1-dodecene. Solely (Vogelpohl et al., 2013) have performed experiments regarding CO in 1-dodecene and iso-dodecene. Therein, the mole fraction of CO in 1-dodecene and iso-dodecene is measured for different temperatures and pressures. Seeing a quadratic behavior in the experimental data set regarding the solubility for various temperatures, an equation of the type Eq. (4.87) has been determined to be adequate. Using this equation, multi-nonlinear regression of the data set from (Vogelpohl et al., 2013) is performed. Additionally, in the experiments carried out by Vogelpohl et al. (2014), the solubility of hydrogen (H_2) in 1-dodecene and iso-dodecene is analyzed as well. Just as for the experiment for the solubility of CO in 1-dodecene, the temperature and pressure are varied. The data sets are then also fitted to Eq. (4.87). Fig. 4.25 shows the experimental data sets and the fitted model for both gases. The model deviation from the data is sufficiently small.

Syngas solubility in tridecanal: The next essential component in the system is the product 1-tridecanal. The solubility of syngas in the product 1-tridecanal and iso-tridecanal is of interest, because the amounts continuously increase to an expected value of roughly 50 wt.-% in the oil phase. Consequently, tridecanal appears in larger quantities in the liquid phase within the reactor and poses a potential reservoir of syngas for the reaction. Vogelpohl et al. (2013) also measured the solubility of CO in tridecanal. Again, the approach shown in Eq. (4.87) is selected to fit the data. The results are shown in Fig. 4.26(a) and the parity plots in Fig. 4.26(b). The parity plots show a very good fit for the solubility model for tridecanal.

Besides, the solubility of hydrogen in tridecanal is required. At the current point in time, no data are available. Therefore, a workaround is required. A data set for the solubility of hydrogen in dodecanal is available. Due to the similarity of the chemical structure between 1-dodecanal and 1-tridecanal only a minimal offset is expected. The used data set stems from (Vogelpohl et al., 2014). The same calculation of the quadratic temperature-dependent Henry coefficient as for the previous fittings is thus carried out. Fig. 4.25 shows this fit. Here, the results are not as exact due to the variance of the measurement data.

Syngas solubility in n-dodecane: Another relevant component in the oil phase is n-dodecane. Dodecane is the main byproduct of the reaction and will amount to roughly 2 wt.-% in the oil phase. In (Gao et al., 1999) the solubility of CO and H_2 in dodecane are measured.

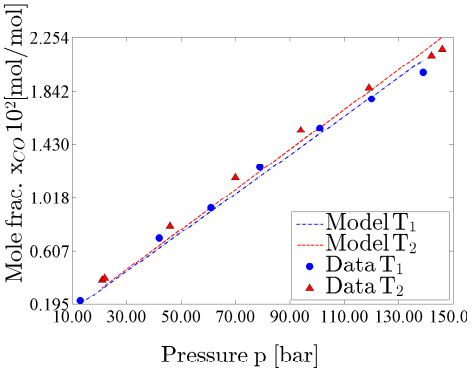

(a) CO in dodecene

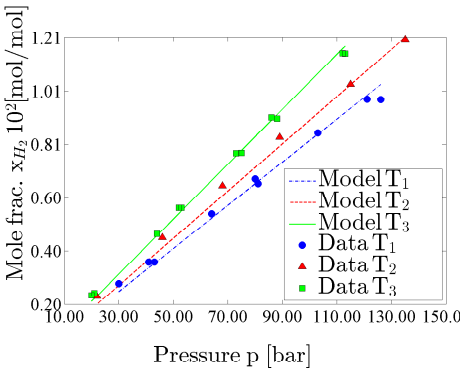

(b) H_2 in dodecene

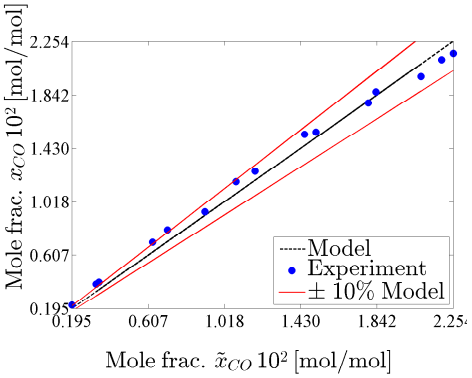

(c) Parity plot: CO in dodecene

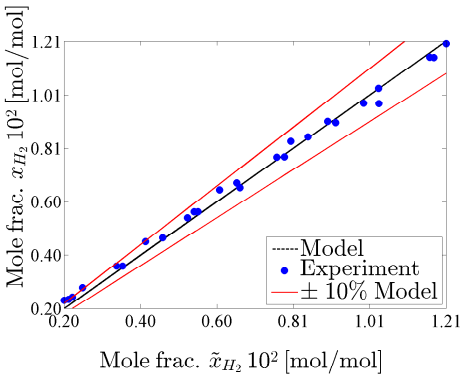

(d) Parity plot: H_2 in dodecene

Figure 4.25.: Gas solubility: CO & H_2 in dodecene. For CO, T_1 = 310.7 K and T_2 = 364.0 K. For H_2, T_1 = 304.9 K, T_2 = 333.2 K, and T_3 = 364.5 K. The data stems from (Vogelpohl et al., 2014).

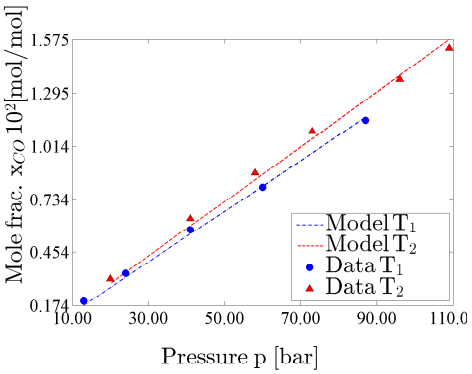

(a) CO in tridecanal

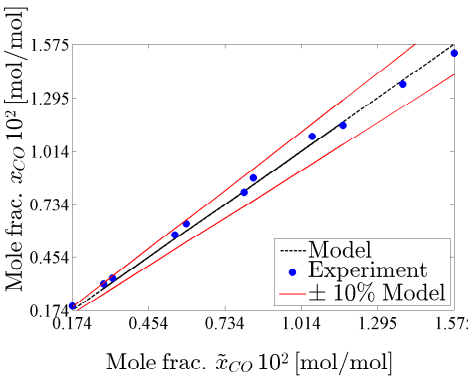

(b) Parity plot

Figure 4.26.: Gas solubility: CO in tridecanal (T_1 = 303.1 K and T_2 = 362.4 K). The data stems from (Vogelpohl et al., 2013)

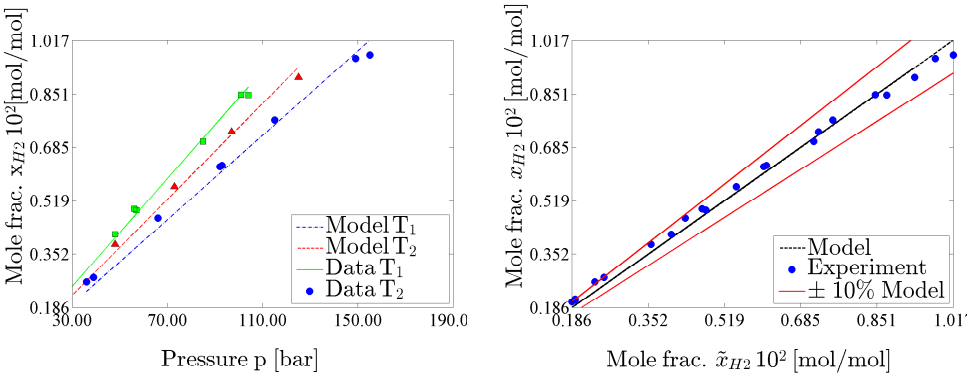

(a) H_2 in tridecanal (b) Parity plot

Figure 4.27.: Gas solubility: H_2 in dodecanal (T_1 = 303.8 K, T_2 = 335.7 K, and T_3 = 363.1 K). The data stems from (Vogelpohl et al., 2014).

Again, the equation shown in Eq. (4.87) is used to fit the data. The models for CO and H_2 are shown in Fig. 4.28(a) and in Fig. 4.29(a) respectively. The parity plots are shown in Fig. 4.28(b) and Fig. 4.29(b). For both CO and H_2 decent fitting can be achieved, the errors are well below a 5 % deviation from the model.

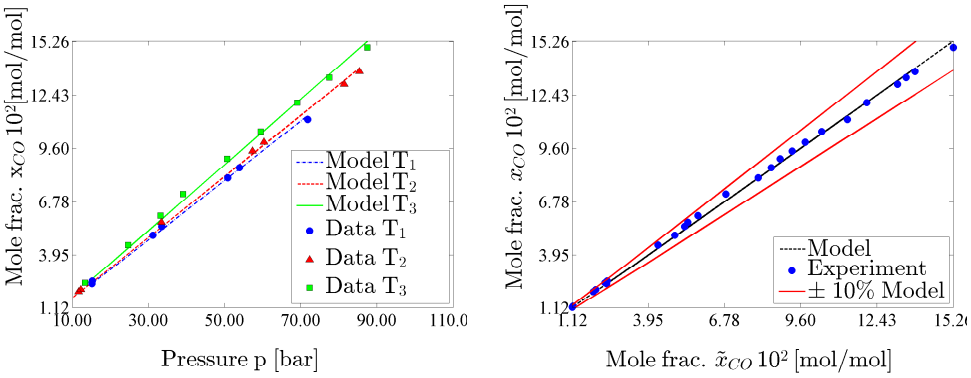

(a) CO in n-dodecane (b) Parity plot

Figure 4.28.: Gas solubility: CO in n-dodecane (T_1 = 344.3 K, T_2 = 377.6 K, and T_3 = 410.9 K). The data stems from (Gao et al., 1999).

Syngas solubility in water: The component with the largest mass fraction in the reactor is water. Therefore, special attention is given to the modeling of the solubility of syngas in water. At the National Institute of Standards and Technology (*NIST*) correlations for CO in (NIST, 2014a) and H_2 in (NIST, 2014b) can be found. These correlations presented on the *NIST* chemistry webbook are taken from (Lide and Frederiksen, 1995). Eq. (4.88) shows the general structure of these correlations.

$$H_{g,i} = H^o_{g,i} \cdot e^{\left(\frac{d(ln(k_H))}{d(1/T)} \cdot \left(\frac{1}{T} - \frac{1}{T_{ref}}\right)\right)} \tag{4.88}$$

Herein, $H^o_{g,i}$ is Henry's law's constant for the solubility in water at 298.15 K (mol/kg*bar)

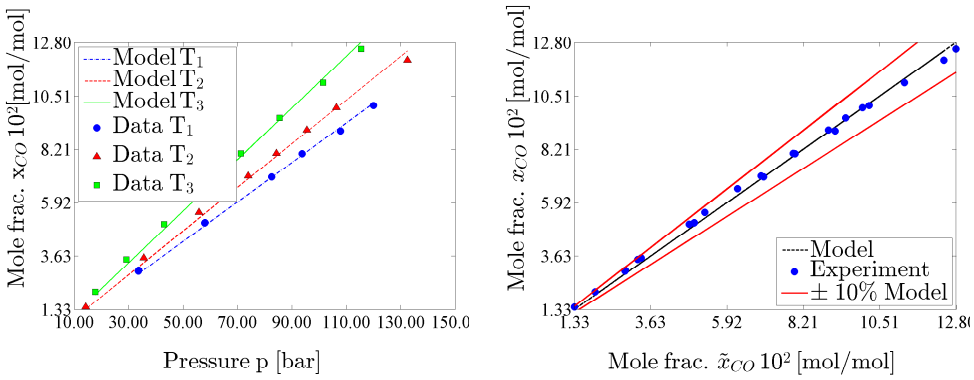

(a) H_2 in n-dodecane (b) Parity plot

Figure 4.29.: Gas solubility: H_2 in n-dodecane (T_1 = 344.3 K, T_2 = 377.6 K, and T_3 = 410.9 K). The data stems from (Gao et al., 1999).

and $d(ln(k_H))/d(1/T)$ is the temperature dependence constant (K) . To determine the mole amount dissolved in the solvent, Eq. 4.89 is applied.

$$n_{g,i} = H_{g,i} \cdot p_g \cdot m_i \tag{4.89}$$

$$x_{g,i} = \frac{H_{g,i} \cdot p_g}{\frac{1}{\tilde{M}_i} + H_{g,i} \cdot p_g} \tag{4.90}$$

Eq. (4.89) is then expanded to Eq. (4.90), in order to determine the mole fraction of syngas in water. Here, p_g is the partial pressure of the gas in the gas phase and $\tilde{M}_i$ is the molar mass of the solvent. From (NIST, 2014a) and (NIST, 2014b) constants for CO and H_2 are obtained. The values are listed in Tab. 4.9. Based on these correlations, a data set for 1 bar in the range of 273 to 363 K in 5 K steps is generated. This generated data set is then used to fit the equation presented above.

Table 4.9.: NIST syngas in water solubility parameters.

Gas	$\mathbf{H}^{o}_{g,S}$ [mol/kg*bar]	$d(ln(k_H))/d(1/T)$ [K]
CO	$9.9 \cdot 10^{-7}$	1300
H_2	$7.8 \cdot 10^{-7}$	500

The generated data set is mixed with experimental data for higher pressures from (Wiebe and Gaddy, 1934). Fig. 4.30 shows the model for the solubility of CO and H_2 in water for different temperatures across a pressure range.

Summary of results for the main liquid components: As a reminder, dissolved gas in the mixture is calculated with the previously presented equations Eq. 4.83 to Eq. 4.85. This general assumption from Eq. (4.83) is now tested with available data. A comparison between syngas dissolved in 1-dodecene and the sum of hydrogen and carbon monoxide dissolved in 1-dodecene is made. The data set for syngas dissolved in 1-dodecene is taken

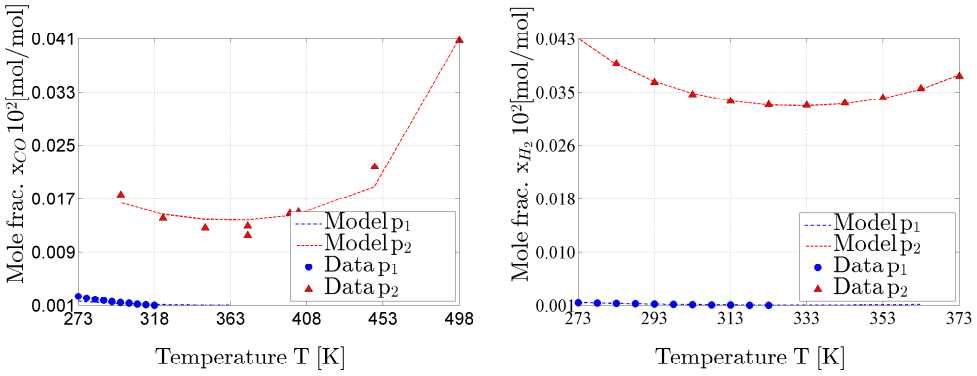

(a) Solubility CO in water

(b) Solubility H_2 in water

Figure 4.30.: Mol fraction of dissolved CO and H_2 in water at different temperatures for two pressures. For CO the pressures are 1.013 bar and 10.13 bar. For H_2 the pressures are 1.013 bar and 25.325 bar. The correlations stem from (NIST, 2014a), (NIST, 2014b), and (Lide and Frederiksen, 1995) respectively and are displayed as data points in the figures above.

from (Vogelpohl et al., 2014). Again, as for the data sets presented for all other solubilities, a quadratic temperature dependent Henry correlation is used. Fig. 4.31 shows the result for a temperature of 358 K and pressures ranging from 1 to 30 bar. The difference is marginal, which validates the assumption.

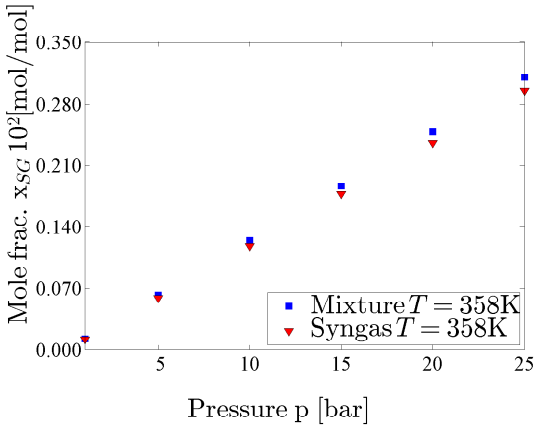

Figure 4.31.: Comparison between syngas in 1-dodecene and a mixture of CO and H_2 in 1-dodecene.

For the components dodecene, tridecanal, dodecane, and water the following parameter values shown in Tab. 4.10 are used to determine the solubility of syngas in the mixture:

$$H_{g,i} = H_{0,g,i} + H_{1,g,i} \cdot T + H_{2,g,i} \cdot T^2$$

Table 4.10.: Solubility parameter values for the main liquid components.

Component	$H_{1,g,i}$ [-]	$H_{2,k,i}$ [1/K]	$H_{3,k,i}$ [1/K^2]
Gas: carbon monoxide			
1-dodecene	297.607	41.362	-0.067
1-tridecanal	171.854	51.663	-0.091
n-dodecane	-792.899	8.371	-0.012
water	-273,312.539	1,905.848	-2.624
Gas: hydrogen			
1-dodecene	2,221.272	96.558	-0.210
1-tridecanal	55,975.538	-200.442	0.218
n-dodecane	-667.053	13.315	-0.023
water	-544,626.028	3,761.933	-5.682
Gas: syngas, ratio 1:1			
1-dodecene	1,247.608	82.478	-0.177

Chapter 5.

Process Uncertainty Analysis

In the previous chapters information regarding the actual process concept, the mini-plant, and the model of the mini-plant was presented. The goal in this thesis is to perform online-optimization under uncertainty. In order to do this additional information is required: the relevant uncertainty surrounding the process concept. In Section 2.3 a classification as well as a quantification for different uncertainty types for chemical engineering systems was discussed. This classification and quantification is now applied for the hydroformylation process concept. A focus is hereby laid on the first two types: process-inherent uncertainty and model-inherent uncertainty. Additionally, the results of the applied uncertain parameter selection method discussed in Section 2.3.3 for the parameter estimation of the reaction kinetics of the process are presented and discussed herein.

5.1. Process Inherent Uncertainty

Process inherent uncertainty contains variations of streams, temperatures, pressures, and concentrations and is often obtained from online measurements. Of utmost importance for the online-optimization of the process is the uncertainty concerning the controls of the process. For the hydroformylation mini-plant these controls are the flow rates controlled by the three feed pumps and the three recycle pumps, the temperature of the reactor and settler, and the opening of the gas valve of syngas. Of high relevance is the variance of the feed streams from the feed pumps. All other measurement devices have such low measurement errors, that their impact on the process operating strategies in negligible. Fig. 5.1 shows a normalized histogram for the alkene feed stream.

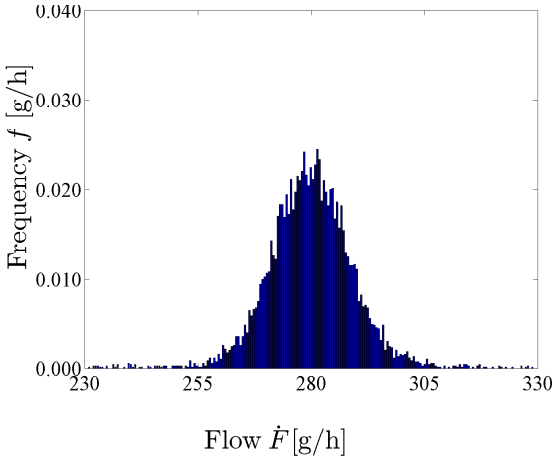

Figure 5.1.: Variance of the alkene feed stream values for a constant operating point of 280 g/h.

To shed light upon the issue of uncertainty in measurements, data sets from performed mini-plant operations are used. Time intervals of one to two hours are analyzed in which the process is operated at steady-state. Using the data points, an according variance analysis is carried out. Tab. 5.1 shows the determined standard deviations for a row of set-points.

Table 5.1.: Process uncertainty: standard deviations of the feed streams from set-point values. $F_{s=1,2,3}$ are the alkene feed stream, the catalyst feed stream, and the surfactant feed stream

	$F_{s=1}$ $[g/h]$	$F_{s=2}$ $[g/h]$	$F_{s=3}$ $[g/h]$
Set-point 1	300	200	270
σ	30	28	30
Set-point 2	200	50	150
σ	20	4	25
Set-point 3	100	20	30
σ	10	2	1

The measurement error of the implemented FIC is determined to be at least 4.7 %. This value stems from the manufacturer-defined operating point of 60 bar. For every 1 bar of pressure deviating from this operating point, an error of 0.1 % is expected with a base error or 0.2 %. As discussed in several previous contributions, such as (Müller et al., 2013a, 2014d,c), our operating point lies at 15 bar. Nevertheless, an analysis of the data points presented in Tab. 5.1 shows that the standard deviation of the measurement is dependent on the actual value of the stream. For each of the feed streams the standard deviation is roughly 10 % of the nominal value of the stream. An implementation of this concept into the chance-constrained framework is done as shown in Eq. 5.1 exemplarily for stream S_4 (which equals S_1 and is the alkene feed stream).

$$F_{s=4} = (1 + \xi_3) \cdot F_{s=4}^{SP} \qquad \text{with} \qquad \xi_3 = \mathcal{N}(0, 0.1) \tag{5.1}$$

The set-point of stream S_4 is thus manipulated by the uncertain parameter ξ_3. This parameter has an expected value of 0, but a standard deviation of 0.1. That way, the true value of the stream is changed within the desired range. The same applies for the other feed streams as well as for the three recycle streams[1]. For the other controls, a close analysis of the measurements has shown, that the variance of the reactor temperature as well as of the settler temperature is negligibly small. This also applies to the opening time of the gas valve.

5.2. Model Inherent Uncertainty

As mentioned in Chapter 4, the main uncertain parameters in the mini-plant model can be found in the reaction kinetics. In this section, a summary of those results is presented and the uncertainty of each relevant parameter is highlighted.

Sensitivity Analysis: Of interest is the effect of the uncertainty of the parameters (expressed via their variance) on the output of the model. Therefore, a sensitivity analysis of the two most relevant parameters is performed. The two parameters were previously determined in

[1]The same ξ_3 is used for all the streams

the parameter estimation process, $E_{r=5}$ and K_{cat}. Hereby, the values of the parameters are deviated by ± 10 % and their effect on the output of the the product 1-tridecanal is observed for the semi-batch reaction performed at 85 °C and 15 bar. Only the final output value is analyzed (after 4 h of batch reaction). Tab. 5.2 shows the eight cases with the corresponding values used for the uncertain parameters in the sensitivity study.

Table 5.2.: Expected values of uncertain parameters modified by ± 10 % for sensitivity analyses.

	$\Delta E_{r=5}$ [%]	ΔK_{cat} [%]	$E_{r=5}$ $[J/mol]$	K_{cat} $[l/mol]$
Case 1:	-10 %	0 %	$1.7 \cdot 10^4$	$4.2 \cdot 10^2$
Case 2:	+10 %	0 %	$2.1 \cdot 10^4$	$4.2 \cdot 10^2$
Case 3:	0 %	-10 %	$1.9 \cdot 10^4$	$3.8 \cdot 10^2$
Case 4:	0 %	+10 %	$1.9 \cdot 10^4$	$4.7 \cdot 10^2$
Case 5:	-10 %	-10 %	$1.7 \cdot 10^4$	$3.8 \cdot 10^2$
Case 6:	+10 %	+10 %	$2.1 \cdot 10^4$	$4.7 \cdot 10^2$
Case 7:	-10 %	+10 %	$1.7 \cdot 10^4$	$4.7 \cdot 10^2$
Case 8:	+10 %	-10 %	$2.1 \cdot 10^4$	$3.8 \cdot 10^2$

The result of the value change is displayed in Fig. 5.2. It is obvious, that the activation energy parameter has the largest influence on the output. As depicted for Case 1, a reduction of the activation energy leads to a massive production of 1-tridecanal, doubling the concentration in the analyzed time-frame (4 h batch reaction). On the other hand, an increase of the activation energy by 10 % completely stops the production of 1-tridecanal (Case 2, 6, & 8). In all cases, where the activation energy is increased, no production of tridecanal took place. A change of the parameter K_{cat} on the other hand only has a minor effect. Here, a decrease of the inhibition factor leads to an increase of 1-tridecanal by roughly 7.5 % and vice versa. In comparison to the influence caused by a change of $E_{r=5}$, this result is almost negligible. Therefore, concluding it can be said that the parameter containing the most relevant uncertainty is the activation energy of the hydroformylation reaction.

Nevertheless, a reduction of both uncertain parameters leads to an even greater increase in the 1-tridecanal output (Case 5). This may become extremely important during the optimization, in which a prediction of the 1-tridecanal production in the reactor is performed. The result has an influence on the subsequent separation step and strongly determines the operation strategy.

Monte Carlo Simulations: To analyze the effect of the actually determined uncertain parameters with their variance, Monte Carlo Simulations (MCS) are carried out exemplarily for the semi-batch reaction performed at 85 °C and 15 bar. For this purpose, 100 MCS are done. Fig. 5.3 shows the MCS results for 1-dodecene ($i = 1$) and 1-tridecanal ($i = 5$), while Fig. 5.4 depicts the distribution of the final simulation value (t=4 hours) for 1-tridecanal. Tab. 5.3 presents the expected values as well as the variances of the parameters. Those parameters with a variance of 0 are the inactive parameters from the parameter estimation and subset selection. These parameters are fixed. The other parameters are the uncertain parameters that are used as in ξ_i in the optimization studies.

It is apparent from Fig. 5.3 that for the experiment performed at 85 °C and 15 bar the reaction of 1-dodecene is slightly too small. For 1-tridecanal on the other hand, the experimental results lie within the MCS results. This can especially be seen in the histogram in Fig. 5.4, if a comparison between the MCS results and the line in the plots is done. The

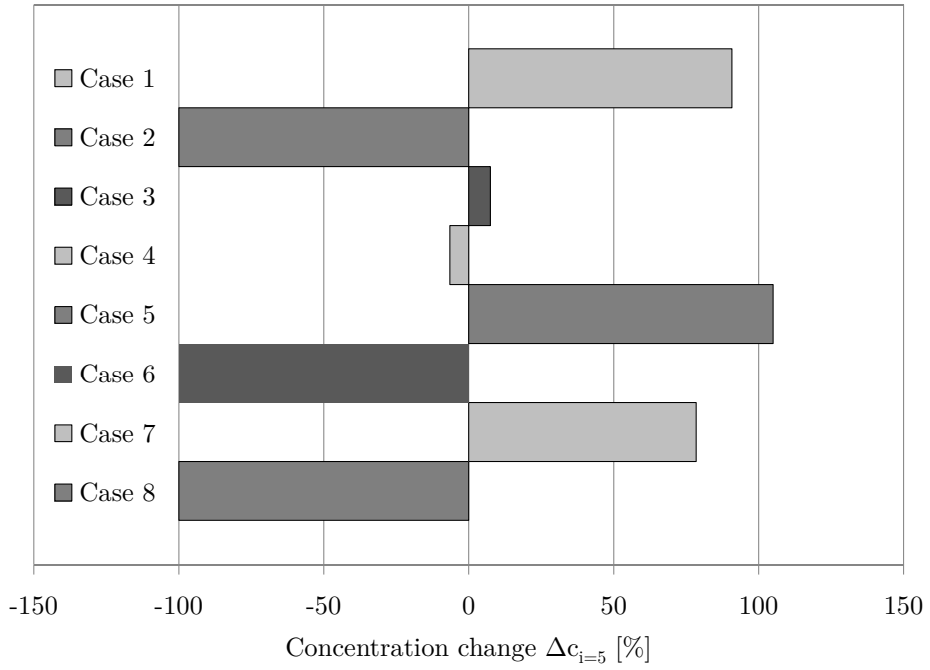

Figure 5.2.: Parameter sensitivity study for 85 °C and 15 bar: 1-tridecanal output.

Table 5.3.: Expected values and variances of kinetic parameters after the all subset selections I& II& III. The last two parameters are identical to the parameters directly above.

	$E_{r=1}$ $[J/mol]$	$E_{r=3}$ $[J/mol]$	$E_{r=5}$ $[J/mol]$	$k_{r=1}$ $[l/(mol\ g)]$	$k_{r=2}$ $[l/(mol\ g)]$	$k_{r=3}$ $[l/(mol\ g)]$
μ	$6.3 \cdot 10^{-3}$	$5.3 \cdot 10^{4}$	$1.9 \cdot 10^{4}$	$2.2 \cdot 10^{5}$	$1.9 \cdot 10^{7}$	$2.3 \cdot 10^{10}$
σ	0	0	$1.9 \cdot 10^{2}$	0	0	0
	$k_{r=4}$ $[l/(mol\ g)]$	$k_{r=5}$ $[l^2(mol^2\ g)]$	$k_{r=6}$ $[l^2/(mol^2\ g)]$	K_{cat} $[l/mol]$	$K_{r=5,e=1}$ $[l/mol]$	$K_{r=5,e=2}$ $[l^2/mol^2]$
μ	$3.4 \cdot 10^{2}$	$6.2 \cdot 10^{10}$	$2.8 \cdot 10^{8}$	$4.2 \cdot 10^{2}$	$1.8 \cdot 10^{-2}$	$2.1 \cdot 10^{4}$
σ	0	0	0	$3.2 \cdot 10^{1}$	0	0
	$K_{r=1,e=1}$ $[l/mol]$	$K_{r=2,e=1}$ $[l/mol]$	$K_{r=3,e=1}$ $[l/mol]$	$K_{r=4,e=1}$ $[l/mol]$	$K_{r=6,e=1}$ $[l/mol]$	$K_{r=6,e=2}$ $[l^2/mol^2]$
μ	$3.9 \cdot 10^{3}$	$3.3 \cdot 10^{5}$	$9.2 \cdot 10^{-1}$	$6.4 \cdot 10^{5}$	$1.8 \cdot 10^{-2}$	$2.1 \cdot 10^{4}$
σ	0	0	0	0	0	0

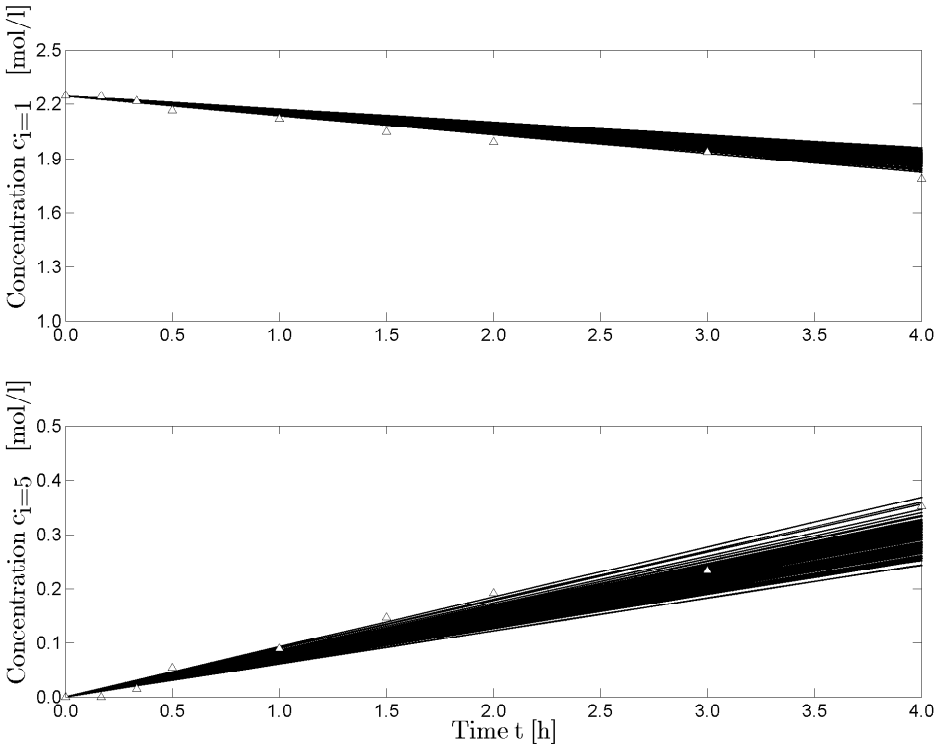

Figure 5.3.: Monte Carlo simulations for 85 °C and 15 bar: main components. The measured data set (triangles) stems from Tobias Hamerla, Technische Universität Berlin.

line represents the experimental result. Nevertheless, the result in total is satisfying enough, so that the determined parameters are applicable for optimization purposes.

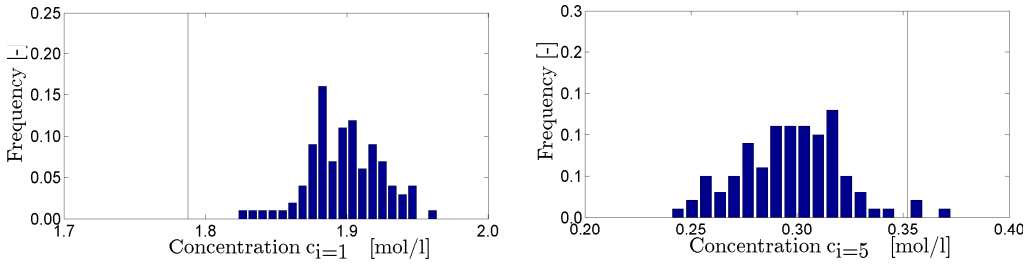

(a) 1-dodecene (b) 1-tridecanal

Figure 5.4.: Monte Carlo simulations result distribution vs. experimental results. The vertical line going to ∞ displays the position of the experimental results.

Chapter 6.

Optimization of Trajectories Under Uncertainty

In this chapter, the operation strategy for the hydroformylation mini-plant is presented. On the one hand, results from performed mini-plant operations are shown, in which no model-assisted operating strategies are used. These results are later on compared to results concerning the theoretically optimized, model-assisted operation using the model as well as the uncertainty described in the previous two chapters.

6.1. Plant Operation Without Model-based Approaches

To test the viability of the process concept of hydroformylation in microemulsions the mini-plant is initially operated without the assistance of a model. The general aim is to perform the "proof of concept" and to identify unexpected challenges during the operation of the plant. Additionally, because of always present plant-model mismatch, these plant operations are needed to fit the model to a certain degree. Finally, it must also be said that before a comparison between the different optimization cases can be performed, a test run must be carried out, in which no model-assisted approaches are applied. Otherwise a quantification of the actual benefit of the optimized case is barely possible. In the following, the reaction conditions as well as the results of the phase separation of these plant operations are presented and discussed.

Of interest in this section are three aspects:

- the difference of the product concentration between the oil and water phase,
- the amount of rhodium lost with the product phase,
- and the amount of byproducts produced during the reaction.

The first two of these aspects are indicators for the efficiency of the phase separation. They determine the cost-efficiency of the process. If the product concentration can be maximized in the oil phase, the following separation steps would become less expensive. Furthermore, if the rhodium-loss is minimized in the oil phase, this means less rhodium has to be replenished in the reactor and the reaction can continue as desired. The byproduct production is an indicator for the efficiency and is an important aspect regarding the economic feasibility of the reaction. Just as for the maximization of product in the oil phase, if less byproducts are produced, the subsequent purification steps can be minimized as well.

In the following, these aspects for two mini-plant operations without model-assisted approaches are discussed. Some of the results have already been published in contributions such as (Müller et al., 2013a), (Müller et al., 2014d), (Müller et al., 2014e), and (Müller et al., 2014c). Nevertheless, they will be revisited here, so that a later quantification of the betterment by model-assisted operation strategies can be carried out.

6.1.1. Operation 1: Mini-plant Operation with Phase Separation

In a first operation performed in the mini-plant, the aim is simply to present the proof of concept. This first mini-plant operation is performed for a duration of 130 hours. In order to operate the plant four teams of three people are required. Each day consists of three shifts and each shift lasts nine hours, while the last hour of each shift overlaps with the first hour of the next. Thus, issues that occur during the first shift can be communicated accordingly. The results of the first operation are divided into two parts: results concerning the phase separation and results concerning the reaction. Before these are presented though, the reaction conditions as well as the operation strategy are discussed.

Reaction Conditions: The reaction conditions are selected based on the results performed in the batch experiments presented in section 4.2. The aim is to produce as much 1-tridecanal as possible, while keeping the byproducts at a minimum. Therefore, a pressure of 15 bar(g) and a starting temperature of 95 °C are chosen. The composition of the mixture inside the reactor is the same, as in the mini-plant operation described in (Müller et al., 2013a) and consists of "roughly 46 wt.-% catalyst solution, 46 wt.-% 1-dodecene, and 8 wt.-% surfactant [...]. The catalyst solution consists roughly of 300 ppm $Rhacac(CO)_2$ and 4500 ppm Ligand. The ratio of metal-to-ligand of the catalyst complex is 1:4". As mentioned in section 4.2 the reaction rate in the three phase region is higher than in the upper two phase or lower two phase region. In this experiment the temperature in the reactor is kept constant at 95 °C.

Operation Strategy: The operation of a chemical plant is strongly dependent of the process as well as the available equipment and process units themselves. Nevertheless, according to (Weber, 2006) several general principles can be adhered to hereby, which were followed during the operation of the plant:

- The start-up should be carried out by separately starting up specific units.
- The operation of these as a whole should be carried out step by step, in which each unit is coupled, thus creating unit groups to finally operate the entire plant.
- The plant should be operated between 60 to 70 % of its nominal load. Thus, the sensors and actuators can be observed accordingly. Additionally, material and energy costs are kept low. Furthermore, in case of an emergency, the plant can be shut down quickly.
- "In classical continuous chemical plants with synthesis and separation parts, the separation sections should be started-up first [...]" (Weber, 2006).

The description of the operation strategy for the hydroformylation mini-plant focuses on three parts: feed streams, temperatures, and system pressure. This entire operation strategy is shown in Fig. 6.1. The operation can be summarized into three categories: filling of the mini-plant (start-up), stabilization of the process, and continuous operation. In the first hours, the plant is filled with alkene, catalyst solution, and surfactant to roughly reach the desired reaction mixture described above. The topmost diagram of Fig. 6.1 shows the feed streams into the reactor. The entire volume of the system is about two liters. The filling of the system takes roughly three hours. This can be seen in the upmost diagram of Fig. 6.1 by the spike of the three feeds in the first five to seven hours of operation. After the system is filled, the feed streams are reduced to zero and the reactor is heated to the desired 95 °C. A slight overshoot of the reactor temperature is visible in middle diagram of Fig. 6.1.

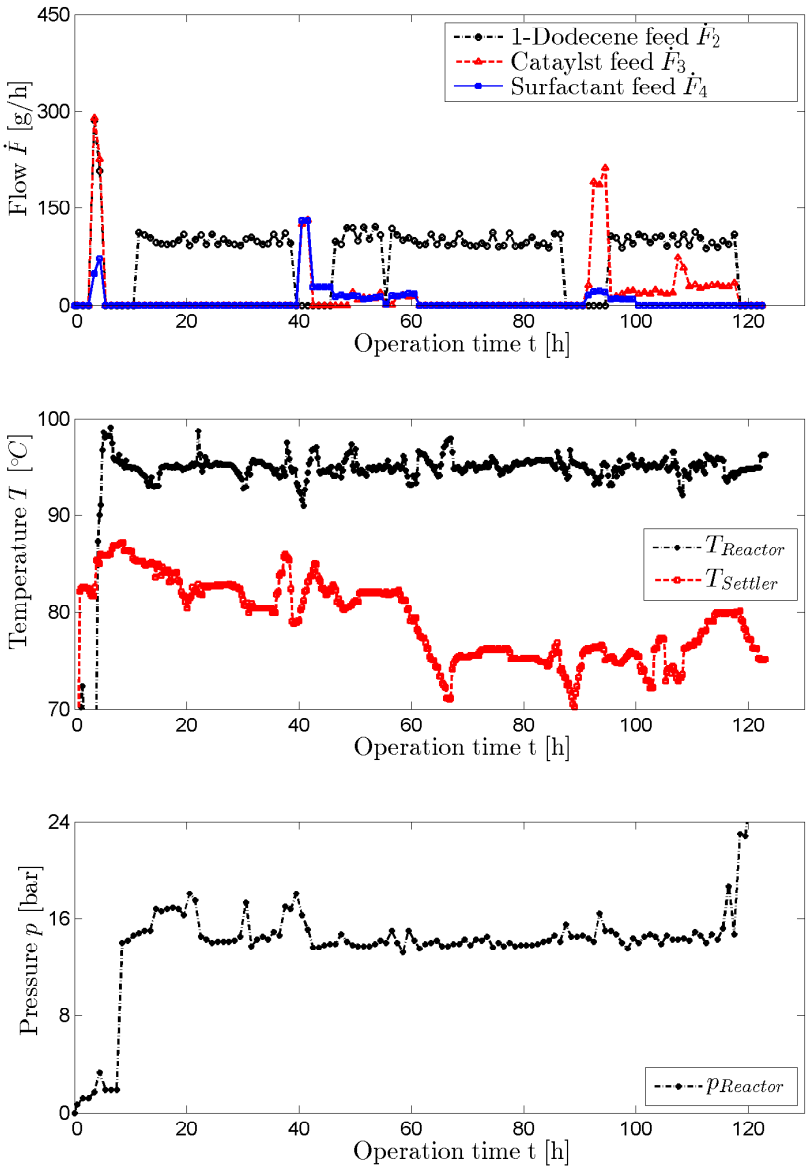

Figure 6.1.: Operation strategy in the first mini-plant operation.

Simultaneously, the settler temperature is set to a desired 85 °C, which was observed to be the correct separation temperature for the mixture at this current state. This state is part of the start-up of the process. Here though, no feed material is added and the process is operated in such a way that the correct reaction temperature and the correct phase separation temperature is set.

Afterwards, the stabilization phase of the process is started. Here, the reaction is initiated by feeding syngas into the system. The process is operated as a batch process for three hours with a continuous recycle. No material leaves the process during this phase.

After a total of ten hours of operation, the alkene feed is restarted at 100 g/h. This feed is kept constant for the entire operation of the plant, except for two intervals of five hours, where a refilling was necessary and additional surfactant and catalyst solution are fed into the system to reach desired concentrations. During the entire operation, the pressure of the plant is kept more or less constant at 15 bar(g).

Regarding the settler temperature, repeated changes throughout the mini-plant operation

can be observed. The reason for this is, that the optimal temperature in the settler had to be manually adjusted according to heuristics. At the point in time of this operation, not all information regarding the shift of the optimal separation region was available. Furthermore, samples from the top and bottom of the settler could only be analyzed every hour. Thus, a constant readjustment of the settler temperature according to estimated concentration changes in the process were carried out.

Operation Results: Fig. 6.2 shows the concentration of 1-tridecanal in the oil and the water phase. In the beginning, the phase separation works very well. A clear concentration difference of 1-tridecanal in the oil and water phase is visible. At around 20 hours of operation, the phase separation fails and the concentration of 1-tridecanal is equal in both phases.

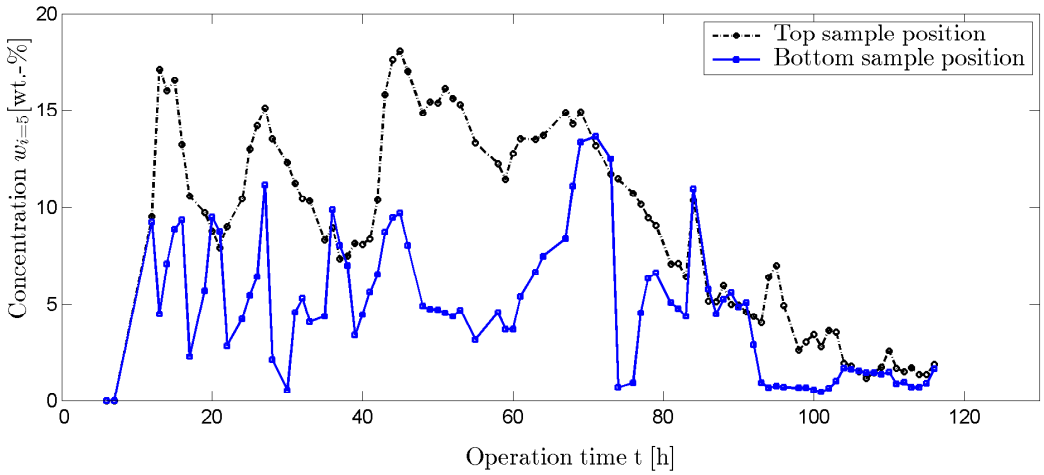

Figure 6.2.: Operation 1: product concentration.

The reason for this is, that a shift out of the viable phase separation region occurs. As shown in Section 3.1 the temperature interval in which the phase separation works well has a width of roughly 4 K. In this temperature interval the separation is adequately fast and results in a pure oil phase. The small temperature interval poses a challenge, especially if this interval shifts due to concentration changes in the system. After a correction of the temperature, shown in the middle diagram of Fig. 6.1, the phase separation starts again. This shift of the desired separation region makes the process difficult to operate continuously in steady-state, even though the feed streams and the reaction temperature remain more or less constant. Due to the fact that the exact composition of the recycle stream is unknown, it is difficult to estimate the concentration of the mixture entering the settler. That is the reason why a repeated "break-down" of the phase separation can be observed. Fig. 6.3 shows an excerpt of Fig. 6.2 where this repeated phase separation initiation and "break-down" can be seen by the concentration changes of product in the respective sample positions in the settler. After 70 hours of operation, no clear phase separation is possible and the production of product is slowly reduced.

During the operation hours, in which the phase separation works as desired, the catalyst loss remains at a minimal level. Fig. 6.4 and Fig. 6.5 show another detailed excerpt of Fig. 6.2 where this is the case. The separation was kept stable for over 24 hours of operation. The oily components in the top sample position of the settler amounted to values between 95 wt.-% and 99 wt.-% (Müller et al., 2014d).

In the optimal area the rhodium loss is below 0.01 ppm, because used ligand is highly water soluble. Seeing that the reaction is initiated with 120 ppm rhodium (equivalent to 300ppm precursor-complex), this means that more than 99.99% of the catalyst remains in the catalyst phase. This mini-plant result mimics lab-scale test-tube results and is thus a satisfying result regarding economic viability of the process concept (Müller et al., 2013a). At these catalyst loss rates, an economically feasible process is thinkable as the effort of subsequent catalyst recovery steps can be minimized.

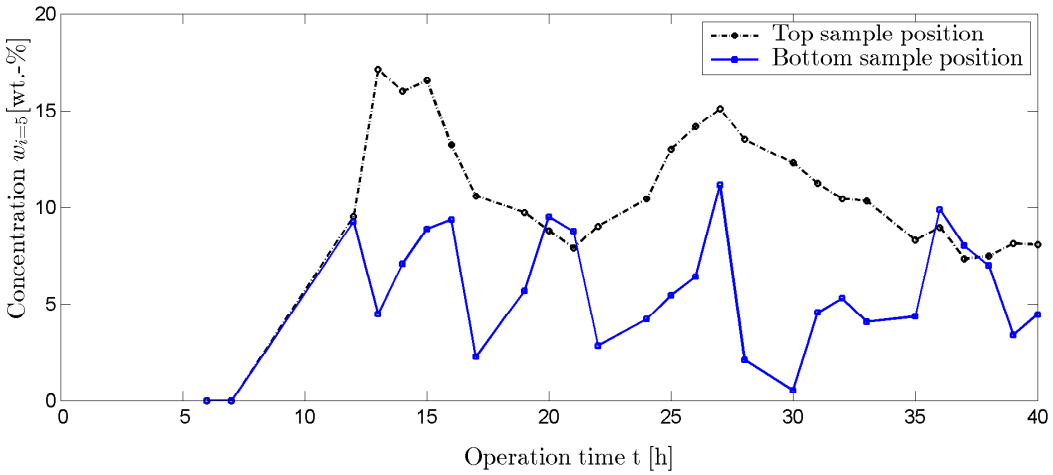

Figure 6.3.: Operation 1: loss of the viable phase separation temperature interval.

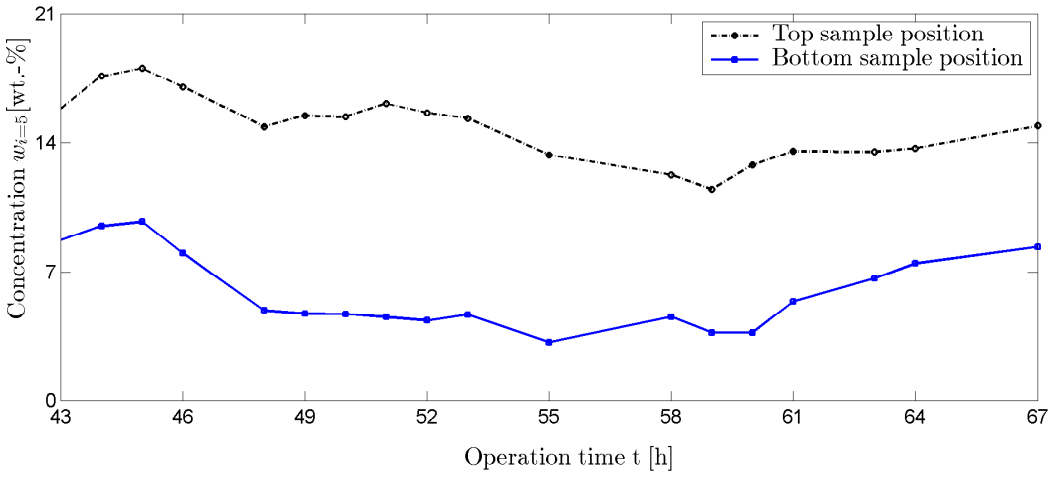

Figure 6.4.: Operation 1: functioning phase separation.

The main byproducts of the reaction are iso-tridecanal and n-dodecane. Fig. 6.6 shows the byproduct concentrations in the oil and the water phase. During this operation, the production of n-dodecane is very high reaching values above 25 wt.-% (Müller et al., 2014d). Simultaneously larger quantities of iso-tridecanal are produced. The selectivity of 1-tridecanal vs. iso-tridecanal lies around 96.7:3.3 (Fig. 6.7). If this is compared with batch experiments in the lab shown in (Hamerla et al., 2013b), where values between 98:2 and 99:1 were reached, this result is not completely satisfactory for a mini-plant operation.

Both byproducts n-dodecane and iso-tridecanal are highly undesired. Possible reasons for this massive production of n-dodecane and iso-tridecanal are an inconvenient shift of the

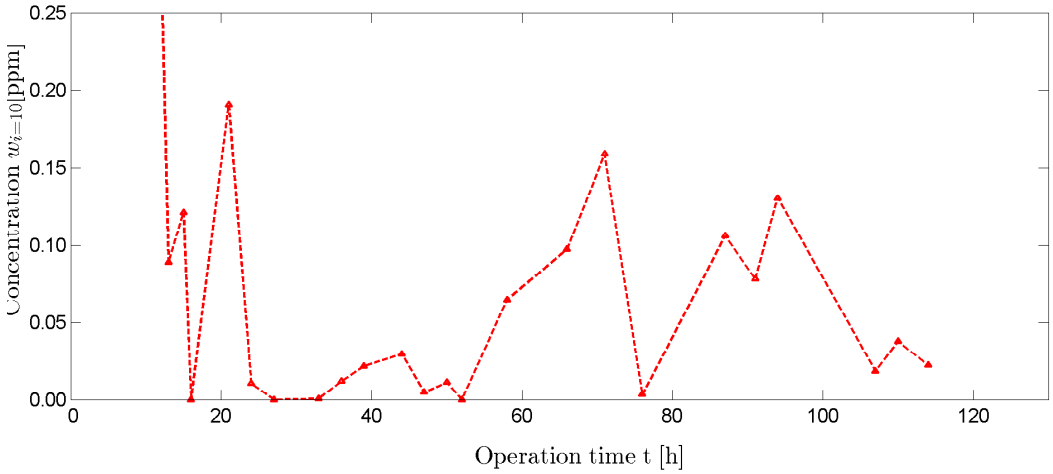

Figure 6.5.: Operation 1: catalyst loss.

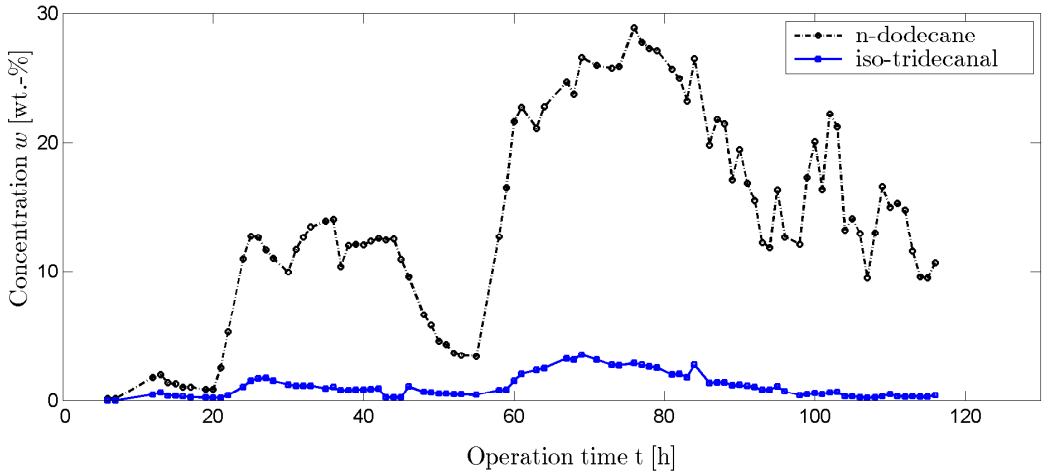

Figure 6.6.: Operation 1: byproduct concentration at the top sample position of the settler.

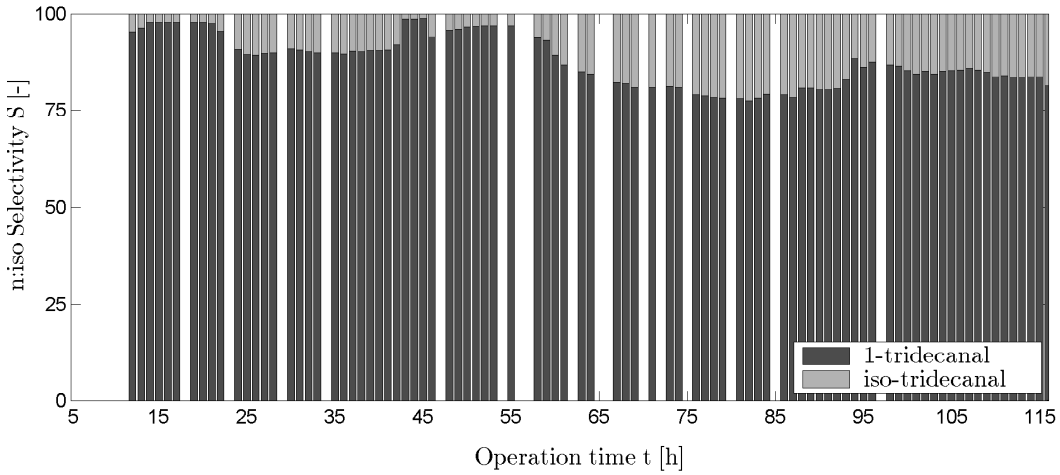

Figure 6.7.: Operation 1: n:iso selectivity.

syngas composition in the reactor as well as the relatively high reaction temperature. It has been observed in batch experiments that the isomerization of 1-dodecene and the hydrogenation reaction of 1- and iso-dodecene are more likely to occur at higher temperatures. Nevertheless, such large amounts of byproducts as those produced during the mini-plant operation have not been observed in batch experiments. Based on these observations, a second mini-plant operation, in which the reaction is improved, is carried out. The improvements are discussed in the next section.

6.1.2. Operation 2: Mini-plant Operation without Phase Separation

In the second mini-plant operation two goals are strived for:

- Firstly the aim is to reduce the amount of n-dodecane being produced during the reaction.
- Secondly, an increase of the n:iso tridecanal selectivity is targeted at.

Therefore, several conceptual and operational changes were made. As mentioned in the previous section, it is assumed that the high reaction temperature and gas composition variation in the reactor are the reasons for the undesired n-dodecane and iso-tridecanal production. "First of all, the reaction temperature was lowered [...]. Thus, the hydrogenation reaction should be avoided. Secondly, a gas purge was installed to ensure a constant syngas renewal and thus avoid a [variation] of the gas composition. Thirdly, the reactor residence time is increased to two hours to increase the yield" (Müller et al., 2014d).

The plant is operated for a total of 100 hours. Again, a similar team set-up as in the first operation is used. Furthermore, to observe the reaction more adequately two sample points are added in the reactor. The first is to analyze the liquid samples with the offline gas chromatograph. The second sample point is connected with the online gas chromatograph and analyzes the gas composition in the reactor. That way it can be guaranteed that no oxygen is left in the reactor before the reaction is initiated and a possible gas composition shift can be observed.

Reaction Conditions: First of all, the same starting liquid composition as in the first operation is fed into the reactor: 46 wt.-% 1-dodecene, 46 wt.-% catalyst solution, 298 ppm rhodium precursor and a molar metal to ligand ratio of 1:4. The reaction temperature is fixed to 358 K (85 $°C$) to minimize the production of byproducts. Finally, the reaction pressure is kept at 15 bar, just as in the first operation.

Operation Strategy: Since the aim in this mini-plant operation was not to find the best operation strategy, but to solely improve the reaction, no detailed operation strategy is designed. Nevertheless, the whole operation is shown in Fig. 6.8 and the general idea of start-up phase, stabilization phase, and continuous operation are maintained. The reactor residence time was increased from one to roughly two hours. Hereby, recycle stream values ranging between 400 and 500 g/h were chosen.

At certain points in time, a refeeding of catalyst solution, 1-dodecene, and surfactant were carried out to refill the liquid amount in the plant lost through sampling. This can be seen in the upper diagram in Fig. 6.8.

Operation Results: An overview of the operation results is given in Fig. 6.9. As mentioned in the beginning of this section, the goal here was to test the reaction and catalyst stability. The operation can thus be viewed as a long-term semi-batch operation.

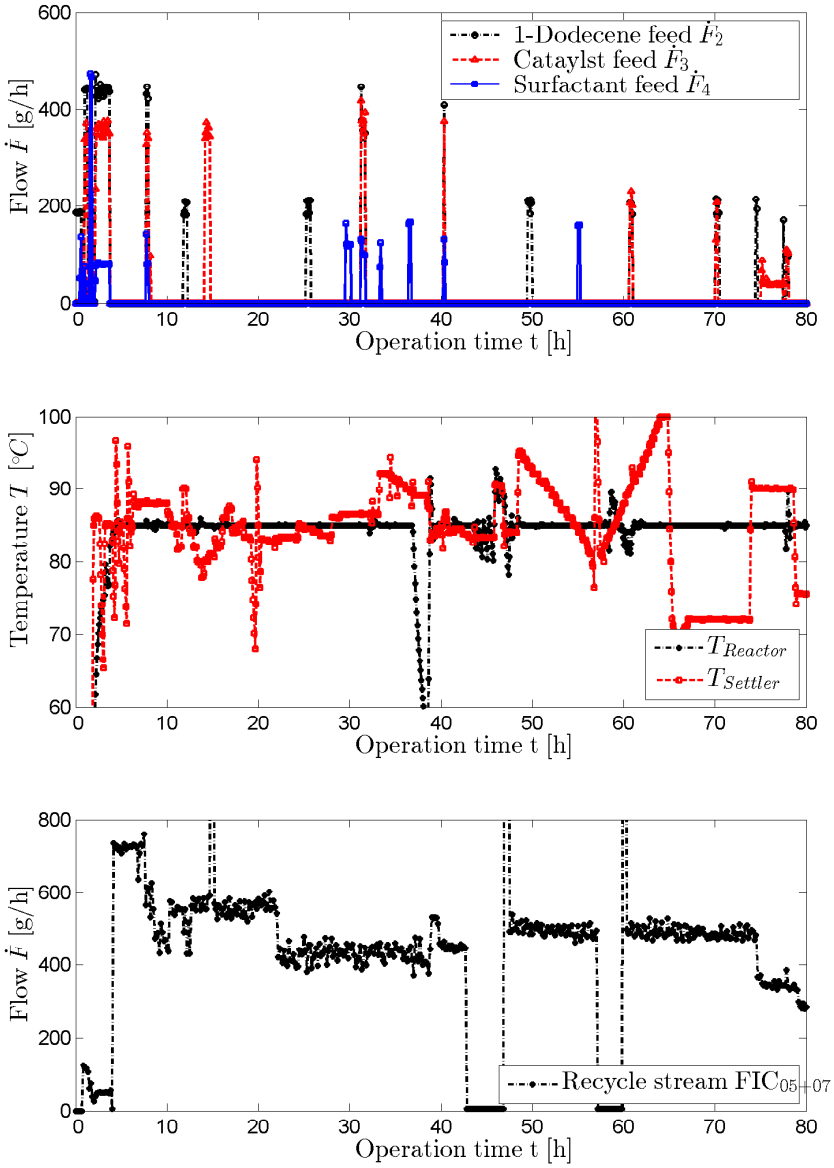

Figure 6.8.: Operation strategy in the second mini-plant operation.

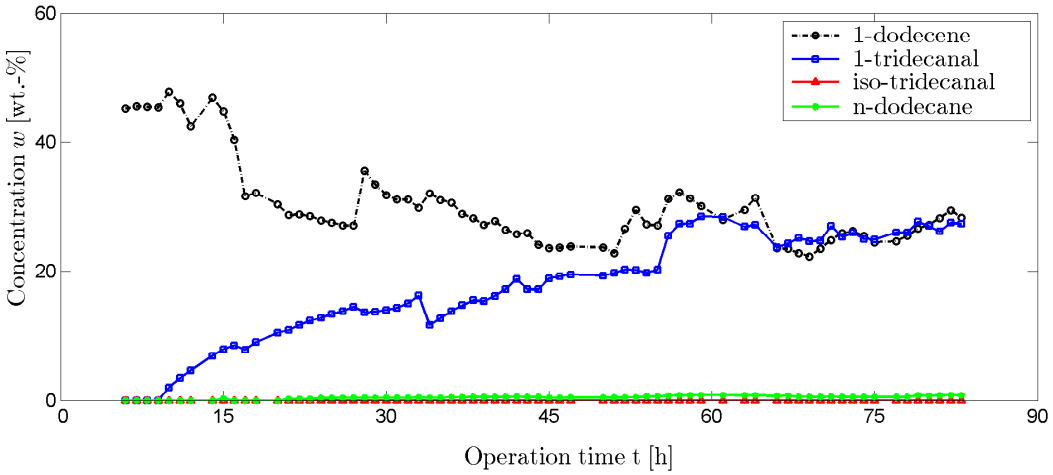

Figure 6.9.: Operation 2: reaction results showing the production of 1-tridecanal, iso-tridecanal, and n-dodecane as well as the consumption of 1-dodecene.

Müller et al. (2014d) discuss that the selectivity towards the n-aldehyde in comparison to the iso-aldehyde during the entire operation is at 100:0, meaning that the amount of iso-aldehyde lies below the detectability limit of the applied gas chromatographs. Nevertheless it is known, that small iso-aldehyde amounts are produced during the reaction, thus resulting in a realistic selectivity of 99:1. The selectivity regarding all other byproducts such as n-dodecane and iso-dodecene is roughly 97:3 to 98:2. This matches the results from batch experiments. Fig. 6.10 shows the selectivity for roughly eighty hours of operation. The production of n-dodecane is considerably smaller compared to the first mini-plant operation. Furthermore, Fig. 6.10 proves that the rhodium-based catalyst complex is stable as well as selective for a long period in time (>100 hours).

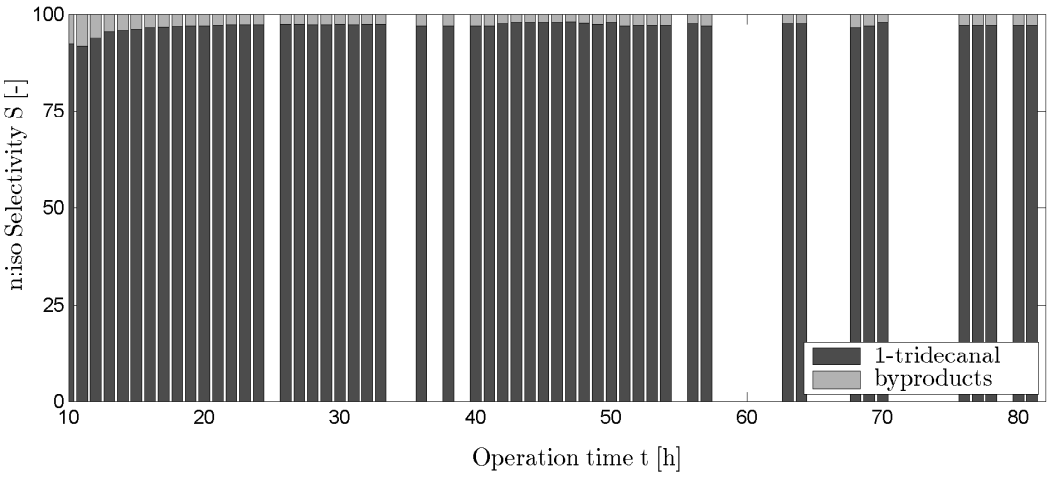

Figure 6.10.: Operation 2: selectivity of product vs. sum of byproducts. The empty spacing corresponds to left out measurements.

Applicability of Raman spectroscopy: As mentioned in the previous sections, the concentrations of the liquids in the process are analyzed offline using a gas chromatograph (GC). Based on the analysis data obtained with the GC, the changes of compounds are

determined and thus the temperature of the settler thermostat could be adjusted with a certain delay. For adequate online-optimization of the process, however, fast and accurate analysis techniques are needed. In the second operation of the mini-plant the concentration analysis is additionally performed by a Raman spectrometer affixed directly in the product stream of the settler. At this point in time, no adequate model for the analysis with Raman spectroscopy is available. For future process operation, the online Raman spectra shall enable real-time process control. Critical questions concerning the application of Raman spectroscopy are at this point:

- Which components can the Raman spectrometer observe and which phase should be analyzed?
- How exact are the measurements?
- Is the Raman spectrometer capable of analyzing an emulsion?

To ease analysis, it was decided to affix the probe in the product outlet of the settler. Thus, the oil phase was analyzed. Efforts were made before the operation of the plant to design a chemometric model and to determine, which components are actually visible in the Raman spectra. "The Raman spectra of the mixtures prepared offline enable the multivariate prediction of the educt 1-dodecene and the product 1-tridecanal in the oil phase with 5 and 10 % accuracy respectively. The non-ionic surfactant Marlipal 24/70 can only be estimated with an accuracy of 37 %. Prediction was performed after the evaluation of spectra both by partial least squares regression (PLS), support vector machines (SVM), and by indirect hard modeling (IHM)" (Müller et al., 2014c). Using this developed model, no sensible results concerning the spectra of the mini-plant operation were attainable. Therefore, "in a second step, chemometric models were refined using the actual process GC data of the oil phase. Based on these results, models with higher prediction power could be calculated" (Müller et al., 2014c). The main difference between the offline analyzed samples and the online in situ measurement is the syngas activation of the system. The Raman spectra of the syngas activated system are clearly different than those of the non-activated system.

The spectra of the oil-phase obtained during the operation of the pilot plant exhibited a high quality, even though the phase separation in the process did not occur. This result is exceptionally interesting, as it means that an analysis of the components is possible, even if the Raman measures inside an emulsion. By combining manually taken samples with online spectra, the components 1-tridecanal and 1-dodecene could successfully be analyzed. Fig. 6.11 shows the concentrations of the two components over the number of spectra, which indirectly represents the operation time.

Results Summary: In (Müller et al., 2014d) the results of the mini-plant operations are summarized: "Firstly, the proof of concept has been made. The reaction, applying the water-soluble rhodium-based catalyst modified with SulfoXantPhos as a ligand is stable and remains selective towards the desired product for a long time period". Even though a breakdown of the selectivity was observed in the middle of plant operation it is not credited to catalyst degeneration, but rather a syngas composition shift. In general, the application of the technical-grade surfactant Marlipal 24/70 enabled a successful phase separation resulting in minimal rhodium losses even below 0.01ppm. It must be mentioned though that "the phase separation region of the surfactant is very small, thus making the stable operation [rather] challenging. The selection of an adequate surfactant, which functions well in the reaction and has a large ideal phase separation area, is critical for the success of this process concept" (Müller et al., 2014d).

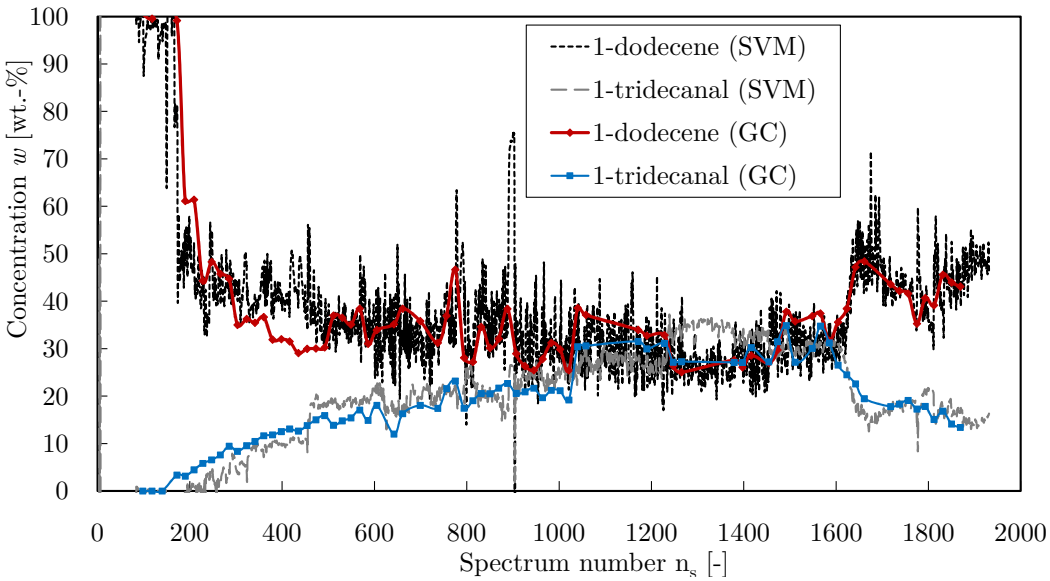

Figure 6.11.: Operation 2: concentration monitoring by GC and predicted concentrations Raman spectroscopy.

The long-term operation of the mini-plant revealed noteworthy effects. Among these are the following:

- A fractioning of the surfactant takes place during the phase separation step. The surfactant consists of a multitude of components, some of which are more hydrophobic than others. These hydrophobic components leave the system with the product phase. Hence, the overall composition of the surfactant changes after several hours of operation and leads to another undesired effect: a shift of the optimal separation temperature in the settler. Possible counter measures, such as preliminary surfactant rectification as well as continuous surfactant feeding during operation should be taken into consideration.

- In certain operating areas foaming of the oil-water-surfactant system occurs. Foam appears when the system is degassed, which becomes especially relevant in the flash or product container. In general, foaming can cause problems such as blockage of pipes and the reduction of mass and heat transfer. To avoid foaming, the gassing stirrer speed was reduced. Furthermore, in preliminary research it was discovered, that foam containing an abundance of oil is less stable than foam containing an abundance of water (>30 wt.-%). This knowledge was used during the operation - a product stream was only allowed, if the system was in the correct phase separation region.

The identification of the ideal surfactant is vital for the success of this process concept. After this operation, the statement can be made, that the surfactant must provide two important characteristics for the reaction mixture: a large phase separation region (large temperature interval) in which the phase separation is fast (Müller et al., 2013a).

The results of the mini-plant operation show that a sophisticated model is required to predict the reaction behavior and the phase separation. In the next section, a deterministic optimization of the process operation strategies is performed to stabilize the phase separation over a longer period in time and to reach a constant 1-tridecanal concentration in the product

phase. To express the target for the optimization in numbers, the following goals are to be achieved and constraints adhered to:

1. The n:iso selectivity of the reaction is to remain above the mass ratio of 98:2.
2. During the product removal, the product stream should have at least 20 % product.
3. The phase separation is to remain stable for a period longer than 24 h.
4. Catalyst loss is to remain below 0.1 ppm throughout the operation time.
5. The mass fraction of byproducts should remain below 0.5 wt.-%.

6.2. Simulated Plant Operation

Before an actual optimization of the operation strategies of the mini-plant is carried out, a simulation of a non-optimized operation is performed. For this purpose, the second mini-plant operation is selected. In this operation a long-term semi-batch run was done. Besides at the beginning of the operation, no phase separation was achieved. Thus, the results of this operation can be used to refit the kinetics accordingly. The idea is to see if the reaction kinetics in the mini-plant reactor (1000 ml) are similar to those observed in the lab-scale reactor (roughly 50 ml). Due to different scales, non-ideal mixing, apparatus residence times, or other issues, it is expected that the kinetics of the reaction in the plant differ to those obtained in the lab-scale reactor.

The simulation is performed in gPROMS version 3.3.1 on an Intel core 2 Duo CPU 3.00 GHz with 4 GB RAM on a 32 bit system using the model code exported from MOSAIC. The operation is modeled for 32 hours. This time frame is seen as adequate to depict the entire range of desired control actions as well as the maximum production of 1-tridecanal. The reaction is initiated after eight hours of operation. Thus, the simulation shows 24 hours of reaction in the process.

6.2.1. Model Modifications and Initial Conditions

To carry out the simulation several changes or modifications of the model are made. These modifications can be grouped into equation-based changes and operation commands. Due to a different configuration of the plant as well as DOF removal in the system for simulation purposes, the equation-based changes are made. The operation commands on the other hand are the commands carried out during the operation.

Equation-based changes: First of all, the pump for stream S_{24} does not exist in the plant configuration of the second operation. Therefore, it is simply connected to unit 14. All component balances for the tank u_{14} are modified accordingly.

Apart from that, several of the triggers important for optimization purposes, are inadequate for the simulation. These are also removed from the model, because the decision of when and how an operation procedure is to be carried out, was done by the operator. Among these triggers are the feeding triggers as well as the reaction initiation triggers. Also, the phase separation trigger is turned off, because it did not occur in the mini-plant operation. The equation containing the splitter for the oil phase stream S_{12} is set to zero, thus eliminating the oil phase stream.

The settler used in the second operation is drastically smaller than the settler in the current plant configuration. It has a volume of 309 ml. Therefore, the parameters in the

cubic equation used to describe the liquid height of the settler are changed to $Pl1$ = 2.085, $Pl2$ = -6.784, and $Pl3$ = 14.013.

Lastly, a new trigger is introduced, which starts the actual reaction and hinders the isomerization before the reaction actually begins. This trigger has the same form as the previous triggers and is connected to the concentration of hydrogen in the system: $c_{i=7}$ = 0.004. As soon as enough hydrogen is present, the reaction is initiated.

Operation-based commands: For the simulation, an update of certain input values is performed. The operation strategy shown in the previous section for the second operation is used for this purpose. The following variables are fixed to the process control data averaged every minute:

- the three feed streams as well as the recycle and product streams,
- the reactor temperature and settler temperature, and
- the system pressure.

Additionally, the measured pump streams are adapted to the real process behavior with linear factors. Stream S_4 is multiplied with 1.07, stream S_5 is multiplied with 1.11, and stream S_6 with 1.40[1]. The recycle streams S_{16} and S_{25} are multiplied with 1.25.

In addition to the measured product stream leaving the settler to the product tank, additional mass leaving the system needs to be modeled. During the actual operation, three samples for GC analysis were taken every hour. Based on actual sample amounts including dead volume removal in the sample positions, a total averaged hourly sample mass of 23 g is assumed. Thus in the simulation, every hour 1380 g are removed in the time frame of one minute (1380/60 = 23) at every hour of operation.

Initial conditions: The most important initial conditions used to simulate the process are given in Tab. 6.1. A full list of parameter values is given in the appendix.

6.2.2. Simulation Results

The results concerning the reaction in the model and in the mini-plant are compared in Fig. 6.12 and Fig. 6.13. In Fig. 6.12 only the main components 1-dodecene and 1-tridecanal are shown, while in Fig. 6.13 the components iso-dodecene as well as n-dodecane are analyzed. Iso-tridecanal is left out, because it was not produced during the mini-plant operation. The two figures show two simulation results: Simulation and Simulation (Modified). The former is the original, unmodified simulation regarding the reaction equations. Here, it is obvious that the reaction, which is initiated at roughly eight hours of operation, is much too fast. The educt 1-dodecene is rapidly used up and reacts to 1-tridecanal within only four further hours of operation. The creation of byproducts is also much too fast.

Because of this result the decision is made to introduce a reduction factor in the reaction rate equations, so that a correct depiction of the reaction kinetics in the plant can be carried out. This modification is carried out based on the following thoughts:

- In the small, lab-scale reactor, the system is stirred at 1200 rpm. In the mini-plant, however, the reactor is stirred at below 650 rpm to avoid foaming. It has been shown in results by Hamerla et al. (2013a) that the stirrer speed has a drastic influence on

[1] In the Master's thesis of Mr. Alexander Fleck, the FI measured values were compared to the actual mass that left the system. The values for the feed stream pumps are taken from these measurements.

Table 6.1.: Initial conditions for the simulation of operation 2.

Variable	Value	Unit	Description
$HU_{u=1}$	7600	[g]	Hold-up of alkene in the alkene tank
$HU_{u=2}$	9696	[g]	Hold-up of catalyst solution in the catalyst tank
$HU_{u=3}$	9600	[g]	Hold-up of surfactant in the surfactant tank
$HU_{u=9}$	0	[g]	Hold-up in the reactor (liquid)
$HU_{u=13}$	0	[g]	Hold-up in the settler (mixed phase)
$HU_{u=14}$	0	[g]	Hold-up in the intermediate storage
$HU_{u=20}$	0	[g]	Hold-up in the product tank
$HU^{L}_{u=9,i=1}$	0.50	[g/g]	Mass frac. of alkene in the reactor
$HU^{L}_{u=9,i=9}$	0.42	[g/g]	Mass frac. of water in the reactor
$HU^{L}_{u=9,i=12}$	0.08	[g/g]	Mass frac. of surfactant in the reactor
$HU^{L}_{u=12,i=1}$	1.00	[g/g]	Mass frac. of alkene in the oil hold-up of settler
$HU^{L}_{u=13,i=9}$	1.00	[g/g]	Mass frac. of water in the mixed hold-up of settler
$HU^{L}_{u=14,i=1}$	1.00	[g/g]	Mass frac. of alkene in the intermediate tank
$HU^{L}_{u=20,i=1}$	1.00	[g/g]	Mass frac. of alkene in the product tank
$w_{s=1,i=2}$	0.025	[g/g]	Mass frac. of iso-dodecene in first feed stream
$w_{s=2,i=9}$	0.988	[g/g]	Mass frac. of water in second feed stream
$w_{s=2,i=10}$	0.001	[g/g]	Mass frac. of precursor in second feed stream
$w_{s=2,i=11}$	0.011	[g/g]	Mass frac. of ligand in second feed stream
$w_{s=3,i=12}$	1.000	[g/g]	Mass frac. of surfactant in third feed stream
$w_{u=20,i=1}$	1.000	[g/g]	Mass frac. of alkene in product tank
$T_{u=9}$	300	[K]	Reactor temperature
$T_{u=13}$	300	[K]	Settler temperature
p_{Start}	1.013	[bar]	Reactor pressure

the reaction rate of the system. If the therein presented diagram is believed, then the stirrer speed of 600 rpm yields roughly 50 % of the reaction rate compared to 1200 rpm. Of course, the stirrer-type must be considered hereby. In the plant, a six-bladed Rushton turbine-type stirrer is used. In the lab-scale reactor a standard four-bladed gassing stirrer is applied.

- Additionally, the dimensions of the applied reactors differ greatly. The ratio of stirrer diameter to tank diameter in the lab-scale reactor is 1:2.3 (17 mm vs. 40 mm) while in the mini-plant the ratio is roughly 1:1.9 (45 mm vs. 84 mm). The liquid volume in the lab reactor is roughly 50 ml and in the plant is 700 ml, which is a factor of 14. Based on this information, another crucial difference becomes apparent: the ratio of stirrer diameter to stirrer height, which plays a significant role in the efficiency of the mixing process. In the lab reactor the liquid height is roughly 40 mm (ratio = 1:2.3), in the mini-plant, however, the liquid height is 150 mm (ratio = 1:4.4). This means that the stirring in the plant is bound to be less effective considering the amount of liquid inside the reactor and height up to which the stirrer has to mix the liquid, which showed a beginning phase separation in the gauge glass of the reactor at too low stirrer speeds.

- Furthermore, due to a multitude of dead volumes in the plant (e.g. pipes in general, pulsation dampeners after the pumps, etc.), not all of the catalyst present in the plant is immediately activated when CO and H_2 are fed into the system. It takes roughly two hours to have all of the catalyst cycle through the reactor at least once. Thus, it is possible that inactivated catalyst is continuously fed into the reactor for at least two hours after pressurization of the system.

- On top of that, much larger amounts of catalyst are prepared for the mini-plant operation than for the lab-scale reactor. It is possible that during the storage of the catalyst solution in the mini-plant's feed tanks some deactivation has occurred. The presence of oxygen leads to an immediate deactivation of the catalyst.

- Finally, the performed batch reactions only reached a certain production of tridecanal. The exact influence of an enhanced tridecanal concentration on the reaction rate has not been investigated yet. Each lab-scale batch reaction was performed for four hours. At this point the assumption is made that tridecanal has a dampening influence on the reaction rate by inhibiting the development of the active form of the catalyst.

Based on these thoughts, a reduction factor is introduced for the catalyst mass, which influences all kinetic equations in the same manner:

$$m_{cat,mod} = m_{cat} \cdot C_1 \cdot (1 - (w_{u=9,i=5} + w_{u=9,i=3}))^{C_2} \tag{6.1}$$

The parameters C_1 and C_2 are modification constants. For the modified simulation they are set to 0.135 and 5 respectively. These values were obtained with a few simulation runs. No optimization was carried out here. Furthermore, as can be observed in the original parameter estimation, the production of byproducts is higher than actual measured values. Therefore, all reactions associated with iso-dodecene are multiplied with 1 %.

By using these modifications of the reaction kinetics, adequate simulation results for all components shown in the figures Fig. 6.12 and Fig. 6.13 in "Simulation (Modified)" are obtained. The simulation results for 1-dodecene, iso-dodecene, n-dodecane, and iso-tridecanal are in the 3σ error range of all of the measurements. For the product tridecanal

on the other hand, 17 of the 23 measurements points are met correctly by the simulation. The offsets occur mainly, when the feeding is started or when the recycle is drastically increased from roughly 500 g/h to 1500 g/h. This is especially visible in the period between 14 to 17 hours as well as 26 to 27 hours of operation.

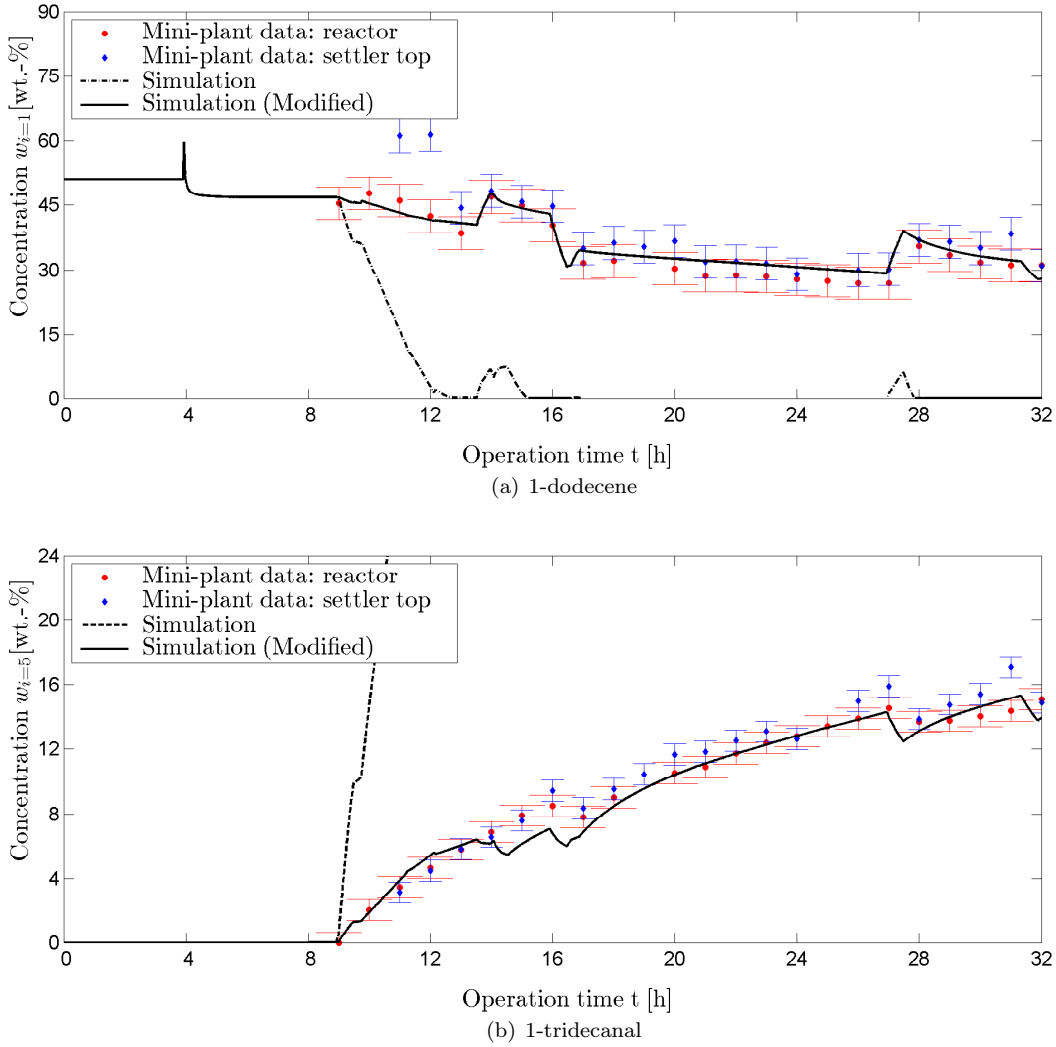

(a) 1-dodecene

(b) 1-tridecanal

Figure 6.12.: Operation 2 main components: simulation vs. plant operation.

6.2.3. Conclusions Based on the Simulation Results

With the modifications regarding the reaction, over 24 hours can be depicted correctly. As soon as the recycle is drastically changed, deviations are observable. A resimulation must be carried out periodically. This yields values for the state variables of the system, which can be used as starting values for the optimization of the process. It must be underlined though that these modifications are a mathematical workaround. They are not phenomenologically correct descriptions. Once correct descriptions of mass transfer effects are available, an update on the kinetics can be done.

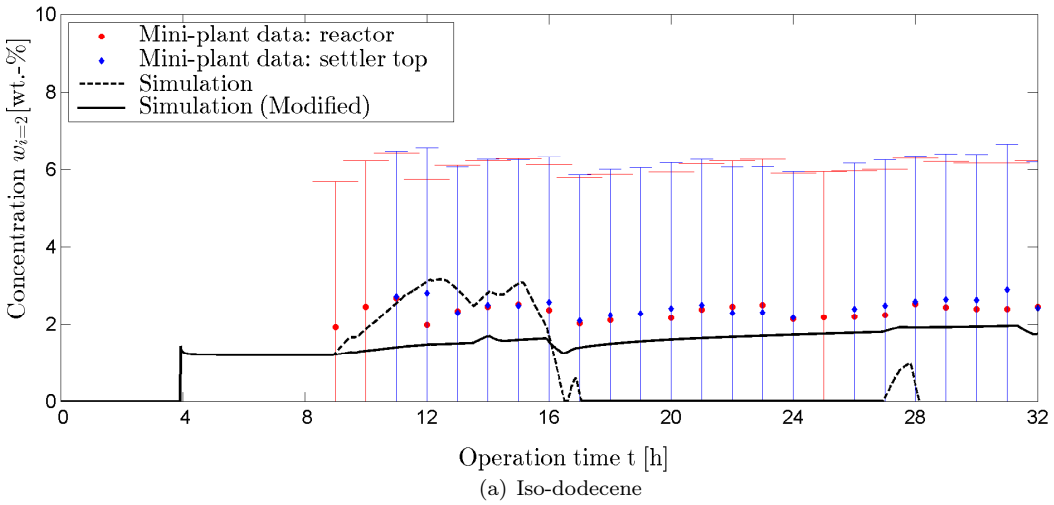

(a) Iso-dodecene

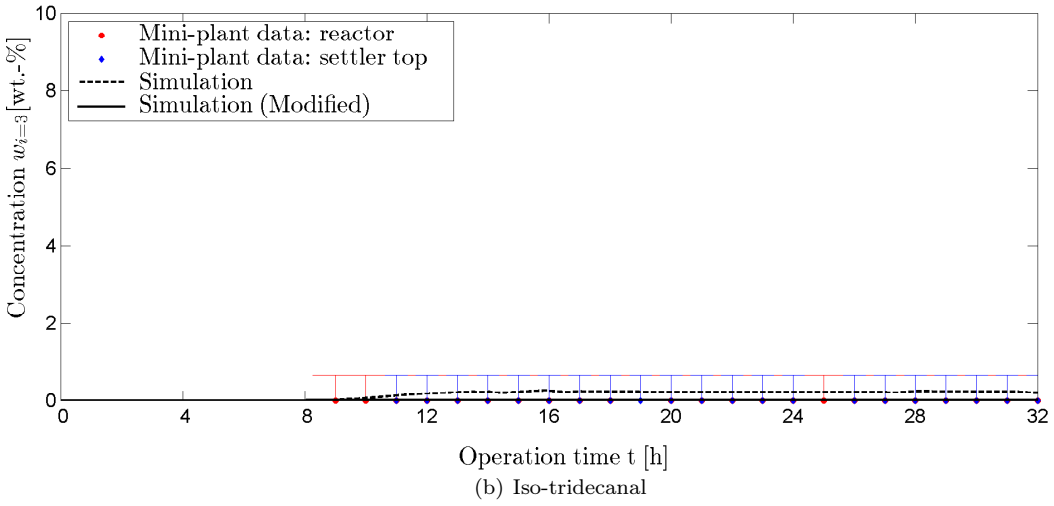

(b) Iso-tridecanal

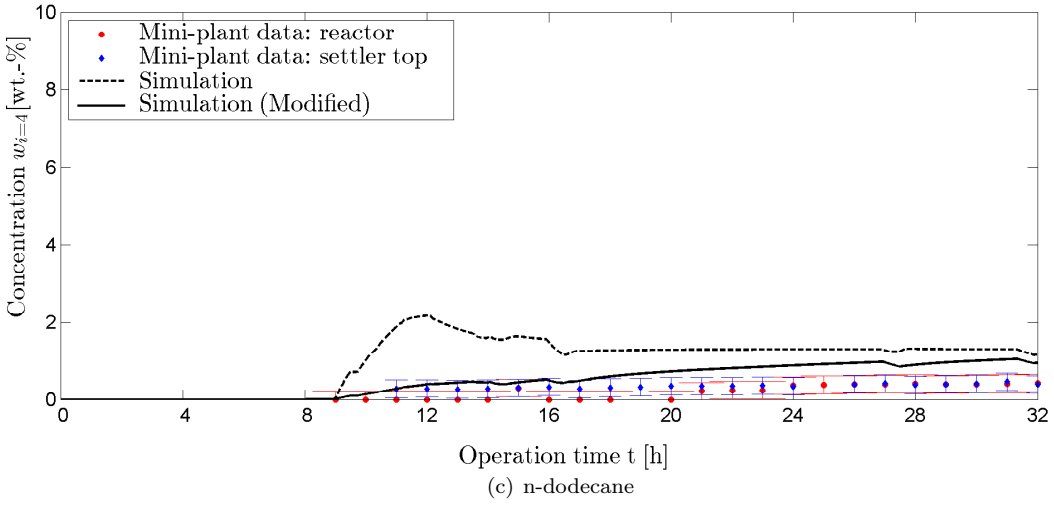

(c) n-dodecane

Figure 6.13.: Operation 2 byproducts: simulation vs. plant operation.

6.3. Deterministic Optimization: Trajectory Development

The general goal of the optimization of the hydroformylation mini-plant is to achieve an adequate yield in a short amount of time. After the plant is started up, a stabilization of the process should occur leading to the continuous operation in which a constant and, more importantly, stable production is carried out. A stable plant operation is of higher importance here opposed to maximizing 1-tridecanal yield. The determined controls should therefore not be sporadic or prone to extreme jumps. This can generally be avoided by two measures: selection of according control variable bounds or additional equations in which the change of the control variable value is bounded, e.g. the settler temperature is not allowed to increase by more than 5 K in 15 minutes. In this study, the former strategy is selected to avoid extreme control variable value jumps.

Before looking at the chance-constrained optimization problem, a deterministic optimization of the process is carried out. Since deterministic optimization is not the core topic of this thesis, this presented study serves simply as a preliminary analysis for the later to be performed chance-constrained optimization. Of interest hereby are the following questions:

- Is an optimization with the currently available model possible?
- How long does the optimization with a "standard", commercially available solver on a "standard" CPU take?
- What does the result of the deterministic optimization look like and are constraints violated?
- What are achievable targets in the given time frames?

In accordance to the operation strategy carried out with the mini-plant, the objective function of the deterministic optimization problem is divided into several sub-problems: start-up of the plant and stabilization leading to a continuous operation. In the following, the according objective functions, constraints, and controls including their respective results are presented.

6.3.1. Optimization of the Start-up Process

For the start-up of the plant, the aim is to reach a maximum product concentration in the reactor outlet after four hours. The optimization problem can be expressed as follows:

$$\min_{u} \quad -X_{s=11,FE=final} \tag{6.2}$$

$$s.t. \quad \text{all model equations} \tag{6.3}$$

$$0.40 \leq \alpha_{s=11,FE} \leq 0.60 \tag{6.4}$$

$$0.07 \leq \gamma_{s=11,FE} \leq 0.10 \tag{6.5}$$

$$0 \leq L_{u=12,FE} \leq 0.25 \tag{6.6}$$

$$0 \leq L_{u=13,FE} \leq 0.50 \tag{6.7}$$

$$1.20 \leq L_{u=14,FE=final} \tag{6.8}$$

Hereby, $X_{s=11,FE=final}$ is the yield value at the end of the final finite element. The yield is calculated as shown in Eq. 6.9.

$$X_{s=11} = \frac{w_{s=11,i=5}}{\sum_{i=1}^{5} w_{s=11,i}} \tag{6.9}$$

This objective is subject to several constraints though. Firstly, all model equations, which have been presented in Chapter 4, must be adhered to. Secondly, the oil:water ratio $\alpha_{s=11}$ in stream S_{11} should remain in the vicinity of 50 % (± 10 %). Thirdly, the surfactant concentration $\gamma_{s=11}$ in stream S_{11} should lie between 7 % and 10 %, because the model has been validated for these concentrations. Hereby, 7 % is selected instead of 6 % as a lower bound, because the temperature jump due to catalyst activation in the phase separation model occurs around 6 %. The oil:water ratio $\alpha_{s=11}$ and the surfactant concentration $\gamma_{s=11}$ are calculated as shown in Eq. 6.10 and Eq. 6.11 respectively:

$$\alpha_{s=11} = \frac{\sum_{i=1}^{5} w_{s=11,i}}{(\sum_{i=1}^{5} w_{s=11,i}) + w_{s=11,i=9}} \tag{6.10}$$

$$\gamma_{s=11} = w_{s=11,i=12} \tag{6.11}$$

The oil and water levels in the settler ($L_{u=12}$ & $L_{u=13}$) are bounded by maximum values of 0.25 dm and 0.50 dm respectively. The settler is full around 0.55 dm. These two liquid levels in the settler are calculated as shown in Section 4.3 in Eq. 4.59 and Eq. 4.60. Additionally, an end-point inequality constraint for the liquid height in the intermediate tank is defined: $L_{u=14} \geq 1.2$ dm. This is to guarantee a smooth switch to the continuous operation. The liquid height $L_{u=14}$ is calculated in the model via Eq. 6.12. The dynamic part of the three liquid heights stems from the differential hold-up equations in the respective tanks.

$$HU^{L}_{u=14} \cdot \sum_{i=1}^{Ni} \frac{w_{s=16,i}}{\rho_i} = A_{u=14} \cdot L_{u=14} \tag{6.12}$$

The initial controls and their bounds can be seen in Tab. 6.2, Tab. 6.3, and Tab. 6.4. The splitting factor λ_{u15} is removed as a control and set to 1 and the reactor temperature $T_{u=9}$ is set to 368.15 K, so that solely a maximization of product in the system can be achieved. The recycle stream $F^{SP}_{s=25}$ is initially guessed as 0 g/h and bounded by 0 and 300 g/h. The controls are turned into piece-wise constant controls for intervals with a fixed length of 15 minutes. The idea here is that a certain amount of time is needed, so that a change of the set-point value actually has an effect on the state of the plant. 15 minutes is seen as adequate. These intervals are denoted with the index FE for finite element. The used starting values for the hold-ups can found in the Appendix in Section A.4 in Tab. A.9.

The alkene feed is given a lower bound of 50 g/h so that a constant feed is guaranteed. Otherwise, the optimizer may find a solution in a batch operation mode. For the current goal, of quickly reaching a continuous production of 1-tridecanal, a batch operation mode is not desired. Later, if goals change, this option should be considered in case higher yields are desired.

The optimization problem is solved in gPROMS with the standard solver "CVP_SS" using the default solver parameters. The computation is carried out on an Intel Core2 Duo CPU E8400 @ 3.00 GHz with 4.00 GB RAM on a 32 bit system. Additional information on selectively modified parameters can be found in the Appendix in Section A.4 in Tab. A.6. In the "CVP_SS" solver the differential-algebraic equation solver "DASOLV" is used. The problem is solved in 16 seconds, which is an adequate time frame for real-time optimization. It also shows that the model can be used for the chance-constrained optimization problems.

The results of the optimization are summarized in Tab. 6.5 and can be seen in the following figures.

Hereby, Fig. 6.14 shows the streams that are to be implemented to achieve a maximum yield. Fig. 6.15 shows the levels of the different containers in the plant and Fig. 6.16 shows

Table 6.2.: Lower bounds, initial guess, and upper bounds for the alkene feed $F_{s=4}^{SP}$.

Interval Nr. [-]	Time frame [h]	Lower bound [g/h]	Initial guess [g/h]	Upper bound [g/h]
1	0.00 - 0.25	500	500	500
2	0.25 - 0.50	500	500	500
3	0.50 - 0.75	500	500	500
4	0.75 - 1.00	50	500	500
5	1.00 - 1.25	50	500	500
6	1.25 - 1.50	50	300	500
7	1.50 - 1.75	50	200	500
8	1.75 - 2.00	50	100	500
9	2.00 - 2.25	50	100	500
10	2.25 - 2.50	50	100	500
11	2.50 - 2.75	50	100	500
12	2.75 - 3.00	50	100	500
13	3.00 - 3.25	50	100	500
14	3.25 - 3.50	50	100	500
15	3.50 - 3.75	50	100	500
16	3.75 - 4.00	50	100	500

Table 6.3.: Lower bounds, initial guess, and upper bounds for the catalyst feed $F_{s=5}^{SP}$.

Interval Nr. [-]	Time frame [h]	Lower bound [g/h]	Initial guess [g/h]	Upper bound [g/h]
1	0.00 - 0.25	500	500	500
2	0.25 - 0.50	500	500	500
3	0.50 - 0.75	500	500	500
4	0.75 - 1.00	0	500	500
5	1.00 - 1.25	0	150	300
6	1.25 - 1.50	0	150	300
7	1.50 - 1.75	0	100	300
8	1.75 - 2.00	0	50	300
9	2.00 - 2.25	0	50	300
10	2.25 - 2.50	0	50	300
11	2.50 - 2.75	0	50	300
12	2.75 - 3.00	0	50	300
13	3.00 - 3.25	0	0	300
14	3.25 - 3.50	0	0	300
15	3.50 - 3.75	0	0	300
16	3.75 - 4.00	0	0	300

Table 6.4.: Lower bounds, initial guess, and upper bounds for the surfactant feed $F_{s=6}^{SP}$.

Interval Nr. [-]	Time frame [h]	Lower bound [g/h]	Initial guess [g/h]	Upper bound [g/h]
1	0.00 - 0.25	88	88	88
2	0.25 - 0.50	88	88	88
3	0.50 - 0.75	88	88	88
4	0.75 - 1.00	0	88	88
5	1.00 - 1.25	0	88	88
6	1.25 - 1.50	0	35	88
7	1.50 - 1.75	0	17.5	88
8	1.75 - 2.00	0	8.7	88
9	2.00 - 2.25	0	8.7	88
10	2.25 - 2.50	0	8.7	88
11	2.50 - 2.75	0	8.7	88
12	2.75 - 3.00	0	8.7	88
13	3.00 - 3.25	0	0	88
14	3.25 - 3.50	0	0	88
15	3.50 - 3.75	0	0	88
16	3.75 - 4.00	0	0	88

Table 6.5.: Deterministic start-up operation optimization: controls.

Interval Nr. [-]	Time frame [h]	$F_{s=4}^{SP}$ [g/h]	$F_{s=5}^{SP}$ [g/h]	$F_{s=6}^{SP}$ [g/h]	$T_{u=9}$ [K]	$F_{s=25}^{SP}$ [g/h]	$\lambda_{u=15}$ [-]
1	0.00 - 0.25	500.00	500.00	88.00	368.15	100.00	1.00
2	0.25 - 0.50	500.00	500.00	88.00	368.15	100.00	1.00
3	0.50 - 0.75	499.29	500.00	88.00	368.15	100.00	1.00
4	0.75 - 1.00	493.49	300.00	87.01	368.15	100.00	1.00
5	1.00 - 1.25	263.21	300.00	79.74	368.15	100.31	1.00
6	1.25 - 1.50	132.30	300.00	17.39	368.15	66.84	1.00
7	1.50 - 1.75	50.00	229.77	0.00	368.15	111.01	1.00
8	1.75 - 2.00	50.00	6.77	0.00	368.15	116.52	1.00
9	2.00 - 2.25	50.00	8.55	0.00	368.15	110.99	1.00
10	2.25 - 2.50	50.00	7.65	0.00	368.15	111.72	1.00
11	2.50 - 2.75	50.00	26.74	0.00	368.15	75.51	1.00
12	2.75 - 3.00	50.00	5.79	0.07	368.15	113.61	1.00
13	3.00 - 3.25	50.00	11.09	3.79	368.15	103.19	1.00
14	3.25 - 3.50	50.00	19.80	16.93	368.15	86.64	1.00
15	3.50 - 3.75	50.00	37.69	44.11	368.15	53.36	1.00
16	3.75 - 4.00	50.00	37.69	44.11	368.15	53.36	1.00

the effect that the streams have on the composition of the process via the composition parameters $\alpha_{s=11}$, $\gamma_{s=11}$, and via the yield in $X_{s=11}$.

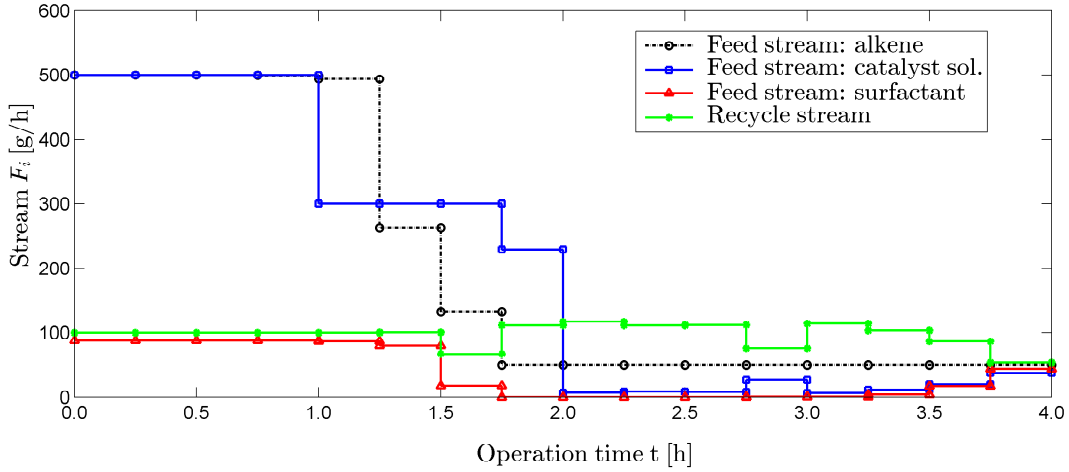

Figure 6.14.: Deterministic start-up optimization: control results for streams.

Before discussing the influence of the results on the plant state, a clarification must be made between set-points and actually implemented values. This can best be explained with the set-point of the recycle stream. At the beginning, when the plant is started-up, the settler is empty. Hence, nothing can be recycled. Nevertheless, a set-point can be chosen that demands a recycle of 100 g/h. Effectively, nothing will happen in the model, because a trigger function, in which the liquid height of the settler is used as an argument, hinders the implementation of the set-point into the process.

Initially, the feed streams are set to their respective maximum values, so that a filling of the process with the desired composition is carried out as quickly as possible. After 3 intervals, the degree of freedom is increased and the three feed streams are turned to optimization variables to maximize the yield of 1-tridecanal. This can be seen in the Fig. 6.15. The reactor is filled from the start. Once the reactor is full ($L_{u=9} \approx 1.72$ dm) the settler is filled. Here, roughly 80 % of the oil in the entering stream is split into the oil phase. Thus, the oil phase is smaller than the water phase. After 1.75 hours the settler reaches its critical value and oil flows out through the top outlet into the intermediate tank. The intermediate tank begins to fill up and eventually reaches a value of slightly under 1.25 dm.

From Fig. 6.16 it can be seen that all constraints concerning the composition are adhered to at all times. The oil:water ratio $\alpha_{s=11}$ is slightly increased in the beginning, when more oil is fed into the system between 1.0 and 1.25 operation hours. Afterwards it is reduced, because the recycle stream and the larger water stream start to have an effect. Oil is split in the settler and fed into the intermediate product tank. Thus, the oil:water ratio being recycled back to the settler is reduced and the overall composition shifts. The surfactant amount $\gamma_{s=11}$ stays at an adequate level of roughly 9 wt.-%. This is maintained throughout the operation. The yield $X_{s=11}$ increases after 0.75 hours. At this point the reactor is full and the reaction is initiated. The slope of the yield is slightly increased, once the feeding is reduced and the recycle is started (at around 1.75 hours). As desired, the oil and water levels stay at a desired height without overly fluctuating.

The final figure shows the results concerning the temperature in the reactor and settler. The reactor temperature is set to 368.15 K. The settler temperature is calculated depending on the composition entering the settler. For the plant, piece-wise linear controls can

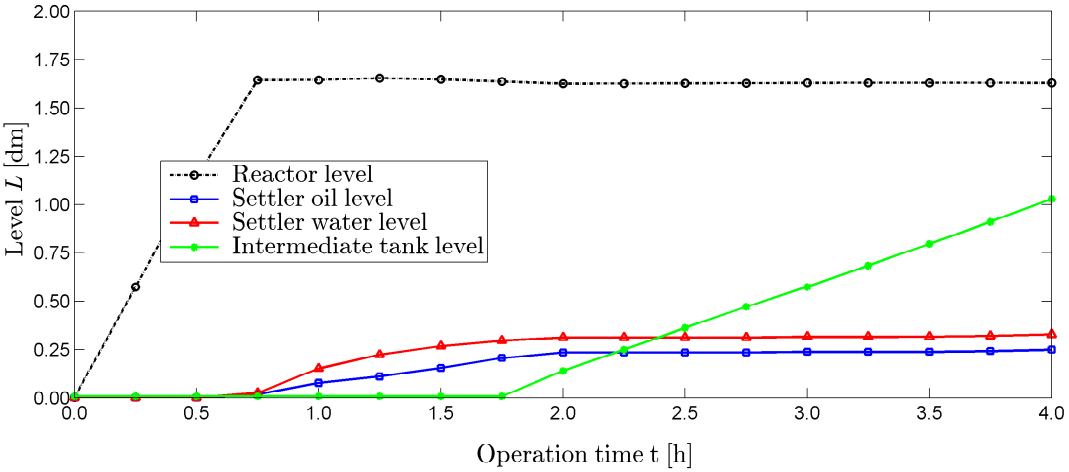

Figure 6.15.: Deterministic start-up optimization: liquid levels in the plant.

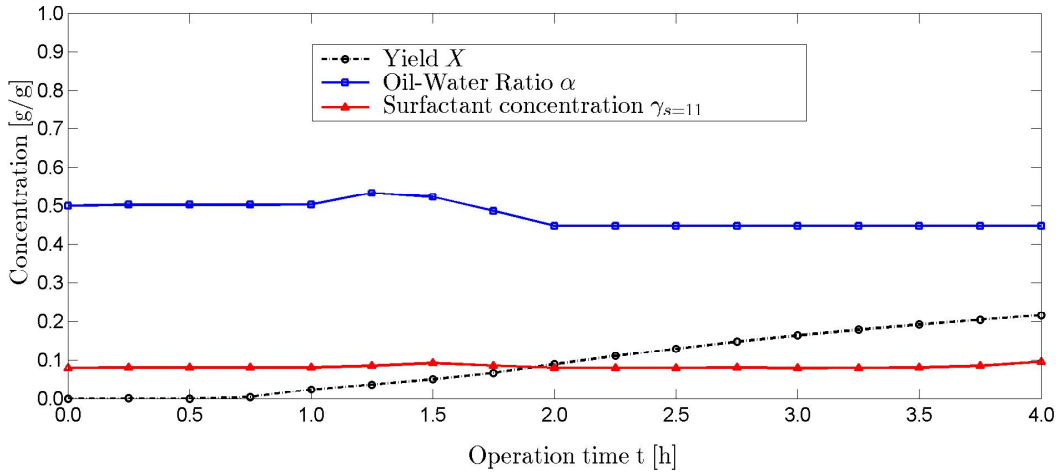

Figure 6.16.: Deterministic start-up optimization: composition parameters.

be imaged to achieve this temperature and thus remain within the ideal phase-separation temperature bounds. Due to the concentration shift at 1.5 h of operation leading to a higher surfactant containing system, the settler temperature has a slight drop. By adding more water and simultaneously reducing the recycle, the necessary settler temperature is increased and kept constant. Using the values concerning concentrations, levels, hold-ups, temperatures, and pressures after four operation hours, the optimization of the continuous process is started.

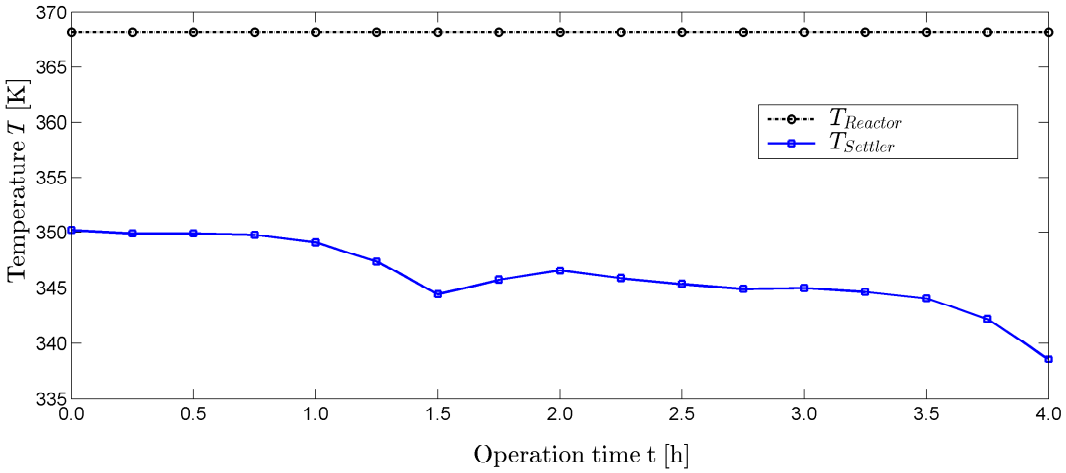

Figure 6.17.: Deterministic start-up optimization: reactor and settler temperature.

6.3.2. Optimization of the Continuous Operation of the Process

In the continuous operation of the plant, the objective function is switched from maximum product yield to maximum product outflow concentration. The aim is to determine controls, which stabilize the plant in terms of streams and concentrations and lead to a constant production of 1-tridecanal.

$$\min_{u} \quad -F_{s=18,i=5,FE=final} \tag{6.13}$$

$$s.t. \quad \text{all model equations} \tag{6.14}$$

$$0.40 \leq \alpha_{s=11,FE} \leq 0.60 \tag{6.15}$$

$$0.07 \leq \gamma_{s=11,FE} \leq 0.10 \tag{6.16}$$

$$0.15 \leq L_{u=12,FE} \leq 0.25 \tag{6.17}$$

$$0.25 \leq L_{u=13,FE} \leq 0.50 \tag{6.18}$$

$$0.15 \leq X_{s=11,FE} \tag{6.19}$$

$$0.1 \leq \frac{HU^{L}_{u=20,i=5,FE=final}}{HU^{L}_{u=20,FE=final}} \tag{6.20}$$

The constraints of the previous section concerning $\alpha_{s=11}$, $\gamma_{s=11}$, $L_{u=12}$, and $L_{u=13}$ are kept, only adding two additional constraints as an advancement for the continuous process. Firstly, the concentration of product in the product tank $u = 20$ after the additional four hours of operation should at least be 10 wt.-%. Secondly, the yield $X_{s=11}$ should always lie above 15 %.

The initial controls, as well as lower and upper bounds for the continuous operation are displayed in Tab. 6.6 to Tab. 6.8. The alkene feed is bounded to a minimum of 70 g/h and 100 g/h. This is done, because it has been observed in previously carried out optimization studies that a wider range (example: 0 to 500 g/h) leads to drastic control changes, which is not desired.

Table 6.6.: Lower bounds, initial guess, and upper bounds for the alkene feed $F^{SP}_{s=4}$.

Interval Nr. [-]	Time frame [h]	Lower bound [g/h]	Initial guess [g/h]	Upper bound [g/h]
1	4.00 - 4.25	70	90	100
2	4.25 - 4.50	70	90	100
3	4.50 - 4.75	70	90	100
4	4.75 - 5.00	70	90	100
5	5.00 - 5.25	70	90	100
6	5.25 - 5.50	70	90	100
7	5.50 - 5.75	70	90	100
8	5.75 - 6.00	70	90	100
9	6.00 - 6.25	70	90	100
10	6.25 - 6.50	70	90	100
11	6.50 - 6.75	70	90	100
12	6.75 - 7.00	70	90	100
13	7.00 - 7.25	70	90	100
14	7.25 - 7.50	70	90	100
15	7.50 - 7.75	70	90	100
16	7.75 - 8.00	70	90	100

The other two streams, catalyst solution and surfactant, have an upper bound of 40 g/h

and 30 g/h respectively. The idea is to use these two streams as correctors to keep the concentration of the reactor outlet stream in the desired range. The recycle stream is kept at a constant value of 500 g/h as this is optimal. This is done, to speed up the computation process. It has been observed that higher recycle values are generally obtained.

Table 6.7.: Lower bounds, initial guess, and upper bounds for the catalyst solution feed $F_{s=5}^{SP}$.

Interval Nr. [-]	Time frame [h]	Lower bound [g/h]	Initial guess [g/h]	Upper bound [g/h]
1	4.00 - 4.25	0	38	40
2	4.25 - 4.50	0	38	40
3	4.50 - 4.75	0	38	40
4	4.75 - 5.00	0	38	40
5	5.00 - 5.25	0	38	40
6	5.25 - 5.50	0	38	40
7	5.50 - 5.75	0	38	40
8	5.75 - 6.00	0	38	40
9	6.00 - 6.25	0	38	40
10	6.25 - 6.50	0	38	40
11	6.50 - 6.75	0	38	40
12	6.75 - 7.00	0	38	40
13	7.00 - 7.25	0	38	40
14	7.25 - 7.50	0	38	40
15	7.50 - 7.75	0	38	40
16	7.75 - 8.00	0	38	40

Again, the optimization problem is solved in gPROMS using the same selectively modified solver parameters shown in Section A.4. The problem is solved even faster this time, taking only 6 seconds to find an optimal solution. This relatively short computation time is expected, because the controls are greatly restricted. The determined controls are summarized in Tab. 6.9

The optimization results can be seen in Fig. 6.18 regarding the streams. It can be seen that the alkene feed stream is kept more or less constant, while slight corrections are performed regarding the catalyst solution and surfactant stream to maintain the desired composition in the plant. The recycle stream is kept at a stable value of 500 g/h. The other controls, temperature in the reactor and splitting factor, are more or less constant. The reactor temperature stays at 368.15 K and the splitting factor at 0.6. Leaving the splitting factor as a full optimization variable for each interval results in very drastic jumps regarding the feed streams, as sudden purges of product occur. This is not desired for a stable operation. Thus, the splitting factor is optimized to a constant value for the full four hours of operation.

The stability of the optimizer's results can be seen in Fig. 6.19 in which the levels in the process are displayed. All remain at constant values for all intervals.

The same can be said regarding the composition of the stream leaving the reactor in the plant. The oil:water ratio is slightly increased over time. Simultaneously, the yield is also slightly increased. The surfactant composition is kept constant and the product concentration in the product storage tank is increased, showing an asymptotic behavior towards the yield value. This can be explained by the fact that at the beginning, the intermediate tank is filled with pure dodecene. The longer the operation time, the more of the dodecene in that tank gets recycled. After enough time, the entire tank is eventually filled with a similar composition as in the stream leaving the reactor. Thus, the stream split

Table 6.8.: Lower bounds, initial guess, and upper bounds for the surfactant feed $F_{s=6}^{SP}$.

Interval Nr. [-]	Time frame [h]	Lower bound [g/h]	Initial guess [g/h]	Upper bound [g/h]
1	4.00 - 4.25	0	20	30
2	4.25 - 4.50	0	20	30
3	4.50 - 4.75	0	20	30
4	4.75 - 5.00	0	20	30
5	5.00 - 5.25	0	20	30
6	5.25 - 5.50	0	20	30
7	5.50 - 5.75	0	20	30
8	5.75 - 6.00	0	20	30
9	6.00 - 6.25	0	20	30
10	6.25 - 6.50	0	20	30
11	6.50 - 6.75	0	20	30
12	6.75 - 7.00	0	20	30
13	7.00 - 7.25	0	20	30
14	7.25 - 7.50	0	20	30
15	7.50 - 7.75	0	20	30
16	7.75 - 8.00	0	20	30

Table 6.9.: Deterministic continuous operation optimization: controls.

Interval Nr. [-]	Time frame [h]	$F_{s=4}^{SP}$ [g/h]	$F_{s=5}^{SP}$ [g/h]	$F_{s=6}^{SP}$ [g/h]	$T_{u=9}$ [K]	$F_{s=25}^{SP}$ [g/h]	$\lambda_{u=15}$ [-]
1	4.00 - 4.25	70.00	35.91	0.00	368.15	500.00	0.60
2	4.25 - 4.50	70.00	31.34	0.00	368.15	500.00	0.60
3	4.50 - 4.75	70.00	28.24	0.00	368.15	500.00	0.60
4	4.75 - 5.00	70.00	0.00	0.00	368.15	500.00	0.60
5	5.00 - 5.25	70.00	0.00	0.00	368.15	500.00	0.60
6	5.25 - 5.50	70.00	0.00	0.00	368.15	500.00	0.60
7	5.50 - 5.75	70.00	0.00	0.00	368.15	500.00	0.60
8	5.75 - 6.00	100.00	0.00	0.00	368.15	500.00	0.60
9	6.00 - 6.25	100.00	0.00	0.00	368.15	500.00	0.60
10	6.25 - 6.50	100.00	0.00	0.00	368.15	500.00	0.60
11	6.50 - 6.75	100.00	0.00	0.00	368.15	500.00	0.60
12	6.75 - 7.00	100.00	0.00	0.00	368.15	500.00	0.60
13	7.00 - 7.25	100.00	0.00	0.00	368.15	500.00	0.60
14	7.25 - 7.50	100.00	0.00	0.00	368.15	500.00	0.60
15	7.50 - 7.75	100.00	0.00	0.00	368.15	500.00	0.60
16	7.75 - 8.00	100.00	40.00	30.00	368.15	500.00	0.60

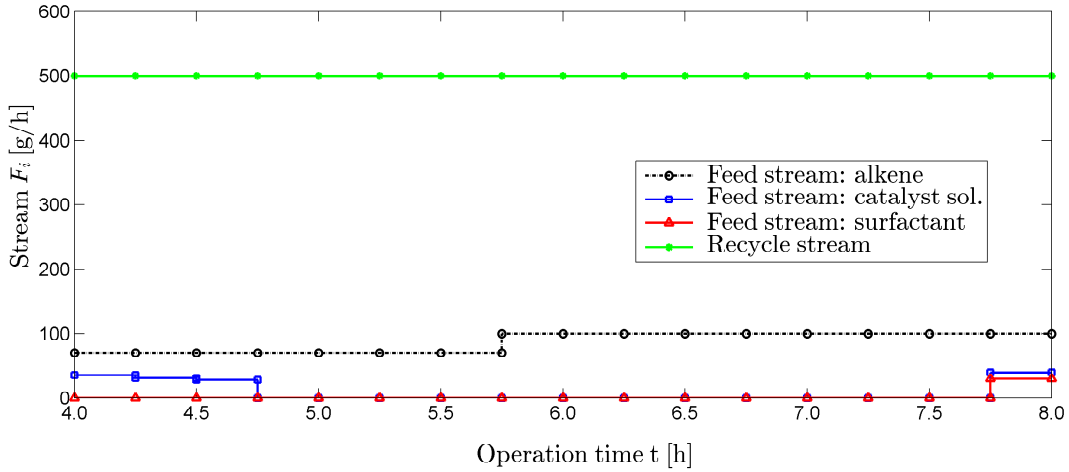

Figure 6.18.: Deterministic continuous operation optimization: control results for streams.

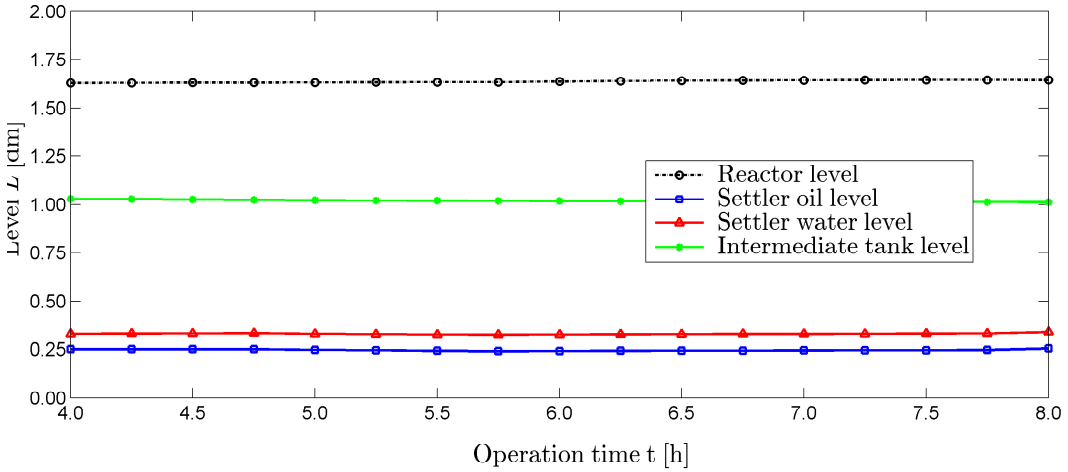

Figure 6.19.: Deterministic continuous operation optimization: liquid levels in the plant.

into the product tank takes on the composition of $X_{s=11}$ and the product concentration in the product tank asymptotically approaches the value of $X_{s=11}$.

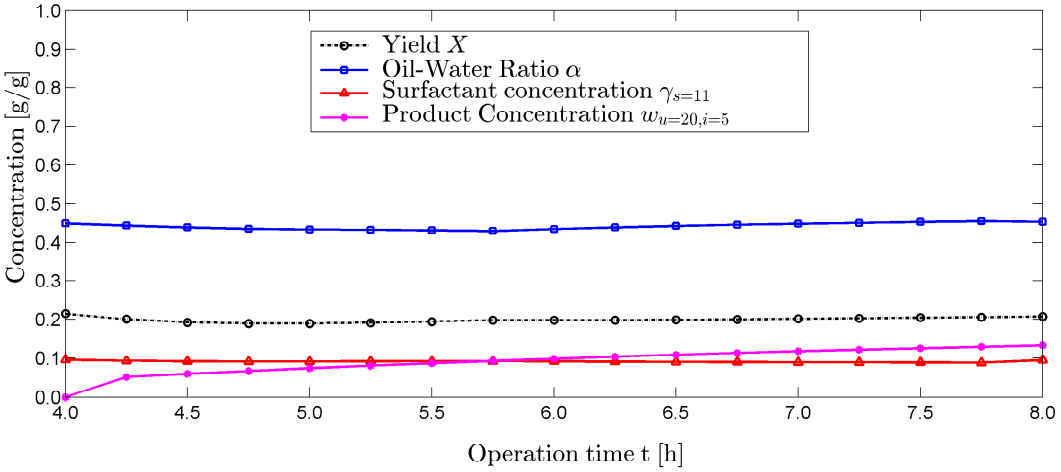

Figure 6.20.: Deterministic continuous operation optimization: composition parameters.

The settler temperature is also constant throughout the process. At the end, when a refeeding of surfactant and catalyst solution occurs, a slight drop is necessary so that the separation is continued.

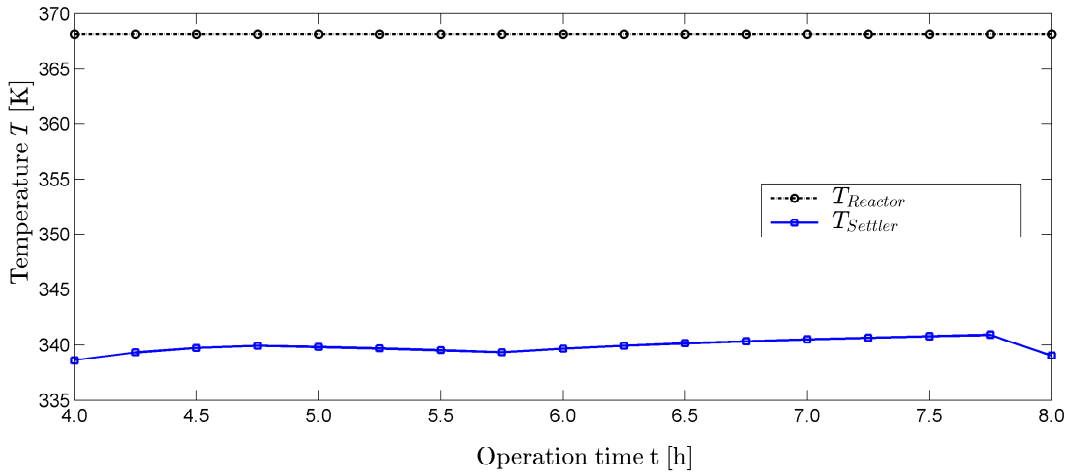

Figure 6.21.: Deterministic continuous operation optimization: reactor and settler temperature.

The currently implemented result leads to a constant, but very small loss of catalyst. The concentration of rhodium precursor in the product tank after the eight hours of operation roughly equal 0.12 ppm. The product stream contains 0.16 ppm precursor after eight hours at a yield of 21 %. This value can be explained by the implemented concentration equations for the oil phase. The higher the amount of 1-tridecanal at the inlet of the settler, the higher the water and surfactant concentration in the oil phase. This directly leads to an increased rhodium leaching. The value of 0.16 ppm is similar to the actually achieved rhodium leaching values during the mini-plant operation. As shown in Section 6.1 in Fig. 6.5, the rhodium concentration in the oil phase samples were below 0.20 ppm for the times, when the phase separation was functioning. Thus, the calculated result of 0.16 ppm from the simulation of

the optimal controls is an acceptable value. It is necessary that value lies below 0.5 ppm, to reduce subsequent separation steps.

Nevertheless, further investigation is required on this part, so that a correct description of the water and rhodium concentration in the oil phase can be made. At this point, it must be kept in mind that the concentration equations describing the rhodium loss into the oil phase are purely empirical and estimation based. It is necessary to improve these equations with according measurements, so that a better and more trustworthy estimation of actual values is possible.

Concluding it can be said that the results are satisfactory and the overall operation implementable into the actual process. A continuous production of 1-tridecanal can thus be achieved already after only 4.0 hours of operation. If higher yield values are desired, a longer start-up period must be considered as well as alternative feeding strategies in which the reactor residence time is increased. Based on the results of the deterministic dynamic optimization, initial values are obtained which are used in the dynamic chance-constrained optimization.

Additionally, for the sake of completeness, a steady-state optimization study is carried out with the same starting values obtained after the 4.0 hours start-up of the process. In gPROMS, steady-state optimization of a dynamic model is performed via a method called time relaxation. No sensible result is obtainable with the currently implemented model. Several equations must be changed, including a removal of the triggering functions, the product tank, and feed tanks. The entire model would have to be rewritten to obtain an adequate result. Additionally, the question arises, whether a steady-state result is truly implementable in the plant with the currently desired constraints. If a yield of 20 % is desired, the ingoing alkene feed stream is not allowed to be too high, i.e. over 200 g/h, to ensure a high enough reactor residence time. Secondly, if the feed stream of alkene is that low, then a refeeding of catalyst and surfactant would occur in very small amounts, e.g. continuously 3 g/h. This result is not implementable with the currently installed pumps in the plant, because the value is simply too small.

6.4. Chance-Constrained Optimization: Trajectory Development

The objective function of the chance-constrained optimization problem is divided into several parts.

$$\min_{u} \sum_{FE=1}^{NFE} \left(E\left[\Phi_1 + \Phi_2 + \Phi_3 + \Phi_4\right]\right) \tag{6.21}$$

The terms in Eq. 6.21 are each objective functions by themselves. Just as in the deterministic optimization problem, the aim during the start-up of the process is to maximize the yield of 1-tridecanal in stream S_{11}. The value is multiplied by minus ten, so that its influence on the objective function result is larger and to account for the fact that we wish to maximize this value and not minimize it.

$$\Phi_1 = -10 \cdot X_{S=11} \tag{6.22}$$

Here, the main units with larger hold-ups, reactor ($u = 9$), settler ($u = 12 + 13$), and the intermediate product tank ($u = 14$), are filled as quickly as possible. Once the reactor is full, the reaction is initiated and the production of 1-tridecanal can begin. After this has been carried out for the first four hours of operation, the second entry in the objective function becomes relevant. Here, the 1-tridecanal product stream is to be maximized.

$$\Phi_2 = -F_{s=18,i=5,FE} \tag{6.23}$$

Depending on whether the start-up or the continuous operation are of interest, Φ_1 or Φ_2 are eliminated from Eq. 6.21. Additionally, two penalty functions or regulation terms are required, to keep the concentrations of surfactant and oil:water ratio in the vicinity of 0.08 g/g and 0.5 g/g respectively. These values are chosen, because the reaction kinetics have been validated for these concentrations. Additionally, these concentrations represent the center point of the phase separation model. The objective is calculated for each finite element to force the optimizer to find a solution in which the concentrations are maintained throughout the process.

$$\Phi_3 = W_1 \cdot \left(\frac{\gamma_{S=11,FE} - 0.08}{0.08}\right)^2 \tag{6.24}$$

$$\Phi_4 = W_2 \cdot \left(\frac{\alpha_{S=11,FE} - 0.5}{0.5}\right)^2 \tag{6.25}$$

The weighting factors W_1 and W_2 are required, so that the penalty part of the objective function is effective. Otherwise the values would be very small in comparison to the hold-up of product in the product tank. They are set as $W_1 = 10$ and $W_2 = 5$. These values are chosen so that the influence on the phase separation temperature caused by a concentration variation of the surfactant amount is equal to that of a concentration variation of the oil content.

Applied Chance Constraints: The objective function in Eq 6.21 may be subject to different constraints. The first chance constraint is concerned with the product concentration, which should be reached in the product tank ($u = 20$) after a given time frame. For the start-up, the product concentration should be at least 10 wt.-%, if any product is to be purged into the product tank. In the stabilization procedure towards the continuous operation, the product

should be at least 15 wt.-%. The constraint may seem trivial, yet under the circumstances that the reaction kinetics themselves are uncertain and the feed streams are prone to vary, an operating procedure must be found which guarantees a certain yield.

Secondly and of higher relevance for the process is the rhodium loss: The loss of course should not exceed a certain bound, in this case being 0.5 ppm, for economic reasons. This value has been achieved in the actual mini-plant operation, but has also been exceeded. With the currently implemented concentration equations, a too high yield would lead to an increased rhodium loss. Therefore, a trade-off between rhodium loss and product yield will be reached in the optimization. It is possible to determine the critical product concentration manually beforehand. If the bound lies at 0.5 ppm, then that means a yield of slightly over 22 wt.-% should not be exceeded. This can be shown in the following calculation, in which a yield of 22 wt.-% is assumed. The oil phase is contaminated with surfactant and water, the higher the product amount in the inlet stream of the settler. The ratio of surfactant to water in the splitted oil stream (s=12) is the same as that in the outlet reactor stream (s=12). The same applies to the catalyst amount. Thus, the catalyst loss in the oil stream can be calculated. In the case below, a yield of 22 wt.-% would lead to a catalyst loss of 0.475 ppm.

$$w^{oil}_{s=12} = 1 - (w_{s=11,i=5} + w_{s=11,i=4}) \cdot 0.4 \quad \rightarrow w^{oil}_{s=12} = 0.912 \tag{6.26}$$

$$w_{s=11,i=12} = (1 - w^{oil}_{s=12}) \cdot \frac{0.08}{0.46} \quad \rightarrow w_{s=11,i=12} = 0.015 \tag{6.27}$$

$$w_{s=11,i=9} = (1 - w^{oil}_{s=12}) - w_{s=11,i=12} \quad \rightarrow w_{s=11,i=9} = 0.073 \tag{6.28}$$

$$w_{s=11,i=10} = w_{s=11,i=9} \cdot \frac{300 \cdot 10^{-6}}{0.46} \cdot 0.01 \rightarrow w_{s=11,i=10} = 0.475 \cdot 10^{-6} \tag{6.29}$$

Again, the issue here is that with the uncertain parameters in the reaction kinetics and the uncertain pump behavior, concentration changes are prone to happen. These changes may cause undesired fluctuations. Thus, an operation procedure is required which takes these changes into account and makes certain that the rhodium loss bound is not violated.

Both of these constraints are formulated as chance constraints and are shown in Eq. 6.30. The α_i are set to 0.80 and 0.98 respectively. The constraint concerning the rhodium loss is "stricter" than that concerning the product yield.

$$s.t.\ Pr\left\{\frac{HU^L_{u=20,i=5}}{HU^L_{u=20}} - 0.5 \geq 0\right\} \geq \alpha_1 \text{ or } \left\{0.5 \cdot 10^{-6} - \frac{HU^L_{u=20,i=10}}{HU^L_{u=20}} \geq 0\right\} \geq \alpha_2. \tag{6.30}$$

Sparse Grid: For these constraints, the activation energy of the hydroformylation reaction, the catalyst inhibition factor, and the feed stream uncertainty factor are seen as uncertain. To calculate the probability that the determined controls adhere to these constraints, a sparse grid is created. Fig. 6.22 shows the grid for the two parameters K_{cat} and ξ. The boundary of the inequality constraints is then determined for $E_{r=5}$. This is done, because a monotonous relationship between the uncertain input $E_{r=5}$ and the output is assumed for most cases, which speeds up the calculation process of the critical $E_{r=5}$ value for the inequality constraints.

To avoid repetition at this point, a closer description of this method, the determination of the critical uncertain parameter bound, and thus the calculation of the probability of adhering to the constraints can be found in (Esche, 2015).

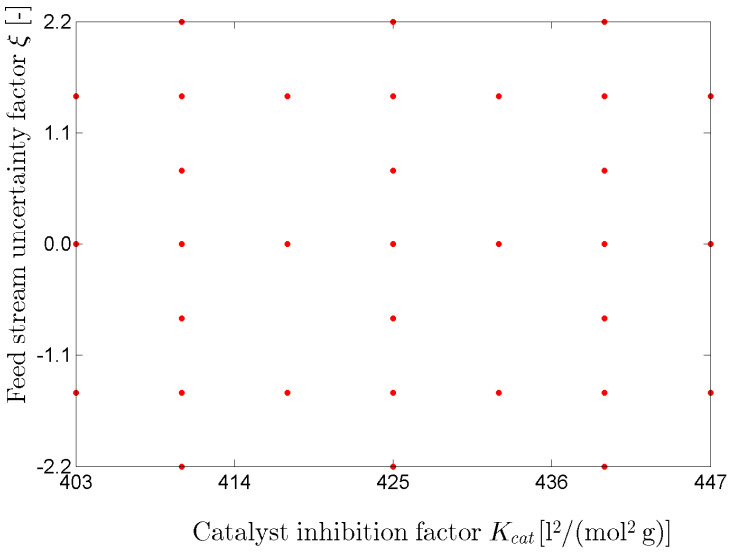

Figure 6.22.: Sparse grid of K_{cat} and ξ.

6.4.1. Chance-Constrained Optimization: Start-up

In this section, the results concerning the chance-constrained optimization of the start-up of the plant are presented. Hereby, the results using the chance constraints from Eq. 6.30 are analyzed separately. The problem is solved with NLPQLP, described in (Exler and Schittkowski, 2007), using the settings shown in the Appendix in Tab. A.8. The graphical comparison of the results is carried out at the end of the section.

Chance-constrained product optimization: As mentioned in the previous section, the aim is to keep the system from purging product, if the product concentration is too low. For this purpose, the same controls and control variable bounds as in the deterministic optimization are used. The results of the deterministic optimization are used as initial values. Initially, the probability using these initials is calculated. Hereby, a value of $Pr \geq 0.41$ is obtained. This means that if the deterministic results are implemented into the problem, an adhering to the constraints at an α_1 of greater or equal to 80 % can not be guaranteed.

The optimization problem is solved in 19 min. The primary objective was to optimize the yield. The initial product value from the deterministic optimization yields roughly 20.33 %. The chance-constrained optimization slightly improves this value to 20.39 %, which is almost negligible. More importantly, the operation is modified in such a way that the probability of adhering to the chance constraint lies above 98 %. The following control values shown in Tab. 6.10 should be implemented to obtain this result:

Compared to the deterministic optimization controls, the main difference lies in the purging at the end and slight modifications concerning the feeding policy. More alkene is fed in the beginning and less catalyst solution. Additionally, more surfactant is fed over time.

Chance-constrained Rhodium Loss: The second constraint of interest is the rhodium loss. If the originally determined deterministic controls are implemented, the probability lies above 98 %. This means that concerning the rhodium loss, the desired constraint value is fully adhered to. Nevertheless, a slight improvement regarding the objective is performed: 20.33 % vs. 20.38 %. This result is obtained in less than 36 minutes. The resulting

Table 6.10.: Chance-constrained start-up operation optimization: controls - product optimization.

Interval Nr. [-]	time frame [h]	$F_{s=4}^{SP}$ [g/h]	$F_{s=5}^{SP}$ [g/h]	$F_{s=6}^{SP}$ [g/h]	$T_{u=9}$ [K]	$F_{s=25}^{SP}$ [g/h]	$\lambda_{u=15}$ [-]
1	0.00 - 0.25	500.00	500.00	88.00	368.15	100.00	1.00
2	0.25 - 0.50	500.00	500.00	88.00	368.15	100.00	1.00
3	0.50 - 0.75	500.00	500.00	88.00	368.15	100.00	1.00
4	0.75 - 1.00	500.00	500.00	87.96	368.15	100.00	1.00
5	1.00 - 1.25	500.00	300.00	87.95	368.15	100.00	1.00
6	1.25 - 1.50	260.00	300.00	79.95	368.15	100.00	1.00
7	1.50 - 1.75	160.00	270.01	39.95	368.15	94.68	1.00
8	1.75 - 2.00	80.00	130.01	15.95	368.15	83.82	1.00
9	2.00 - 2.25	70.00	110.01	6.96	368.15	84.68	1.00
10	2.25 - 2.50	50.00	80.01	0.36	368.15	80.55	1.00
11	2.50 - 2.75	50.00	50.01	1.36	368.15	149.91	1.00
12	2.75 - 3.00	50.00	10.00	3.96	368.15	114.56	1.00
13	3.00 - 3.25	50.00	0.35	2.97	368.15	125.02	1.00
14	3.25 - 3.50	50.00	0.74	5.61	368.15	123.57	1.00
15	3.50 - 3.75	50.00	1.61	11.31	368.15	121.34	1.00
16	3.75 - 4.00	50.00	15.13	35.77	368.15	200.00	0.90

controls are displayed in Tab. 6.11. Also for these controls, the probability of adhering to the constraint remains above 98 %. Just as for the previous optimization, a purging of product in the final interval is carried out.

Chance-constrained Start-up Optimization - Result Comparison: A comparison between the different control strategies is presented below. The focus hereby lies on the three feed streams. In Fig. 6.23 to Fig. 6.25 the results for the feed streams are shown. CC1 is the chance constraint which belongs to the product specification and CC2 is the chance constraint which belongs to the rhodium loss. It immediately becomes obvious, that the results of the chance-constrained optimization are very similar to the deterministic one.

Concerning the alkene feed, both chance constraint optimizations increase the alkene feed slightly (Fig. 6.23). This leads to an increase in the oil:water ratio in the plant and thus ultimately to a higher oil phase in the settler. This is required, to be able to purge a certain amount of product. The oil ratio shift is enhanced by the reduced catalyst solution feed. Interestingly enough, the solution for both chance constraints for the catalyst solution are the same. In both cases, less catalyst solution is initially fed into the system. Integrally seen though, roughly the same amount is introduced after four hours. The slight differences suffice to avoid the violation of the constraints. If more alkene is fed into the system, the intermediate tank is filled sooner and thus the recycle of alkene begins earlier. This leads to a higher concentration of product in the intermediate tank. Thus, the purged stream has a high 1-tridecanal concentration and a constraint violation can be avoided. Additionally, the amount of product in the reactor outlet stream is below the critical 22 %. The catalyst concentration is low enough so that a violation of the rhodium loss is also avoided as well.

6.4.2. Chance-Constrained Optimization: Stabilization

Besides the two chance constraints, other critical questions arise for the continuous operation. What controls are generally determined for the continuous operation? How are controls modified if more product is created during the start-up phase than expected? What happens,

Table 6.11.: Chance-constrained start-up operation optimization: controls - rhodium loss reduction.

Interval Nr. [-]	time frame [h]	$F_{s=4}^{SP}$ [g/h]	$F_{s=5}^{SP}$ [g/h]	$F_{s=6}^{SP}$ [g/h]	$T_{u=9}$ [K]	$F_{s=25}^{SP}$ [g/h]	$\lambda_{u=15}$ [-]
1	0.00 - 0.25	500.00	500.00	88.00	368.15	100.00	1.00
2	0.25 - 0.50	500.00	500.00	88.00	368.15	100.00	1.00
3	0.50 - 0.75	500.00	500.00	88.00	368.15	100.00	1.00
4	0.75 - 1.00	500.00	500.00	87.70	368.15	100.00	1.00
5	1.00 - 1.25	500.00	300.00	87.60	368.15	100.00	1.00
6	1.25 - 1.50	268.00	300.00	79.60	368.15	100.00	1.00
7	1.50 - 1.75	160.00	270.00	39.60	368.15	94.70	1.00
8	1.75 - 2.00	87.50	130.00	15.70	368.15	83.80	1.00
9	2.00 - 2.25	71.50	110.00	6.69	368.15	84.70	1.00
10	2.25 - 2.50	50.00	80.00	0.12	368.15	80.50	1.00
11	2.50 - 2.75	50.00	50.00	1.13	368.15	150.00	1.00
12	2.75 - 3.00	50.00	10.00	3.75	368.15	115.00	1.00
13	3.00 - 3.25	50.00	0.38	2.77	368.15	125.00	1.00
14	3.25 - 3.50	50.00	0.77	5.45	368.15	124.00	1.00
15	3.50 - 3.75	50.00	1.62	11.20	368.15	121.00	1.00
16	3.75 - 4.00	50.00	15.10	35.70	368.15	200.00	0.90

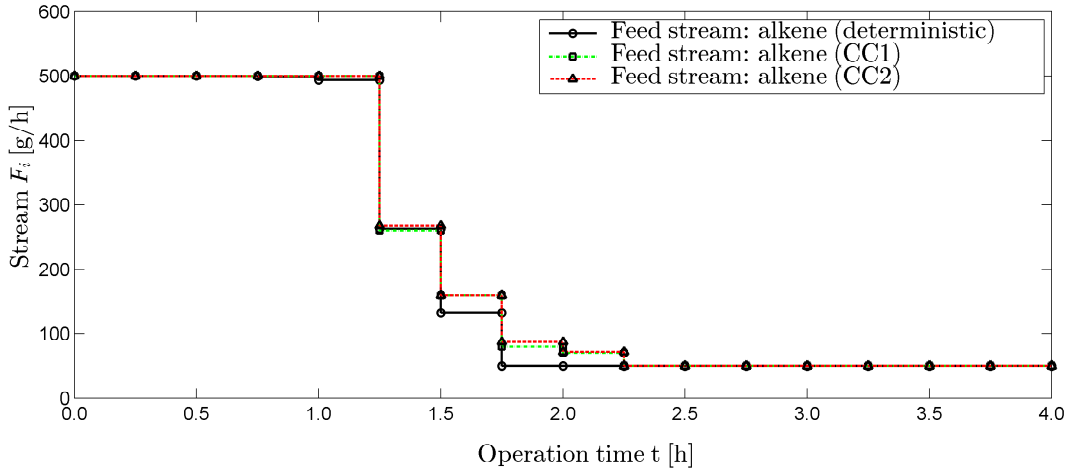

Figure 6.23.: Comparison of deterministic and chance-constrained optimization results: controls for alkene feed.

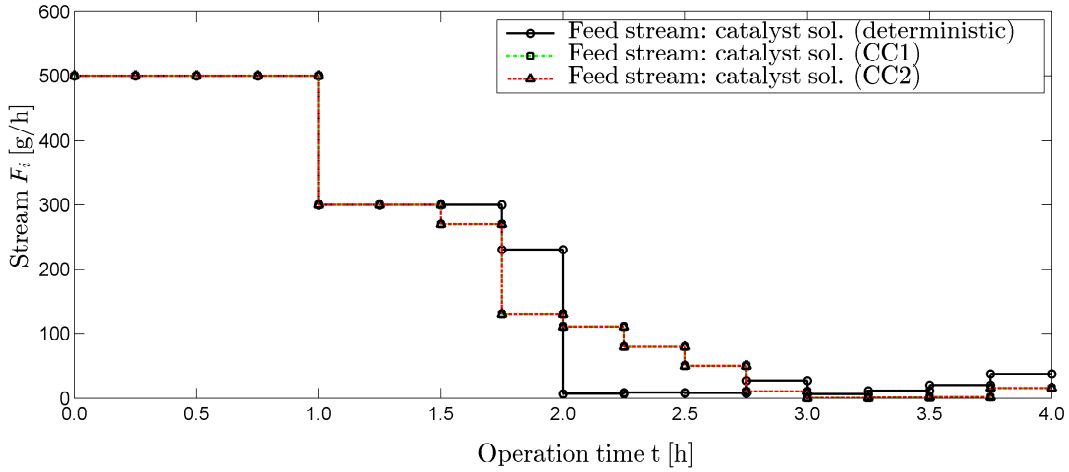

Figure 6.24.: Comparison of deterministic and chance-constrained optimization results: controls for catalyst solution feed.

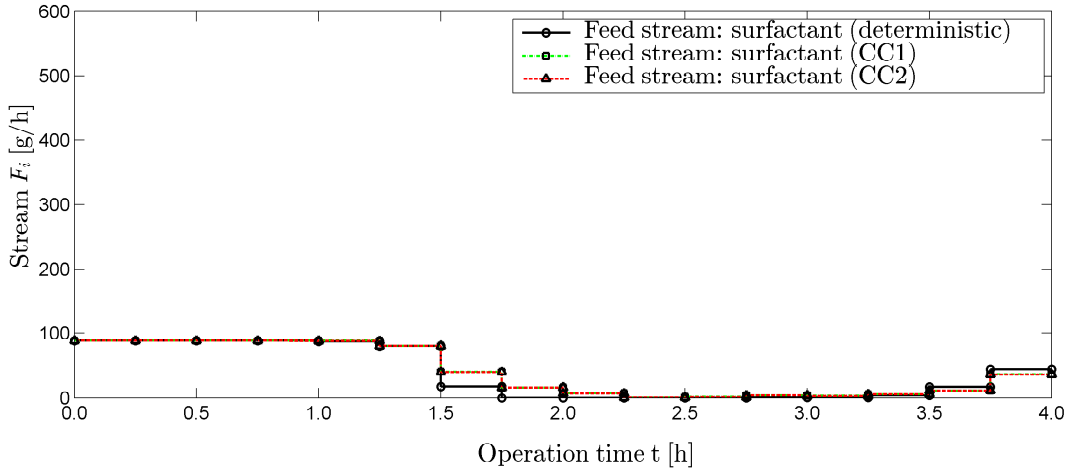

Figure 6.25.: Comparison of deterministic and chance-constrained optimization results: controls for surfactant feed.

if the operator has not implemented the determined controls correctly for the last interval of the start-up and the plant is in a different state? This is especially important for the phase separation, e.g. the wrong settler temperature is implemented. What happens if no oil phase is present and the entire settler is filled with mixed phase? Based on these questions, different scenarios can be imagined for the chance-constrained optimization of the process. Exemplarily, two of these shall be exercised to show the functionality of the model and the applied chance-constrained optimization.

- Case 1: ideal operation - everything goes as planned after start-up
- Case 2: the wrong settler temperature has been set.

In the following, these two cases will be presented.

Case 1: This is the standard case, in which everything goes according to plan. After the start-up of the plant, the correct concentrations are reached and perfectly estimated by the model. For this case, an optimization using the two chance constraints, catalyst loss and the product quality, are implemented. The same controls and control bounds are used just as for the deterministic optimization. The optimization result is obtained in 17 minutes, showing that a product stream containing 18.3 g/h 1-tridecanal, at a yield of $X_{s=11}$ 19.17 wt.-%. In this case, IPOPT converges at a point of local infeasibility. Nevertheless, none of the chance constraints are violated. Both the probability of not violating the catalyst constraint and the probability of not violating the product specification stay above 98 %. The determined controls are shown in Tab. 6.12.

Table 6.12.: Chance-constrained continuous operation optimization: case 1 controls.

Interval Nr. [-]	time frame [h]	$F_{s=4}^{SP}$ [g/h]	$F_{s=5}^{SP}$ [g/h]	$F_{s=6}^{SP}$ [g/h]	$T_{u=9}$ [K]	$F_{s=25}^{SP}$ [g/h]	$\lambda_{u=15}$ [-]
1	4.00 - 4.25	99.60	39.41	0.14	365.45	495.96	0.65
2	4.25 - 4.50	70.69	39.30	0.13	365.45	495.85	0.65
3	4.50 - 4.75	70.70	39.16	0.12	365.45	495.70	0.65
4	4.75 - 5.00	70.71	0.19	0.10	365.45	495.53	0.65
5	5.00 - 5.25	70.75	0.18	0.08	365.45	495.30	0.65
6	5.25 - 5.50	70.87	0.12	0.07	365.45	494.96	0.65
7	5.50 - 5.75	71.28	0.06	0.06	365.45	494.45	0.65
8	5.75 - 6.00	98.84	0.06	0.06	365.45	493.56	0.65
9	6.00 - 6.25	98.92	0.06	0.06	365.45	491.95	0.65
10	6.25 - 6.50	98.91	0.06	0.05	365.45	489.60	0.65
11	6.50 - 6.75	98.92	0.06	0.05	365.45	486.64	0.65
12	6.75 - 7.00	98.92	0.06	0.05	365.45	483.06	0.65
13	7.00 - 7.25	98.92	0.07	0.05	365.45	478.29	0.65
14	7.25 - 7.50	98.96	0.08	0.05	365.40	471.02	0.65
15	7.50 - 7.75	98.97	0.13	0.05	365.45	455.15	0.65
16	7.75 - 8.00	98.98	39.42	28.69	365.44	496.69	0.65

Using NLPQLP with the current settings, no result is obtainable within one hour. This issue of obtaining infeasible results can be tackled in multiple ways:

- modification of the initial conditions (consistency check required),
- modification of the optimization variable bounds,
- tuning of the starting values of the optimization variables,

- reduction of the degree of freedom,
- tuning of the solver parameters, or
- switching the objective function.

The first five options are not desired herein, because of the fact that many manual modifications are required. Since a "good and stable" solution is desired quickly the workaround by switching the objective function is used. The aim is no longer to maximize the product stream leaving the system, but to let it reach a value of 19.5 g/h. This value is selected, because it is the result of the deterministic optimization and is a result that has been observed during the actual plant operation. The new objective function therefore is:

$$\Phi_2 = (F_{s=18,i=5,FE=final} - 19.5)^2 \tag{6.31}$$

Here, only the final interval is considered, because we are still in the stabilization phase of the process. Once this has been achieved, the objective can be switched so that the aim is to keep the stream around 19.5 g/h for all intervals. Satisfactory results are obtained and the optimization problem is solved in less than 6 minutes using IPOPT as a solver. The controls are slightly modified and can be seen in Tab. 6.13. Using the NLPQLP, the result is obtained in 20 s, but no change to the controls is done. In general, the result is fairly similar to that of the deterministic optimization. A graphical comparison between each of the results will be shown in a summary later in this chapter.

Table 6.13.: Chance-constrained continuous operation optimization: case 1 - optimal controls.

Interval Nr. [-]	time frame [h]	$F^{SP}_{s=4}$ [g/h]	$F^{SP}_{s=5}$ [g/h]	$F^{SP}_{s=6}$ [g/h]	$T_{u=9}$ [K]	$F^{SP}_{s=25}$ [g/h]	$\lambda_{u=15}$ [-]
1	4.00 - 4.25	99.97	29.97	0.00	368.15	500.00	0.60
2	4.25 - 4.50	86.76	29.96	0.00	368.15	500.00	0.60
3	4.50 - 4.75	83.78	29.95	0.00	368.15	500.00	0.60
4	4.75 - 5.00	92.19	14.92	0.00	368.15	500.00	0.60
5	5.00 - 5.25	99.88	14.62	0.00	368.15	500.00	0.60
6	5.25 - 5.50	99.92	0.44	0.00	368.15	500.00	0.60
7	5.50 - 5.75	99.95	0.10	0.00	368.15	500.00	0.60
8	5.75 - 6.00	99.97	0.05	0.00	368.15	500.00	0.60
9	6.00 - 6.25	99.98	0.03	0.00	368.15	500.00	0.60
10	6.25 - 6.50	99.99	0.02	0.00	368.15	500.00	0.60
11	6.50 - 6.75	99.99	0.02	0.00	368.15	500.00	0.60
12	6.75 - 7.00	99.99	0.02	0.01	368.15	500.00	0.60
13	7.00 - 7.25	99.99	0.01	0.01	368.15	500.00	0.60
14	7.25 - 7.50	100.00	0.01	0.01	368.15	500.00	0.60
15	7.50 - 7.75	100.00	0.01	0.01	368.15	500.00	0.60
16	7.75 - 8.00	100.00	30.00	30.00	368.15	500.00	0.60

Case 2: This case is of high interest, because it is a very plausible case that may occur. Since currently the concentration measurements in the plant can only be carried out every hour, a misinterpretation of the development of the concentration in the reactor is possible. Also, if the optimization fails or takes longer than expected, the operator may keep the currently installed controls. Therefore, the case can be imagined in which, due to a slightly different plant behavior or non-availability of optimal results, the operator has decided to

operate the settler at the current temperature. The operator operates the settler in a wrong manner for the last two intervals (30 minutes) of an operation. First of all, to account for this case, modifications of the equations are necessary. The current model does not account for an outflowing oil stream if there is no inlet oil stream in the settler. Therefore, the equation concerning the outflowing oil stream is modified accordingly. It is assumed that the operator uses the results of the deterministic optimization for the oil stream, which is roughly 100 g/h.

Additionally, a kill switch $TRIG^{kill}$ for the phase separation trigger is introduced into the equation for stream S_{12}. The kill switch is a binary variable with a value 0 or 1 and will be implemented as an additional degree of freedom in the optimization process. However, it is be bounded in such a way, that the optimizer has no freedom to change its set value. For the first interval, it will be set to 0. Thus, no stream 12 is established and the hold-up of the oil phase is reduced. After the interval, the kill switch is set to 1 and the stream is restored.

$$\begin{aligned} Old: \quad & F_{s=12} = \lambda_{u=10}^{Oil} \cdot w_{s=11}^{Oil} \cdot F_{s=11} \cdot TRIG^{Tmax} \cdot TRIG^{Tmin} \\ New: \quad & F_{s=12} = TRIG^{kill} \lambda_{u=10}^{Oil} \cdot w_{s=11}^{Oil} \cdot F_{s=11} \cdot TRIG^{Tmax} \cdot TRIG^{Tmin} \end{aligned} \tag{6.32}$$

$$\begin{aligned} Old: \quad & F_{s=16} = TRIG_{Settler}^{Lvl} \cdot (TRIG_{Settler}^{OilLvl}) \cdot F_{s=12} + KP_{u=12} \cdot (L_{Settler}^{tot,L} - L_{Settler}^{tot,L,SP})) \\ New: \quad & F_{s=16} = 100 \cdot (1 - TRIG^{kill}) + TRIG^{kill} \cdot F_{s=16}^{Old} \end{aligned} \tag{6.33}$$

For the first two intervals, the controls of the last interval of the start-up optimization are implemented. This part can be seen as a simulation, because the controls are fixed at their lower and upper bound values. The kill switch is set to 1.0E-3 for these two intervals. Setting it to exactly 0 leads to convergence issues. For the remaining 16 intervals, the determined optimal results of the "ideal" operation are used as starting values for the optimization. The initial conditions for the hold-ups are taken from the final results of the start-up optimization.

The optimization is solved in under 10 minutes reaching a product stream value of 19.5 g/h 1-tridecanal and a yield of 18.64 %. The objective function value lies at around 0.4, which is established due to a deviation from the desired oil:water ratio and surfactant concentration. The results of the operation can be seen in Tab. 6.14. The probability of adhering to the catalyst constraint remains above 98 %. The product specification bound is met with a probability of 95 %.

The result of the optimization problem is logical. The oil phase is reduced due to the not functioning phase separation. Thus, the system needs to replenish it by increasing the feed stream in comparison to originally determined optimal result. Since too much surfactant has been fed into the system at the beginning (interval -2 and -1), nothing is fed during the 16 remaining intervals. The same applies for the catalyst solution, whose values are more spread out rather than forcefully being added at selected intervals.

Chance-constrained continuous operation optimization - result comparison: A comparison between each of the results can be seen in the Fig. 6.26 to Fig. 6.27. The axis of the figures are kept so large to focus on drastic changes in set-points opposed to changes in the range of 2 or 3 g/h.

Firstly, a comparison between Case 1 and the deterministic case is legitimate. Here, the same constraints apply. In contrast to the deterministic solution, the chance-constrained solution suggests to implement more alkene into the system, so that the product specification can definitely be met. As stated before, looking at Case 2, to account for the higher sur-

Table 6.14.: Chance-constrained continuous operation optimization: case 2 - optimal controls with bounded rhodium loss. The grey means that no optimizer action is allowed during this interval.

Interval Nr. [-]	time frame [h]	$F_{s=4}^{SP}$ [g/h]	$F_{s=5}^{SP}$ [g/h]	$F_{s=6}^{SP}$ [g/h]	$T_{u=9}$ [K]	$F_{s=25}^{SP}$ [g/h]	$\lambda_{u=15}$ [-]	$TRIG^{Kill}$ [-]
-2	3.50 - 3.75	50.00	15.10	35.7	368.1	200.0	0.9	0.001
-1	3.75 - 4.00	50.00	15.10	35.70	368.1	200.0	0.9	0.001
1	4.00 - 4.25	99.95	29.96	0.0	368.1	500.0	0.6	1.000
2	4.25 - 4.50	99.94	14.96	0.0	368.1	500.0	0.6	1.000
3	4.50 - 4.75	99.92	14.95	0.0	368.1	500.0	0.6	1.000
4	4.75 - 5.00	99.91	14.94	0.0	368.1	500.0	0.6	1.000
5	5.00 - 5.25	99.90	14.93	0.0	368.1	500.0	0.6	1.000
6	5.25 - 5.50	99.89	14.93	0.0	368.1	500.0	0.6	1.000
7	5.50 - 5.75	99.88	14.92	0.0	368.1	500.0	0.6	1.000
8	5.75 - 6.00	99.87	14.91	0.0	368.1	500.0	0.6	1.000
9	6.00 - 6.25	99.86	14.90	0.0	368.1	500.0	0.6	1.000
10	6.25 - 6.50	99.85	14.88	0.0	368.1	500.0	0.6	1.000
11	6.50 - 6.75	99.83	14.85	0.0	368.1	500.0	0.6	1.000
12	6.75 - 7.00	99.80	14.82	0.0	368.1	500.0	0.6	1.000
13	7.00 - 7.25	99.75	29.78	0.0	368.1	500.0	0.6	1.000
14	7.25 - 7.50	99.66	29.71	0.0	368.1	500.0	0.6	1.000
15	7.50 - 7.75	99.46	29.57	0.0	368.1	500.0	0.6	1.000
16	7.75 - 8.00	96.01	24.88	0.0	368.1	500.0	0.6	1.000

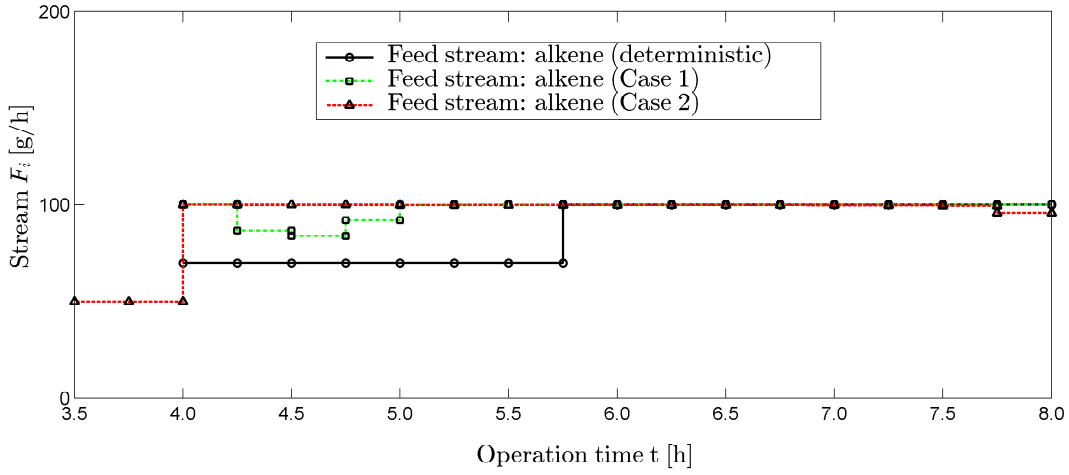

Figure 6.26.: Comparison of deterministic and chance-constrained optimization results for the continuous operation: controls for alkene feed.

factant and catalyst concentration in the system, the alkene feed is increased in the second chance-constrained optimization even more than in Case 1. A direct comparison between Case 2 and the deterministic solution is not valid, because the settings, due to the fixed controls for $t_i = 3.5$ to 4.0 h.

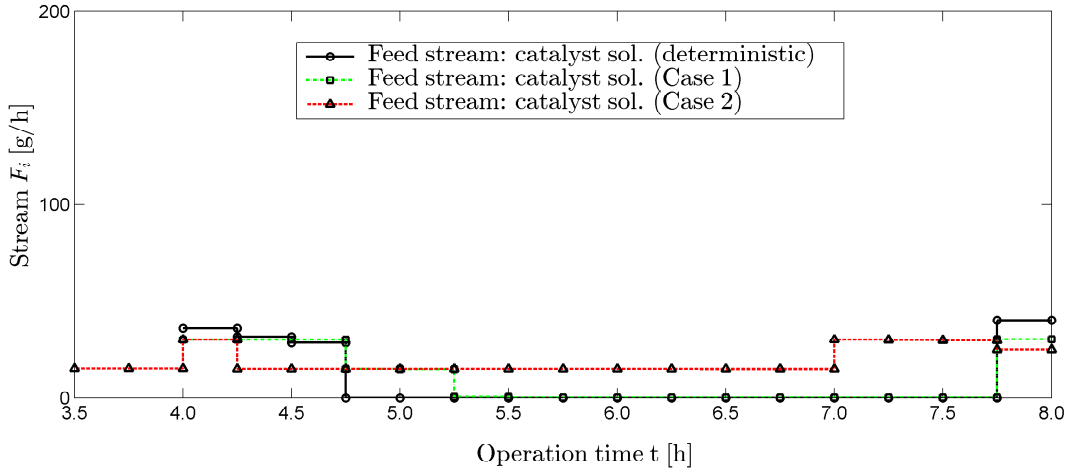

Figure 6.27.: Comparison of deterministic and chance-constrained optimization results for the continuous operation: controls for catalyst solution feed.

Overall, the chance-constrained optimization results show that an increase in the catalyst solution is required. The feeding value is maintained for a longer time period (4.5 to 5.25 h).

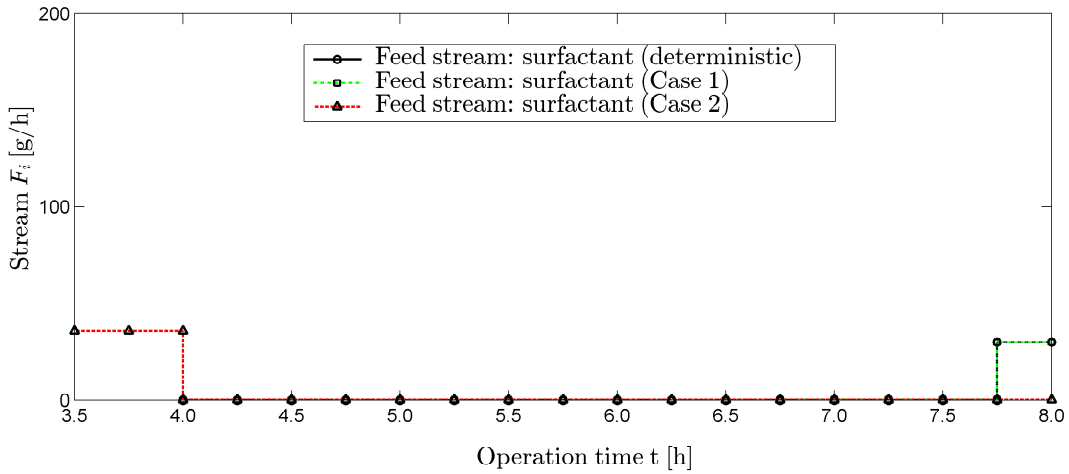

Figure 6.28.: Comparison of deterministic and chance-constrained optimization results for the continuous operation: controls for surfactant feed.

In conclusion, for the continuous cases it can be said, that the model can be applied for online-optimization purposes. Convergence to adequate solutions is achieved within less than one hour, sometimes even less than ten minutes. The consideration of the uncertainty caused by the feed streams and the reaction kinetic parameters is accounted for and flows into the optimization problem. The results of the objective function are generally slightly better than those of the deterministic optimization. The reasons for this can be, because

- different DAE solvers are used in the two cases, which may result in slightly different values regarding the gradients,

- different optimization solvers are used in gPROMS and in the chance-constrained optimization framework, which may lead to different local optima, and lastly
- the chance constraint allows for a slight violation of the constraint.

A critical remark at the end must be made though. The question has to be raised, whether the currently implemented strategy of a kill switch for the phase separation is correct? How should the operator know, that the current temperature is or is not suitable? This can only be done, if some form of state estimator of the plant is used beforehand. The plant state estimator can then decide, based on available concentration measurements of the past, if the plant was operated correctly. Based on this information, according initial values for the states and for the controls including their bounds can be set. This automation is yet to be implemented though and is not the focus of this thesis.

Quantification of the Potential Operation Improvement: Now, a quantification of the improvement caused by the determined optimal operation trajectories is made. It must be said beforehand, a true quantification at this point is hardly possible, because the existing data set stems from older plant configurations without the according settler modifications and addition of salt to enhance the phase separation. Nevertheless, a quantification is exemplarily carried out, to show how such a betterment may look like. In Fig. 6.29 the results of a simulation run in gPROMS using the determined optimal controls of the chance-constrained optimization for the start-up and continuous operation are compared to that of the first mini-plant operation. Hereby, the amount of 1-tridecanal in the product and in the water stream are analyzed.

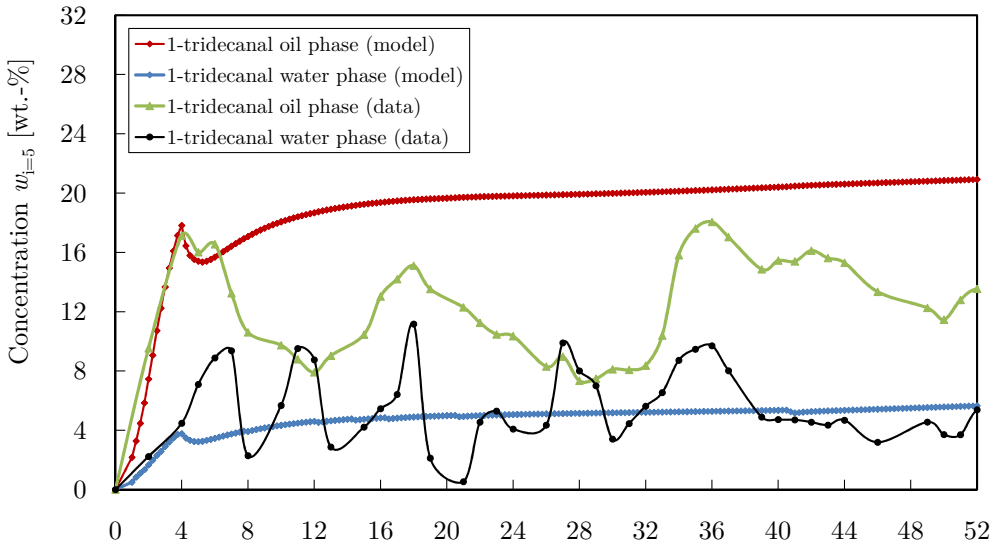

Figure 6.29.: Quantification of results: comparison of optimal results and non-optimal mini-plant operation.

Comparing the two results, several points worthy of notice should be mentioned.

- Firstly, the start-up of the reaction in the model and in the actual mini-plant operation must be looked at. For this purpose, the initial hours, in which the actual plant was filled, have been removed. Thus, the data points at the start of the reaction are compared, not including the filling process. It is apparent that the same amount of 1-tridecanal can be found in the oil phase in the model as in the plant. Even the

established maximum 1-tridecanal value is the same. The 1-tridecanal in the water phase of the model also has the same value as in the plant data. This underlines the validity of the determined reaction kinetics.

- Secondly, it can be concluded that the main difference between model and data begins, when the phase separation starts to fail in the real mini-plant operation. The repeated establishment and breakdown of the phase separation leads to a massive difference between mini-plant's 1-tridecanal concentration and model's 1-tridecanal concentration. Additionally, if the phase separation does not work properly, more catalyst and surfactant are lost in the product stream. Thus, less catalyst is present in total, which ultimately leads to less production of 1-tridecanal in the long run. Thus, even if the phase separation begins to function afterwards, the amount produced in the model prediction will not be reached, unless the catalyst amount is replenished.

- During the operation hours in which the phase separation functioned, the value of 1-tridecanal in the water phase in the model is similar to that in the real plant data set. This can especially be seen during 22 to 26 and 38 to 52 hours of operation. Since more 1-tridecanal is present in the model prediction in total, the values of 1-tridecanal in the water phase are of course slightly higher in the model than in the real data set.

The improvement that the results of the optimal controls would yield can be interpreted as the area between the model and the data points. It is obvious, that the results of the optimization would drastically improve the results of the mini-plant operation. A purer 1-tridecanal stream would be established and the loss of catalyst could be drastically reduced. In order to test these theoretical results and thus validate the model, an additional operation with the current plant configuration is carried out.

Comparison - Optimal Trajectories and Operation with Current Plant Configuration: Finally, at the end of this thesis, a comparison between determined optimal trajectories and a final operation of the mini-plant is made. With this final comparison, not only the validity of the model is shown, but also the implementability and reachability of the determined results. A close look is therefore taken on a third mini-plant operation performed in April 2015. Here, the new settler from Fig. 3.22 with the internal fittings was tested and 1 wt.-% Na_2SO_4 was added to the reaction mixture. In this operation, the phase separation was kept stable for several days with oil concentrations in the oil phase staying above 95 wt.-% at all times. The entire operation lasted over 200 hours. Of special interest for this thesis is the time frame from noon of the 21.04.2015, to midnight of the 22.04.2015. Here, a repeated 1.0 hour simulation followed by a 3.5 to 4.0 hour optimization of the plant operating trajectories is carried out.

Because real-time optimization was not the focus of this 200 hour mini-plant operation, the calculated results are not directly implemented in real-time into the process control system of the plant. They are solely used for comparison purposes[2]. The aim is to test the theoretical implementability as well as applicability of the results while using actual plant data for the simulation-optimization loop. The objective function shown in Eq. 6.34 is used

[2]The operation decisions were carried out by three Ph.D. students: Erik Esche, Markus Illner, and myself.

for the chance-constrained optimization:

$$\min_{u} \sum_{FE=1}^{NFE} \left(E\left[\Phi_2 + \Phi_3 + \Phi_4\right]\right) \tag{6.34}$$

$$s.t. \quad \text{all model equations} \tag{6.35}$$

$$Pr\left\{\frac{HU^{L}_{u=20,i=5}}{HU^{L}_{u=20}} - 0.5 \geq 0\right\} \geq 0.98 \tag{6.36}$$

Hereby, Φ_2, Φ_3, and Φ_4 represent different targets. The goal is to maximize the product stream leaving the system at the end while keeping the concentrations of surfactant and oil:water ratio in adequate values. Simultaneously, the catalyst loss should be kept below 0.5 ppm with a probability of 98 %.

$$\Phi_2 = -F_{s=18,i=5,FE=final} \tag{6.37}$$

$$\Phi_3 = W_1 \cdot \left(\frac{\gamma_{S=11,FE} - 0.08}{0.08}\right)^2 \tag{6.38}$$

$$\Phi_4 = W_2 \cdot \left(\frac{\alpha_{S=11,FE} - 0.5}{0.5}\right)^2 \tag{6.39}$$

The controls of the process are the feed streams, the reaction temperature, and the recycle of the lower settler stream. The outlet ratio is kept constant at 0.65. The bounds of the optimization can be summarized as follows:

- 30 g/h $\leq F^{SP}_{s=4} \leq$: 100 g/h
- 0 g/h $\leq F^{SP}_{s=5} \leq$: 10 g/h
- 0 g/h $\leq F^{SP}_{s=6} \leq$: 10 g/h
- 348 K $\leq T_{u=9} \leq$ 368 K
- 60 g/h $\leq F^{SP}_{s=25} \leq$: 90 g/h

For each simulation-optimization loop the final simulation value (implemented control in the plant) is used as an initial guess. For starting values of the concentrations in the reactor, settler, and tanks the offline GC concentration measurements of reactor, settler-oil, and settler-water phase as well as the controls implemented into the process are used.

In the beginning of the operation, the switch from batch operation mode to continuous operation mode (21.04.2015 12:00 h) can be seen by the decrease of the yield. Here, a stream of 31 g/h alkene feed is initially used. The optimization is started using the data set of 14:00 (2 p.m.) on the 21.04.2015. Initially, a simulation is done for one hour. This is then followed by an optimization for roughly four hours. Around 18:00 (6 p.m.), an accumulation of surfactant before the knitted fabric in the settler was observable. Here, clearly a mismatch between reality and model becomes visible. This accumulation of the surfactant means that less surfactant is being recycled back to the reactor. Thus, a reduction of the yield in the process takes place. At 3:00 (3 a.m.), on the 22.04.2015, this accumulation of surfactant was actively countered by the operators by heating up the settler to higher temperatures and increasing the recycle of the middle phase while keeping the entire recycle constant.

Then, after the accumulation is kept under control, the data set of 05:00 (5 a.m.) is used and the simulation and optimization is restarted and carried out until 23:00 (11 p.m.) on the 22.04.2015. During this period, an increase in the yield is observable. Each result

was calculated in under 1700 seconds. Each result has a probability greater than 98 % of adhering to the constraint. The results are summarized in Fig. 6.30. In this figure four different sets of points are visible:

- The diamond is used for the measured 1-tridecanal yield in the stream leaving the reactor ($X_{s=11}$). Additionally, the error bar of the measurement is portrayed.
- Secondly, the triangle (green) is used for the 1 hour simulation. These points belong to the time frame in which the accumulation of surfactant in the settler was not present.
- Triangle (red) for a 1 hour simulation in which the model is not valid due to the accumulation of surfactant in the settler.
- Square for a 3.5 to 4.0 hour optimization of the operating trajectories under uncertainty.

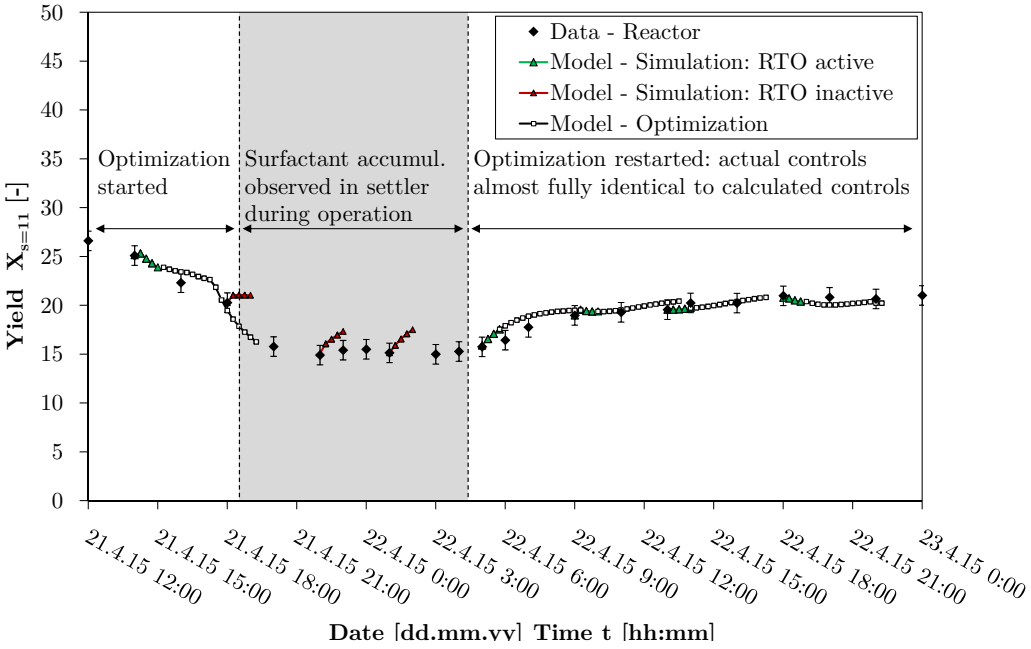

Figure 6.30.: Comparison: repeated optimization and mini-plant data.

The determined optimal controls are very similar to those implemented during the operation. These can be seen in the Appendix in Fig. A.10 to Fig. A.12 for the optimization carried out at 05:00 on the 22.04.2015. In general, the optimization determines that the best solution lies at the lowest bound of the alkene feed stream of 30 g/h, negligible to no surfactant and catalyst feed, the reactor should be operated at 95 °C, and the highest recycle stream of 90 g/h should be applied. During the operation, all of these values were used except for the recycle stream value, which was kept at its lower bound opposed to the calculated upper bound. A reactor residence time of roughly 2.5 hours was implemented during this time. A detailed comparison of the controls can be found in the Appendix in Fig. A.10 to Fig. A.12. The optimization of the mini-plant operation shows that the values obtained by the model regarding process yield are almost identical to the measurements.

Next to these extremely satisfying results, a discussion regarding two issues must be made:

1. Objective function formulation: The objective function leads to the result that at the end of the final optimization interval a drastic jump of the alkene feed is performed

(30 g/h to 100 g/h). This is obviously done to maximize the $F_{s=18,i=5,FE=final}$ value. Since this jump occurs at the end of the optimization time, the effect of this jump does not immediately drastically influence the other parts of the plant. To counter this effect, the objective function may be changed to something slightly different such as the difference between a certain concentration in the output or the optimization time horizon can be increased, but only the first set of results used.

2. Model adequacy throughout the operation. In the time frame between the 21.04.2015 18:00 (6 p.m.) and 22.04.2015 06:00 (6 a.m.) the yield in the mini-plant operation is significantly lower. Later, model and data points reach the same value, which is kept more or less constant for another 24 hours later on. The reason for this initial difference can be traced back to the recycle ratios and the surfactant accumulation in particular. After 22.04.2015 03:00 (3 a.m.), the recycle ratio of oil, middle, and water stream after the settler had to be switched from 1:0.6:1 to 0.6:1:06, since the middle phase in the settler was increasing and the accumulation became more and more obvious. The middle stream, which contains the largest amount of surfactant if the settler is operated in the 3 phase region, was thus doubled. The other two streams were reduced by a third, thus keeping the overall recycle stream of roughly 200 g/h intact. Over the course of 6 hours (from 03:00 (3 a.m.) to 09:00 (9 a.m.) on the 22.04.2015) the yield was significantly increased by roughly 6 %. This extreme sensitivity of the reaction regarding the surfactant concentration is currently not depicted by the model or by the reaction kinetics. The model currently assumes a homogeneous recycling of surfactant in the middle and water streams. This is obviously not the case, as some of the surfactant phase is blocked by the internal displacer in the settler. This fact also strengthens the demand for a correct measurement of surfactant concentrations entering and leaving the settler. Without this information, a key state variable for the estimation of the overall plant state is missing. Therefore, an enhancement on two sides must be made, modeling and process analytics, so that online-optimization under uncertainty can truly be carried out.

Even with this mismatch, the successful continuous result of roughly 20.5 % yield is reached both by the process and the model in a short time frame. This result lays a sturdy foundation for future work on the process concept as well as further implementation efforts on optimization under uncertainty.

Chapter 7.

Conclusions and Future Research Directions

In current industrial practice, uncertainty is often overestimated which leads to conservative decisions, be it design decisions or operating decisions. These conservative decisions, in consequence, reduce the economic viability of processes. In contrast to these conservative decisions stand aggressive strategies, which are preferably used to present high profit expectations. Due to unconsidered uncertainty these aggressive strategies are likely to lead to process constraint violations. Therefore, it can be said that systematic procedures are required to evaluate the trade-off between profitability and reliability (Arellano-Garcia, 2006). The herein applied approach of chance-constrained optimization can tackle both issues mentioned above. The determined optimization results on the one hand adhere to the constraints to a certain probability and on the other hand present a solution, whose profitability is higher than that of worst-case solutions. In this approach, the trade-off between profitability and reliability can be quantified.

In this thesis, the focus was laid on two main aspects, which were brought into connection with each other: uncertainty in process engineering problems and the development of a novel process concept known as hydroformylation in microemulsions. Because the process concept is new and currently no industrial process utilizing the described components exists, the uncertainty here is very high. This makes the operation of a mini-plant, in which the process concept is tested, exceptionally challenging. The main task was therefore to design a systematic framework to determine optimal operation trajectories under uncertainty for this novel process. Hereby, within the greater framework, several workflows were developed to achieve this goal. A complex optimization problem under uncertainty was solved using the chance-constrained optimization approach. As described by Arellano-Garcia (2006), "The major challenge when solving chance-constrained optimization problems lies in the computation of the probability and its derivatives of satisfying inequality constraints". This challenge was effectively met. In contrast to existing approaches, the computation of the results was achieved in an adequately short time frame applicable for dynamic real-time online-optimization for the mini-plant. Concluding it can therefore be said that since uncertainty is taken into account chance-constrained optimization potentially leads to more reliable results. Constraint violations not predicted by deterministic results are estimable.

This work thus presents advancements to the research of optimization under uncertainty and provides theoretical developments as well as actual practical applications of chance-constrained programming techniques.

7.1. Summary of Contributions

The contributions of this thesis can be summarized as follows:

- *The realization of a novel process concept known as hydroformylation in microemulsions:* As shown in this thesis in Chapter 3, several academic publications exist, in which microemulsions are used for reaction media. In all of these publications, the reactions are performed on a lab-scale. One of the primary results of this thesis is the proof of concept of the process known as hydroformylation in microemulsions. The process is realized on a mini-plant scale totaling an operation time of over 200 hours. This result means that new process possibilities are available in the field of multi-liquid-phase systems and promotes the application of surfactants as solvents in various media.

- *General workflow for critical steps of model preparation for optimization purposes:* The success of many, currently available model-based optimizers can be ascribed to the utilized models. These models show a high accuracy regarding depiction of process outputs and have acceptable characteristics regarding the computational effort for optimization problems. The workflow presented herein aims at guiding process systems engineers, whose goal is to develop models for optimization purposes, in designing a model that has the two mentioned characteristics.

- *A list of reformulation strategies to enhance the numerical behavior of optimization problems:* In accordance with the workflow for model development for optimization purposes, a fundamental step is the removal of nonlinearities and non-convexities in the model that lead to undesirable computational behavior. In this thesis, sets of potential mathematical equation structures are discussed that negatively influence the computational behavior during the optimization process. The aim hereby is to tell process systems engineers what, where, and why the formulation is inconvenient as well as how to alleviate the inconvenient formulation to achieve an improvement.

- *A framework to identify relevant uncertain parameters for optimization under uncertainty:* In stochastic optimization uncertain parameters or variables are applied. Often enough, these are randomly selected and their uncertainty description is assumed. In this thesis, a framework for parameter estimation problems is presented, in which the optimization function is considered in the uncertain parameter selection process. The reduction of the set of uncertain parameters is based on subset selection strategies and can be summarized by three steps: first, a parameter estimation is done to calculate expected values. This is then followed by a linear dependency analysis. Hereby a ranking of the uncertain parameters is carried out. The uncertain parameters with a high linear dependency are fixed, while others are left uncertain. This is followed by an analysis of the sensitivity of the uncertain parameters on a user-defined objective function regarding optimization of process operation or similar. Thus, one obtains a reduced set of uncertain parameters as well as their variance. These can then be used for optimization under uncertainty.

- *A workflow for the solution of nonlinear dynamic systems under uncertainty:* The herein developed workflow is divided into the six steps: definition of process goals, systems analysis, model development, uncertainty analysis, selection of desired stochastic optimization strategy, and solution of the optimization problem. The workflow incorporates the other contributions of this thesis and it is successfully applied on the model of the mini-plant for hydroformylation in microemulsions.

- *A guideline for the analysis of surfactant containing multiphase systems:* The analysis of real, surfactant containing multiphase systems still poses a challenge today. Chemists and engineers are often faced with the challenge of handling a multicomponent surfactant. This increases the difficulty of a correct concentration-analysis and of obtaining reproducible results. In this thesis, an approach is presented, in which the phase separation characteristics of surfactant containing multiphase systems are systematically investigated, so that modeling, process and equipment design, and general system analysis efforts are assisted.

- *An empirical phase separation model for oil-water-surfactant systems:* Using the guideline for the analysis of surfactant-containing multiphase systems, an empirical phase separation model has been developed. This model explicitly yields two temperature bounds, between which an adequate phase separation in terms of time and quality can be achieved. The model is easily implementable in a general settler model and applicable for optimization studies.

- *A modular settler for the extraction of multiple phases:* Again, using the guideline for the analysis of surfactant-containing multiphase systems a modular settler is developed. This settler consists of different modules, each fulfilling a different purpose such as enhancements for observability, coalescence, or operability. The general settler can easily be scaled-up and applied for other multiphase separation processes.

- *Application of insitu, online-Raman spectroscopy:* To analyze the components in the system Raman spectroscopy is employed insitu and online while the process was being operated. For the future, a chemometric model of the hydroformylation system is available which allows for the fast analysis. This analysis can be used for further application in model assisted plant operation. The achievement thus presents a step forward in the field of online process analytics.

- *A dynamic model of a hydroformylation process:* A dynamic model of the hydroformylation mini-plant was developed. This model may be specific for the mini-plant investigated in this thesis, but it contains ideas and strategies transferable to other processes. Among these ideas is that of triggering functions. The current model is capable of depicting the full operation of the process from start-up, to continuous operation, to shut-down. The implemented triggering functions change the model and the according optimization problem from a dynamic mixed-integer nonlinear problem to a solely dynamic nonlinear problem. Additionally, the concept of splitting the settler-unit into a splitter and a tank has proven to be suitable.

- *Combination of experiments and modeling:* Additionally, a process model to be applied for actual operation is only useful if it shows a certain repeatability of the measurements. In this work, it was shown in a 32 h simulation that the developed dynamic model of the hydroformylation mini-plant is capable of predicting the concentrations within the measurement error range. Based on this successful application, striving for optimization of the process using this model is a valid target.

- *Development of operation trajectories under uncertainty:* Lastly, and most importantly, the model is used to determine operation trajectories for the plant. Initially, this is done deterministically in gPROMS to test the applicability of the model for optimization purposes. Due to the design of the model equations as discussed in the in the mentioned optimization model development workflow, the optimization problems are solved rapidly. Afterwards, optimization under uncertainty is carried out using

the chance-constrained optimization approach. Again, the solution of the problems can be found in an adequate time frame for real-time optimization. This is done repeatedly using experimental data points, thus showing the functionality of repeated optimization and simulation. The validity of the determined operation trajectories becomes obvious when these are compared with actual set-points of a final mini-plant operation.

The advancements presented in this thesis are presented both from a theoretical as well as practical point of view. They can thus be transferred to other systems, so that efforts for optimization under uncertainty can be assisted, the utilization of the chance-constrained optimization approach can be propagated, and the development of surfactant based multiphase systems can be improved.

7.2. Outlook and Future Work

The outlook focuses on three parts: enhancements of the current framework, improvements regarding the process concept of hydroformylation in microemulsions, and improvements regarding model development for oil-water-surfactant systems.

Enhancements of the Framework: The focus of this thesis was to develop operation trajectories for a chemical plant with the chance-constrained optimization approach. Essential preceding steps, such as data reconciliation or model-adjustment via parameter estimation, which may improve the optimization process were neglected. For online-optimization of any larger chemical plant however, there is always a mismatch between model and reality. Additionally, data coming from the chemical plant may be prone to errors or failures of measurements. Therefore, it is necessary that the data is validated before it is sent to the model of the plant. Secondly, to reduce the mismatch between model and plant, the current model can be enhanced with adjustable parameters that can be fitted according to the measurement data. Fig. 7.1 highlights the position of the data reconciliation and model update steps in the online-optimization framework.

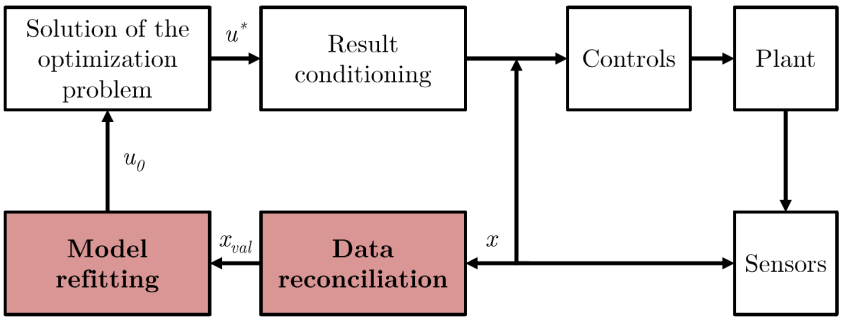

Figure 7.1.: General model-based RTO loop highlighting data reconciliation and model update steps. The figure is adapted from (Forbes et al., 1994).

For the hydroformylation process specifically, an idea to achieve the model update is to use the introduced reduction factors of the catalyst mass, C_1 and C_2, to fit the outcome of the reactions:

$$m_{cat,true} = m_{cat} \cdot C_1 \cdot (1 - (w_{u=9,i=5} + w_{u=9,i=3}))^{C_2} \tag{7.1}$$

Hereby, data points from the past hours of operation including the resulting concentrations can be used to update the model regarding the reaction efficiency via Eq. 7.1. This has proven to be useful during the simulation of the mini-plant operation. Of course the amount of required data points and the time interval in which the data points are fitted must be decided upon.

Secondly, an improvement on the platform side can be carried out. The chance-constrained optimization problem is solved on a 16 core machine. Obviously, for the employed sparse grid with 32 grid points, a machine with more cores could solve the problem faster (approx. 2 times as fast). This would make a noteworthy difference, if reinitialization or recalculation is required.

Improvements for the Process Concept: The success of the process concept depends on several aspects. Among these are the reaction yield during the reaction and the catalyst leaching during the product separation. Improvements can be made both on the substance as well as the process side of the concept.

The identification of an ideal surfactant is crucial for the success of the process concept. The currently used surfactant consists of a multitude of components. This increases the difficulty on all research fronts such as reaction kinetic experiments, general phase separation modeling, process optimization, and mini-plant operation. During the mini-plant operation, effects such as separation of the surfactant into more hydrophilic and more hydrophobic components during the phase separation step was observed (Müller et al., 2013a). This leads to an undesired shift of the optimal operating point. In general, a concentration shift takes place, thus rendering the phase separation model invalid and enhancing plant model mismatch. Possible counter measures for this observation are listed below:

1. A first counter measure would be to selectively feed the leached parts of the surfactant. Continuous surfactant feeding of the initial surfactant used in the beginning may cause an unwanted buildup of the hydrophilic compounds.

2. A second possibility is the switch of the surfactant to a one-component surfactant. In general, the surfactant must fulfill two requirements. First of all, the region or temperature interval in which the phase separation takes place must be large. Additionally, the phase separation must take place in an adequately short time frame. "The surfactant that was applied in the mini-plant run has a very small appropriate temperature interval. This is not ideal for a large, industrial scale process. An optimal surfactant should have a relatively large temperature interval of at least 10 K, within which the separation is fast. Secondly, the reaction must lead to high yields. Not all surfactants, that have ideal separation characteristics, provide satisfactory results during the reaction. The reaction should therefore be tested in each of the existing separation regions (lower 2 phase, 3 phase, and upper 2 phase region)" (Müller et al., 2013a). Thirdly, a surfactant which is prone to cause foaming in an oil-water system is also not desirable.

There is potential for improvement on the current process set-up of the mini-plant. Firstly, the concentration analysis of the components in the process can be enhanced. Raman spectroscopy has proven to be useful for 1-tridecanal and 1-dodecene. It is thinkable, that with multivariate curve resolution models, the concentrations of n-dodecane and the surfactant are also measureable. For this to be successful, more measurements and more reference data sets are required. Secondly, the current strategy to reduce the loss of rhodium in the product separation step can be improved. An idea is the addition of a membrane separation unit or

an extra extraction unit to the process. These ideas have already been proposed in contributions such as (Müller et al., 2013c), (Schwarze et al., 2015), and (Müller et al., 2012d). Nevertheless, the challenge remains of finding the right membrane-surfactant combination or the adequate extraction substance with the according purification and recycle steps.

Modeling Improvements of Oil-Water-Surfactant Systems: The currently implemented phase separation model is an empirical model valid only for the system at hand. The model describes the required temperature bounds for phase separation region, in which an oil and a mixed phase is established. During the optimization process, the settler's temperature is an output variable and not an optimization variable. The area within the two bounding functions T_{min} and T_{max} is insensitive for the optimization process. As long as $T_{settler}$ is within T_{min} and T_{max} any temperature can be set. There is no influence on the purity of the oil phase or the height of the oil phase. This is of course not accurate from a thermodynamic point of view. An equation of state for this liquid mixture would be desirable to actually predict concentrations and phase ratios. Thus, the results concerning the phase separation, the product isolation, and the catalyst loss in particular could be calculated more correctly. To develop this model additional experimental results are required, which examine the respective concentrations in the various phases.

Outlook Summary: With the improvements concerning data reconciliation and model update techniques a complete framework can be developed that takes uncertainty into account, removes measurement errors, and performs a model update to thus counter plant model mismatch. The framework can then help to increase the profitability and stability of model-assisted operation approaches. This framework should in future be tested on the industrial application discussed herein. Within this thesis the proof of concept for hydroformylation in microemulsions has been made. Hence, the target of developing new liquid-liquid multiphase processes promoting the application of new reactants from renewable resources has been achieved. Regarding hydroformylation in microemulsions, the rhodium losses in the mini-plant operation ranged below 0.1 ppm in the product stream, thus letting economic viability of the concept seem attainable. The challenge of a stable, maintainable phase separation still remains though. With the herein developed model and online-optimization scheme assisted with adequate concentration analysis techniques such as Raman spectroscopy this vision is turned into an achievable task, which can be carried out in the future.

Appendix A.

Supplementary Material

The appendix is divided into several chapters. Each chapter corresponds to the actual chapter in the thesis. This is done to ease the search for tables or figures from the respective chapters. In Appendix: Chapter 3 the experimental results concerning the ideal phase separation temperature at various concentrations are given. Additionally, the P&ID in A3 format can be found. In Appendix: Chapter 4 results concerning the parameter estimation of the reaction kinetics are presented. Secondly, the modeled upper and lower separation temperatures at various concentrations are shown. In Appendix: Chapter 5 the distribution of the liquid flow for the feed streams for a fixed set-point is displayed. In Appendix: Chapter 6 the model parameters, initial conditions, solver parameters, and additional results are given.

A.1. Appendix: Chapter 3

Table A.1.: Experimental results: lower and upper phase separation temperatures.

Composition			Inactive		Active		
α	γ	X	T_{min}	T_{max}	T_{min}	T_{max}	ΔT
40	6	0	81	85	84	90	3
40	8	0	74	79			
40	10	0	69	73			
40	6	20	79	86	84	91	5
40	8	20	68	72			
40	10	20	65	67	65	67	0
40	6	40	83	89	90	94	7
40	8	40	66	72			
40	10	40	62	64	62	64	0
50	6	0	84	88			
50	8	0	76	85	76	85	0
50	10	0	70	74			
50	6	20	79	85			
50	8	20	69	76			
50	10	20	63	68			
50	6	40	83	91			
50	8	40	68	73			
50	10	40	62	66			
60	6	0	88	92			
60	8	0	75	79	75	83	0
60	10	0	66	70			
60	6	20	85	91	91	94	6
60	8	20	73	77			
60	10	20	63	68	66	69	3
60	6	40	88	91	88	89	0
60	8	40	76	80			
60	10	40	63	69	63	71	0

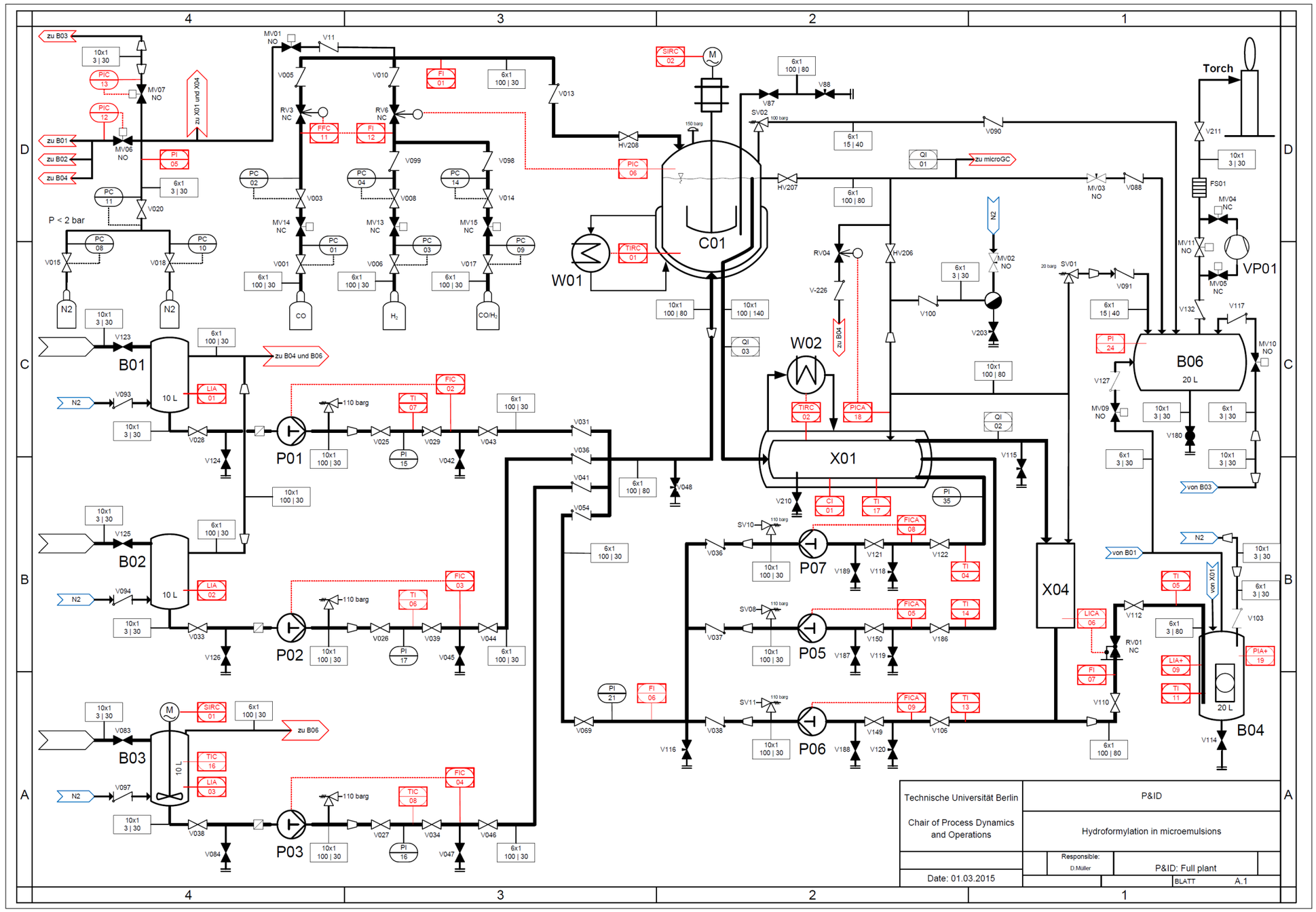

Figure A.1.: Hydroformylation mini-plant piping and instrumentation diagram.

A.2. Appendix: Chapter 4

Section 2: Reaction Section

Selected results from the parameter estimation are displayed in Fig. A.2 to Fig. A.5.

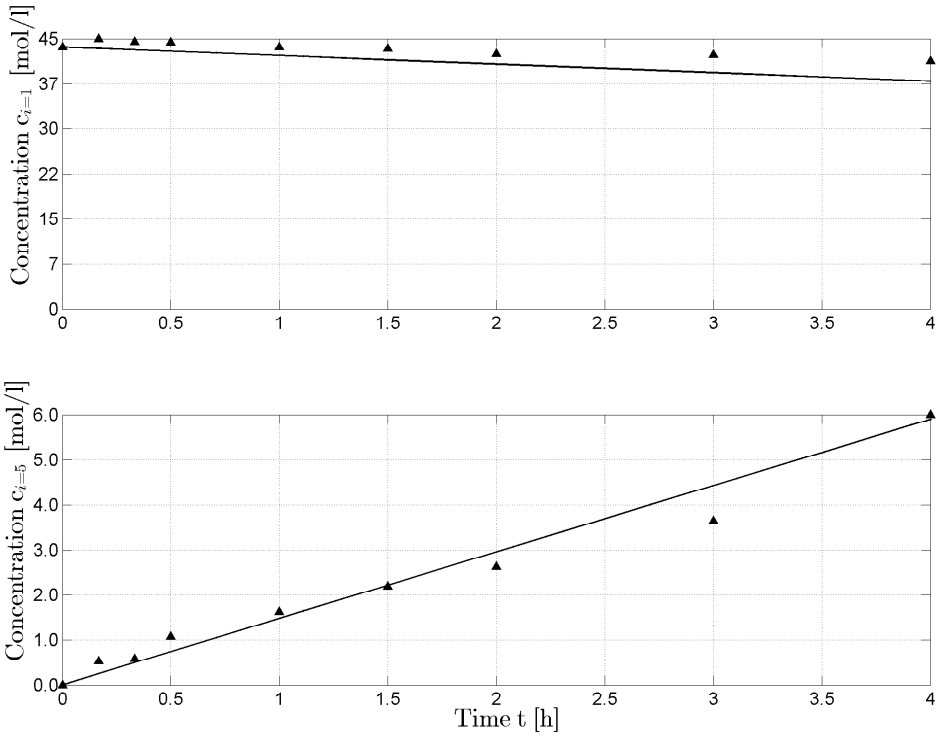

Figure A.2.: Parameter estimation result for 75 °C and 20 bar: main components.

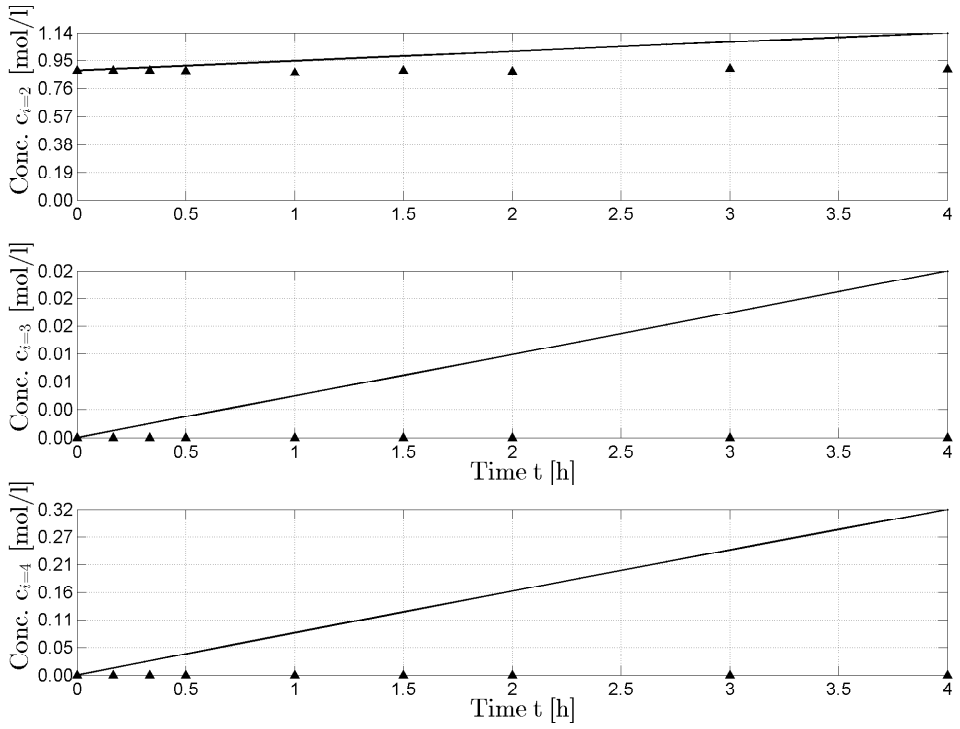

Figure A.3.: Parameter estimation result for 75 °C and 20 bar: byproducts.

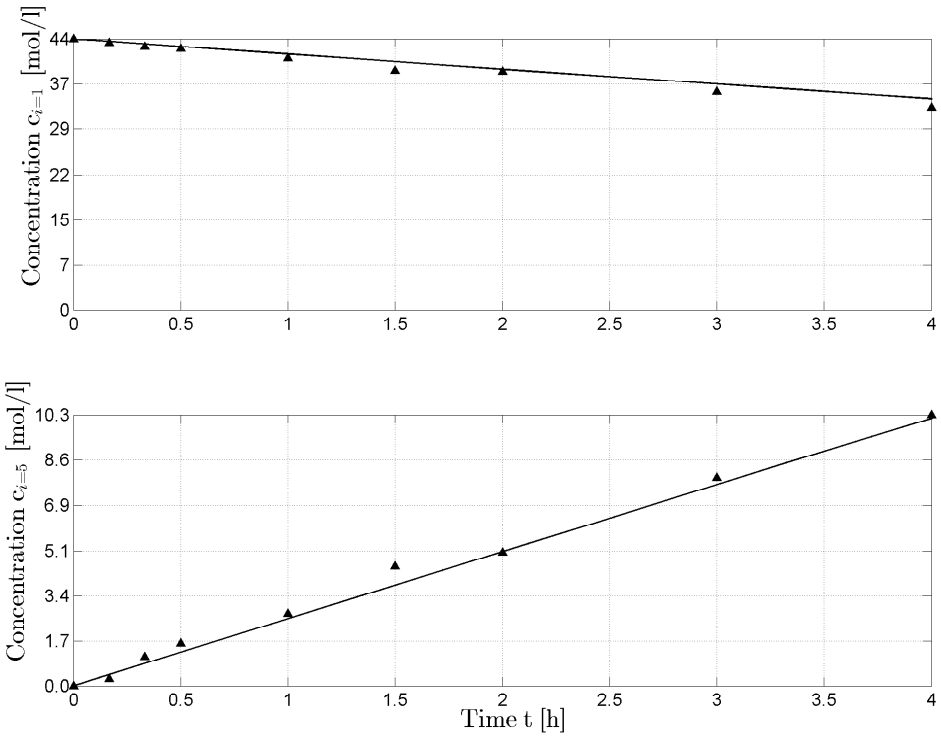

Figure A.4.: Parameter estimation result for 95 °C and 30 bar: main components.

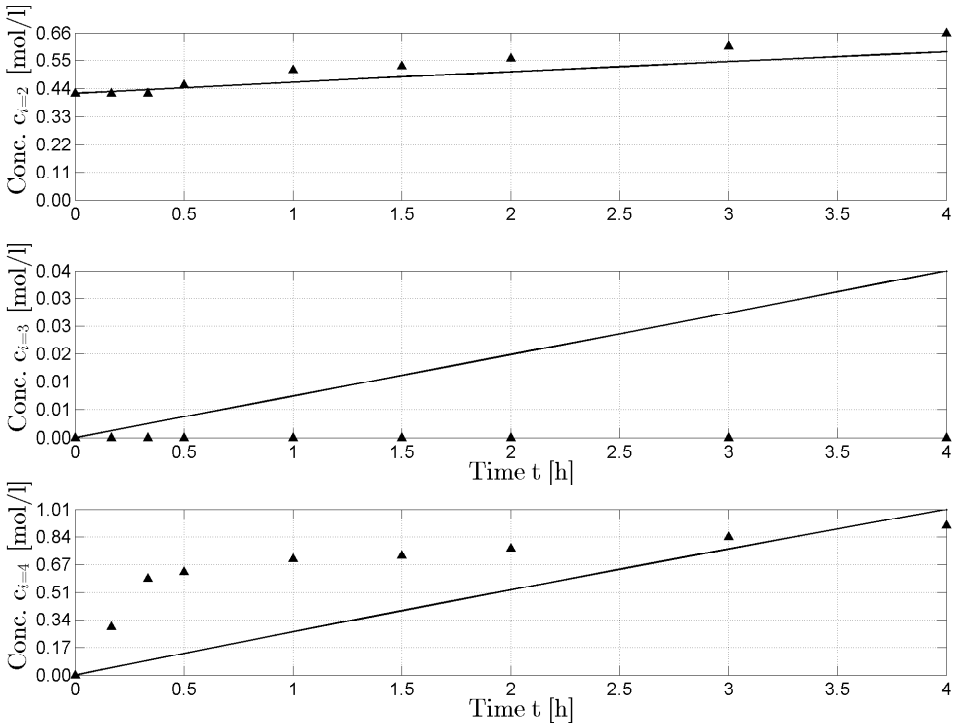

Figure A.5.: Parameter estimation result for 95 °C and 30 bar: byproducts.

Section 3: Separation Section

The full mapping of the phase separation results for the lower and upper temperature bounds can be found in the following three figures.

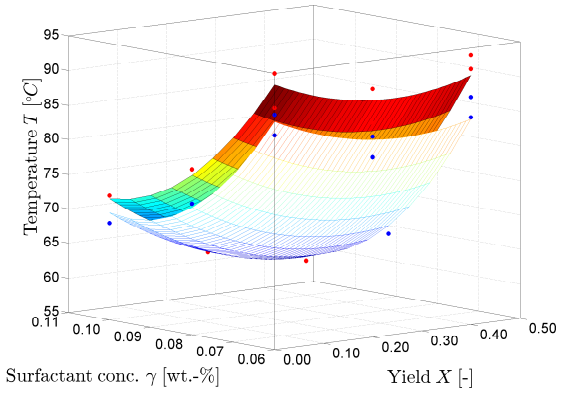

(a) $\alpha = 40$ %.

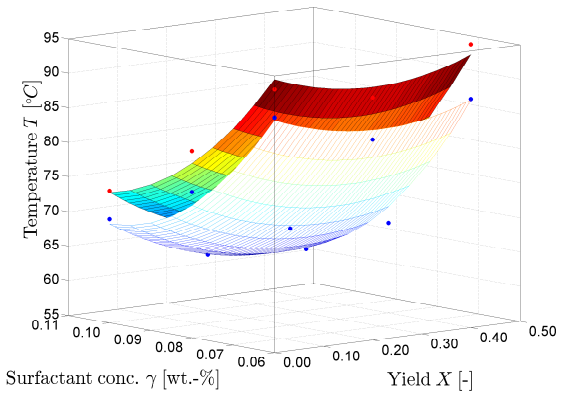

(b) $\alpha = 50$ %.

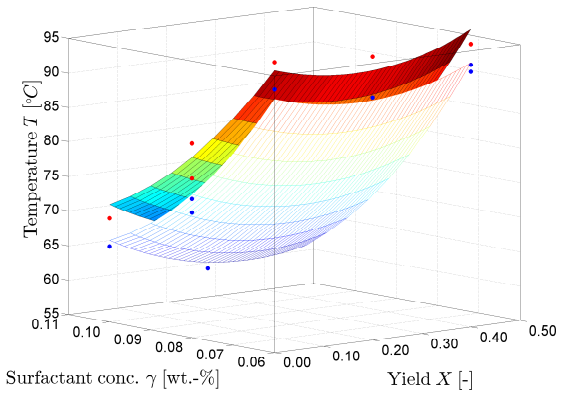

(c) $\alpha = 60$ %.

Figure A.6.: Model for lower and upper temperature bound for constant α values.

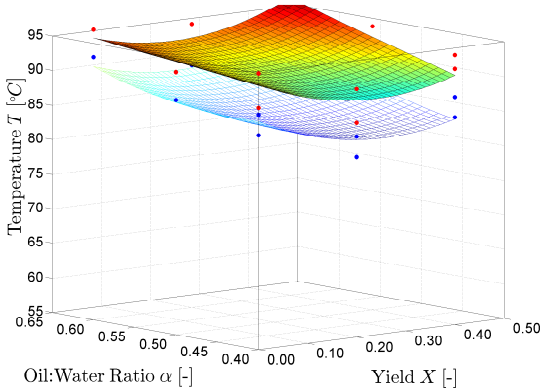

(a) $\gamma = 6$ %.

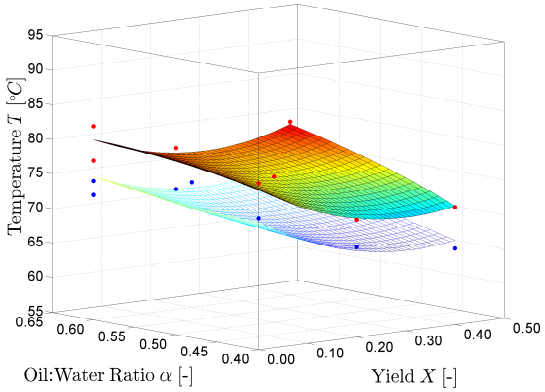

(b) $\gamma = 8$ %.

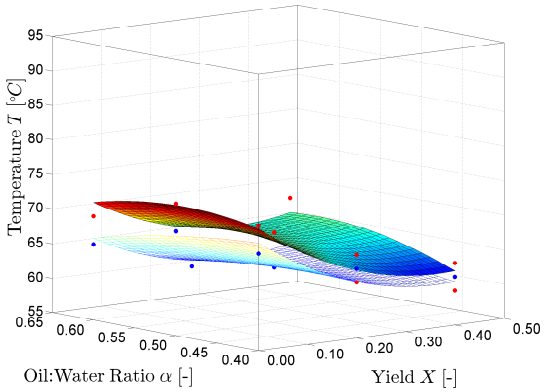

(c) $\gamma = 10$ %.

Figure A.7.: Model for lower and upper temperature bound for constant γ values.

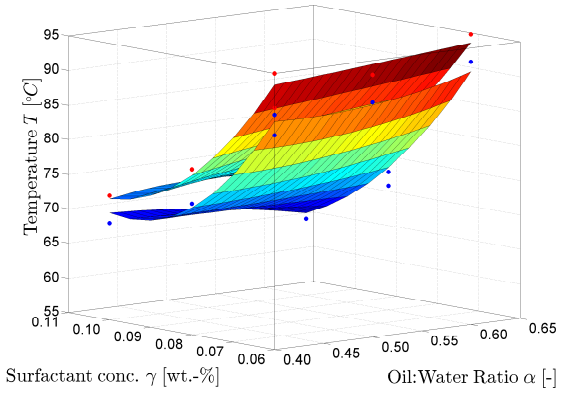

(a) $X = 0$ %.

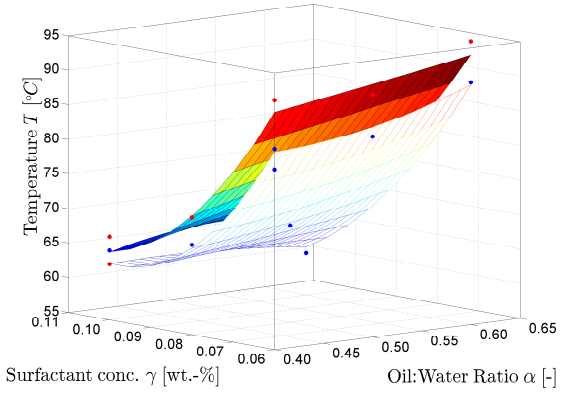

(b) $X = 20$ %.

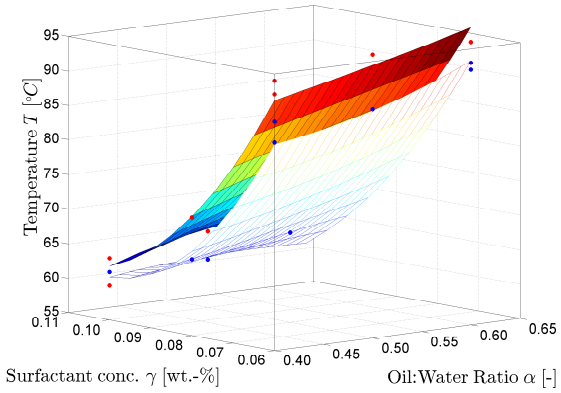

(c) $X = 40$ %.

Figure A.8.: Model for lower and upper temperature bound for constant X values.

A.3. Appendix: Chapter 5

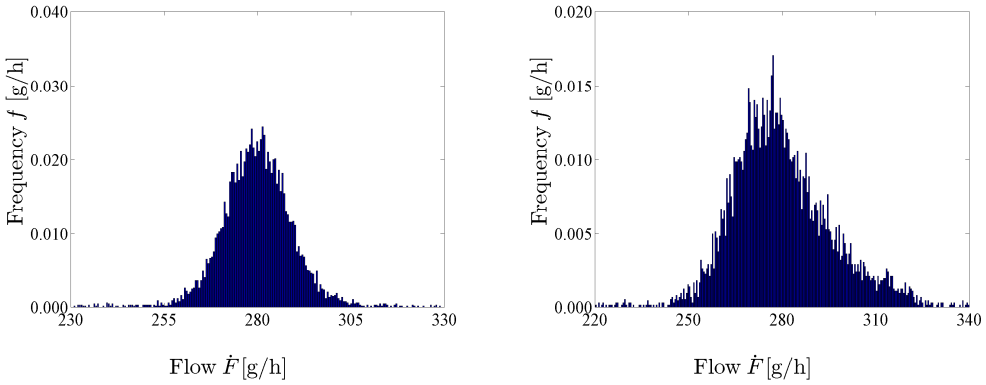

(a) Alkene feed pump

(b) Catalyst feed pump

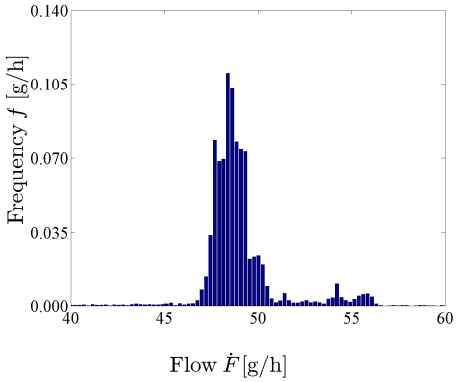

(c) Surfactant feed pump

Figure A.9.: Variance of feed stream values for a constant operating point.

A.4. Appendix: Chapter 6

In the following, several tables are presented, which contain vital information for the simulations and for the optimization studies. The first is Tab. A.2, in which the mass fractions of the feed streams is visible. The parameters used in gPROMS during the simulation of the model are shown in Tab. A.3. The solution parameters used in gPROMS are shown in Tab. A.6, those used for IPOPT are shown in Tab. A.7, and those used for the NLPQLP are shown in Tab. A.8. The starting values used for the start-up optimization are shown in Tab. A.9.

Table A.2.: Mass fractions of concentrations in feed tanks

Alkene [g/g]		Catalyst [g/g]		Surfactant [g/g]	
$w_{s=1,i=2}$	0	$w_{s=2,i=2}$	0	$w_{s=3,i=2}$	0
$w_{s=1,i=3}$	0	$w_{s=2,i=3}$	0	$w_{s=3,i=3}$	0
$w_{s=1,i=4}$	0	$w_{s=2,i=4}$	0	$w_{s=3,i=4}$	0
$w_{s=1,i=5}$	0	$w_{s=2,i=5}$	0	$w_{s=3,i=5}$	0
$w_{s=1,i=6}$	0	$w_{s=2,i=6}$	0	$w_{s=3,i=6}$	0
$w_{s=1,i=7}$	0	$w_{s=2,i=7}$	0	$w_{s=3,i=7}$	0
$w_{s=1,i=8}$	0	$w_{s=2,i=8}$	0	$w_{s=3,i=8}$	0
$w_{s=1,i=9}$	0	$w_{s=2,i=9}$	0.98943	$w_{s=3,i=9}$	0
$w_{s=1,i=10}$	0	$w_{s=2,i=10}$	0.000648	$w_{s=3,i=10}$	0
$w_{s=1,i=11}$	0	$w_{s=2,i=11}$	0.009922	$w_{s=3,i=11}$	0
$w_{s=1,i=12}$	0	$w_{s=2,i=12}$	0	$w_{s=3,i=12}$	1

Table A.3.: Model parameters - 1

Density [kg/m^3]		Molar mass [g/mol]		Gas solubility parameters [-]		Gas solubility parameters [-]	
$\rho_{i=1}$	760	$M_{i=1}$	168.32	$Ho_{i=7,Sol=1}$	297.61	$Ho_{i=6,Sol=1}$	2221.27
$\rho_{i=2}$	760	$M_{i=2}$	168.32	$Ht1_{i=7,Sol=1}$	41.36	$Ht1_{i=6,Sol=1}$	96.56
$\rho_{i=3}$	835	$M_{i=3}$	198.34	$Ht2_{i=7,Sol=1}$	-0.07	$Ht2_{i=6,Sol=1}$	-0.21
$\rho_{i=4}$	703	$M_{i=4}$	170.33	$Ho_{i=7,Sol=2}$	171.85	$Ho_{i=6,Sol=2}$	55975.54
$\rho_{i=5}$	835	$M_{i=5}$	198.34	$Ht1_{i=7,Sol=2}$	51.66	$Ht1_{i=6,Sol=2}$	-200.44
$\rho_{i=6}$	1	$M_{i=6}$	2.02	$Ht2_{i=7,Sol=2}$	-0.09	$Ht2_{i=6,Sol=2}$	0.22
$\rho_{i=8}$	18	$M_{i=7}$	28.01	$Ho_{i=7,Sol=3}$	-792.90	$Ho_{i=6,Sol=3}$	-667.05
$\rho_{i=7}$	18	$M_{i=8}$	28.01	$Ht1_{i=7,Sol=3}$	8.37	$Ht1_{i=6,Sol=3}$	13.32
$\rho_{i=9}$	969	$M_{i=9}$	18.02	$Ht2_{i=7,Sol=3}$	-0.01	$Ht2_{i=6,Sol=3}$	-0.02
$\rho_{i=10}$	969	$M_{i=10}$	258.03	$Ho_{i=7,Sol=4}$	-273312.54	$Ho_{i=6,Sol=4}$	-544626.03
$\rho_{i=11}$	969	$M_{i=11}$	784.71	$Ht1_{i=7,Sol=4}$	1905.85	$Ht1_{i=6,Sol=4}$	3761.93
$\rho_{i=12}$	960	$M_{i=12}$	513.00	$Ht2_{i=7,Sol=4}$	-2.62	$Ht2_{i=6,Sol=4}$	-5.68

Table A.4.: Model parameters - 2

Area [dm^2]		Flow [g/h]		Trigger function parameter [-]	
$A_{u=1}$	3.766848	$F^{SP}_{s=4}$	30	ϵ_{Kin}	1.00E-08
$A_{u=2}$	3.766848	$F^{SP}_{s=5}$	0	$\epsilon_{u=9}$	1.00E-11
$A_{u=3}$	3.766848	$F^{SP}_{s=6}$	0	$\epsilon_{u=11}$	1.00E-09
$A_{u=9}$	0.5541769	$F^{Conti}_{s=9}$	20	$\epsilon_{u=12}$	1.00E-09
$A_{u=14}$	0.16666667	$F^{Conti}_{s=15}$	1000	$\epsilon_{u=13}$	1.00E-09
$A_{u=20}$	5.5401664	$F^{SP}_{s=25}$	500	$\epsilon_{u=14}$	1.00E-08

Table A.5.: Model parameters - 3

Phase sep. parameters [-]		Phase sep. parameters [-]		Flow parameters [-]	
$P^{T_{max}}_{ps=1}$	177.34167	$P^{T_{min}}_{ps=1}$	236.49294	$KP_{u=8}$	2000
$P^{T_{max}}_{ps=2}$	-99.658455	$P^{T_{min}}_{ps=2}$	-304.19388	$KP_{u=9}$	200
$P^{T_{max}}_{ps=3}$	33.39854	$P^{T_{min}}_{ps=3}$	212.28723	$KP_{u=12}$	0
$P^{T_{max}}_{ps=4}$	-2199.9321	$P^{T_{min}}_{ps=4}$	-2990.6033	$KP_{u=14}$	0
$P^{T_{max}}_{ps=5}$	8247.481	$P^{T_{min}}_{ps=5}$	12379.95	Settler volume parameters	
$P^{T_{max}}_{ps=6}$	-24.638256	$P^{T_{min}}_{ps=6}$	-34.087173	[-]	
$P^{T_{max}}_{ps=7}$	68.139656	$P^{T_{min}}_{ps=7}$	70.07212	Pl3	0.52339786
$P^{T_{max}}_{ps=8}$	2382.4487	$P^{T_{min}}_{ps=8}$	3525.664	Pl1	0.8437006
$P^{T_{max}}_{ps=9}$	56.23059	$P^{T_{min}}_{ps=9}$	56.694252	Pl2	-0.8360981
$P^{T_{max}}_{ps=10}$	-487.20267	$P^{T_{min}}_{ps=10}$	-396.09802		
$P^{T_{max}}_{ps=11}$	-17546.555	$P^{T_{min}}_{ps=11}$	-27660.4		

Table A.6.: Solver options chosen for the optimization in gPROMS v.3.6.0

Option	Default Value	Applied Value
`DOSolver`	`CVP_SS`	`CVP_SS`
`DASolver`	`DASOLV`	`DASOLV`
`AbsoluteTolerance`	`1e-012`	`1e-014`
`EventTolerance`	`1e-005`	`1e-005`
`RelativeTolerance`	`1e-005`	`1e-005`

Table A.7.: Solver options chosen for the optimization with IPOPT

Option	Applied Value
warm_start_init_point	yes
linear_solver	ma57
ma57_pivot_order	4
ma57_automatic_scaling	yes
mu_init	1e-3
mu_strategy	adaptive
mu_min	1e-15
mu_max	1e-2
mu_oracle	loqo
warm_start_mult_bound_push	1e-3
warm_start_bound_push	1e-3
max_iter	1e5
constr_viol_tol	1e-7
acceptable_constr_viol_tol	1e-6
tol	1e-6

Table A.8.: Solver options chosen for the optimization with NLPQLP

Option	Applied Value
acc	1e-5
accqp	1e-8
stpmin	0
maxfun	50
maxit	1e3
maxnm	25
rho	1e0
mode	0

Table A.9.: Starting values for the start-up optimization.

Hold-up	[g]	Hold-up	[g]	Hold-up	[g]
$HU_{i=1}^{Reactor}$	0.46	$HU_{u=12,i=1}^{L}$	1.0	$HU_{u=13,i=1}^{L}$	0.0
$HU_{i=2}^{Reactor}$	0.0	$HU_{u=12,i=2}^{L}$	0.0	$HU_{u=13,i=2}^{L}$	0.0
$HU_{i=3}^{Reactor}$	0.0	$HU_{u=12,i=3}^{L}$	0.0	$HU_{u=13,i=3}^{L}$	0.0
$HU_{i=4}^{Reactor}$	0.0	$HU_{u=12,i=4}^{L}$	0.0	$HU_{u=13,i=4}^{L}$	0.0
$HU_{i=5}^{Reactor}$	0.0	$HU_{u=12,i=5}^{L}$	0.0	$HU_{u=13,i=5}^{L}$	0.0
$HU_{i=6}^{Reactor}$	1.0E-5	$HU_{u=12,i=6}^{L}$	0.0	$HU_{u=13,i=6}^{L}$	0.0
$HU_{i=7}^{Reactor}$	1.0E-5	$HU_{u=12,i=7}^{L}$	0.0	$HU_{u=13,i=7}^{L}$	0.0
$HU_{i=8}^{Reactor}$	1.41	$HU_{u=12,i=8}^{L}$	0.0	$HU_{u=13,i=8}^{L}$	0.0
$HU_{i=9}^{Reactor}$	0.46	$HU_{u=12,i=9}^{L}$	0.0	$HU_{u=13,i=9}^{L}$	1.0
$HU_{i=10}^{Reactor}$	0.0	$HU_{u=12,i=10}^{L}$	0.0	$HU_{u=13,i=10}^{L}$	0.0
$HU_{i=11}^{Reactor}$	0.0	$HU_{u=12,i=11}^{L}$	0.0	$HU_{u=13,i=11}^{L}$	0.0
$HU_{i=12}^{Reactor}$	0.08	$HU_{u=12,i=12}^{L}$	0.0	$HU_{u=13,i=12}^{L}$	0.0
$HU_{u=14,i=1}^{L}$	1.0	$HU_{u=20,i=1}^{L}$	1.0		
$HU_{u=14,i=2}^{L}$	0.0	$HU_{u=20,i=2}^{L}$	0.0		
$HU_{u=14,i=3}^{L}$	0.0	$HU_{u=20,i=3}^{L}$	0.0		
$HU_{u=14,i=4}^{L}$	0.0	$HU_{u=20,i=4}^{L}$	0.0		
$HU_{u=14,i=5}^{L}$	0.0	$HU_{u=20,i=5}^{L}$	0.0		
$HU_{u=14,i=6}^{L}$	0.0	$HU_{u=20,i=6}^{L}$	0.0		
$HU_{u=14,i=7}^{L}$	0.0	$HU_{u=20,i=7}^{L}$	0.0		
$HU_{u=14,i=8}^{L}$	0.0	$HU_{u=20,i=8}^{L}$	0.0		
$HU_{u=14,i=9}^{L}$	0.0	$HU_{u=20,i=9}^{L}$	0.0		
$HU_{u=14,i=10}^{L}$	0.0	$HU_{u=20,i=10}^{L}$	0.0		
$HU_{u=14,i=11}^{L}$	0.0	$HU_{u=20,i=11}^{L}$	0.0		
$HU_{u=14,i=12}^{L}$	0.0	$HU_{u=20,i=12}^{L}$	0.0		

The next set of important data are the used starting values for the repeated simulation and optimization from the final mini-plant operation. These can be seen in Tab. A.10. The table is then followed by a set of figures, in which a comparison between actually implemented controls during the mini-plant operation and controls determined as optimal in the chance-constrained optimization problem is made. The full set of determined controls can be seen in Tab. A.11 to Tab. A.14.

Table A.10.: Starting values for repeated simulation and optimization from mini-plant data in April 2015

Date:	21.04.	21.04.	21.04.	22.04.	22.04.	22.04.	22.04.	22.04.
Time:	14:00	18:00	22:00	01:00	05:00	09:00	14:00	18:00
$HU_{i=1}^{Reactor}$	232.0	230.1	265.00	494.18	370.69	344.11	300.51	278.21
$HU_{i=2}^{Reactor}$	12.0	18.0	12.00	36.81	30.02	26.80	23.37	29.59
$HU_{i=3}^{Reactor}$	0.5	0.0	0.50	1.14	0.86	1.07	0.93	1.22
$HU_{i=4}^{Reactor}$	10.0	6.9	10.00	14.72	13.44	13.44	11.44	21.87
$HU_{i=5}^{Reactor}$	85.0	64.8	51.00	97.55	77.61	90.26	81.76	83.90
$HU_{i=6}^{Reactor}$	0.3	0.3	0.25	0.25	0.25	0.25	0.25	0.25
$HU_{i=7}^{Reactor}$	3.5	3.5	3.53	3.53	3.53	3.53	3.53	3.53
$HU_{i=8}^{Reactor}$	0.0	0.0	0.00	0.00	0.00	0.00	0.00	0.00
$HU_{i=9}^{Reactor}$	305.0	305.0	305.00	305.00	305.00	305.00	305.00	305.00
$HU_{i=10}^{Reactor}$	0.2	0.2	0.20	0.21	0.21	0.21	0.21	0.20
$HU_{i=11}^{Reactor}$	3.2	3.2	3.16	3.16	3.16	3.16	3.16	3.16
$HU_{i=12}^{Reactor}$	63.0	63.0	63.00	63.00	63.00	63.00	63.00	63.00
$HU_{u=12.i=1}^{L}$	240.0	193.5	230.00	209.26	212.62	203.03	221.45	188.71
$HU_{u=12.i=2}^{L}$	14.9	15.8	14.90	17.39	15.43	15.96	17.48	16.90
$HU_{u=12.i=3}^{L}$	0.0	0.0	0.00	1.02	0.00	1.11	1.29	1.14
$HU_{u=12.i=4}^{L}$	6.0	6.6	6.00	7.78	7.60	7.78	8.59	7.57
$HU_{u=12.i=5}^{L}$	31.4	46.2	41.40	46.62	44.05	54.46	62.85	55.74
$HU_{u=12.i=6-12}^{L}$	0.0	0.0	0.00	0.00	0.00	0.00	0.00	0.00
$HU_{u=13.i=1}^{L}$	60.0	60.0	60.00	60.00	60.00	60.00	60.00	100.00
$HU_{u=13.i=2}^{L}$	5.0	5.0	5.00	5.00	5.00	5.00	5.00	5.00
$HU_{u=13.i=5}^{L}$	5.0	5.0	5.00	5.00	5.00	5.00	5.00	5.00
$HU_{u=13.i=3.4.6-8}^{L}$	0.0	0.0	0.00	0.00	0.00	0.00	0.00	0.00
$HU_{u=13.i=9}^{L}$	400.0	400.0	400.00	400.00	400.00	400.00	400.00	360.00
$HU_{u=13.i=10}^{L}$	0.3	0.3	0.24	0.27	0.27	0.27	0.27	0.26
$HU_{u=13.i=11}^{L}$	3.9	3.9	3.91	3.91	3.91	3.91	3.91	3.91
$HU_{u=13.i=12}^{L}$	88.9	88.9	88.89	88.89	88.89	88.89	88.89	88.89
$HU_{u=14.i=1}^{L}$	155.0	129.7	128.37	112.87	114.68	130.51	145.44	131.79
$HU_{u=14.i=2}^{L}$	2.7	5.6	8.51	9.38	8.32	8.61	9.43	9.11
$HU_{u=14.i=3}^{L}$	0.0	0.0	0.00	0.55	0.00	0.60	0.69	0.62
$HU_{u=14.i=4}^{L}$	0.0	1.8	3.55	4.19	4.10	10.19	4.64	4.08
$HU_{u=14.i=5}^{L}$	0.0	12.5	5.90	25.15	23.76	10.37	0.90	0.07
$HU_{u=14.i=6-12}^{L}$	0.0	0.0	0.00	0.00	0.00	0.00	0.00	0.00

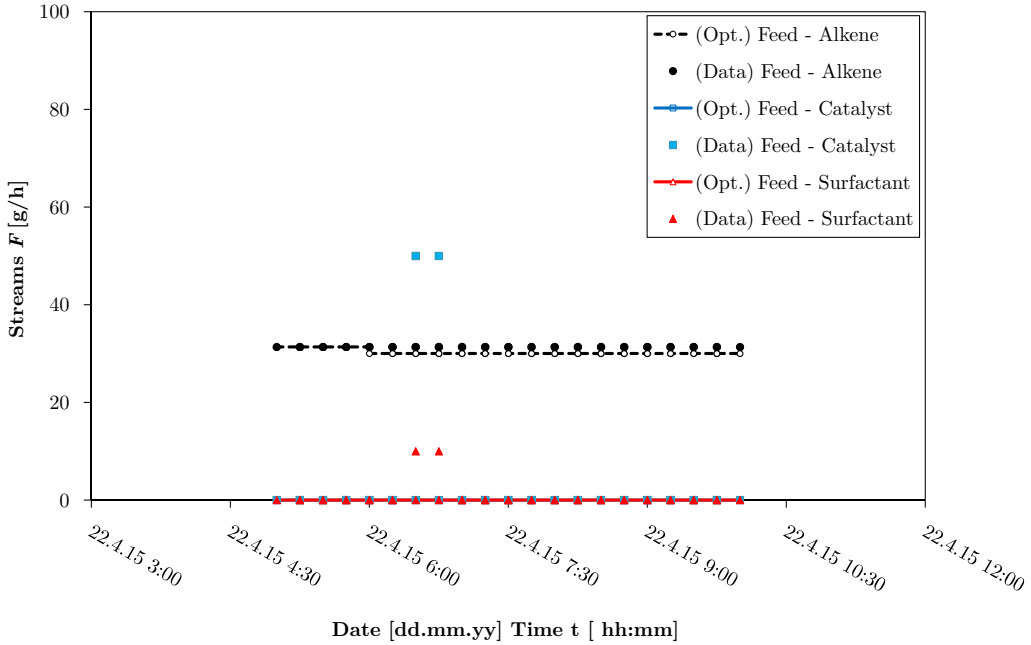

Figure A.10.: Comparison: determined optimization and implemented mini-plant controls for the feed streams for the 22.04.2015 at 05:00. It can be seen that the determined result for the alkene feed stream is almost identical to the actually implemented control. Except for a short refeeding of catalyst and surfactant in the actual operation (because samples had to be taken), the results are identical.

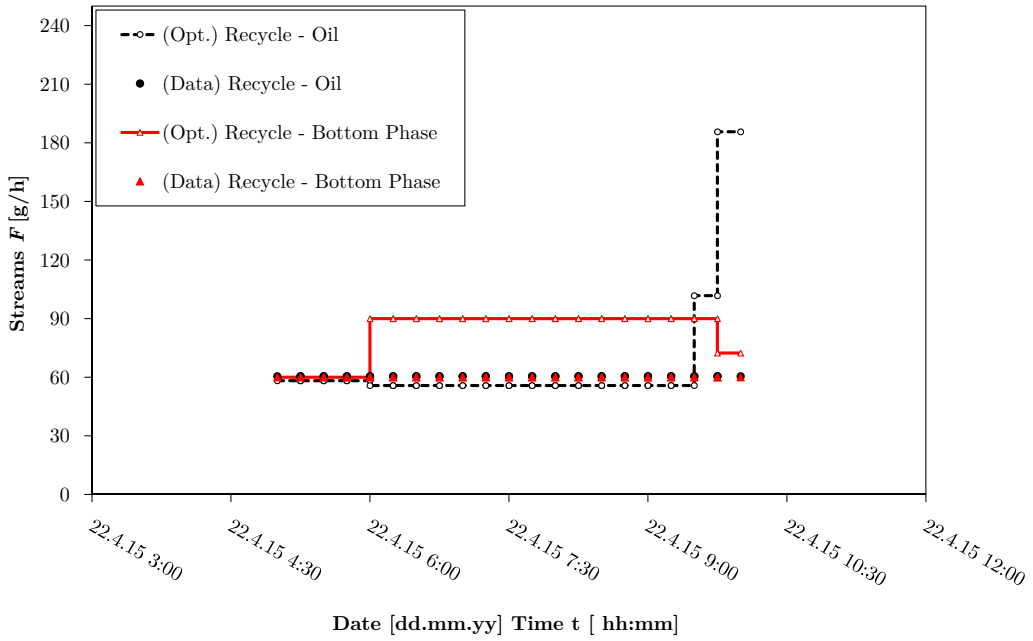

Figure A.11.: Comparison: determined optimization and implemented mini-plant controls for the recycle streams for the 22.04.2015 at 05:00. The difference between optimal and implemented controls for the oil recycle is marginal. At the end the optimizer determines a drastic increase in the recycle stream though, which is not implemented.

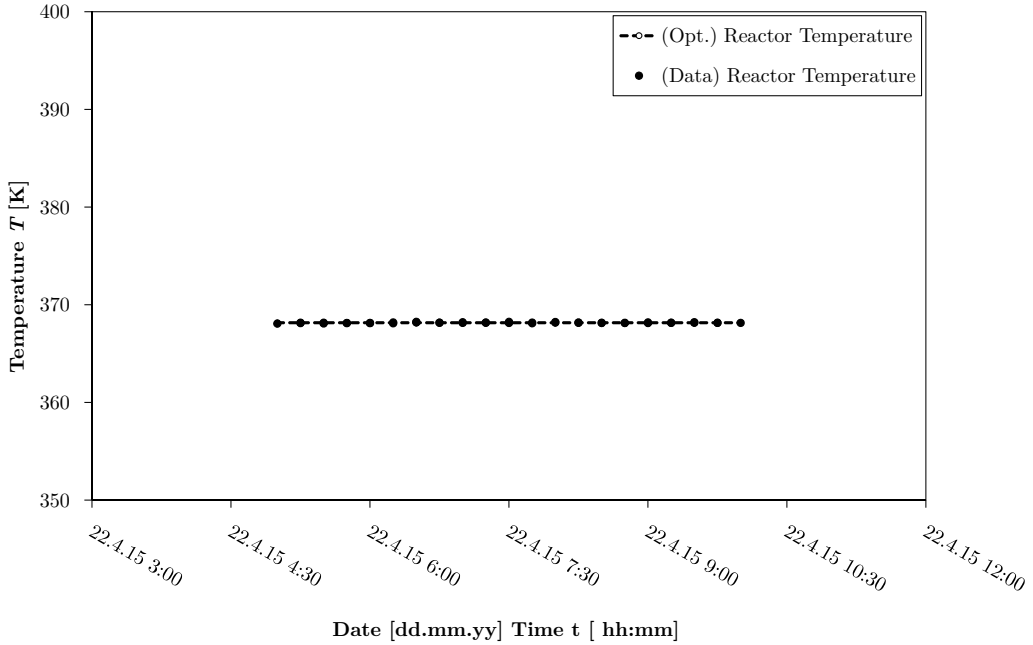

Figure A.12.: Comparison: determined optimization and implemented mini-plant controls for the reactor temperature for the 22.04.2015 at 05:00. No difference between implemented and determined controls is visible.

Table A.11.: Determined controls for the chance-constrained optimization of the final mini-plant operation on the 22.04.2015 at 05:00.

Time [hh:mm]	Time frame [h]	$F^{SP}_{s=4}$ [g/h]	$F^{SP}_{s=5}$ [g/h]	$F^{SP}_{s=6}$ [g/h]	$T_{u=9}$ [K]	$F^{SP}_{s=25}$ [g/h]	$\lambda_{u=15}$ [-]
05:00	0.00 - 0.25	31.35	0.01	0.01	368.15	60.00	0.65
05:15	0.25 - 0.50	31.35	0.01	0.01	368.15	60.00	0.65
05:30	0.50 - 0.75	31.35	0.01	0.01	368.15	60.00	0.65
05:45	0.75 - 1.00	31.35	0.01	0.01	368.15	60.00	0.65
06:00	1.00 - 1.25	30.00	0.01	0.01	368.15	89.99	0.65
06:15	1.25 - 1.50	30.00	0.01	0.01	368.15	89.99	0.65
06:30	1.50 - 1.75	30.00	0.01	0.01	368.15	89.99	0.65
06:45	1.75 - 2.00	30.00	0.01	0.01	368.15	89.99	0.65
07:00	2.00 - 2.25	30.00	0.01	0.01	368.15	89.99	0.65
07:15	2.25 - 2.50	30.00	0.01	0.01	368.15	89.99	0.65
07:30	2.50 - 2.75	30.00	0.01	0.01	368.15	89.99	0.65
07:45	2.75 - 3.00	30.00	0.01	0.01	368.15	89.99	0.65
08:00	3.00 - 3.25	30.01	0.01	0.01	368.15	89.99	0.65
08:15	3.25 - 3.50	30.01	0.01	0.01	368.15	89.98	0.65
08:30	3.50 - 3.75	30.01	0.01	0.01	368.15	89.98	0.65
08:45	3.75 - 4.00	30.01	0.01	0.01	368.15	89.98	0.65
09:00	4.00 - 4.25	30.01	0.01	0.01	368.15	89.98	0.65
09:15	4.25 - 4.50	30.03	0.01	0.01	368.15	89.98	0.65
09:30	4.50 - 4.75	54.79	0.01	0.01	368.15	89.97	0.65
09:45	4.75 - 5.00	99.97	0.01	0.01	368.15	89.97	0.65

Table A.12.: Determined controls for the chance-constrained optimization of the final mini-plant operation on the 22.04.2015 at 09:00.

Time [hh:mm]	Time frame [h]	$F^{SP}_{s=4}$ [g/h]	$F^{SP}_{s=5}$ [g/h]	$F^{SP}_{s=6}$ [g/h]	$T_{u=9}$ [K]	$F^{SP}_{s=25}$ [g/h]	$\lambda_{u=15}$ [-]
09:00	0.00 - 0.25	31.35	0.01	0.01	368.15	60.00	0.65
09:25	0.25 - 0.50	31.35	0.01	0.01	368.15	60.00	0.65
09:50	0.50 - 0.75	31.35	0.01	0.01	368.15	60.00	0.65
10:15	0.75 - 1.00	31.35	0.01	0.01	368.15	60.00	0.65
10:40	1.00 - 1.25	30.00	0.01	0.01	368.15	90.00	0.65
11:05	1.25 - 1.50	30.00	0.01	0.01	368.15	90.00	0.65
11:30	1.50 - 1.75	30.00	0.01	0.01	368.15	90.00	0.65
11:55	1.75 - 2.00	30.00	0.01	0.01	368.15	90.00	0.65
12:20	2.00 - 2.25	30.00	0.01	0.01	368.15	90.00	0.65
12:45	2.25 - 2.50	30.00	0.01	0.01	368.15	90.00	0.65
13:10	2.50 - 2.75	30.00	0.01	0.01	368.15	90.00	0.65
13:35	2.75 - 3.00	30.00	0.01	0.01	368.15	90.00	0.65
14:00	3.00 - 3.25	30.00	0.01	0.01	368.15	90.00	0.65
14:25	3.25 - 3.50	30.00	0.01	0.01	368.15	90.00	0.65
14:50	3.50 - 3.75	30.00	0.01	0.01	368.15	90.00	0.65
15:15	3.75 - 4.00	30.00	0.01	0.01	368.15	90.00	0.65
15:40	4.00 - 4.25	30.00	0.01	0.01	368.15	90.00	0.65
16:05	4.25 - 4.50	30.00	0.01	0.01	368.15	90.00	0.65
16:30	4.50 - 4.75	79.85	0.01	0.01	368.15	90.00	0.65
16:55	4.75 - 5.00	100.00	0.01	0.01	368.15	76.03	0.65

Table A.13.: Determined controls for the chance-constrained optimization of the final mini-plant operation on the 22.04.2015 at 14:00.

Time [hh:mm]	Time frame [h]	$F^{SP}_{s=4}$ [g/h]	$F^{SP}_{s=5}$ [g/h]	$F^{SP}_{s=6}$ [g/h]	$T_{u=9}$ [K]	$F^{SP}_{s=25}$ [g/h]	$\lambda_{u=15}$ [-]
14:00	0.00 - 0.25	31.35	0.01	0.01	368.15	60.00	0.65
14:15	0.25 - 0.50	31.35	0.01	0.01	368.15	60.00	0.65
14:30	0.50 - 0.75	31.35	0.01	0.01	368.15	60.00	0.65
14:45	0.75 - 1.00	31.35	0.01	0.01	368.15	60.00	0.65
15:00	1.00 - 1.25	30.00	0.01	0.01	368.15	89.99	0.65
15:15	1.25 - 1.50	30.00	0.01	0.01	368.15	89.99	0.65
15:30	1.50 - 1.75	30.00	0.01	0.01	368.15	89.99	0.65
15:45	1.75 - 2.00	30.00	0.01	0.01	368.15	89.99	0.65
16:00	2.00 - 2.25	30.00	0.01	0.01	368.15	89.99	0.65
16:15	2.25 - 2.50	30.00	0.01	0.01	368.15	89.99	0.65
16:30	2.50 - 2.75	30.01	0.01	0.01	368.15	89.99	0.65
16:45	2.75 - 3.00	30.01	0.01	0.01	368.15	89.98	0.65
17:00	3.00 - 3.25	30.01	0.01	0.01	368.15	89.98	0.65
17:15	3.25 - 3.50	30.01	0.01	0.01	368.15	89.98	0.65
17:30	3.50 - 3.75	30.01	0.01	0.01	368.15	89.98	0.65
17:45	3.75 - 4.00	30.02	0.01	0.01	368.15	89.97	0.65
18:00	4.00 - 4.25	31.89	0.01	0.01	368.15	89.96	0.65
18:15	4.25 - 4.50	99.96	0.01	0.01	368.15	89.90	0.65
18:30	4.50 - 4.75	99.99	0.01	0.01	368.15	80.70	0.65
18:45	4.75 - 5.00	99.99	0.01	0.01	368.15	60.19	0.65

Table A.14.: Determined controls for the chance-constrained optimization of the final mini-plant operation on the 22.04.2015 at 18:00.

Time [hh:mm]	Time frame [h]	$F^{SP}_{s=4}$ [g/h]	$F^{SP}_{s=5}$ [g/h]	$F^{SP}_{s=6}$ [g/h]	$T_{u=9}$ [K]	$F^{SP}_{s=25}$ [g/h]	$\lambda_{u=15}$ [-]
18:00	0.00 - 0.25	31.35	0.01	0.01	368.15	60.00	0.65
18:15	0.25 - 0.50	31.35	0.01	0.01	368.15	60.00	0.65
18:30	0.50 - 0.75	31.35	0.01	0.01	368.15	60.00	0.65
18:45	0.75 - 1.00	31.35	0.01	0.01	368.15	60.00	0.65
19:00	1.00 - 1.25	30.02	0.01	0.01	368.15	89.82	0.65
19:15	1.25 - 1.50	30.02	0.01	0.01	368.15	89.77	0.65
19:30	1.50 - 1.75	30.03	0.01	0.01	368.15	89.75	0.65
19:45	1.75 - 2.00	30.03	0.01	0.01	368.15	89.72	0.65
20:00	2.00 - 2.25	30.03	0.01	0.01	368.15	89.68	0.65
20:15	2.25 - 2.50	30.03	0.01	0.01	368.15	89.63	0.65
20:30	2.50 - 2.75	30.04	0.01	0.01	368.15	89.57	0.65
20:45	2.75 - 3.00	30.05	0.01	0.01	368.15	89.49	0.65
21:00	3.00 - 3.25	30.06	0.01	0.01	368.15	89.33	0.65
21:15	3.25 - 3.50	30.10	0.01	0.01	368.15	89.14	0.65
21:30	3.50 - 3.75	30.19	0.01	0.01	368.15	86.38	0.65
21:45	3.75 - 4.00	47.48	0.01	0.01	368.15	61.34	0.65
22:00	4.00 - 4.25	99.80	0.01	0.01	368.15	60.44	0.65
22:15	4.25 - 4.50	99.92	0.01	0.01	368.15	60.20	0.65
22:30	4.50 - 4.75	99.95	0.01	0.01	368.15	60.11	0.65
22:45	4.75 - 5.00	99.97	0.01	0.01	368.15	60.07	0.65

Bibliography

Albuquerque, J. S. and Biegler, L. T. (1996). Data reconciliation and gross-error detection for dynamic systems. *AIChE Journal*, 42(10):2841 – 2856.

Amarger, R., Biegler, L., and Grossmann, I. (1992). An automated modelling and reformulation system for design optimization. *Computers & Chemical Engineering*, 16(7):623 – 636. An International Journal of Computer Applications in Chemical Engineering.

Anderson, M. J. and Whitcomb, P. J. (2000). *DOE Simplified: Practical Tools for Effective Experimentation*, chapter 1, page 1. John Wiley & Sons, Inc.

Arellano-Garcia, H. (2006). *Chance constrained Optimization of Process Systems under Uncertainty*. PhD thesis, Technische Universität Berlin.

Arellano-Garcia, H., Martini, W., Wendt, M., Li, P., and Wozny, G. (2003a). Chance constrained batch distillation process optimization under uncertainty. In *Proceedings of the International Conference on Foundations of Computer-Aided Process Operations*, pages 609 – 612.

Arellano-Garcia, H., Martini, W., Wendt, M., and Wozny, G. (2003b). Nichtlineare stochastische Optimierung unter Unsicherheiten. *Chemie Ingenieur Technik*, 75:814 – 822.

Arellano-Garcia, H., Martini, W., Wendt, M., and Wozny, G. (2004). A new optimization framework for dynamic systems under uncertainty. In Barbosa, A. and Matos, H., editors, *European Symposium on Computer-Aided Process Engineering-14 37th European Symposium of the Working Party on Computer-Aided Process Engineering*, volume 18 of *Computer Aided Chemical Engineering*, pages 553 – 558. Elsevier.

Arellano-Garcia, H., Schöneberger, J., and Körkel, S. (2007a). Optimale Versuchsplanung in der chemischen Verfahrenstechnik. *Chemie Ingenieur Technik*, 79(10):1625 – 1638.

Arellano-Garcia, H., Wendt, M., Barz, T., and Wozny, G. (2007b). Close-loop stochastic dynamic optimization under probabilistic output-constraints. In Findeisen, R., Allgöwer, F., and Biegler, L. T., editors, *Assessment and Future Directions of Nonlinear Model Predictive Control*, volume 358 of *Lecture Notes in Control and Information Sciences*, pages 305 – 315. Springer Berlin Heidelberg.

Arellano-Garcia, H. and Wozny, G. (2009). Chance constrained optimization of process systems under uncertainty: I. strict monotonicity. *Computers and Chemical Engineering*, 33:1568 – 1583.

Arora, N. and Biegler, L. T. (2001). Redescending estimators for data reconciliation and parameter estimation. *Computers & Chemical Engineering*, 25(11):1585 – 1599.

Bard, Y. (1974). *Nonlinear Parameter Estimation*. Academic Press, New York.

Barz, T., Kuntsche, S., Wozny, G., and Arellano-Garcia, H. (2011). An efficient sparse approach to sensitivity generation for large-scale dynamic optimization. *Computers & Chemical Engineering*, 35(10):2053 – 2065.

Berger, R. (1986). Koaleszenzprobleme in chemischen Prozessen. *Chemie Ingenieur Technik*, 58(6):449 – 456.

Bhanage, B., Divekar, S., Deshpande, R., and Chaudhari, R. (1997). Kinetics of hydroformylation of 1-dodecene using homogeneous $HRh(CO)(PPh_3)_3$ catalyst. *Journal of Molecular Catalysis A: Chemical*, 115:247 – 257.

Binder, T. (2012). *Optimization under uncertainty: Robust Parameter Estimation with Erroneous Measurements and Uncertain Model Coefficients*. PhD thesis, Philipps-Universität Marburg.

Blaß, E. and Rommel, W. (1993). *VDI-Gesellschaft Verfahrenstechnik und Chemieingenieurwesen*, chapter Tropfenabscheidung in Flüssig-Flüssig-Systemen, pages 259 – 283. VDI-Verlag.

Bohnet, M. (1976). Trennen nicht mischbarer Flüssigkeiten. *Chemie Ingenieur Technik*, 48(3):177 – 189.

Brandt, H. W., Reissinger, K.-H., and Schröter, J. (1978). Moderne Flüssig/Flüssig-Extraktoren-Übersicht und Auswahlkriterien. *Chemie Ingenieur Technik*, 50(5):345 – 354.

Brun, R., Kühni, M., Siegrist, H., Gujer, W., and Reichert, P. (2002). Practical identifiability of {ASM2d} parameters – systematic selection and tuning of parameter subsets. *Water Research*, 36(16):4113 – 4127.

Brunsch, Y. and Behr, A. (2013). Temperature-controlled catalyst recycling in homogeneous transition-metal catalysis: Minimization of catalyst leaching. *Angewandte Chemie International Edition*, 52:1586 – 1589.

Burth, M., Verghese, G. C., and Velez-Reyes, M. (1999). Subset selection for improved parameter estimation in on-line identification of a synchronous generator. *Power Systems, IEEE Transactions on*, 14(1):218 – 225.

Chatterjee, M. R. (1998). *Dimensionierung liegender Flüssig-Flüssig-Abscheider mit Platteneinbauten*. PhD thesis, Rheinisch-Westfälische Technische Hochschule Aachen.

Cornils, B. (1980). *New Syntheses with Carbon Monoxide*. Springer.

Cornils, B., Hibbel, J., Konkol, W., Lieder, B., Much, J., Schmidt, V., and Wiebus, E. (1984). Verfahren zur Herstellung von Aldehyden. Patent: 3234701. Country: Germany.

Darby, M. L., Nikolaou, M., Jones, J., and Nicholson, D. (2011). RTO: An overview and assessment of current practice. *Journal of Process Control*, 21(6):874 – 884.

Davis, T. A. (2004). Algorithm 832: Umfpack v4.3 – an unsymmetric-pattern multifrontal method. *ACM Trans. Math. Softw.*, 30(2):196–199.

Diwekar, U. (2003). Optimization under uncertainty in chemical engineering. *Proc. Indian Nat. Sci. Acad.*, 69(3/4):267 – 283.

Diwekar, U. M. and Kalagnanam, J. R. (1997). Efficient sampling technique for optimization under uncertainty. *AIChE Journal*, 43(2):440 – 447.

Drown, D. C. and Thomson, W. J. (1977). Fluid mechanic considerations in liquid-liquid settlers. *Industrial & Engineering Chemistry Process Design and Development*, 16(2):197 – 206.

Dyer, M. and Stougie, L. (2006). Computational complexity of stochastic programming problems. *Math. Program.*, Ser. A 106:423 – 432.

Endress+Hauser (2015a). *Levelflex FMP50 Guided Level-Radar Level measurement in liquids*, ti01000f/00/en/13.11 edition. Technical Information.

Endress+Hauser (2015b). *Levelflex FMP51, FMP52, FMP54 Guided Level-Radar Level and interface measurement in liquids*, ti01001f/00/en/14.11 edition. Technical Information.

Esche, E. (2011). Optimal operation of a membrane reactor network. Master's thesis, Technische Universität Berlin.

Esche, E. (2015). *MINLP Optimization Under Uncertainty for the Oxidative of Coupling of Methane*. PhD thesis, Technische Universität Berlin. Submitted and accepted PhD Thesis.

Esche, E., Müller, D., Kraus, R., and Wozny, G. (2014a). Systematic approaches for model derivation for optimization purposes. *Chemical Engineering Science*, 115:215 – 224.

Esche, E., Müller, D., and Wozny, G. (2014b). Systematic modeling for optimization. In Eden, M. R., Siirola, J. D., and Towler, G. P., editors, *8th International Conference on Foundations of Computer-Aided Process Design (FOCAPD 2014)*, volume 34 of *Computer-Aided Chemical Engineering*, pages 699 – 704.

Esche, E. B., Müller, D. N., Song, S., and Wozny, G. (2013). Optimization of a membrane-absorption-hybrid system for the removal of CO_2 from OCM product gas. In Manan, Z. A., Hussain, M. A., and Zahedi, G., editors, *Proceedings of the 6th International Conference on Process systems Engineering (PSE ASIA 2013)*, pages 295 – 300.

Escobedo, F. A. (2000). Molecular and macroscopic modeling of phase separation. *AIChE Journal*, 46(10):2086 – 2096.

Exler, O. and Schittkowski, K. (2007). A trust region SQP algorithm for mixed-integer nonlinear programming. *Optimization Letters*, 1(3):269 – 280.

Faber, R., Arellano-Garcia, H., Li, P., and Wozny, G. (2007). An optimization framework for parameter estimation of large-scale systems. *Chemical Engineering and Processing: Process Intensification*, 46(11):1085 – 1095. Special Issue on Process Optimization and Control in Chemical Engineering and Processing.

Fiessler, B., Rackwitz, R., and Neumann, H. (1979). Quadratic limit states in structural reliability. *Journal of Engineering Mechanics*, 105:661 – 676.

Finanzen.net (2015). Goldpreis. `http://www.finanzen.net/rohstoffe/goldpreis/Chart`.

Finlayson, B. A. (1980). *Nonlinear Analysis in Chemical Engineering*. Mc-Graw-Hill International Book Company.

Flemming, T., Bartl, M., and Li, P. (2007). Set-point optimization for closed-loop control systems under uncertainty. *Industrial & Engineering Chemistry Research*, 46(14):4930 – 4942.

Forbes, J., Marlin, T., and MacGregor, J. (1994). Model adequacy requirements for optimizing plant operations. *Computers & Chemical Engineering*, 18(6):497 – 510. An International Journal of Computer Applications in Chemical Engineering.

Franke, R., Selent, D., and Börner, A. (2012). Applied hydroformylation. *Chemical Reviews*, 112(11):5675 – 5732.

Gao, W., Jr., R. L. R., and Gasem, K. A. M. (1999). High-pressure solubilities of hydrogen, nitrogen, and carbon monoxide in dodecane from 344 to 410 K at pressures to 13.2 MPa. *Journal of Chemical & Engineering Data*, 44:130 – 132.

Geletu, A., Hoffmann, A., Klöppel, M., and Li, P. (2011). Monotony analysis and sparse-grid integration for nonlinear chance constrained process optimization. *Engineering Optimization*, 43(10):1019 – 1041.

Geletu, A., Klöppel, M., Hoffmann, A., and Li, P. (2014). A tractable approximation of non-convex chance constrained optimization with non-gaussian uncertainties. *Engineering Optimization*, 47(4):495 – 520.

Geletu, A., Klöppel, M., Zhang, H., and Li, P. (2013). Advances and applications of chance-constrained approaches to systems optimisation under uncertainty. *International Journal of Systems Science*, 44(7):1209 – 1232.

Geletu, A. and Li, P. (2014). Recent developments in computational approaches to optimization under uncertainty and application in process systems engineering. *Chem. Bio. Eng. Reviews*, 1(4):170 – 190.

Ghanem, R. and Spanos, P. (2003). *Stochastic Finite Elements: A Spectral Approach*. Civil, Mechanical and Other Engineering Series. Dover Publications.

Goedheijt, M. S., Kamer, P. C., and van Leeuwen, P. W. (1998). A water-soluble diphosphine ligand with a large 'natural' bite angle for two-phase hydroformylation of alkenes. *Journal of Molecular Catalysis A: Chemical*, 134:243 – 249.

Grah, A. (2004). *Entwicklung und Anwendung modularer Software zur Simulation und Parameterschätzung in gaskatalytischen Festbettreaktoren*. PhD thesis, Martin-Luther-Universität Halle-Wittenberg.

Grötschel, M., Krumke, S. O., Rambau, J., Winter, T., and Zimmermann, U. (2001). Combinatorial online optimization in real time. Report. Konrad-Zuse-Zentrum für Informationstechnik Berlin.

Hamel, C., Markert, J., Kiedorf, G., Minh, D. H., Arellano-Garcia, H., Brunsch, Y., Behr, A., and Seidel-Morgenstern, A. (2012). Hydroformylierung von 1-Dodecen in einem thermomorphen Lösungsmittelsystem: Netzwerkanalyse und kinetische Modellierung. In *Jahrestreffen Reaktionstechnik 2012. Würzburg, Germany.*

Hamerla, T., Paul, N., Kraume, M., and Schomäcker, R. (2013a). Aufklärung der Stofftransportwege in mizellaren Mehrphasenreaktionen am Beispiel der Hydroformylierung. *Chemie Ingenieur Technik*, 85(10):1530 – 1539.

Hamerla, T., Rost, A., Kasaka, Y., and Schomäcker, R. (2013b). Hydroformylation of 1-Dodecene with Water-Soluble Rhodium Catalysts with Bidentate Ligands in Multiphase Systems. *ChemCatChem*, 5(7):1854 – 1862.

Hamerla, T., Schwarze, M., and Schomäcker, R. (2012). Katalyse in modifizierten Flüssig/flüssig- Mehrphasensystemen. *Chemie Ingenieur Technik*, 84:1861 – 1872.

Haumann, M., Koch, H., Hugo, P., and Schomäcker, R. (2002a). Hydroformylation of 1-dodecene using Rh-TPPTS in a microemulsion. *Applied Catalysis A: General*, 225:239 – 249.

Haumann, M., Yildiz, H., Koch, H., and Schomäcker, R. (2002b). Hydroformylation of 7-tetradecene using Rh-TPPTS in a microemulsion. *Applied Catalysis A: General*, 236:173 – 178.

Heitzig, M., Sin, G., Sales-Cruz, M., Glarborg, P., and Gani, R. (2011). Computer-aided modeling framework for efficient model development, analysis, and identification: Combustion and reactor modeling. *Industrial & Engineering Chemistry Research*, 50(9):5253 – 5265.

Henrion, R., Li, P., Möller, A., Steinbach, M. C., Wendt, M., and Wozny, G. (2001). Stochastic optimization for operating chemical processes under uncertainty. In Grötschel, M., Krumke, S., and Rambau, J., editors, *Online Optimization of Large Scale Systems*, pages 457–478. Springer Berlin Heidelberg.

Henrion, R. and Möller, A. (2003). Optimization of a continuous distillation process under random inflow rate. *Computers and Mathematics with Applications*, 43:247 – 262.

Henschke, M. (1994). *Dimensionierung Liegender Flüssig-Flüssig-Abscheider Anhand Diskontinuierlicher Absetzversuche*. PhD thesis, RWTH Aachen.

Henschke, M. and Hartmann, H. (1993). Auslegung kontinuierlich betriebener liegender Flüssig-Flüssig-Abscheider anhand diskontinuierlicher Absetzversuche. *Chemie Ingenieur Technik*, 65(9):1114 – 1114.

Henschke, M., Schlieper, L. H., and Pfennig, A. (2002). Determination of a coalescence parameter from batch-settling experiments. *Chemical Engineering Journal*, 85(2 - 3):369 – 378.

Herder, P., Verwater-Lukszo, Z., and Weijnen, M. (1997). How to define the quality of plant design and operation. In *Proceedings: ECCE-1, the First European Congress on Chemical Engineering*, volume 1, pages 671 – 680. Associazione Italiana di Ingegneria Chimica and European Federation of Chemical Engineering.

Hirasaki, G., Miller, C. A., and Puerto, M. (2011). Recent Advances in Surfactant EOR. *SPE Journal*, 16:889.

Homma, T. and Saltelli, A. (1996). Importance measures in global sensitivity analysis of nonlinear models. *Reliability Engineering & System Safety*, 52(1):1 – 17.

Ierapetritou, M., Acevedo, J., and Pistikopoulos, E. (1996). An optimization approach for process engineering problems under uncertainty. *Computers & Chemical Engineering*, 20:703 – 709. 5th International Symposium on Process Systems Engineering.

InPROMPT (2013). Collaborative research center/transregio 63: Integrated chemical processes in liquid multiphase systems (inprompt). `http://www.inprompt.tu-berlin.de/`.

Jalilova, N., Strathman, A. T. M., and Sama, S. (2008a). Optimizing the Azeri Field Asset. *World Oil*, 1:103 – 106.

Jalilova, N., Tautiyev, A., Forcadell, J., Rodriguez, J. C., and Sama, S. (2008b). Production optimization in an oil producing asset - the BP Azeri field optimizer case. In *SPE Gulf Coast Section 2008 Digital Energy Conference and Exhibition*, Houston, Texas.

Jeffreys, G. V., Davies, G. A., and Pitt, K. (1970). Rate of coalescence of the dispersed phase in a laboratory mixer settler unit: Part I. *AIChE Journal*, 16(5):823 – 827.

Jeffreys, G. V. and Dawies, G. A. (1974). *Neuere Fortschritte der Flüssig/Flüssig-Extraktion*, chapter Koaleszenz von Flüssigkeitströpchen und flüssigen Dispersionen. Sauerländer.

Kahlweit, M., LeSSner, E., and Strey, R. (1983). Über das Phasenverhalten ternärer Systeme des Typs H_2O - Öl - Nichtionisches Tensid. *Colloid & Polymer Science*, 261:954 – 964.

Kahlweit, M. and Strey, R. (1985). Phase behavior of ternary systems of the type H_2O - oil - nonionic amphiphile (microemulsions). *Angewandte Chemie International Edition*, 24:654 – 668.

Kamath, R. S., Biegler, L. T., and Grossmann, I. E. (2010). An equation-oriented approach for handling thermodynamics based on cubic equation of state in process optimization. *Computers & Chemical Engineering*, 34(12):2085 – 2096. 10th International Symposium on Process Systems Engineering, Salvador, Bahia, Brasil, 16-20 August 2009.

Kenkare, P. U. and Hall, C. K. (1996). Modeling of Phase Separation in PEG-Salt Aqueous Two-Phase Systems. *AIChE Journal*, 42(12):3508 – 3522.

Kiedorf, G., Hoang, D., Müller, A., Jörke, A., Markert, J., Arellano-Garcia, H., Seidel-Morgenstern, A., and Hamel, C. (2014). Kinetics of 1-dodecene hydroformylation in a thermomorphic solvent system using a rhodium-biphephos catalyst. *Chemical Engineering Science*, 115:31 – 48.

Klöppel, M., Geletu, A., Hoffmann, A., and Li, P. (2011). Using sparse-grid methods to improve computation efficiency in solving dynamic nonlinear chance-constrained optimization problems. *Industrial & Engineering Chemistry Research*, 50(9):5693 – 5704.

Kohlpaintner, C. W., Fischer, R. W., and Cornils, B. (2001). Aqueous biphasic catalysis: Ruhrchemie/Rhône-Poulenc oxo process. *Applied Catalysis A: General*, 221(1-2):219 – 225. Hoelderich Special Issue.

Krebs, T., Schröen, C., and Boom, R. (2012). Separation kinetics of an oil-in-water emulsion under enhanced gravity. *Chemical Engineering Science*, 71:118 – 125.

Kuntsche, S., Arellano-Garcia, H., and Wozny, G. (2009). Web-based object-oriented modeling environment for the simulation of chemical processes. In *Chemical Engineering Transactions*, volume 18, pages 779 – 784.

Kuntsche, S., Arellano-Garcia, H., and Wozny, G. (2010). A new modeling environment based on internet-standards XML and MathML. In *20th European Symposium on Computer Aided Process Engineering*.

Kuntsche, S., Barz, T., Kraus, R., Arellano-Garcia, H., and Wozny, G. (2011). MOSAIC a web-based modeling environment for code generation. *Computers & Chemical Engineering*, 35(11):2257 – 2273.

Kupka, J. (2006). *Hydroformylierung von 1-Octen in Mikroemulsion*. PhD thesis, Technische Universität Carolo-Wilhelmina zu Braunschweig.

Lee, S. and Chen, W. (2009). A comparative study of uncertainty propagation methods for black-box-type problems. *Structural and Multidisciplinary Optimization*, 37(3):239 – 253.

Li, P. (2007). *Prozessoptimierung unter Unsicherheiten*. Oldenbourg Wissenschaftsverlag.

Li, P., Arellano-Garcia, H., and Wozny, G. (2008). Chance constrained programming approach to process optimization under uncertainty. *Computers & Chemical Engineering*, 32:25 – 45.

Li, P., Wendt, M., Arellano-Garcia, H., and Wozny, G. (2002). Optimal operation of distillation processes under uncertain inflows accumulated in a feed tank. *AIChE Journal*, 48(6):1198 – 1211.

Li, P., Wendt, M., and Wozny, G. (2000). Robust model predictive control under chance constraints. *Computers & Chemical Engineering*, 24(2 - 7):829 – 834.

Li, P., Wendt, M., and Wozny, G. (2003). Optimale Produktionsplanung für verfahrenstechnische Prozess unter unsicheren Marktbedingungen. *Chemie Ingenieur Technik*, 75:832 – 842.

Li, P., Wendt, M., and Wozny, G. (2004). Optimal production planning for chemical processes under uncertain market conditions. *Chemical Engineering & Technology*, 27(6):641 – 651.

Lide, D. R. and Frederiksen, H. P. R. (1995). *CRC Handbook of Chemistry and Physics*. CRC Press, Inc., Boca Raton, FL, 76 edition.

Liu, H., Shah, S., and Jiang, W. (2004). On-line outlier detection and data cleaning. *Computers & Chemical Engineering*, 28:1635 – 1647.

López, D., Barz, T., Arellano-Garcia, H., Wozny, G., Villegas, A., and Ochoa, S. (2012). Subset selection for improved paramter identification in a bio-ethanol production process. In *Proceedings of the19th International Conference on Process Engineering and Chemical Plant Design*.

López C., D. C., Barz, T., Penuela, M., Villegas, A., Ochoa, S., and Wozny, G. (2013). Model-based identifiable parameter determination applied to a simultaneous saccharification and fermentation process model for bio-ethanol production. *Biotechnol. Prog.*, 29:1064 – 1082.

Madsen, H., Krenk, S., and Lind, N. (2006). *Methods of Structural Safety*. Dover Civil and Mechanical Engineering Series. Dover Publications.

Marquardt, W. (1996). Trends in computer-aided process modeling. *Computers and Chemical Engineering*, 20(6):591 – 609.

Matthey, J. (2015). Precious metals management: Prices. `http://www.platinum.matthey.com/prices/price-charts`.

Miyagawa, C. C., Kupka, J., and Schumpe, A. (2005). Rhodium-catalyzed hydroformylation of 1-octene in micro-emulsions and micellar media. *Journal of Molecular Catalysis A: Chemical*, 234:9 – 17.

Montgomery, D. C. (2013). *Design and analysis of experiments*. John Wiley & Sons, Inc., 8 edition.

Mungma, N., Chuttrakul, P., and Pfennig, A. (2014). Liquid-liquid phase separation in batch settling with inclined plate. In *Jurnal Teknologi UTM*, volume 67, pages 55 – 58. Penerbit UTM Press.

Murray, D. J. (1979). Equipment development in solvent extraction. *Journal of Chemical Technology and Biotechnology*, 29:367 – 378.

Müller, D., Esche, E., Hamerla, T., Rost, A., Kasaka, Y., Schomäcker, R., and Wozny, G. (2013a). Enabling hydroformylation in micro-emulsion systems: Long-term performance of a continuously operated mini-plant. In *Proceedings of the AIChE Annual Meeting, San Francisco, CA, Online Proceedings.* url: http://www3.aiche.org/proceedings/Abstract.aspx?PaperID=324238.

Müller, D., Esche, E., López C., D. C., and Wozny, G. (2014a). An algorithm for the identification and estimation of relevant parameters for optimization under uncertainty. *Computers & Chemical Engineering*, 71(0):94 – 103.

Müller, D., Esche, E., López C., D. C., and Wozny, G. (2014b). Systematic parameter selection for optimization under uncertainty. In Eden, M. R., Siirola, J. D., and Towler, G. P., editors, *8th International Conference on Foundations of Computer-Aided Process Design (FOCAPD 2014)*, volume 34 of *Computer-Aided Chemical Engineering*, pages 717 – 722.

Müller, D., Esche, E., Müller, M., and Wozny, G. (2012a). Development of a short-cut model for three-phase liquid separation dynamics for a hydroformylation mini-plant. In *Proceedings of the AIChE Annual Meeting, Pittsburgh, PA, Online Proceedings.*

Müller, D., Esche, E., Paul, A., Walter, K., Pogrzeba, T., Hamerla, T., Barz, T., Maiwald, M., Schomäcker, R., and Wozny, G. (2014c). Hydroformylation of long-chained alkenes in microemulsions: Raman-spectrometer assisted mini-plant operation. In *Proceedings of the 9th International Symposium on Catalysis in Multiphase Reactors.*

Müller, D., Esche, E., Pogrzeba, T., Hamerla, T., Barz, T., Schomäcker, R., and Wozny, G. (2014d). *Proceedings of the 20th International Conference on Process Engineering and Chemical Plant Design*, chapter Hydroformylation of 1-Dodecene in Microemulsions: Long-Term Mini-Plant Operation Results, pages 15 – 23. Technische Universität Berlin.

Müller, D., Esche, E., Pogrzeba, T., Illner, M., Leube, F., Schomäcker, R., and Wozny, G. (2015a). Systematic phase separation analysis of surfactant containing systems for multiphase settler design. *Industrial & Engineering Chemistry Research*, 54(12):3205 – 3217.

Müller, D., Esche, E., Werk, S., and Wozny, G. (2015b). Dynamic chance-constrained optimization under uncertainty on reduced parameter sets. In *12th International Symposium on Process Systems Engineering and 25th European Symposium on Computer Aided Process Engineering.*

Müller, D., Esche, E., and Wozny, G. (2013b). Phase Separation Engineering: Trajectories Through Model Regression for a Hydroformylation Mini-Plant. In *Proceedings of the 6th International Conference on Process Systems Engineering - PSE Asia 2013.* url: http://www.sps.utm.my/download/PSEAsia2013-14.pdf.

Müller, D., Höser, S., Kahrs, O., Arellano-Garcia, H., and Wozny, G. (2012b). Optimization of process operation strategies by combining process models with plant operating data.

In Varbanov, P. S., editor, *Chemical Engineering Transactions*, volume 29, pages 1495 – 1500.

Müller, D., Illner, M., Fleck, A., Esche, E., Barz, T., Schomäcker, R., and Wozny, G. (2014e). *Proceedings of the 20th International Conference on Process Engineering and Chemical Plant Design*, chapter Enabling Online-Optimization for a Multiphase System in a Hydroformylation Mini-plant, pages 25 – 36. Technische Universität Berlin.

Müller, D., Kahrs, O., Höser, S., and Arellano-Garcia, H. (2012c). Durchgängige Nutzung von Prozessmodellen während des Prozesslebenszyklus: ein industrielles Fallbeispiel. *Chemie Ingenieur Technik*, 84(11):1971 – 1979.

Müller, D., Minh, D. H., Merchan, V. A., Arellano-Garcia, H., Kasaka, Y., Müller, M., Schomäcker, R., and Wozny, G. (2014f). Towards a novel process concept for the hydroformylation of higher alkenes: Mini-plant operation strategies via model development and optimal experimental design. *Chemical Engineering Science*, 115:127 – 138.

Müller, D., Müller, M., Nguyen, L. A. T., Ludwig, J., Drews, A., Kraume, M., Schomäcker, R., and Wozny, G. (2012d). Development of separation methods for a continuous hydroformylation process in a mini-plant scale. In *Czasopismo Techniczne Mechanika*, volume 1-M, pages 165 – 174.

Müller, M., Kasaka, Y., Müller, D., Schomäcker, R., and Wozny, G. (2013c). Process design for the separation of three liquid phases for a continuous hydroformylation process in a miniplant scale. *Industrial & Engineering Chemistry Research*, 52(22):7259 – 7264.

Müller, M., Kasaka, Y., Müller, D., Wozny, G., and Schomäcker, R. (2012e). A continuous hydroformylation process in a miniplant scale: equipment design for the separation of three liquid phases. In *11th International Symposium on Process Systems Engineering - PSE2012*, volume 31 of *Computer-Aided Chemical Engineering*, pages 710 – 714.

NIST (2014a). National institute for standards and technology chemistry webbook: Carbon monoxide. `http://webbook.nist.gov/chemistry/`.

NIST (2014b). National institute for standards and technology chemistry webbook: Hydrogen. `http://webbook.nist.gov/chemistry/`.

Prékopa, A. (1995). *Stochastic Programming*. Kluwer Scientific Publishers, Dordrecht.

Quaglia, A., Sarup, B., Sin, G., and Gani, R. (2013). A systematic framework for enterprise-wide optimization: Synthesis and design of proprocess networks under uncertainty. *Computers & Chemical Engineering*, 59:47 – 62.

Ramdial, A., Hudson, N., Pike, R., Rodriguez, J., Stratman, M., and Sama, S. (2009). Model Based Optimisation of a Gas Production System: The Trinidad Field Optimiser. In *SPE Annual Technical Conference and Exhibition*. Society of Petroleum Engineers.

Rautenberg, D. (1983). *Koaleszenz von Einzeltropfen an geneigten Platten in Flüssigkeiten*. PhD thesis, Technische Universität München.

Reissinger, K.-H., Schröter, J., and Bäcker, W. (1981). Möglichkeiten und Probleme bei der Auslegung von Extraktoren. *Chemie Ingenieur Technik*, 53(8):607 – 614.

Rodrigues, A. E. and Minceva, M. (2005). Modelling and simulation in chemical engineering: Tools for process innovation. *Computers & Chemical Engineering*, 29(6):1167 – 1183.

Roelen, O. (1938). Verfahren zur Herstellung von sauerstoffhaltigen Verbindungen. Patent: DE849548. Country: Germany.

Roelen, O. (1943). Production of oxygenated carbon compounds. Patent: US2327066. Country: United States of America.

Rost, A. (2013). *Rhodium-katalysierte Hydroformylierung von 1-Dodecen mit zweizähnigen Liganden in Mikroemulsionssystemen*. PhD thesis, Technische Universität Berlin.

Rost, A., Müller, M., Hamerla, T., Kasaka, Y., Wozny, G., and Schomäcker, R. (2013). Development of a continuous process for the hydroformylation of long-chain olefins in aqueous multiphase systems. *Chemical Engineering and Processing: Process Intensification*, 67(0):130 – 135. Special issue: Hybrid and Reactive Separations.

Sarabia, D., de Prada, C., Gómez, E., Gutierrez, G., Cristea, S., Sola, J., and Gonzalez, R. (2012). Data reconciliation and optimal management of hydrogen networks in a petrol refinery. *Control Engineering Practice*, 20(4):343 – 354. Special Section: {IFAC} Symposium on Advanced Control of Chemical Processes - {ADCHEM} 2009.

Schlieper, L. (2001). *Trennung von Flüssig-Flüssig-Dispersionen in liegenden Abscheidern mit Platteneinbauten*. PhD thesis, Rheinisch-Westfälische Technische Hochschule Aachen.

Schlieper, L., Chatterjee, M., Henschke, M., and Pfennig, A. (2004). Liquid-liquid phase separation in gravity settler with inclined plates. *AIChE Journal*, 50:802 – 811.

Schulman, J. H. and Hoar, T. (1943). Transparent water-in-oil dispersion: The oleopathic hydromicell. *Nature*, 152:102.

Schulman, J. H., Stoeckenius, W., and Prince, L. (1959). Mechanism of formation and structure of micro emulsions by electron microscopy. *Journal of Physical Chemistry*, 63:1677 – 1680.

Schwarm, A. T. and Nikolaou, M. (2004). Chance-constrained model predictive control. *AIChE Journal*, 45(8):1743 – 1752.

Schwarze, M., Pogrzeba, T., Volovych, I., and Schomacker, R. (2015). Microemulsion systems for catalytic reactions and processes. *Catal. Sci. Technol.*, 5:24 – 33.

Seo, H. S. and Kwak, B. M. (2002). Efficient statistical tolerance analysis for general distributions using three-point information. *International Journal of Production Research*, 40(4):931 – 944.

Sottmann, T., Lade, M., Stolz, M., and Schomäcker, R. (2002). Phase behavior of nonionic microemulsions prepared from technical-grade surfactants. *Tenside, Surfactants, Detergents*, 39:20 – 28.

Stubenrauch, C. (2009). *Microemulsions Background, new Concepts, Applications, Perspectives*. John Wiley & Sons, Inc.

Tinucci, L. and Platone, E. (1991). Process for the catalytic hydroformylation of olefins. Patent: 4,996,355. Country: United States of America.

Verderame, P. M. and Floudas, C. A. (2009). Operational planning of large-scale industrial batch plants under demand due date and amount uncertainty. I. robust optimization framework. *Industrial & Engineering Chemistry Research*, 48(15):7214 – 7231.

Verderame, P. M. and Floudas, C. A. (2010). Operational planning of large-scale industrial batch plants under demand due date and amount uncertainty: II. conditional value-at-risk framework. *Industrial & Engineering Chemistry Research*, 49(1):260 – 275.

Vijayan, S. and Ponter, A. B. (1975). Drop/drop and drop/interface coalescence in primary liquid/liquid dispersion separators. *Chemie Ingenieur Technik*, 47(18):748 – 755.

Vogelpohl, C., Brandenbusch, C., and Sadowski, G. (2013). High-pressure gas solubility in multicomponent solvent systems for hydroformylation. Part I: carbon monoxide solubility. *Journal of Supercritical Fluids*, 81:23 – 32.

Vogelpohl, C., Brandenbusch, C., and Sadowski, G. (2014). High-pressure gas solubility in multicomponent solvent systems for hydroformylation. part ii: Syngas solubility. *The Journal of Supercritical Fluids*, 88(0):74 – 84.

Weber, K. (2006). *Inbetriebnahme verfahrenstechnischer Anlagen: Praxishandbuch mit Checklisten und Beispielen*. VDI-Buch. Springer.

Wendt, M. (2005). *Untersuchungen zur stochastischen Online Optimierung kontinuierlicher Destillationsprozesse unter Unsicherheiten*. PhD thesis, Technische Universität Berlin.

Wendt, M., Li, P., and Wozny, G. (2002). Nonlinear chance-constrained process optimization under uncertainty. *Industrial & Engineering Chemistry Research*, 41:3621 – 3629.

Werk, S., Barz, T., Wozny, G., and Arellano-Garcia, H. (2012). Performance analysis of shooting algorithms in chance-constrained optimization. In *Proceedings of the 11th International Symposium on Process Systems Engineering (PSE2012)*, volume 31 of *Computer-Aided Chemical Engineering*, pages 1512 – 1516.

Wiebe, R. and Gaddy, V. L. (1934). The solubility of hydrogen in water at 0, 50, 75 and 100°c from 25 to 1000 atmospheres. *Journal of the American Chemical Society*, 56(1):76 – 79.

Wiese, K.-D. and Obst, D. (2006). Hydroformylation. In *Catalytic Carbonylation Reactions*, volume 18 of *Topics in Organometallic Chemistry*, chapter Hydroformylation, pages 1 – 33. Springer Berlin Heidelberg.

WIKA (2015a). *Cable resistance thermometer Model TR40*. WIKA data sheet TE 60.40. Technical Information.

WIKA (2015b). *N-10 / N-11 Pressure Transmitter*. Technical Information.

Winsor, P. A. (1954). *Solvent properties of amphiphilic compounds*. Butterworths Scientific Publications.

Wächter, A. and Biegler, L. T. (2006). On the implementation of an interior-point filter line-search algorithm for large-scale nonlinear programming. *Mathematical Programming*, 106(1):25 – 57.

Zagajewski, M., Dreimann, J., and Behr, A. (2014). Verfahrensentwicklung Vom Labor Zur Miniplant: Hydroformylierung von 1-Dodecen in Thermomorphen Lösungsmittelsystemen. *Chemie Ingenieur Technik*, 86(4):449 – 457.

Zhang, H. and Li, P. (2011). Chance constrained programming for optimal power flow under uncertainty. *IEEE Transactions on Power Systems*, 26(4):2417 – 2424.

Zhang, H. and Li, P. (2013). Application of sparse-grid technique to chance constrained optimal power flow. *Generation, Transmission Distribution, IET*, 7(5):491 – 499.